ADSORPTION OF SURFACTANTS FROM SOLUTION ONTO KAOLIN

BY

IAN PATRICK McKEOWN BSc

A thesis submitted in partial fulfilment

of the requirements for the degree of

Doctor of Philosophy

of the

Council for National Academic Awards

School of Natural Sciences
Liverpool Polytechnic
Byrom Street
Liverpool L3 3AF

Collaborating Establishment:
Reservoir Technology Division
Department of Energy
Winfrith Technology
Dorchester, Dorset DT2 8DH

August 1990

TABLE OF CONTENTS

DEDICATION

To my wife, Patricia, and my parents, for all their patience.

ACKNOWLEDGEMENTS

Sincere thanks are extended to Professor G.G. Jayson and Dr. H. Morris for their support throughout this work and their guidance during the writing of this thesis.

Acknowledgement is also made to the Department of Energy, and the Winfrith Atomic Energy Establishment, for the financial assistance given to the project, and additional thanks are extended to the staff at Winfrith for the many useful discussions made during the development of the research.

Abstract

Adsorption of Surfactants from Solution onto Kaolin

Ian Patrick McKeown

A study has been made of the adsorption of a surfactant, sodium dodecylbenzenesulphonate (ϕ-C_{12} ABS), such as might be employed in enhanced oil recovery operations, from aqueous solutions onto kaolin. To grade the isomers of the surfactant for their usefulness in lowering interfacial surface tensions the 1-, 4-, and 6-ϕ-C_{12} ABS forms were synthesised. The 4- isomer was chosen for detailed investigation as regards the effects of pH, solution ionic strength, temperature, the addition of n-butanol, and the presence of n-decane (= oil) on the adsorption (= to loss from aqueous solution). Comparisons were made with the behaviour of a cationic surfactant (cetyltrimethyl ammonium bromide). Electrophoretic mobility measurements of the kaolin particles in some of the solutions were carried out which, together with potentiometric titrations allowed the electrostatic state of the kaolin surface in the various solutions to be established.

Surfactant labelled with ^{35}S, and n-butanol labelled with ^{14}C were used in certain of the experiments. In addition some adsorption studies were undertaken with sandstone and silica as the solid phase.

The results from these experiments showed that under identical conditions the adsorption of the anionic surfactant was always approximately 1000× greater on kaolin than on sandstone or silica. The total available kaolin surface was never covered under any of the conditions investigated, and the smallest adsorption losses were sustained at high pH, low ionic strength, and 60°C. In addition to the loss by adsorption on kaolin, the anionic surfactant could be lost from the aqueous solution (and its property to lower oil/aqueous interfacial tensions) by preferential solubilisation into a separate phase of n-butanol (>8%), or n-decane (oil) when the concentration of the alcohol was high enough (i.e. >8%). In the presence of oil the formation of emulsions creates another phase of complication.

In the absence of butanol the adsorption isotherms of the anionic surfactant onto the kaolin can be analysed, to be due, at low concentrations (10^{-5} to $10^{-4.5}$ mol dm^{-3}) to electrostatic attraction, which is greatly increased at slightly higher concentrations with the build up of hemi- and ad-micelles on the solid. In the concentration region of 10^{-4} to 10^{-3} mol dm^{-3} adsorption is limited by micelle formation in the solution, while at higher concentrations (> 10^{-3} mol dm^{-3}) the surfactant appears to desorb into solution again. Careful examination revealed that aluminium ions from kaolin pass into aqueous solution and form salts or soluble complexes with the anionic surfactant. In either case the re-dissolved surfactant may not be available for the further lowering of interfacial surface tensions.

The study has therefore defined, in operating the surfactant flooding process, the efficient concentration limits of both 4-ϕ-C_{12} ABS and n-butanol. The usefulness of the surfactant in foam formation for reduction of gas mobility and improvement of sweep efficiency has yet to be investigated.

GLOSSARY

a_c, a_h	area of the chain, and headgroup, of a surfactant, respectively, m^2
a_i	activity of component i/mol dm^{-3}
A_s	area/molecule at an interface/m^2
b	a constant $\propto \frac{1}{\text{enthalpy}}$ of adsorption (dimensionless)
Barrel (bbl)	35 UK gallons (0.159 m^3)
c	a constant $\propto$ enthalpy of adsorption (dimensionless)
c_f, c_i	final, and initial, surfactant concentration, respectively/mol dm^{-3}
CMC	surfactant critical micelle concentration/mol dm^{-3}
C	double layer capacitance/F m^{-2}
C_d	diffuse double layer capacitance/F m^{-2}
e	electronic charge = 1.602×10^{-19} C
edl	electrical double layer
E	applied potential for electrophoresis/V
k	Boltzmann's constant = 1.38066×10^{-23} J K^{-1}
K	a constant, related to free energy of adsorption/ mol dm^{-3}
K_{eq}	partition coefficient
M_{Co}, m_{Co}	equilibrium concentration of n-butanol/mol dm^{-3}
M_D, m_D	equilibrium concentration of surfactant/mol dm^{-3}
m_s	concentration of salt in solution/mol dm^{-3}
n_c	a constant which is less than 1 and $\propto$ enthalpy of adsorption (dimensionless)
n_o	the bulk concentration of ions/mol m^{-3}
N	$2.303\frac{kT}{e}$ /V

N_c	capillary number (dimensionless)
N_s	total surface site density/sites m^{-2}
$pM_D(20)$	$-\log_{10}$ of the efficiency of adsorption at an interface/ mol dm^{-3}
pzc	point of zero charge/V
ΔP	pressure gradient/N m^{-2}
r	pore radius/m
T	absolute temperature/K
U_E	electrophoretic mobility/m^2 s^{-1} V^{-1}
V	electrophoretic velocity/m s^{-1}
x	distance from a particle surface/m
Z	valency of ions
γ	surface (or interfacial) tension/N m^{-1}
γ_c	minimum in oil-water interfacial tension/N m^{-1}
Γ	surface excess concentration of surfactant/mol m^{-2}
δ	thickness of the Stern layer/m
Δ	distance from the Outer Stern Plane to the electrokinetic shear plane/m
ε	the static permittivity of the solvent medium/F m^{-1}
ζ	zeta potential/V
η	viscosity of the medium/Pa s
θ	fraction of surface coverage (dimensionless)
θ_c	fraction of charged sites on the solid surface at the pzc (dimensionless)
$\frac{1}{\kappa}$	the electrical double layer thickness/m
μ_i	the chemical potential of species i
π	surface pressure/N m^{-1}

π_{CMC}	the effectiveness of adsorption at an interface/N m^{-1}
σ_o	surface charge density/C m^{-2}
Ψ	electrical potential/V

Chapter One

Introduction

1.1 The Oil Market and Enhanced Oil Recovery

During the latter part of the 1980's the oil industry was subjected to a number of changes in the world market ranging from the fall in oil prices during 1986, to the growth, by 27%, of proven reserves in 1987. This, together with the announcement of a ceasefire in the Iran-Iraq war during 1988/9, suggested that OPEC might finally agree on a strict quota system and end its endemic overproduction. This latter put $1.50 onto the price of a barrel of Brent crude, an action which proved to be unjustified since the anticipated OPEC accord did not arise [O1]. The price of oil is now expected to remain fairly stable in the immediate decade as a consequence of the expanding global consumption of gas; proven global reserves of which have quadrupled in the past 18 years to over 110 trillion cubic metres.

As a result of the price stabilisation of oil, producers have been forced to improve their recovery factors and a great deal of investment has been made to fund research into methods aimed toward improving oil recovery, a move exemplified by the American Department of Energy meeting in Washington on 31st January 1990 [O2].

In the UK, the Department of Energy has a statutory duty to regulate the development of the oil and gas fields of the Continental Shelf in the best interests of the nation. In order to exercise this duty effectively, it must be technically informed, both to engage in dialogue with oil companies and to direct research funds effectively, and to this end the

DOE has undertaken to support an Enhanced Oil Recovery (EOR) programme for North Sea oilfields.

Most of the oil in Britain's North Sea reservoirs is light and of premium quality. The low viscosity of the oil and the good reservoir characteristics of the oil-bearing rock ensure a high degree of productivity and, by world standards, a reasonably good recovery factor (∿ 40% of oil-in-place) when using water drive production methods (section 1.2.1). Nevertheless, using these conventional techniques, an average North Sea field is expected to end its life with about 60% of the original oil-in-place unrecovered [D1], amounting to some 2500 million tonnes, which at present prices* (∿ $20 per barrel) represents a potential asset of over £300 billion. Even a small increase in the percentage recovered could earn a substantial additional revenue, so there is clearly an incentive to encourage developments which may achieve this [L1]. The work presented in this report is designed toward application to oil recovery from North Sea reservoirs, and a brief account of the nature of these reservoirs is given below.

North Sea Reservoirs

Petroleum reservoirs consist of porous and permeable rock, made of silicates and clays, through which fluids (oil, water and gas) may flow toward recovery openings (wells), either under pressures that exist in the system (primary recovery, section 1.2.1) or under pressure applied to the

*Recent events have pushed the price to around $25 a barrel.

system (secondary recovery, section 1.2.2). All communicating pore space within the productive formation is properly a part of the rock, and may include several individual rock strata. The lateral expanse of a reservoir is therefore contingent only upon the continuity of the pore space, and the ability of fluids to move through the rock under the pressures available. An oil-field is thus regarded as an aggregate of well-bores penetrating one, or more, of these petroleum reservoirs.

In addition to being below several hundred feet of water, the oil reservoirs of the North Sea present complex geological structures at depths down to 20,000 feet and consist mainly of porous Jurassic sandstones originally deposited in river deltas, although other depositional formations, such as the giant Forties field, do occur as offshore submarine fans. Most of the reservoir sands are highly permeable, with thicknesses of up to 300 feet in the principal sand layer, although many of the geological structures are highly faulted, so making development more difficult. Very permeable layers in the formation can also act as thief zones for oil-production by water-drive, causing reduction in vertical sweep efficiency and a consequent early breakthrough of water into production wells. Reservoir pressures range between 300 ($2-48\times10^{6}\ N\,m^{-2}$) and 7000 psi, with temperatures in the region of 80-100°C, and salinities of up to 120,000 ppm total dissolved salts. They vary considerably in size, from the Forties field, covering 60 square kilometres, and originally containing about 500 million tonnes of oil, to the smallest economically viable

fields of about 15 million tonnes of oil. The oils are usually under-saturated, although in the case of the Brent field there is a free gas cap in contact with saturated oil, which can provide energy for driving oil to the surface (see section 1.2.1).

Because of the complexity of oil-production, and the possible benefits that may be gained from efficient recovery, much research has been undertaken into methods by which its recovery can be improved. The following section gives an outline of enhanced oil recovery today, and provides a means of introduction to the processes involved in enhanced oil recovery.

Enhanced Oil Recovery Today

Much of the early research into enhanced oil recovery processes has centred upon the research laboratories of the major American oil companies. Processes studied have included miscible gas displacement, surfactant, polymer, and alkaline flooding, in addition to thermal methods such as steam injection and *in situ* combustion [B1,J1,P1]. The US Government has encouraged such research by giving tax incentives for all enhanced oil recovery processes. The USA has some 32,000 million tonnes of unrecovered oil as a potential target which is almost double the nation's oil production over 50 years.

In Europe, research into EOR technology has been carried out at the Institut Francais du Petrole, BP, and by Shell KPL

Laboratories in the Netherlands and studies using surfactants have become prominent at the University of Clausthal in Germany [O1].

Previous American research is not completely relevant to the North Sea because of the rather special reservoir conditions here. The supply of materials to remote platforms presents substantial problems, particularly because loading and storage space is limited. In addition to the logistic problems, due to large well spacings in North Sea fields, considerable well-depths (leading to long lead-times on injection schedules), high temperatures and high salinities make the economics of EOR less attractive than for the land-based reservoirs of the US. As a consequence, much of the surfactant and polymer experience acquired in American projects has little relevance to North Sea oil recovery.

The viability of EOR applications is limited to oil price and such consideration obviously generates priorities for the various processes. Surfactant flooding is at present the area of most interest to the DOE in the UK, since this method of recovery offers the possibility of application to a wider range of oil-fields than other techniques [L1].

1.2 Reservoir Production Methods

1.2.1 Primary Oil Recovery

In the primary recovery process, wells bored into the reservoir rock formations serve as pressure sinks that allow

oil to be recovered, the recovery pressure being sustained by fluid expansion forces of the oil, and release of natural gas from the liquid as pressures fall to below the bubble-point of the under-saturated fluid. This natural pressure maintenance by gas release is referred to as "solution gas drive". In addition to the expansive energy of the petroleum hydrocarbons, reservoir pressures of most North Sea fields are augmented by large water aquifers below, or at the flank of the hydrocarbon phase, the contiguous water expanding into the pore space, as reservoir pressures fall, and displacing hydrocarbon by a natural water-drive mechanism. Thus, reservoir pressure in the early stages of production is supported by natural mechanisms. However, this form of production will generally only give a recovery of between 5 and 15% of the reservoir oil-in-place. In practice therefore, measures are undertaken to maintain the pressure drive by a secondary operation early in the field's life involving a liquid, or gas, injection of carefully selected wells in the field. The following section provides some detail of these procedures.

1.2.2 Secondary Oil Recovery [B2,H1]

Following primary recovery, and in many cases supplementing the process, fluids such as sea-water, miscible gas (e.g. CO_2), or re-cycled natural gas, provide a secondary pressure drive. The success of this additional recovery procedure depends upon the efficiency with which the injected fluid displaces the oil (the displacement

efficiency), the volume of the reservoir the fluid enters (the conformance, or sweep efficiency), and the careful selection of injection wells, around the production well, such that a pattern designed to sweep the field with the injected fluids and maintain the reservoir pressure, avoiding the formation of a free gas phase, is achieved.

The selected pattern of injection and production wells is most often drilled from platforms using deviated drilling techniques. Platforms have been designed to accommodate up to 40 wells and typically such a platform serves an area within a drilling radius about equal to the depth of the drilled well, implying a drainage area of 200 acres, or more, for each well.

The injected fluid displaces much of the resident brine and part of the oil in the contacted regions, driving them to the production wells. Continued injection, however, in time results in ever-increasing production of the injected fluid and eventually production only of this fluid, leaving unrecovered oil as "residual oil".

Field-life in the North Sea (i.e. the time over which economic production takes place) is typically 15-25 years, after which the production of oil from wells will be terminated owing to excessive gas or water production, or because oil production has fallen to below economic rates. The production profile of a typical operating field will give an increasing oil production rate during the first few years, with perhaps 5 years of production at the maximum

rate (usually set to about 10-15% of recoverable reserves per annum), followed by an extended period of declining production. Factors which determine the end-point of production are:

1. the total water-handling capability of the platform,
2. the possible need to install down-hole pumps to raise the oil and water, and
3. the cost of platform maintenance in relation to oil production.

Secondary recovery, using these drive methods, produces between 30 and 50% of oil-in-place, depending on the reservoir geology. The remaining residual oil (50-70%), either trapped by capillary forces, or by-passed by the sweep-pattern of the water-drive, is therefore a potential target for further enhanced recovery. In the North Sea, this target is some 2500 million tonnes, equivalent to over 20 years of UK consumption. In many of the operating fields the question of the feasibility of enhanced oil recovery will arise in less than ten years.

1.2.3 Residual Oil and Enhanced Oil Recovery

At least 30% of the oil originally contained in the pore space of rock, swept by a water flood, remains trapped by capillary forces at interfaces between oil, water and the pore surface. These forces retain the droplets in narrow pores of the structure and must be reduced to recover the oil. The simplest model of a trapped oil-ganglion is

illustrated in Figure 1. Water flowing through adjacent and communicating capillaries establishes a pressure-gradient across the droplet, moving it in the direction closest to the gradient, subject to the pore-wall constraints, until a constriction is met which is too small to permit further advance. Assuming the advancing and receding contact angles (θ_1 and θ_2 respectively) are zero, the pressure gradient required to displace the droplet is given by Laplace's equation (T1):

$$\Delta P = P_1 - P_2 = 2\gamma_i\left(\frac{1}{r_1} - \frac{1}{r_2}\right) \qquad (1.1)$$

in which ΔP = the pressure gradient in mN m^{-2},

r = the pore radius in m,

γ_i = the oil-water interfacial tension in mN m^{-1}.

Typically, ΔP is of the order 500 psi ($\cong 3.4 \times 10^{-6}$ N m^{-2}) [T1] to displace this oil, whereas a practical limit of pressure achievable in real-field situations is between 1 and 2 psi/ft ($\cong (2.3\text{-}4.6) \times 10^{-7}$ N m^{-2}/m) [H2,P1]. Consequently, an interfacial tension reduction to the order of 10^{-2} mN m^{-1} is required for an efficient displacement of the trapped oil [M1,W1].

The interrelationship between the capillary and viscous forces acting on the droplet is expressed by the dimension-less capillary number, N_c [M1,T1]:

$$N_c = \frac{(\text{velocity} \times \text{viscosity})}{\gamma_i} \qquad (1.2)$$

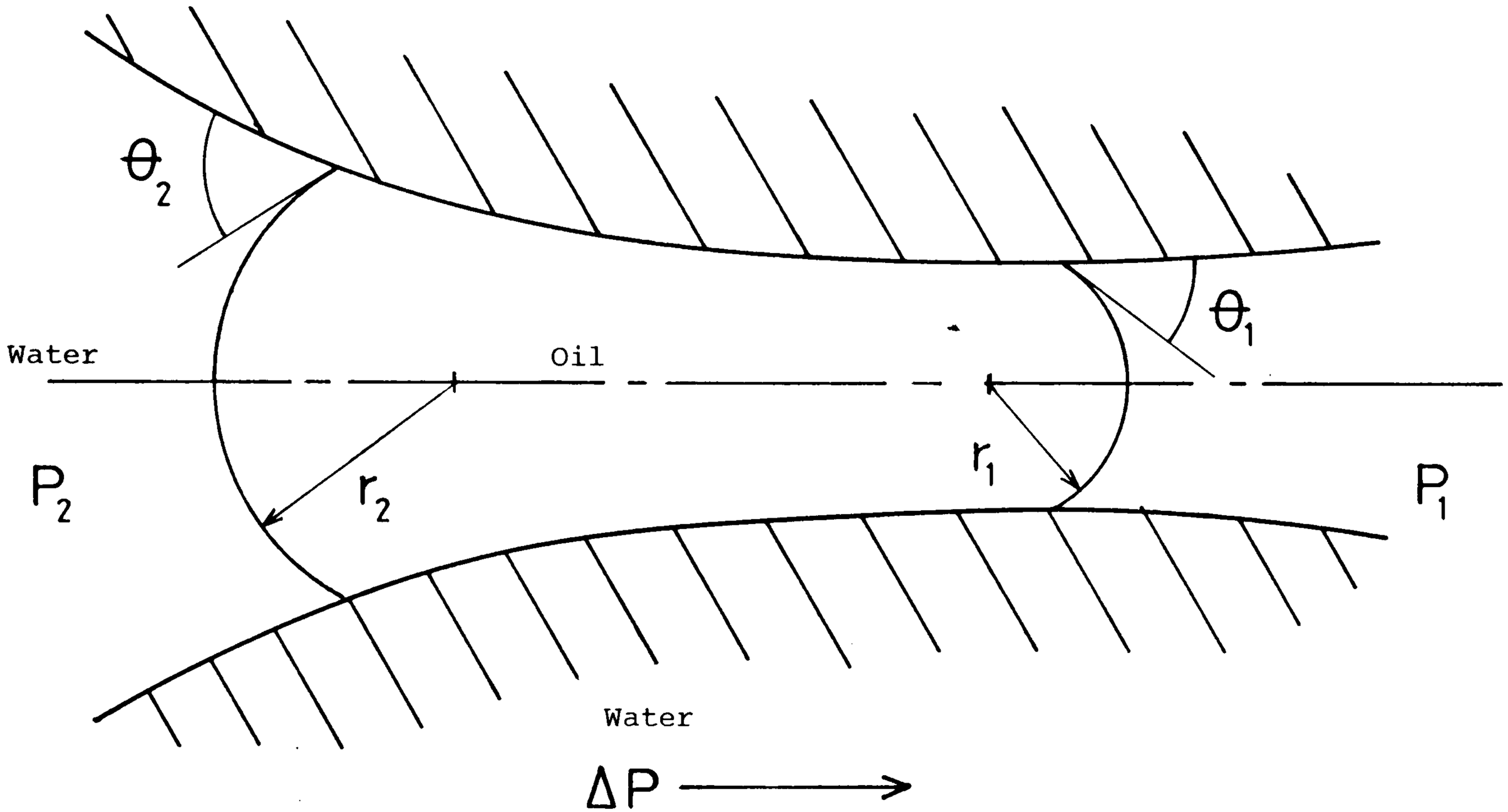

Figure 1. Model of an oil ganglion trapped by capillarity and a pore constriction.

in which the velocity, in ft/day ($\cong 3.6 \times 10^{-6}$ m s^{-1}) and the viscosity, in centipoise ($\cong 10^{-3}$ Ns m^{-2}), refer to the injected fluid, and γ_i (mN m^{-1}) to the interfacial tension between the oil and injected fluid.

The capillary number has been defined by a number of workers [T1,L1,T2] who conclude that high capillary numbers are required to achieve low residual oil saturations. For normal flooding conditions, N_c is of the order 10^{-6} [F1]. In order to recover significant quantities of oil from the pore space, N_c must be increased to about 10^{-2} [S1,G1]. This increase is most practically achieved by the reduction of γ_i to an ultralow value (ca. 10^{-3} mN m^{-1}). In general, methods designed for application to tertiary oil recovery are aimed toward this goal, thus, displacing oil by a miscible process.

1.2.3.1 Surfactant Flooding

In this tertiary oil recovery process, an aqueous solution of a surfactant is injected into the reservoir to displace residual oil. The aim of the surfactant injection is to solubilize the trapped oil and create a mobile microemulsion [R1] through reduction of the oil-water interfacial tension to ultralow values (ca. 10^{-3} mN m^{-1}, see Section 1.2.3). The effectiveness of the surfactant in reducing the interfacial tension depends upon its concentration, monovalent and divalent salt concentrations and the system temperature. Addition of alcohol, or co-surfactants, can be used to improve the efficiency.

Designs of surfactant flooding systems are usually undertaken as high concentration slugs, containing an appropriate composition of other additives as mentioned above. At these high concentrations surfactant micelles form in either the aqueous, or oil, phase. The process is therefore referred to as "micellar displacement" [B3]. The largest reduction in surface tension occurs when the hydrophilic and hydrophobic character of the surfactant is balanced. This can often cause the formation of a third distinct emulsion phase containing oil, water, and surfactant and which is very viscous.

The surfactant fluid is forced through the reservoir system by a polymer-thickened water bank, which increases fluid viscosity and prevents fingering (lateral diffusion into the porous rock, causing dilution of the fluid), and bypass of oil in the system. The desired mobility of the oil-surfactant bank can be adjusted by changes of the polymer concentration and type, and the proper mobility maintains the integrity of the bank and maximises the sweep (conformance) efficiency (Section 1.2.3.2).

1.2.3.2 Polymer Flooding

The water flood performance discussed previously indicated that oil recovery is lost because of the limitations in horizontal and vertial sweep patterns. The sweep efficiency improves through increasing the viscosity of the driving phase. Polymers are therefore employed to "thicken" the water and provide a better sweep. This technique could be

useful to "block-off" highly permeable layers as found in Brent-type sands. The high viscosity of a micellar slug also makes it necessary for a subsequent polymer bank to sweep the slug through the reservoir. A mixed surfactant/ polymer drive can therefore recover additional oil by both releasing trapped oil ("local displacement efficiency") and from improved sweep performance. Figure 2(a) shows a schematic diagram of micellar/polymer flooding.

Polyacrylamides have been used extensively in America for polymer applications, but these degrade rapidly at North Sea temperatures and salinities. Polysaccharides show promise of being more suitable in these conditions. All polymers display shear degradation at high flow rates and the effective viscosity is, therefore, a non-linear function of flow rate in which full viscosity recovery may not occur following very high shears at the injection wells. The long polymer molecules can also be trapped in the smaller pores of a sandstone, thus history dependent changes in rock permeability can also occur [J1].

1.2.3.3 Miscible Gas Techniques

The problems of interfacial tension between residual oil and a driving phase do not arise if the driving fluid can be selected so it is miscible with oil (i.e. a separate phase and interfacial tensions do not exist). Liquid petroleum gas (LPG) products such as ethane, propane and butane, which are miscible with oil, were used many years ago with some success in both laboratory and field trials of miscible

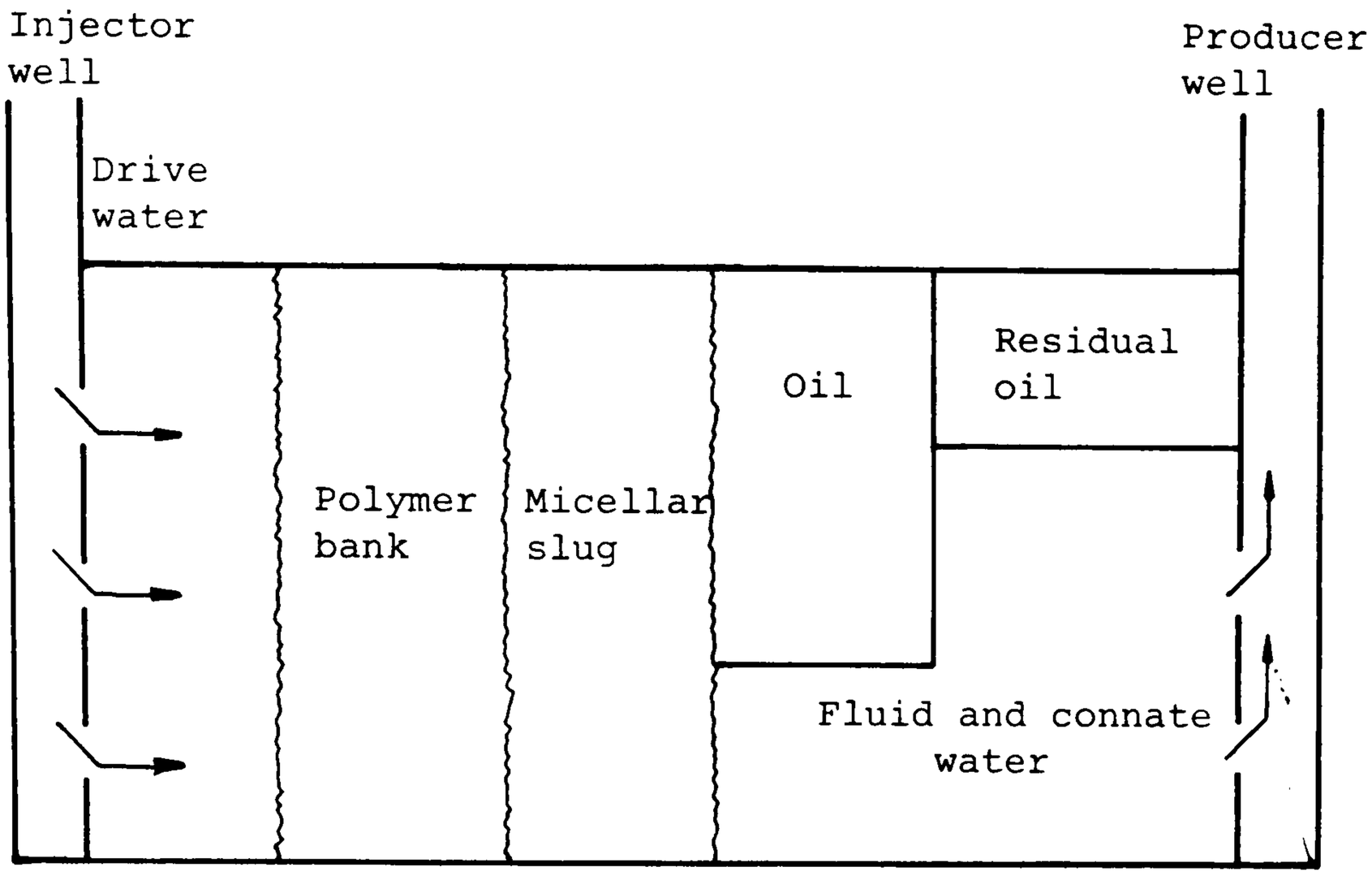

Figure 2(a): Micellar/polymer flood process for enhanced oil recovery.

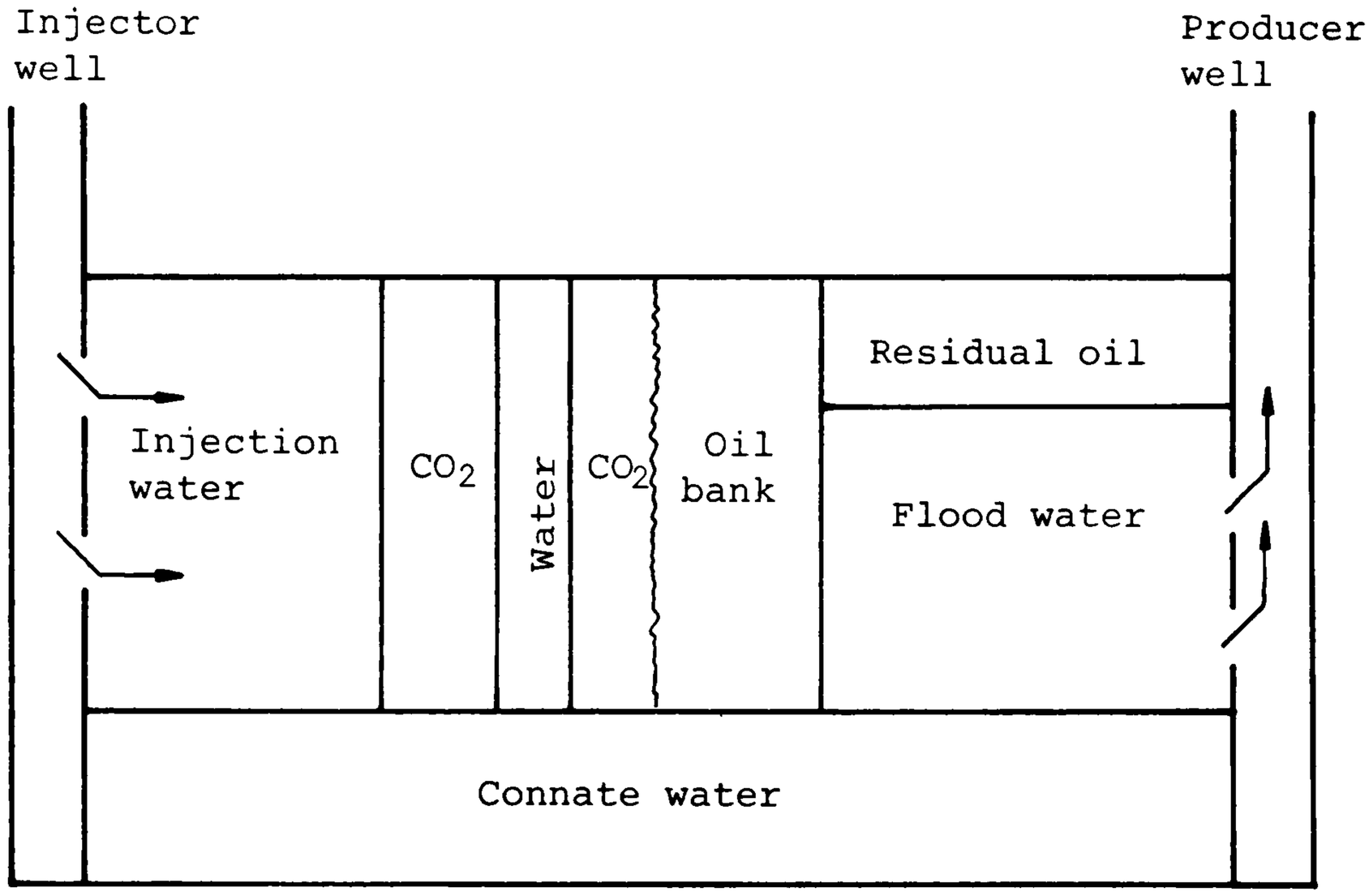

Figure 2(b): Enhanced oil recovery using gas (CO_2) drive.

displacement. LPG is now very expensive, so that interest has moved to less costly natural gas, which can be "tailored" to have some of the LPG properties. This "enriched" gas drive can become miscible with oil, but in this case, miscibility only follows multiple contacts between the gas and oil phases, with the higher components of the gas condensing into the oil and modifying its composition until miscibility is achieved. This is therefore referred to as multiple contact miscibility [S1].

Natural gas itself can become miscible with reservoir oil, provided the pressure is high enough. In the high pressure miscible gas process, the multiple contact miscibility arises as a result of the light ends of the oil vapourising into the gas phase and modifying the gas composition until miscibility is achieved. Both tailored gas and high pressure gas processes have been used in the United States with some success [S1,P2,R1].

The properties of vapourising multiple contact miscibility can also arise with CO_2 (Figure 2(b) at lower pressures than with natural gas. CO_2 also has the attraction that under immiscible conditions it is highly soluble in oil and can significantly swell trapped oil to promote a mobile condition. CO_2 also has a strong vapourising characteristic for removing many components from an oil phase, thereby allowing hydrocarbon production with the flowing gas phase. Consequently CO_2 is a potentially cheap and more effective gas for enhanced oil recovery which is receiving considerable attention in the USA [S1].

Nitrogen, and the more readily available flue gases, also have potential applications, but miscibility with these gases occurs at much higher pressures than with CO_2. The difficulty of the application of CO_2 in the North Sea is the absence of a large and inexpensive source of supply. Logistics and economics are important aspects of assessment studies.

1.2.3.4 Thermal drive methods (Figure 2(c))

Because oil viscosity decreases with increasing temperature, thermal drive methods are particularly relevant to the problems of producing heavy oil. A number of mechanisms contribute towards the effectiveness of steam drive processes, but principally the presence of hot steam will cause the lighter end of the heavy oil to vapourise into the gas flow and this mixed gas can then condense to a fluid containing hydrocarbons, which is less viscous than the original oil. Conditions for multiple contact miscibility between the hot mixture and reservoir oil may also occur and in addition the interfacial trapping forces between phases are also reduced by the increased temperatures [P2].

In the in situ combustion method, the generation of CO_2 in the combustion zone provides another gas component with useful displacement properties. It is found that the combustion process is improved by driving the heat bank, and combustion gases, forward using a water drive alternatively with the air supply for combustion. The additional steam generation assists the fluid displacement ahead of the burn zone.

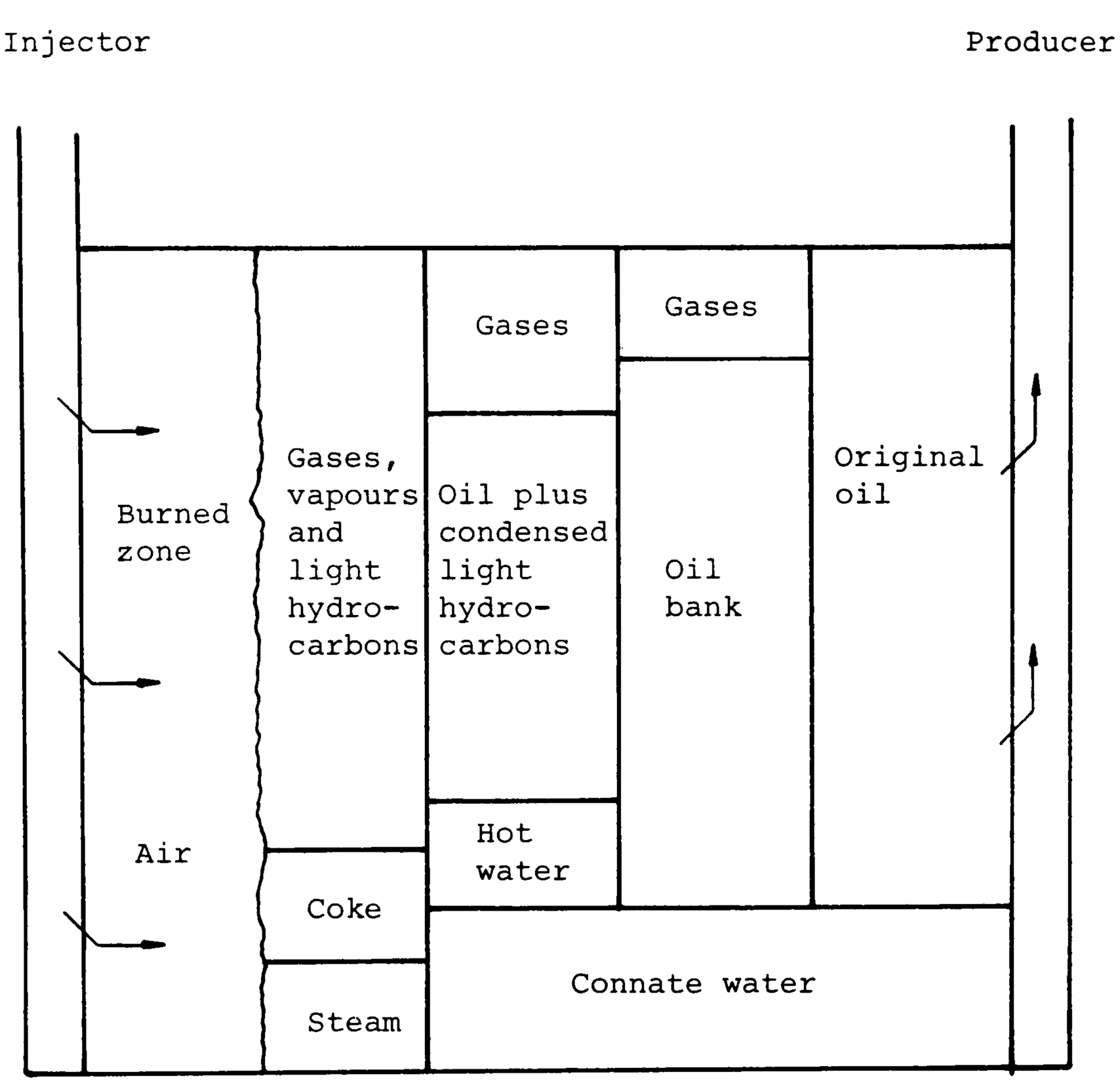

Figure 2(c): In-situ combustion process of enhanced oil recovery with various zones as formed in an oil reservoir.

The use of thermal processes offshore has potential from the raw materials standpoint, oil and air being readily available at a platform. Thermal recovery of oil from the North Sea has received little attention, although there is a large volume of target oil in place which may not be recoverable by other methods.

1.3 Surfactants for Enhanced Oil Recovery

Because of the wide range of surfactants employed in studies that have been aimed towards the formulation of a surfactant-based flooding system for enhanced oil recovery; for example, petroleum sulphonates [T1,W1,M1,H2,C1,D1], Texas I [F2,F3,P3, D2], Aerosol OT [A1], SDS [L3]; it has not been possible to develop a model microemulsion system for use in validating the chemical flood mechanism [F4]. As a consequence a search was instigated to identify potential surfactants for use in a model system; kaolin, n-butanol, n-decane, and NaCl (see present work, Section 1.4). In order to minimise the number of variables, the following constraints were employed [L1]:

(a) Model and field components should be comparable;

(b) Components should be commercially available, reasonably pure and not degradable over long time spans;

(c) Initial coalescence of phases should occur within minutes allowing true thermodynamic equilibrium to be established;

(d) Components should be relatively non-volatile and readily analysed;

(e) Interfacial tension (IFT) of the optimal three-phase region should be approximately 1×10^{-2} mN m^{-1}, or lower, (equation 1.2);

(f) Formation of viscous gels or surfactant precipitation must be avoided.

In view of these constraints a number of surfactant types were rejected:

1. petroleum sulphonates because of ill-defined composition;
2. ethoxylated nonionics, and their sulphonated products - due to temperature sensitivity and viscous gel formation;
3. carboxymethylated ethoxylated surfactants, which, while showing high tolerance to electrolytes (especially Ca^{2+} divalents), and high temperatures, required too great an ethoxylate content to operate efficiently at the low salinity levels present under North Sea conditions [L1].

After considering the available literature it was concluded that the most suitable choice for a model surfactant was, for reasons outlined below, sodium dodecylbenzene sulphonate (SDBS).

Cayais *et al* [C2,C3] first studied the problem of surfactant selection for producing ultra-low interfacial tensions in oil-aqueous solution systems. Their results showed that, at constant salinity, increase in the molecular weight of the petroleum sulphonate produced minimal, optimal interfacial tensions (IFT's) for the high molecular weight fraction of

the oil. Confirmation of this relationship came [C3] when different molecular weight fractions of petroleum sulphonates were contacted with a range of hydrocarbon oils. Only the lighter fraction of the surfactant produced an IFT minima when in contact with the lighter oils. The most important observation made was that measured IFT's were consistently lower for the purer fractions of surfactant.

Doe, Wade and Schecter [D2] extended this work to pure monomeric alkyl benzene sulphonates (ABS) and found these were able to produce ultra-low IFT's (ca. 10^{-3} mN m^{-1}) when in contact with hydrocarbon oils. In addition these workers showed that the positioning of the phenyl group on a hexadecyl chain had marked effects on the behaviour of the surfactants, the optimal conditions for producing the low tensions differing for each isomer.

The model system being considered in this present work is based on sodium dodecylbenzene sulphonate [L1] and in view of the results obtained by Doe, Wade and Schecter [D2], the initial studies were aimed towards a "screening" of the isomers available.

1.4 Adsorption of Surfactants at Solid-Liquid Interfaces

The loss of surfactant from flooding solutions is of great economic importance, such dilution of the solution markedly affecting the viability of the operation. In view of this it is important that the factors contributing to losses are understood and this section serves to introduce some of the

important characteristics involved in the adsorption process.

Adsorption at solid surfaces is the result of favourable interactions between the adsorbate and sites on the solid surface. The extent of adsorption is influenced by the nature of the interaction forces acting between the adsorbate and solvent and it is the presence of solvent species which makes the phenomenon of adsorption from solution more complicated than that of gas adsorption. The possibility of a third phase, as in EOR, can further complicate the adsorption process.

Two cases can be distinguished for adsorption onto solids:

1. In the majority of processes, interactions between the hydrophobic part of a surfactant molecule and the solid surface result in adsorption. This alters the electrical, mechanical and chemical properties of the interface and depends upon the nature of the solid and the hydrophobic and hydrophilic parts of the surfactant molecules [A2].

2. Adsorption can wholly, or partially, be effected through the hydrophilic group, by means of solvation, electrostatic attraction or by ion-exchange [R2]. This is reflected by pH-dependent adsorption. The hydrophilic moiety of the surfactant molecule is directed toward the substrate, rendering it hydrophobic with a close-packed film, an effect utilized in flotation.

Thermodynamics of the Adsorption Process and Adsorption Isotherms

Adsorption isotherms describe the relationship between the activity of adsorbate in the bulk of the solution and the amount of adsorbate adsorbed at constant temperature. A number of equations have been derived to characterise adsorption equilibria and these are briefly outlined below, while full derivation may be found in Appendix A1.

(a) The Gibbs Equation

The Gibbs equation quantitatively relates adsorption to the variation of interfacial tension at the air-liquid, or liquid-liquid, interface. Qualitatively the equation illustrates that dissolved material, which reduces the interfacial tension, accumulates at the interface because less work is required to increase (isothermally and reversibly) the area of the interface.

For a solution of ionic surfactant, in the absence of any other electrolyte, the Gibbs equation is usually expressed as [A1,H3]:

$$\Gamma_2^{(1)} = - \frac{m_D}{n\,RT} \cdot \frac{d\gamma}{dm_D} \qquad (1.3)$$

in which, $\Gamma_2^{(1)}$ = the relative surface excess concentration of the surfactant (component 2), over that of the solvent (component 1), in mol m^{-2}

n = 2 for ionic surfactants in the absence of inert electrolyte

n = 1 for non-ionic surfactants, or ionic surfactants in the presence of excess inert electrolyte

$\frac{d\gamma}{dm_D}$ = the change in surface (or interfacial) tension of the solvent upon addition of component (2) in mN m^{-1}.

That the factor n should be used, and take the values assigned has been supported by evidence from direct measurements of surfactant molecules adsorbed at the air-water interface using radiolabelled materials [C4].

(b) The Langmuir Equation

The Langmuir equation, originally derived from the kinetic theory of gases, relates the amount of adsorbate adsorbed at a plane surface to the equilibrium bulk concentration, and is based on certain simplifying assumptions:

1. adsorption is localised and each site is equivalent,
2. there are no interactions between adsorbed molecules,
3. the heat of adsorption is independent of surface coverage,
4. adsorption is restricted to a monolayer.

Despite these restrictions a great many experimental adsorption isotherms have been shown to fit the Langmuir adsorption model reasonably well, although a satisfactory fit of experimental data does not necessarily imply that the theoretical model is completely fulfilled [S2,S3]. For adsorption from solution, the Langmuir equation may be expressed as [S2]:

$$\Gamma_i = \frac{\Gamma_{i\infty} . a_i}{K + a_i} \quad , \tag{1.4}$$

or

$$\frac{1}{\Gamma_i} = \frac{1}{\Gamma_{i\infty}} + \frac{K}{\Gamma_{i\infty}} \cdot \frac{1}{a_i} \tag{1.5}$$

in which, Γ_i = adsorption density of component i (mol m^{-2}) at a bulk solution activity; a_i (mol dm^{-3})

$\Gamma_{i\infty}$ = the maximum adsorption density of i (mol m^{-2})

and, K is a constant which is related to the standard free energy change of adsorption, $\Delta G^{\ominus}$

$$K = \exp\left(- \frac{\Delta G^{\ominus}}{RT} \right) \quad .$$

Although still used, the Langmuir equation is only of limited value since in practice surfaces are energetically inhomogeneous, and interactions between species often occur. The Tempkin equation, however, is based on a model of surface heterogeneity and expresses the fraction of surface coverage, θ, as a function of log a_i at intermediate coverages of $0.2 < \theta < 0.8$ (see below).

(c) <u>The Tempkin equation</u>

The Tempkin equation is derived by inserting into the Langmuir equation (above) the condition that the heat of adsorption decreases in a linear manner as the surface coverage increases [B4]. This procedure is shown in Appendix A1.

When applied to adsorption data from solution, the Tempkin equation has the form:

$$\Gamma_i = b \ln c + b \ln a_i \qquad (1.6)$$

in which, Γ_i = amount of solute adsorbed (mol m^{-2}) at a bulk solution activity of a_i (mol dm^{-3}),

b = a constant ($\alpha \frac{RT}{\Delta H_o}$, where ΔH_o is the heat of adsorption at $\Gamma_i = 0$),

c = a constant $\left(\alpha \exp \frac{\Delta H_o}{RT} \right)$ which is dimensionless.

From equation (1.6) therefore, a plot of Γ_i against ln a_i would give a straight line with a slope proportional to the absolute temperature. Deviations from linearity occur, however, at low and high values of surface coverage [T3], due to initial adsorption onto the most active sites, and lateral interactions between adsorbed molecules, respectively [Z1]. Hence, the application of the Tempkin equation to coverages of $0.2 < \theta < 0.8$.

(d) The Freundlich Equation

The Freundlich equation, like the Langmuir equation, was originally developed for gas adsorption systems. The equation, however, is empirical depending on no theoretical assumptions, although it may be derived for an adsorption model in which the magnitude of the heat of adsorption varies exponentially with surface coverage (see Appendix A1).

The equation has the general form:

$$\Gamma_i = c \, a_i^{\frac{1}{n}} \qquad (1.7)$$

in which, Γ_i = the number of moles of solute adsorbed per unit area (mols m^{-2})

a_i = the activity of solute at equilibrium (mol dm^{-3})

c = a constant ($\alpha\ \Delta H_m$, the minimum heat of desorption), quoted dimensionless

n = a constant which is less than 1 and $\alpha \frac{\Delta H_m}{RT}$, quoted dimensionless.

The values of c and n vary with the system, although n is usually between 0.2 and 0.7 [A2].

The Freundlich equation is successful with adsorption systems of very variable characteristics, such as adsorption from solution, expressing the rapid increase with concentration in the early part of the isotherm [H4,W3]. Taking logs of equation (1.7) gives:

$$\log \Gamma_i = \log c + \frac{1}{n} \log a_i, \qquad (1.8)$$

thus, a plot of $\log \Gamma_i$ versus $\log a_i$ yields a straight line of slope $\frac{1}{n}$ and intercept $\log c$.

Because the Freundlich isotherm was empirically derived, the constants, c and n, have no simple physical significance. However, they have been used for representing the capacity of an adsorbent (log c) and in providing a description of the functional dependence of the capacity on the equilibrium concentration ($\frac{1}{n}$) for comparative purposes [D4,H4,W3].

1.5 The Electrical Double Layer

Most substances acquire a surface electric charge when brought into contact with a polar (e.g. aqueous) medium, the possible charging mechanisms being ionisation, ion adsorption and ion dissolution. This surface charge generates an ionic atmosphere, part of which is diffuse, in which ions of opposite charge to that of the particle (the "counter-ions") are concentrated close to the surface while those of similar charge (co-ions) are repelled. Such a distribution of charge comprises the electric double layer of the particle, a concept first introduced by Helmholtz in 1879 and later modified by Gouy, Chapman (1919-17), and Stern (1924), and which has been described extensively in the literature of colloid chemistry [O3,V1,H5] and electrochemistry [G2,C5,S3].

The net result of this ion distribution is that close to the charged surface there is an excess of counter-ions over co-ions, the difference decreasing with distance until in bulk solution they are equivalent in order to maintain electro-neutrality. The potential ψ within the diffuse layer decreases exponentially with distance x from its value ψ_o at the surface, until it reaches zero in bulk solution. The mathematical treatment of the double layer is complex and has only been solved satisfactorily for the special cases where the surface is represented as a sphere or a flat plate. For the latter case the fundamental equation for the double layer may be expressed as [O3]:

$$\frac{d^2\psi}{dx^2} = \frac{2Z\ e\ n_o}{\varepsilon} \sinh\left(\frac{Z\ e\ \psi}{kT}\right) \qquad (1.9)$$

with the boundary condition that for $x = 0$, $\psi = \psi_o$, and when $x = \infty$, $\frac{d\psi}{dx} = 0$, the solution of which is given by:

$$\psi = \frac{2kT}{Ze} \ln\left(\frac{1 + \gamma \exp[-\kappa x]}{1 - \gamma \exp[-\kappa x]}\right) \qquad (1.10)$$

where, $$\gamma = \frac{\exp[Ze\psi_o/2kT] - 1}{\exp[Ze\psi_o/2kT] + 1} \qquad (1.11)$$

and $$\kappa = \left(\frac{2e^2\ n_o\ Z^2}{\varepsilon kT}\right)^{\frac{1}{2}} \qquad (1.12)$$

in which, e = the electronic charge/C

n_o = the bulk concentration of ions/mols m^{-3}

Z = the valency of the ions

ε = the static permittivity of the medium/F m^{-1}.

Equation (1.10) describes the reduction in potential as a function of distance from the surface, and at small surface potential, viz: $\psi_o \ll 25$ mV such that $(Ze\psi_o/2kT) \ll 1$, the equation reduces to [S2]:

$$\psi = \psi_o \exp(-\kappa x) \qquad (1.13),$$

showing the potential decreases exponentially with distance from the surface.

The surface charge σ_o is related to the surface potential by [H6]:

$$\sigma_o = (8 n_o\ \varepsilon\ kT)^{\frac{1}{2}} \sinh\left(\frac{Ze\psi_o}{2kT}\right) \qquad (1.14)$$

which for small surface potentials ($\psi_o \ll 25$ mV) reduces to:

$$\sigma_o = (8 n_o \varepsilon kT)^{\frac{1}{2}} . (Z e \psi_o) = \varepsilon \kappa \psi_o \qquad (1.15)$$

and hence the double layer is theoretically equivalent to a parallel plate condenser with a distance $\frac{1}{\kappa}$ between the plates. This is equivalent to assuming that all the ions in the diffuse part of the double layer are located in a single plane at a distance $\frac{1}{\kappa}$ from the surface. The distance $\frac{1}{\kappa}$ is called the "double layer thickness" and its magnitude varies with electrolyte concentration, viz. 10 Å in 0.1 mol dm^{-3} to 1000 Å in 10^{-5} mol dm^{-3} monovalent electrolyte solution.

Electrical Double Layer Capacitance

The Gouy-Chapman theory of the electric double layer, based on the assumptions that:

(i) electrolyte ions are point charges, and

(ii) the solvent is structureless and of constant permittivity,

was modified by Stern to allow for the finite size of hydrated ions. The capacitance C of such a model may be defined by the equation [S2]:

$$C = \frac{d\sigma_o}{d\psi_o} \qquad (1.16)$$

which, upon differentiation of equation (1.14) is given by:

$$\frac{d\sigma_o}{d\psi_o} = \varepsilon \kappa \cosh\left(\frac{Z e \psi_o}{2kT}\right) \qquad (1.17)$$

$$= 228.5 Z c^{\frac{1}{2}} \cosh(19.46 Z \psi_o) \ \mu F \ cm^{-2}$$

where the electrolyte concentration, c, is expressed in mol dm^{-3}, at 25°C, and ψ_o in volts.

Addition of electrolyte to the system, while reducing the double layer thickness, increases the capacitance, thus increasing the σ_o/ψ_o ratio. The response of the two types of double layer (constant charge and constant potential) to the increase in electrolyte concentration will therefore differ [S2]:

ψ_o decreases if σ_o is constant, and

σ_o increases if ψ_o is constant.

Zeta Potential

According to the Stern model of the electric double layer, ions may adsorb strongly at solid surfaces, either specifically or non-specifically (see earlier), such that they overcome thermal agitation. The double layer is then considered as being made up of two parts, the first a compact layer of thickness δ adjacent to the surface and the second consisting of the diffuse Gouy layer (Figure 3). The potential at the boundary between the Stern and Gouy layers ψ_δ, which determines the potential decay within the solution, may have the same or opposite sign to that of the surface, or may be zero.

There is no satisfactory method for evaluating ψ_o and ψ_δ for hydrophobic systems, however, from the measurement of the velocity of a charged particle in an electric field a

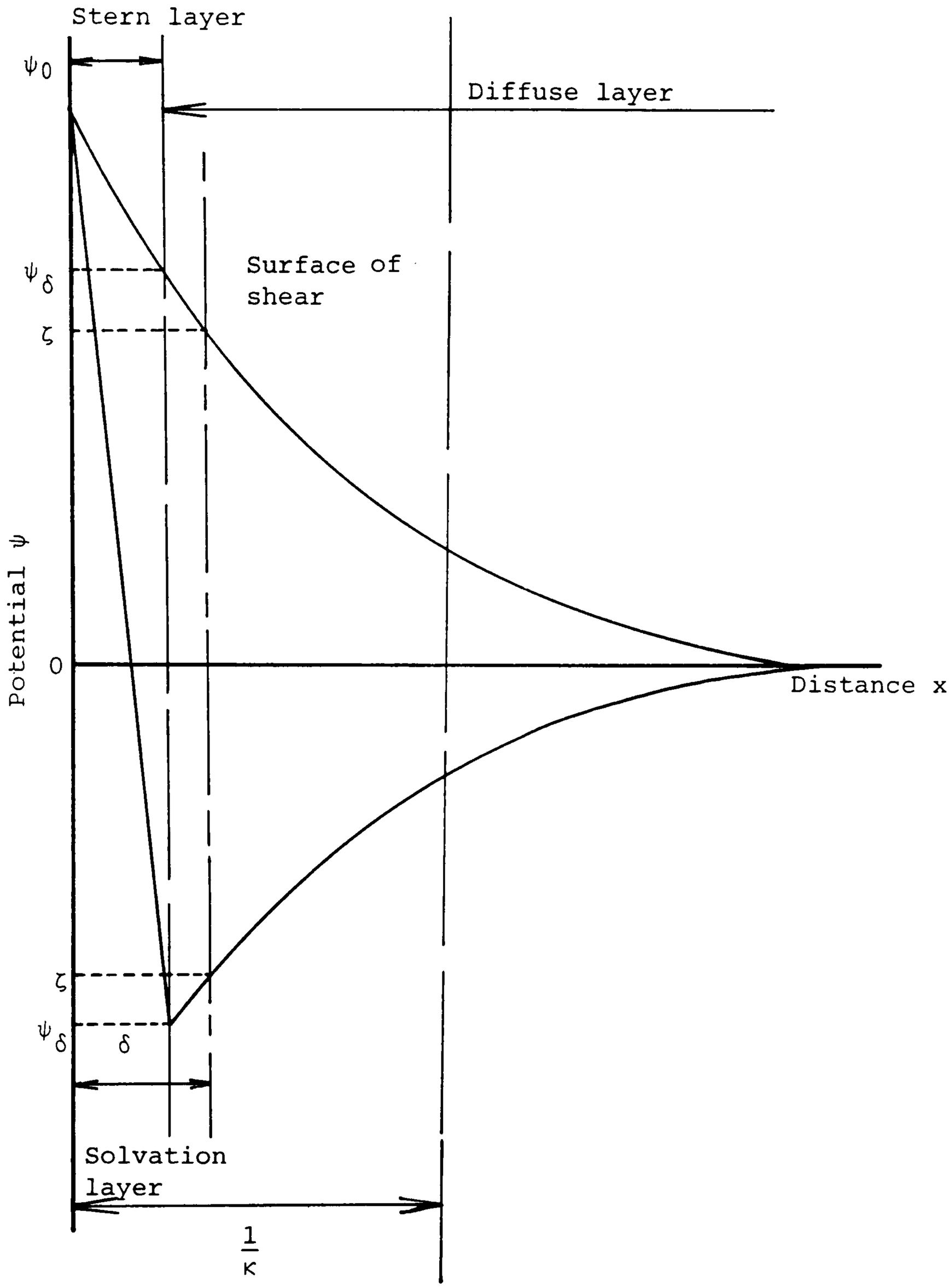

Figure 3: Potential decay curves for an electrical double layer associated with a colloidal particle whose surface potential is ψ_0. The lower curve results from strong adsorption in the Stern layer.

potential, called the "zeta potential" (ζ), can be obtained. The zeta potential is defined as the potential at the surface of shear separating the particle, with any attached solvent and ions which move with the particle, from the electrolyte solution. The technique of microelectrophoresis is the most accurate method for measurement of the electrophoretic velocity of lyophobic systems and provides a number of advantages over other methods of measurement, such as moving boundaries [S4]:

1. the particles are observed in the normal solution environment,
2. very dilute solutions can be studied so that flocculation rates, even at high electrolyte concentration or near the point of zero charge, are negligible,
3. the high magnification of the ultramicroscope system leads to short observation times and high sensitivity, and
4. in a polydisperse solution the particles in a chosen (though wide) size range can be observed while others are ignored.

The relationship between the electrophoretic velocity, V, and zeta potential, ζ, of a particle depends upon the magnitude of the product κa, that is on the relative magnitudes of the particle radius, a, and the double layer thickness:

When $\kappa a \gg 1$, the Smoluchowski approximation [S5],

$$V = \frac{\zeta \varepsilon E}{\eta} \tag{1.18}$$

and when $\kappa a \ll 1$ the Hückel approximation [S5]:

$$V = \frac{2}{3} \cdot \frac{\zeta \varepsilon E}{\eta} \tag{1.19}$$

where, E = the applied potential in volts,

η = the viscosity of the medium in Poise.

For many practical systems κa takes intermediate values and in these cases account must be taken of the fact that the mobile part of the double layer becomes distorted when the particle moves, since a finite time (the relaxation time) is required for the original symmetry to be restored. This "relaxation effect", which retards the motion of the particle, may be neglected for small and large κa values but is significant for intermediate values (see Table 1 below).

The discrepancy between the equations of Smoluchowski and Hückel arises from the different ways in which account was taken of the electric field in the vicinity of the particle, and of the effect of retardation. At small κa, the electrophoretic retardation of the particle is relatively unimportant and the main retarding force is the frictional resistance of the medium; Dukhin and Deryaguin [D3] have shown that the ratio of the retardation force to the viscous force is of the order of κa. Thus, for small particles, although the retardation force acts across the whole double layer, very little of it is transmitted to the particle. For large particles, with thin double layers, essentially all of

the electrophoretic retardation is communicated to the particle [D3].

Henry (1931) resolved the situation by consideration of the applied field. Smoluchoswki had assumed the field to be uniform everywhere parallel to the particle surface, while Hückel had disregarded the deformation of the applied field by the presence of the particle. As Figure 4 shows, these assumptions are justifiable in the extreme situations of $\kappa a \gg 1$ and $\kappa a \ll 1$ respectively.

Henry showed that when the external field was superimposed on the local field around the particle the velocity could be written:

$$V = \frac{2'}{3} \frac{\varepsilon \zeta E}{\eta} \cdot f_1(\kappa a) \qquad (1.20)$$

in which the function $f_1(\kappa a)$ depends on the particle shape. Values of $f_1(\kappa a)$ for a spherical particle are shown in Table 1. Note that $f_1(\kappa a)$ approaches 1 for small κa and $\frac{3}{2}$ for large κa. The smooth transition from the Huckel to the Smoluchowski equation, as κa increases, is shown in Figure 5 for a non-conducting particle.

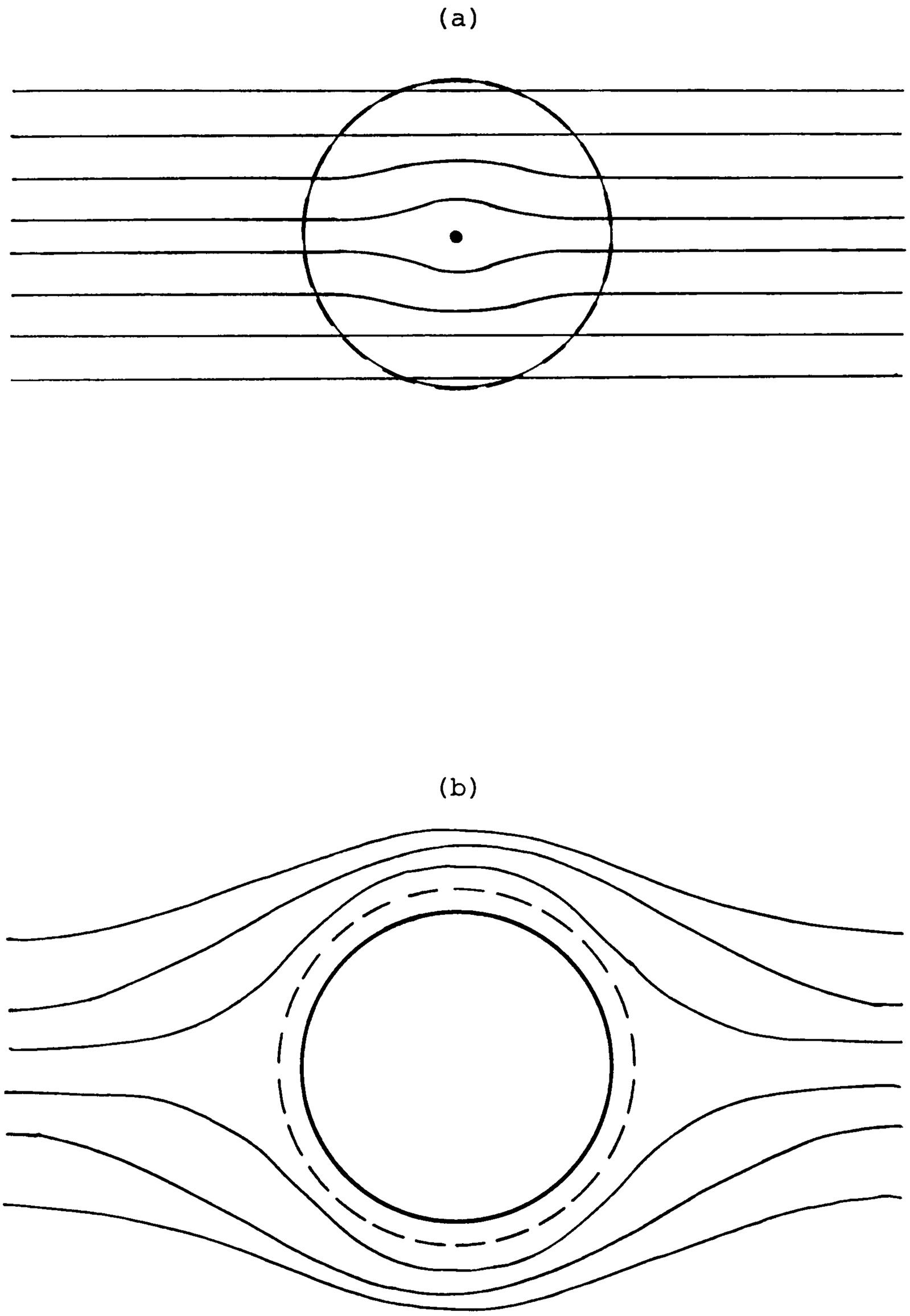

Figure 4: Effect of a non-conducting particle on the applied field

(a) $\kappa a \ll 1$; (b) $\kappa a \gg 1$. The broken line is at a distance $\frac{1}{\kappa}$ from the particle surface.

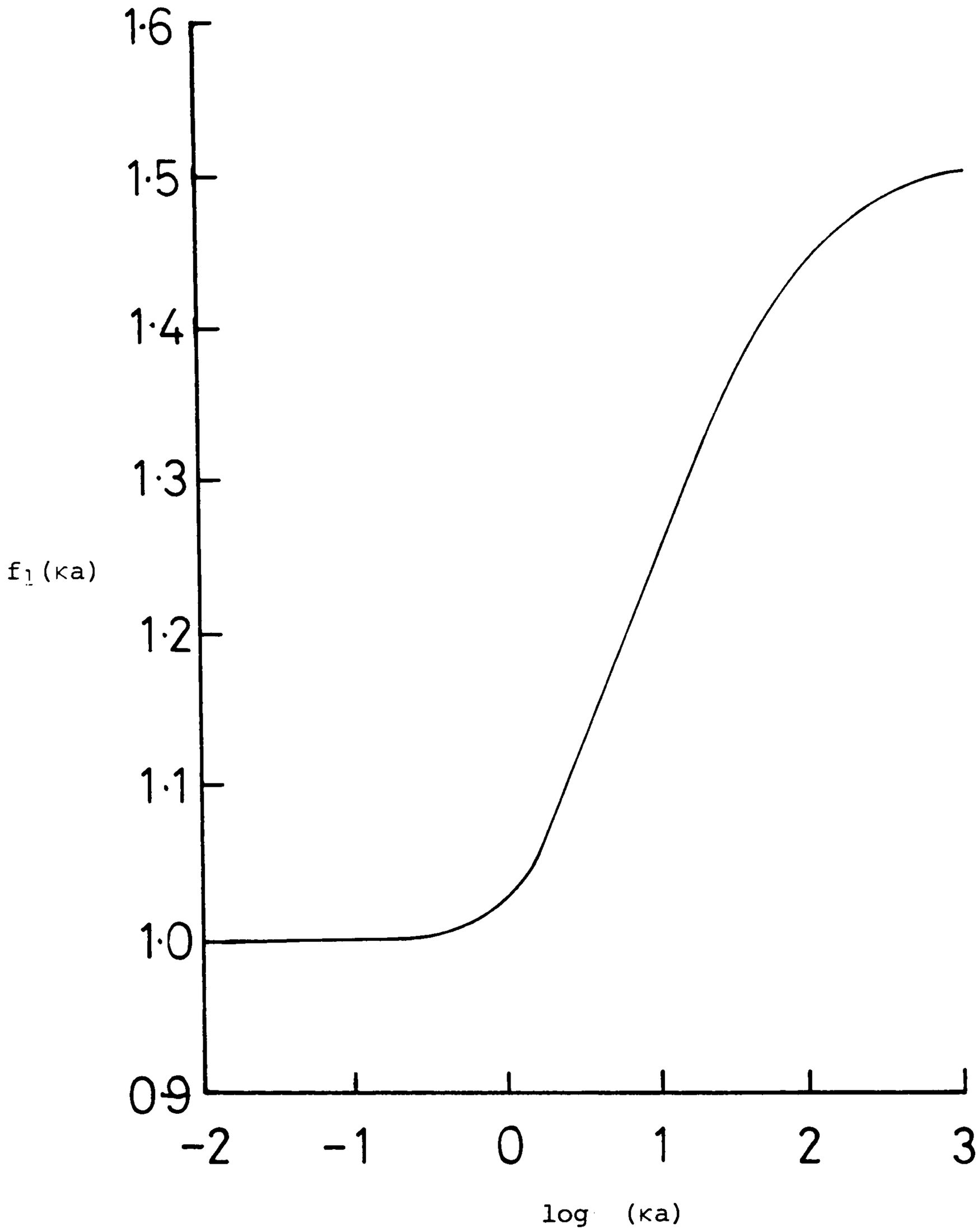

Figure 5: Variation of the Henry function, $f_1(\kappa a)$ with log(κa), showing the influence of an insulating sphere on an imposed electric field.

Table 1. Values of the Henry correction factor, $f_1(\kappa a)$ to be used in equation (1.2), as a function of κa

κa	$f_1(\kappa a)$*	κa	$f_1(\kappa a)$
0	1.000	5	1.160
1	1.027	10	1.239
2	1.066	25	1.370
3	1.101	100	1.370
4	1.333	∞	1.500

*for a sphere, $\kappa a > 1$,

where, $f_1(\kappa a) = \frac{3}{2} - \frac{9}{2\kappa a} + \frac{75}{2\kappa^2 a^2} - \frac{330}{\kappa^3 a^3}$

Electrokinetics of the Oxide-Solution Interface

As outlined above, the electric double layer may be discussed in terms of the electrical capacities of the regions. To determine such capacities involves measurement of charge densities and electric potentials. For oxide systems, where an electrode system is not available, it has been common to assume that the electric potential at the solid surface, ψ_o, can be obtained from measured pH values via a relation of the Nernst form, viz:

$$\Delta\psi_o = -\frac{2.303kT}{e} \cdot \Delta pH \qquad (1.21)$$

$$= N\Delta pH \qquad (1.22)$$

where, e = electron charge, Coulombs

N = -2.303kT/e = 59.2 mV at 298 K.

Thus, derived capacities will reflect the deficiencies of relations (1.21) which are expected [S4] for an interface such as the oxide/solution where the charge results from dissociating surface groups rather than an excess of one constituent of a ionic lattice [L4]. In order to illustrate the deficiencies inherent in equation (1.21) for application to the oxide/solution interfaces, Smith [S6] derived the following expression:

$$\left[\frac{d\,\psi_o}{d(pH)}\right]_{\sigma_o \to 0} = -\frac{2.303kT}{e} - \frac{kT}{2N_s e^2} \cdot \frac{1}{\theta_c} \cdot \frac{d\sigma_o}{dpH} \qquad (1.23)$$

in which, N_s = the total surface density (in sites m^{-2}) of particular sites on the solid

θ_c = the fraction of charged sites on the solid at the point of zero charge, ranging from a maximum of 0.5, down to very small values

σ_o = the surface charge density of the solid.

From equation (1.23), it can be seen that the practice of using a Nernst form relation for $d\psi_o/d(pH)$ corresponds to taking only the first term on the right hand side. The second term, which numerically reduces $d\psi_o/d(pH)$, depends on electrolyte concentration and becomes significant as θ_c tends to zero. The indicated derivation of (1.23) from (1.21) has been used [L5] to correct capacities derived from potentiometric titrations, it is applied in this work to the analysis of electrokinetic data near the point of zero charge of kaolin.

1.6 Clay Mineral Structure and Charge Distributions

The Mineral Structure of Clays

The principal building elements of clay minerals are two-dimensional arrays of silicon-oxygen tetrahedra, and aluminium (or magnesium)-oxygen-hydroxyl octahedra ($Si_xO_yAl_z$). Analogous symmetry and almost identical dimensions between those sheets allows sharing of oxygen atoms (Figure 6), this occurring between either one silica and one alumina sheet, forming "two-layer" minerals, or between two silica and one alumina sheet, forming three-layer minerals. Combination of these sheets constitutes a unit layer and most clay minerals consists of such layers stacked parallel to each other.

Modern studies have organised clay minerals into two main groups [V2]:

(i) an amorphous group which includes allophane and evansite, and

(ii) a crystalline group, the most abundant of which are the kaolins, the montmorillonites and the illites.

In this study we are concerned exclusively with kaolin (china clay) and in the following sections, a description of this clay structure and a discussion of the nature of its surface charge is given.

The Structure of Kaolin

Almost perfect two layer lattices are realized in the clay minerals of the kaolin group, the major members of which are kaolinite, dickite, nacrite and halloysite. In general,

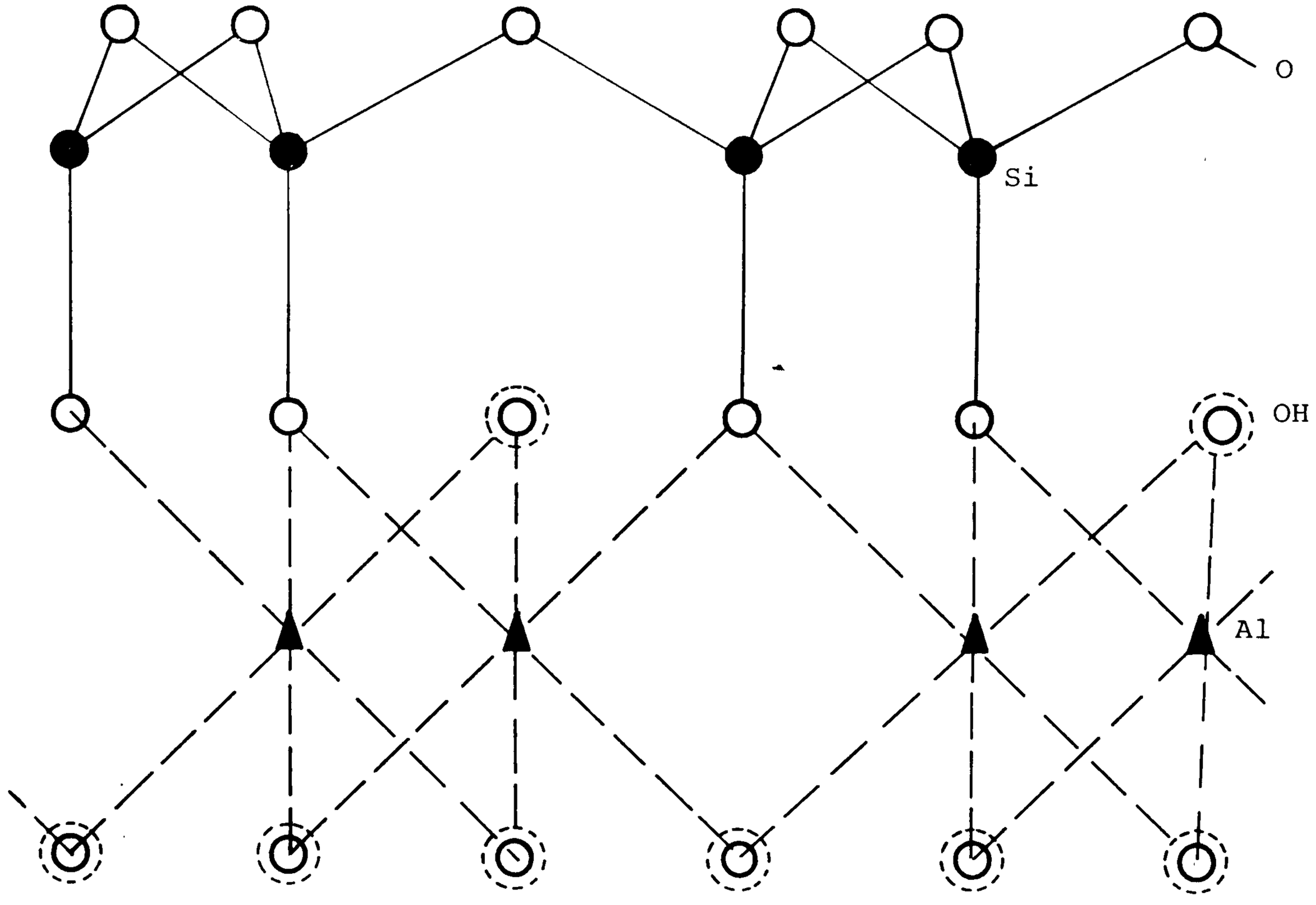

Figure 6: Atom arrangement in the unit cell of a two-layer mineral (schematic).

these minerals are non-expandable (as opposed to montmorillonites - one form of which is expandable, forming a gel in water), and the main difference between these lies in their unit-layer stacking.

Kaolinite is by far the abundant mineral of the kaolin group, and samples of kaolin consist of up to 98% of the mineral. Electron-micrographs of kaolin show the material to consist of pseudo-hexagonal plates of the order of 1 μm in length (Figure 15). The plate-like structure reflects the ease of cleavage along a plane parallel to the silica/alumina unit layer. The lattice structure consists of one sheet of tetrahedrally coordinated silicon (with oxygen) and one sheet of octahedrally coordinated aluminium (with oxygen and hydroxyl species), thus presenting a 1:1 or a "two-layer" structure. An additional layer of hydroxyl ions completes the charge requirements of the octahedron (gibbsite) sheet.

The Origins of Charge and Potential on Clays

Most workers accept the "heteropolar" model for layer silicate surface. This model, based on direct electron-microscopic evidence [T4], was first proposed by van Olphen [V1] and has been supported by Schofield and Samson with results from rheological and ion adsorption measurements [S7]. The results suggest that the distribution of charge on a clay surface is unequal; the face carrying a negative charge which is unaffected by solution conditions and an edge charge which can vary from positive to negative depending on solution conditions [W4,F5,R3,I5,S8,V2].

The face surface charge of the clay particle originates from isomorphous substitutions of Al(III) for Si(IV) at tetrahedral sites, or Mg(II) or Fe(II) for Al(III) at octahedral sites. The resulting negative charge is then internal to the structure, it is not a surface charge. The structural charge on clays is thus fixed by the composition of the clay, a situation which differs markedly from that of other hydrophobic colloids. As the structural charge is not determined by adsorption of ions from solution, there are no particular potential-determining species. The electrical charge is constant and consequently there is no point-of-zero charge (pzc) associated with the structural charge. The electrical charge is distributed throughout the particle volume and hence interacts with the surroundings mainly through the flat-layer surfaces.

Unlike the flat surfaces, the edges of the clay sheets terminate in broken, or unsatisfied, Si-O and Al-O bonds. These bonds hydroxylate in water, producing SiOH and AlOH sites capable of amphoteric behaviour. Like the surfaces of oxides and non-clay silicates, the edges of clay particles develop a pH-dependent "surface" charge, which may be positive or negative, and has a pzc.

The net surface charge of a clay particle is therefore the algebraic sum of the structural and edge charges. When the edge charge is negative (high pH), the overall particle charge is negative. When the edge charge is sufficiently positive to neutralise the face charge (on the acid side of

the edge pzc) [V3,P4,B5] the charge on the particle is zero. The pH corresponding to this zero particle charge is not a pzc, for two reasons:

1. a pzc is defined in terms of a potential-determining ion (pdi) and the particle charge is not determined by pdi adsorption.
2. the surface potential should be zero at the pzc. The potentials between the particle faces and the solution, and between the particle edges and the solution are not zero when the particle charge is zero, since a net positive edge charge is required to neutralise the permanent structural charge.

The pH at which the net particle charge is zero, in the presence of indifferent electrolyte, is the isoelectric point (iep). If the maximum edge charge is small, relative to the structural charge, it may not be possible to acquire a zero net charge without specific adsorption of a positive species.

1.7 Surfactant adsorption at Fluid-Fluid Interfaces

At a fluid-fluid interface, the adsorption of surfactant molecules favours an expansion of the interface, and this must be balanced against the tendency for this area to contract under normal surface tension (internal) forces. This "expanding pressure", π, (or surface pressure) of an adsorbed layer of surfactant is related to the surface (or interfacial) tension, γ, by the expression [G3]:

$$\gamma = \gamma_o - \pi \qquad (1.24)$$

where, γ_o = surface tension of pure solvent/mN m^{-1}

γ = surface tension of solution/mN m^{-1}.

The magnitude of π depends upon the nature of the lyophobic moeity of the surfactant molecules. Its value increases as the group becomes more lyophobic. A rough generalisation, known as Traube's rule, is that for a given homologous series, the concentration of surfactant required for an equal lowering of surfactant tension, in dilute solution, decreases by a factor of about 3 for each additional CH_2 group in the chain [S2].

If, upon addition of a surfactant, the interfacial tension between two liquids is reduced to a sufficiently low value, emulsification will readily take place (see below). This arises because only a relatively small increase in surface energy is involved. If $\pi > \gamma_o$, in equation (1.24), either the liquids will become miscible or spontaneous emulsification will occur.

1.7.1 Formation of Emulsions in Oil Recovery

Emulsions are relatively stable suspensions of droplets of one liquid, in a second, immiscible, liquid. They are generally divided into two classifications: oil-in-water, and water-in-oil emulsions, depending upon the nature of the continuous phase (i.e. the suspending medium). Pure liquids cannot form emulsions and the addition of a stabilising, or emulsifying, agent (e.g. a surfactant) is required.

In oil-field situations, the most commonly encountered emulsion is a water-in-oil emulsion. The process of oil recovery causes these emulsions to form and while, in most cases, this is an undesirable situation, it is one which is deliberately introduced during tertiary oil recovery using surfactants (cf. Section 1.2.3.1). In all cases, the "breaking" of an emulsion, into its original components, is a necessary requirement, a process which can place great demand on economic resources.

Emulsions in Primary and Secondary Oil Recovery

The large pressure drops which occur during primary oil production cause the reservoir fluids to migrate at considerable velocities through the porous structure, providing ample opportunity for mixing and formation of small droplets. Such emulsions are stabilised by surface-active species, such as porphyrins, or long chain fatty acids and esters, which occur naturally in crude oil.

During secondary recovery processes, the addition of surfactants and polymer to a waterflood is common practice, the formation of emulsions here being almost inevitable. A consequence of this process, therefore, is that the selection of polymer and emulsifier must take into account the cost of the breaking of the emulsion at the producing well [J1].

In either primary or secondary processes, once emulsions have been produced and collected, techniques for breaking the emulsions and separating the oil from the other components must be employed. Most emulsions encountered during oil

recovery, as mentioned earlier, are water-in-oil and can range anywhere from 0.5 to 40% water. Many of these are only temporarily stable and can be resolved simply by allowing the fluids to stand until the components separate. This can be time-consuming, although the process can be speeded up by heating, to both reduce the viscosity of the oil and to lessen the effectiveness of naturally occurring emulsifiers. Additionally, centrifugation may be employed [W4].

Emulsions in Tertiary Oil Recovery

Microemulsions [S9,P5] are apparently homogeneous mixtures of oil and water which form spontaneously. They are thermodynamically stable and contain such small particles that turbidity is low. Spontaneous formation of an emulsion, with the associated decrease in free energy, can only be achieved if the remaining liquid-liquid interfacial free energy can be compensated by the entropy of dispersion of the droplets in the medium. While surfactants do lower interfacial tensions, in most cases the cmc or the limit of solubility is reached before the interfacial tension is reduce to a low enough value (ca. 10^{-3}mN m^{-1}) for spontaneous emulsification to occur. The addition of a second surface-active species (a co-surfactant), of a completely different nature to the first, helps to reduce the interfacial tension to an ultralow value.

Consideration of the Gibbs equation (1.3) for a two-component system can be used to illustrate the effectiveness that the addition of co-surfactant can have on the interfacial tension

between two liquids. For a two-component system, the change in interfacial tension, $d\gamma$, can be related to the interfacial excess concentration, Γ_i, and change in chemical potential through:

$$d\gamma = - (\Gamma_1 . d\mu_1 + \Gamma_2 . d\mu_2), \qquad (1.25)$$

where, μ_i = chemical potential of species i,

which shows that the addition of a co-surfactant (which is positively adsorbed at the interface) to a system will always produce a further lowering of γ. It might be noted that, in some cases, certain single surfactants will lower γ far enough for microemulsion formation to occur, for example the surfactant AOT (sodium diethylhexylsulphosuccinate [A3]). However, it is usual practice to add a co-surfactant to a system in order to achieve the ultralow interfacial tension values desired.

Microemulsions in Tertiary Oil Recovery [B6]

The technique of surfactant flooding to recover residual oil in a well has been mentioned earlier (Section 1.2.3.1). As discussed, the mechanism by which oil is recovered using this technique is the reduction of the oil-water interfacial tension to an ultralow value (ca. 10^{-3} mN m^{-1}). Reduction of the interfacial tension to such levels causes spontaneous emulsification to take place, with the consequent formation of a microemulsion occurring. The purpose of forming a micro-emulsion system in the reservoir is to enable the residual oil to be removed from within the sandstone pores, and to

allow the recovered oil to be pushed through the capillary structure, without being hampered by the pressure drop at a curved oil-water interface with a normal interfacial tension. The process is not simple, being complicated by the reservoir temperature, salt concentration, and loss of surfactant by adsorption and precipitation in the well. The loss of surfactant by adsorption is thought to take place at the clay-water interface, and the consequence of its loss is a reduction in the surfactant-solution concentration and subsequent loss of the ultralow interfacial tension condition.

1.8 Present Work

The aim of this present work is to study the effects of solution conditions (ionic strength, pH, added alcohol) on the loss of sodium dodecylbenzene sulphonate onto North Sea reservoir materials - Clashach sandstone, and kaolin clay. The results from the study are to be utilised in a model system of sodium dodecylbenzene sulphonate, sodium chloride, n-butanol and n-decane, designed for phase stability studies at Winfrith AEE [L1].

In order to properly study the adsorption of sodium dodecylbenzene sulphonate onto solid surfaces, specially prepared, isomerically pure surfactants (1-phenyl, 4-phenyl, 6-phenyl isomers; n-ϕ-C_{12} ABS, where n = 1, 4 or 6) have been employed.

Adsorption measurements, comparing the behaviour of these isomers, together with that of cetyltrimethylammonium bromide (CTAB), have been made at the air-liquid interface.

From these measurements the 4-ϕ-C_{12} ABS isomer was selected as the anionic surfactant most suited to the present investigation (see discussion) and using this pure isomer subsequent adsorption studies have been made at both liquid-liquid (n-decane-aqueous), and solid-liquid (kaolin, silica - aqueous), interfaces. Measurements of adsorption at these interfaces have been supported by distribution studies of the surfactant between organic and aqueous phases and those measurements at the solid-liquid interface have additionally been supported by microelectrophoretic studies.

In addition to these surfactant adsorption, and distribution, studies, consideration has been made of interactions between the anionic surfactant and aluminium ions in solution, and of the dissolution of kaolin under varying conditions.

Chapter Two

Experimental

2.1 Minerals

Clashach sandstone: was supplied by Winfrith Petroleum Technology, Winfrith AEE, Dorset, D12 8DH. It was in the form of crushed particles with a size distribution of 300-355 μm diameter. The specific surface area of the material, as determined by nitrogen adsorption and BET analysis, was 2.0 $m^2\ g^{-1}$.

Silica: was obtained from two sources:

(i) BDH (Poole, Dorset) - as precipitated silica. This was found to have a specific surface area of 180 $m^2\ g^{-1}$ (N_2 adsorption, BET analysis). Nitrogen-desorption measurements showed the material to be essentially non-porous (see Section 2.4.1).

(ii) Crosfield Chemicals (Warrington) - as micronised Gasil-35. This sample had a specific surface area of 300 $m^2\ g^{-1}$ and a most abundant pore size of 83 Å, as specified by the supplier (N_2 adsorption-desorption and BET analysis).

Kaolin: was purchased from the Aldrich Chemical Company and specified to be ∿ 95% kaolinite ($Al_2Si_2O_5(OH)_4$). Nitrogen adsorption-desorption measurements showed this material to be non-porous, having a specific surface area of 8.27 $m^2\ g^{-1}$ (see Section 2.4.1).

2.2 Chemicals

2.2.1 General reagents

Sodium chloride, sodium hydroxide, hydrochloric acid (S.G. 1.18) and fuming sulphuric acid (30% SO_3) were obtained from BDH (Poole, Dorset) as "Analar" grade materials.

n-Butanol was obtained as an "Analar" reagent from BDH, gas chromatography showed this to be > 99% n-butanol.

Potassium hydroxide and potassium permanganate, also from BDH, were of "Analar" grade.

Potassium dichromate and concentrated sulphuric acid (S.G. 1.84) for the preparation of chromic acid cleansing solution were purchased from BDH as "Analar" grade materials.

2.2.2 Reagents used for the Preparation of Surfactants

The hydrocarbon, dodecylbenzene used as a starting material for the preparation of a "general" sodium dodecylbenzene-sulphonate was purchased from Ventron Chemicals (Germany) and specified to be C_{12}. Analysis by gas chromatography showed the dodecylbenzene to contain a mixture of chain-lengths i.e. 40% C_{11}, 29% C_{12}, 7.9% C_{13}, with < C_{10} and > C_{14} making up the remainder.

Reagents for the preparation of the isomerically pure samples of sodium dodecylbenzenesulphonate were obtained from the Aldrich Chemical Company (Gillingham, Dorset):

n-Butyrophenone and n-Bromooctane were found to be 99.9% and

99.68% pure by gas chromatography.

Magnesium turnings were 98% magnesium.

Copper sulphate and potassium sulphate were "Analar" grade reagents.

Palladium on activated carbon: Palladium content, 5% and from the Radiochemical Centre, Amersham:

Radioactive sulphur-3S. This was supplied as an aqueous solution of sodium sulphate (S-35) in 185 MBq (525 MBq/mmol) amounts.

The cationic surfactant cetyltrimethylammonium bromide (CTAB) was purchased from BDH (Poole, Dorset) as the "Analar" grade.

2.2.3 Reagents for Two-Phase Titration

These were obtained from BDH:

Chloroform was of "Analar" grade.

Sodium dodecylsulphate was a "specially purified" material. Analysis showed this to be 98.8% sodium dodecylsulphate (see Section 2.4.5).

Hyamine 1622 (benzethonium chloride) was supplied as a 0.004 mol dm^{-3} aqueous solution. This was standardised against sodium dodecylsulphate before use.

The mixed indicator solution of Dimidium Bromide-Disulphine Blue VN was obtained as a concentrated solution which was diluted for use in the titration (Section 2.4.5).

2.2.4 Reagents for Atomic Absorption Spectroscopy

Aluminium nitrate, "Spectrosol" grade, was obtained from BDH as a 1000 ppm (37.1 mmol dm^{-3}) solution in 0.5 mol dm^{-3} HNO_3.

A 100 ppm working solution was prepared by appropriate dilution.

A stock 10% (w/v) solution of potassium chloride "Analar" (BDH) was prepared for experiments.

2.2.5 Other Reagents

Scintillation cocktail, NE260, was purchased from Nuclear Enterprises. This is xylene based and contains 2,5-diphenyl oxazole (PPO) as the scintillant.

Water was doubly distilled from alkaline potassium permanganate (0.05 mol dm^{-3}) at pH 12.5 (using KOH), under an atmosphere of nitrogen, through a 2 m vertical glass column packed with glass. The conductivity of the water collected was 20 $\mu S\ cm^{-1}$ at 25°C, and its surface tension was 71.8 ± 0.2 mN m^{-1} with a pH of 6.95 ± 0.01.

Nitrogen gas: BOC white spot grade.

C-14 labelled n-butanol: This was obtained from Sigma Radiochemicals. It has a specific activity of 1.92×10^8 Bq/mmol.

2.3 Synthesis of Surfactants

2.3.1 Preparation of Radiolabelled Sodium Dodecylbenzenesulphonate (^{35}S)

The preparation of radiolabelled alkylbenzenesulphonate (^{35}S) required the ^{35}S label to be in the form of sulphur trioxide ($^{35}SO_3$) [J4].

Radioactive sodium sulphate (^{35}S) (525 MBq/mmol) was purchased as an aqueous solution (5 cm^3) and carefully taken to dryness in a heated Pyrex tube. The dried salt was then dissolved in 2.4 cm^3 of 30% fuming H_2SO_4 so that the $^{35}SO_4^{2-}$ would exchange with the SO_3. This was ice-cooled and added, dropwise, to 2.9 cm^3 of ice-cooled dodecylbenzene with vigorous stirring, the system being all-enclosed to prevent escape of radioactive $^{35}SO_3$ fumes. Upon complete addition the solution was warmed to 40°C and the temperature maintained for 1 hour. After the mixture had cooled to room temperature it was transferred to a beaker with 4 cm^3 of distilled water and 30 cm^3 of 95% ethanol before being neutralised to pH 7 with drops of a 40% aqueous NaOH solution (with cooling). The neutralised solution was left to stand overnight, to allow sodium sulphate to settle out, after which it was decanted through a filter and the filtrate taken to dryness under vacuum with repeated additions of absolute alcohol to prevent foaming. The residual solid was dissolved in dry chloroform, filtered, and again taken to dryness. The final product was recrystallised from absolute alcohol, dried, and stored over phosphorus pentoxide. The final product had a specific activity of

1.7 MBq per mmol as determined with a calibrated liquid scintillation counter and by weighing (see Section 2.4.4.4).

2.3.2 Preparation of Pure Isomers of Sodium Dodecylbenzenesulphonate

Pure isomers of sodium dodecylbenzenesulphonate surfactant were also prepared for the investigation. These have a C_{12} chain on which the position of the phenyl group is well-defined. The three isomers prepared have the phenyl group attached to position 1, 4 or 6, on the C_{12} chain and were designated as 1-phenyl, 4-phenyl, and 6-phenyl alkylbenzene-sulphonate (ABS). All of the surfactants were synthesised by the same general route and details are given below for the 4-phenyl ABS isomer to illustrate the general procedure.

The isomer, 4-phenyl ABS, was prepared as outlined in the sequence given in Figure 7 [D4]. The synthesis began with a Grignard reaction between n-butyrophenone (1) and octyl-magnesium bromide (2) which afforded the carbinol (3). The alcohol (3) was dehydrated over $CuSo_4/K_2SO_4$ at 180°C to yield an isomeric mixture of 4-phenyl-dodec-3-ene and 4-phenyl-dodec-4-ene (see Figures 8 and 9)), all of which was reduced, with hydrogen, over a carbon-supported palladium catalyst to the hydrocarbon 4-phenyldodecane (4) (Figure 10).

The aromatic hydrocarbon (4) was sulphonated at 70°C with 30% fuming H_2SO_4 (1:1 w/v hydrocarbon) for one hour to yield the sulphonic acid (5) . Upon complete sulphonation water (14% w/v) based on the alkylate) was added to the hot acid mixture

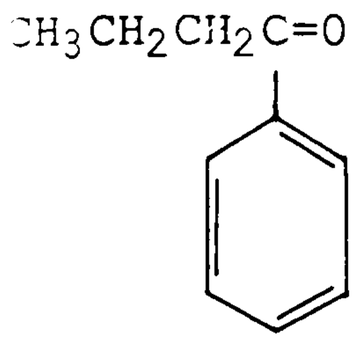

Butyrophenone

(1)

+ $CH_3(CH_2)_7MgBr$ ⟶

Octylmagnesium bromide

(2)

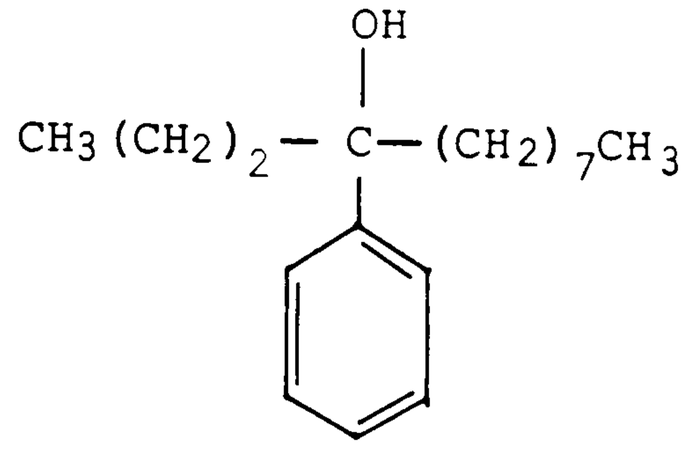

3^0 Carbinol

(3)

Dehydration

Anhyd. $CuSO_4$, K_2SO_4

~180°C

⟶

Olefins mixture

(Fig. 8)

Hydrogenation

Pd/C in EtOH

⟶

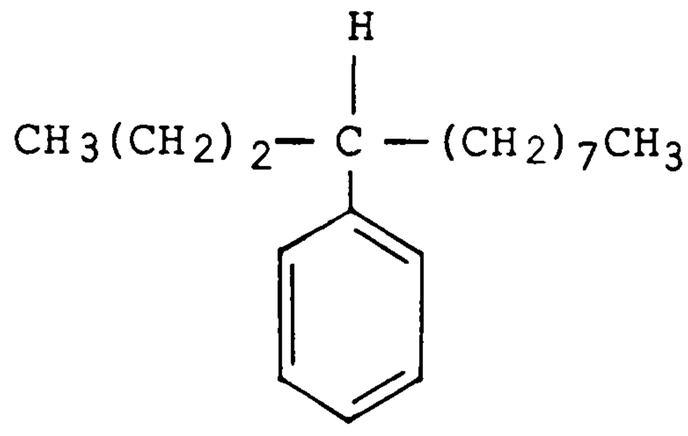

4-Dodecylbenzene

(4)

Sulphonation

Oleum (30% SO_3)

⟶

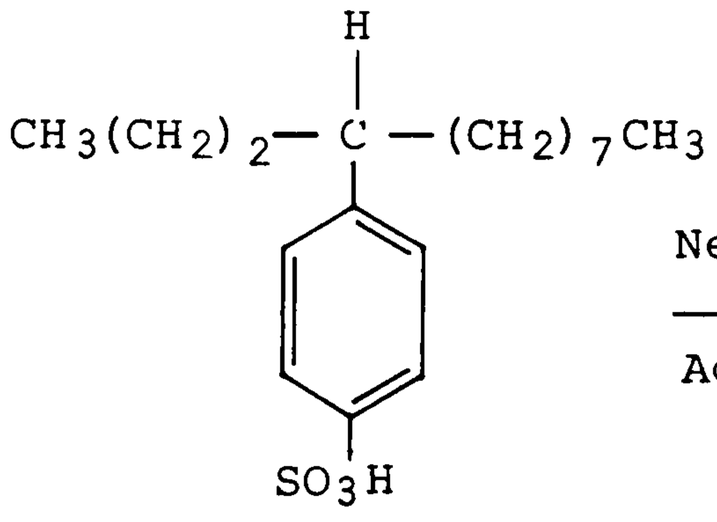

Major Product

Neutralisation

Aq. NaOH (10%)

⟶

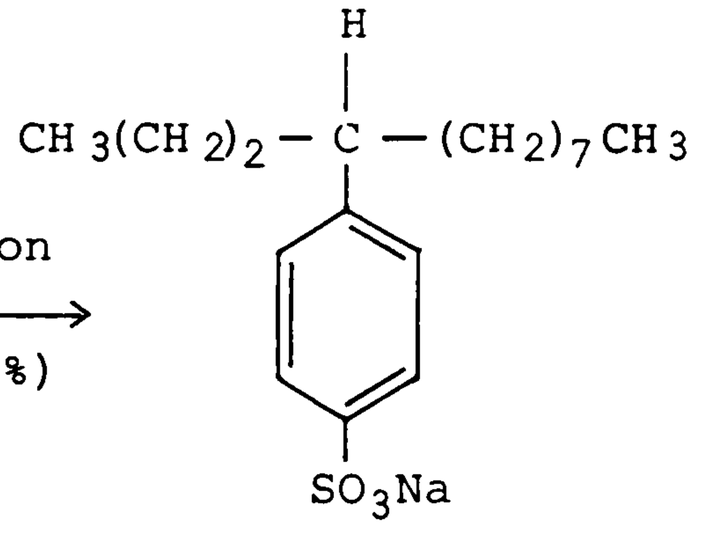

Sodium p-1-propylnonyl benzene sulphonate

(5)

Figure 7 : Preparation of isomerically pure 4-ϕ-C_{12} ABS

Figure 8. Isomers of 4-phenyldecene.

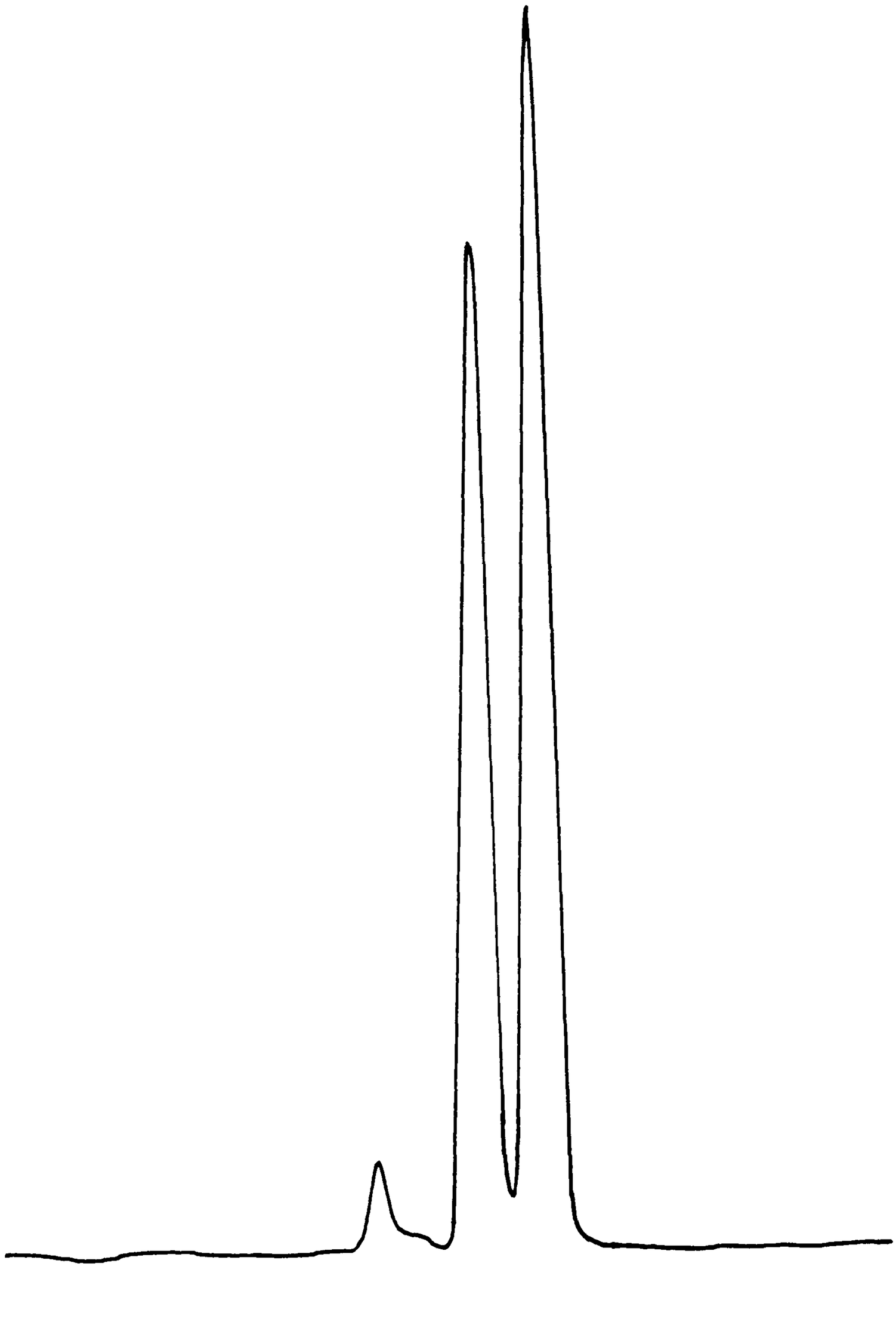

Figure 9: GC analysis of olefins mixture in preparation of 4-ϕ-C_{12} ABS.

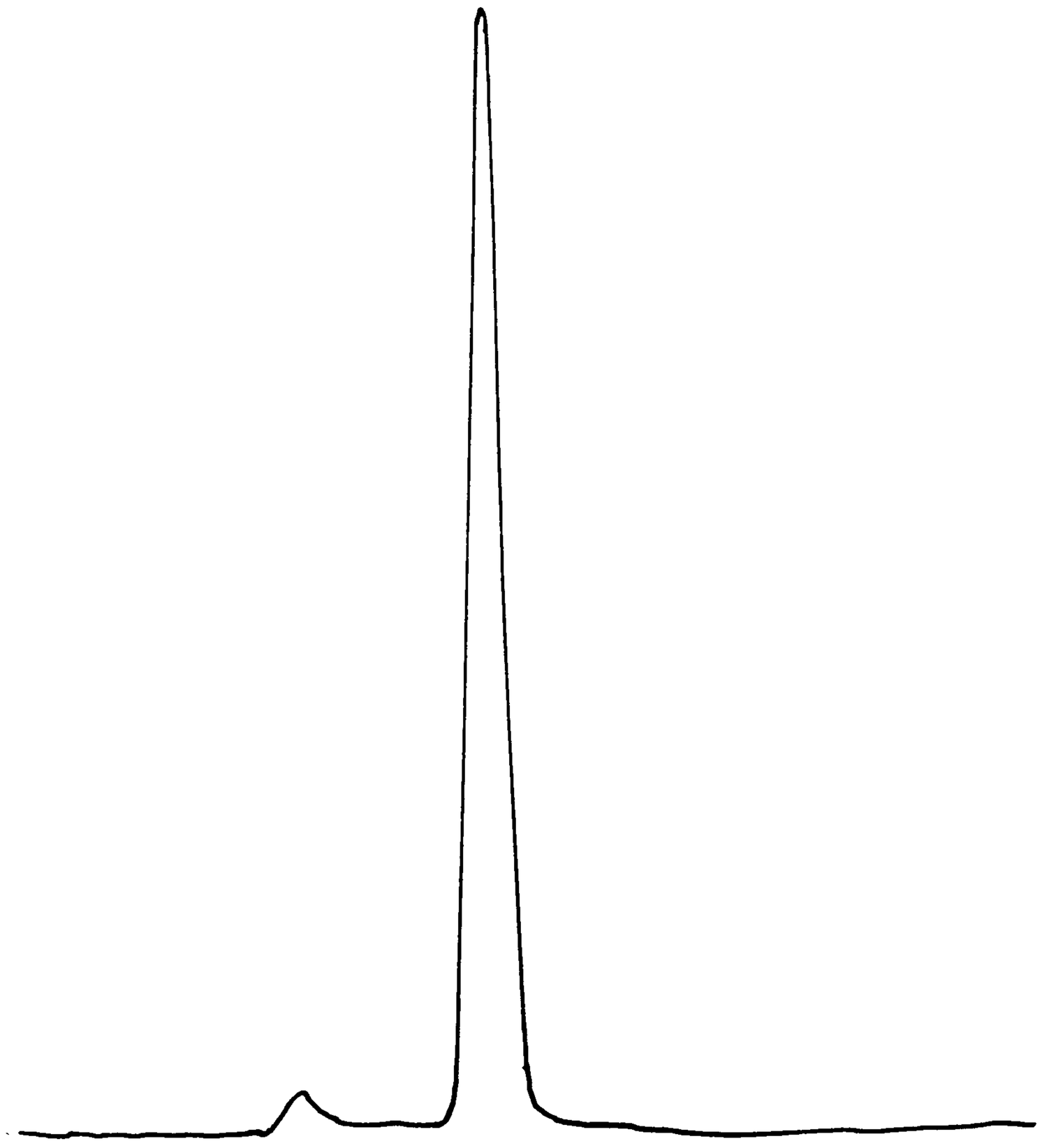

Figure 10: GC analysis of 4-phenyldodecane in preparation of 4-ϕ-C_{12} ABS.

the whole transferred to a separating funnel and allowed to separate into an upper organic, sulphonic acid, layer and a lower aqueous layer. After separation the lower aqueous layer, containing unreacted H_2SO_4, was run-off and the sulphonic acid (5) neutralised to pH 8, with 10% NaOH. The final product, sodium p-[1-propylnonyl]benzenesulphonate (6) was obtained after freeze-drying and recrystallisation from acetone, as a white hygroscopic powder. The overall yield, based on the ketone (1) was 23%.

Analysis of the product by two-phase titration with Hyamine 1622 (Section 2.4.5.3) showed it to be 97.4% anionic-active detergent, with a sulphate content of < 1% as determined by titration with lead nitrate (Section 2.4.5).

In the synthesis of the respective 1-phenyl and 6-phenyl ABS isomers the ketones, benzaldehyde and hexanophenone, together with the Grignard reagents, undecylmagnesium bromide and hexylmagnesium bromide, were employed.

The physical properties of the pure single isomer surfactants were found to differ markedly from those containing isomer mixtures, these depending on the position of the phenyl group on the C-12 chain. The 1-phenyl isomer was obtained as white crystals which were only sparingly soluble in water up to about 60°C. The 6-phenyl isomer was found to be very hygroscopic and some difficulty was experienced in keeping this product completely dry. The 4-phenyl isomer was therefore chosen for most of the subsequent adsorption studies as this offered a balance between the two extremes of solubility. It

was thus prepared several times during the project, each time being checked for purity (infra-red, nmr, and anionic-active content).

2.4 Experimental Procedures

2.4.1 Surface Area Determinations

The surface areas of samples of kaolin, sand and silica (BDH) have been determined by nitrogen adsorption and BET analysis.

Apparatus

A Micrometrics Instrument Corporation (Model 2100D Orr) "accusorb" physical adsorption analyser was used for the measurements.

A 15 cm^3 glass specimen bulb, supplied by Coulter Electronics Ltd. (part number 9961055), held the sample to be measured.

Computations of surface area were made using a DEC system 2060 mainframe computer (see Appendix A2 for program).

Sample Preparation

The gas adsorption apparatus is shown schematically in Figure 11. Approximately 100 mg of sample was accurately weighed (Ws) into one of four sample flasks (1-4), which was then transferred to the apparatus, and degassed under a vacuum of 0.07 N m^{-2} at room temperature overnight. The degassing was completed by raising the temperature of the sample to 573 K for an additional 12 hours while maintaining

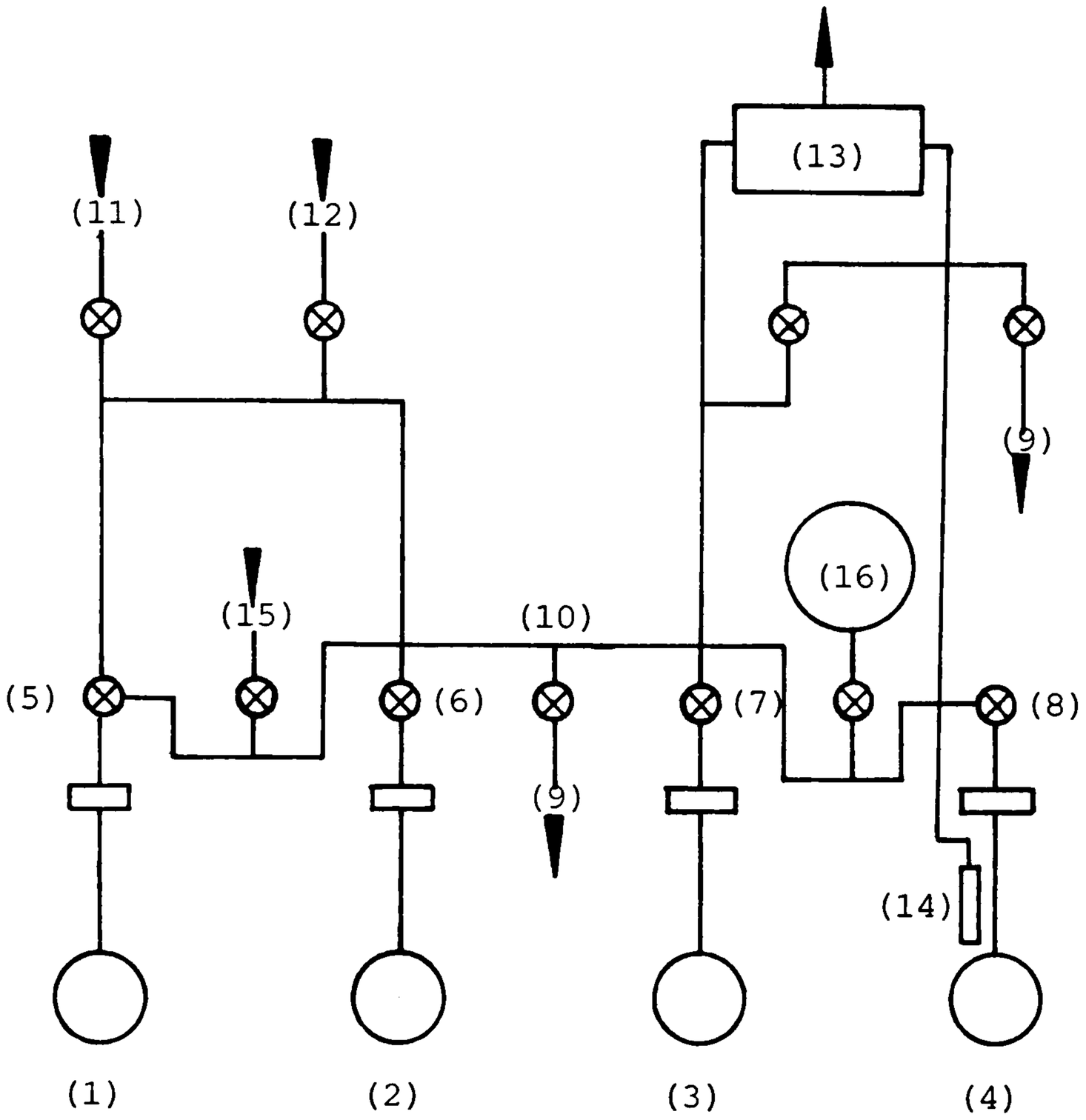

(1)-(4) Sample flasks

(5)-(8) Sample valves

(9) Vacuum line

(10) Manifold

(11)-(12) Adsorbate lines

(13) Pressure transducer

(14) Sorption pump

(15) Helium line

(16) Extra volume

Figure 11: Schematic diagram of the gas adsorption apparatus.

the vacuum. The sample was then tested for residual gas as follows:

The sample valves 5-8, and valve 9 to the vacuum line were closed (see Figure 11). After approximately 10 minutes the valve linking the sample flask to the manifold (10) was re-opened and any increase in the observed pressure was taken as an indication that degassing was not complete. If this was the case then the degassing procedure was repeated until complete. Once total degassing was achieved the heating mantle surrounding the sample flask was removed and the sample allowed to cool to room temperature.

Determination of the Adsorption Isotherm and Surface Area

The valves 11 and 12, leading to the adsorbate gas line (N_2), were closed off thus isolating the sample. The vacuum was then able to pump on both sides of the pressure transducer (13). After the transducer reading had stabilised, it was adjusted to zero. The sample flask and sorption pump (14) were then immersed in liquid nitrogen, the sorption pump acting as a reference by maintaining a constant vacuum to one side of the transducer.

It was important to determine the so-called "dead space" within the sample flask. Helium, which was found not to adsorb on the surface of any of the samplesat liquid nitrogen temperatures ($\sim$ 77 K), was used to determine this dead space as follows [M2]:

The helium line was opened (valve 15 in Figure 11) to give a

pressure in the manifold of approximately 66,660 N m^{-2}, the actual pressure (H_1) was accurately recorded on the transducer. Valve 15 was then closed before opening valve 11 so allowing access of the helium gas from the manifold to the sample flask (located in any one of ports 1-4). After equilibration (indicated by a steady reading at the transducer) the new combined manifold and sample pressure (H_2) was recorded. Valve 5 was then re-opened in order to pump helium from the apparatus. From these readings the dead-space of the system was determined (see computer program in Appendix A2).

Having reduced the pressure in the apparatus to zero on the transducer, the surface area determination could be made as follows:

With valve 1 closed nitrogen was introduced into the manifold, via operation of valve 11, giving a pressure of approximately 26,660 N m^{-2}. The actual pressure reading was noted (P_1) before opening valve 1, which allowed the gas to enter the sample flask. Upon equilibration, the new pressure reading (P_2) was recorded. Valve 1 was then closed and additional nitrogen gas introduced into the manifold to give a further pressure (P_3) in excess of P_1.

Valve 1 was again opened and a new resultant pressure recorded (P_4). This procedure was continued until the pressure in the manifold reached saturation. The saturation vapour pressure of nitrogen for a given temperature was determined from a plot of the vapour pressure of nitrogen versus temperature (Figure 12) [J3,Z2].

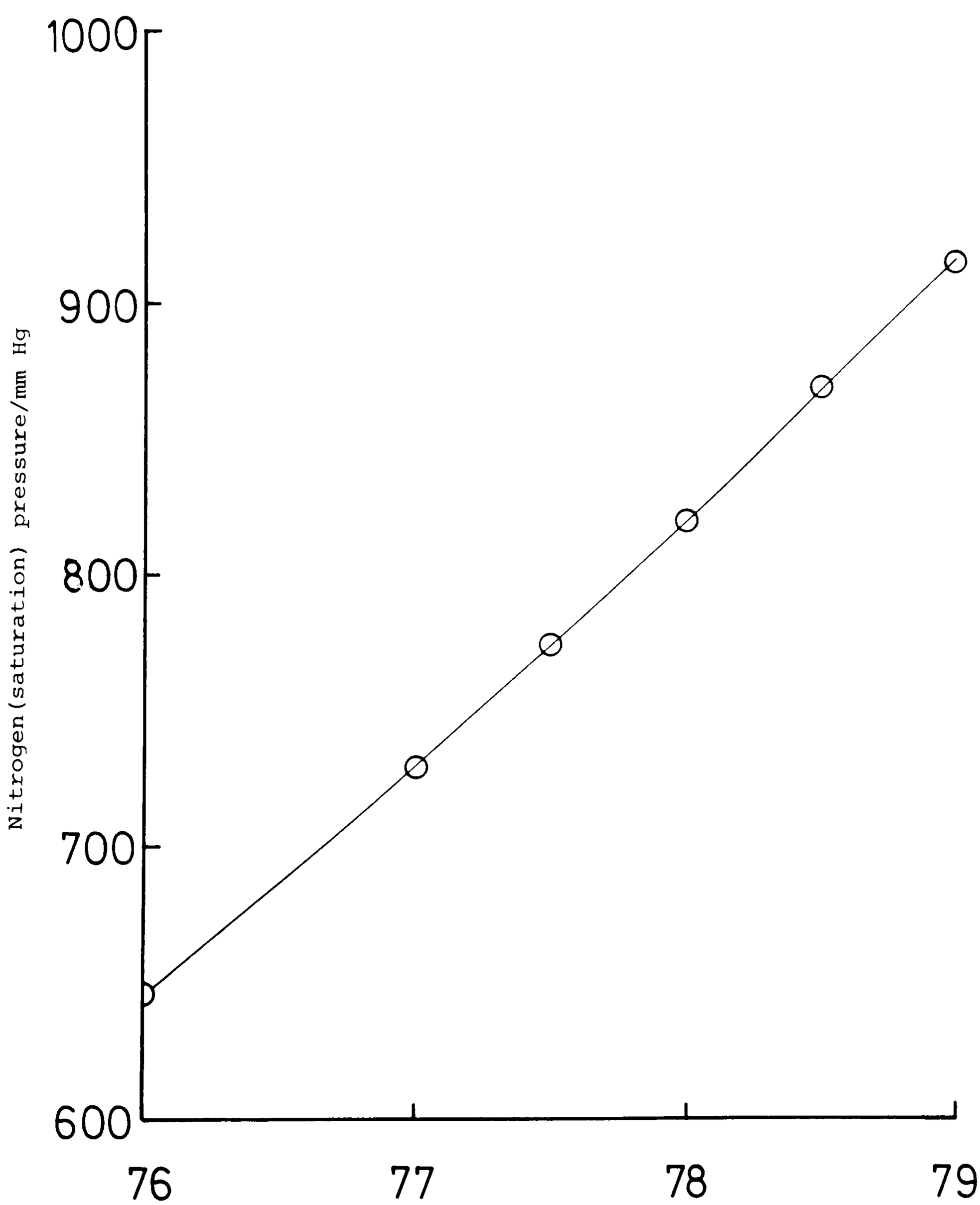

Figure 12: Nitrogen (Saturation) Vapour Pressure as a function of Absolute Temperature. Plotted from data obtained in references J3,Z2.

The desorption isotherms were obtained using the vacuum line to sequentially decrease the pressure in the manifold with respect to the sample flask. Thus, when valve 1 was opened there was an observed rise in the overall pressure of the system.

Nitrogen Adsorption-Desorption Isotherms

Nitrogen adsorption-desorption isotherms for silica and kaolin are shown in Figures 13 and 14 respectively. From these it can be seen that a slight hysteresis of the desorption isotherm is present. The magnitude of the hysteresis, however, indicates that no significant porous structure exists in these samples and the presence of hysteresis may be attributed to sample packing [G3]'.

From the adsorption data, for partial pressures between 0.05 and 0.35 (the region of BET analysis [G3]), the specific surface areas of the sample have been evaluated; silica was found to have a value of 180 $m^2\ g^{-1}$, and kaolin a value of 8.27 $m^2\ g^{-1}$, assuming an N_2 molecular area of 16.2 $Å^2$.

2.4.2 Scanning Electron Microscopy

Scanning electron micrographs of the kaolin, silica, and sand particles were prepared (Figures 15, 16, 17 respectively). The instrument used was a JEM-1200 EX scanning electron microscope. The particles of a specimen were disengaged into free particles by their dispersion into double distilled water followed by the immersion of this suspension in an ultrasonic bath for 30 minutes. The dried specimen was then attached to

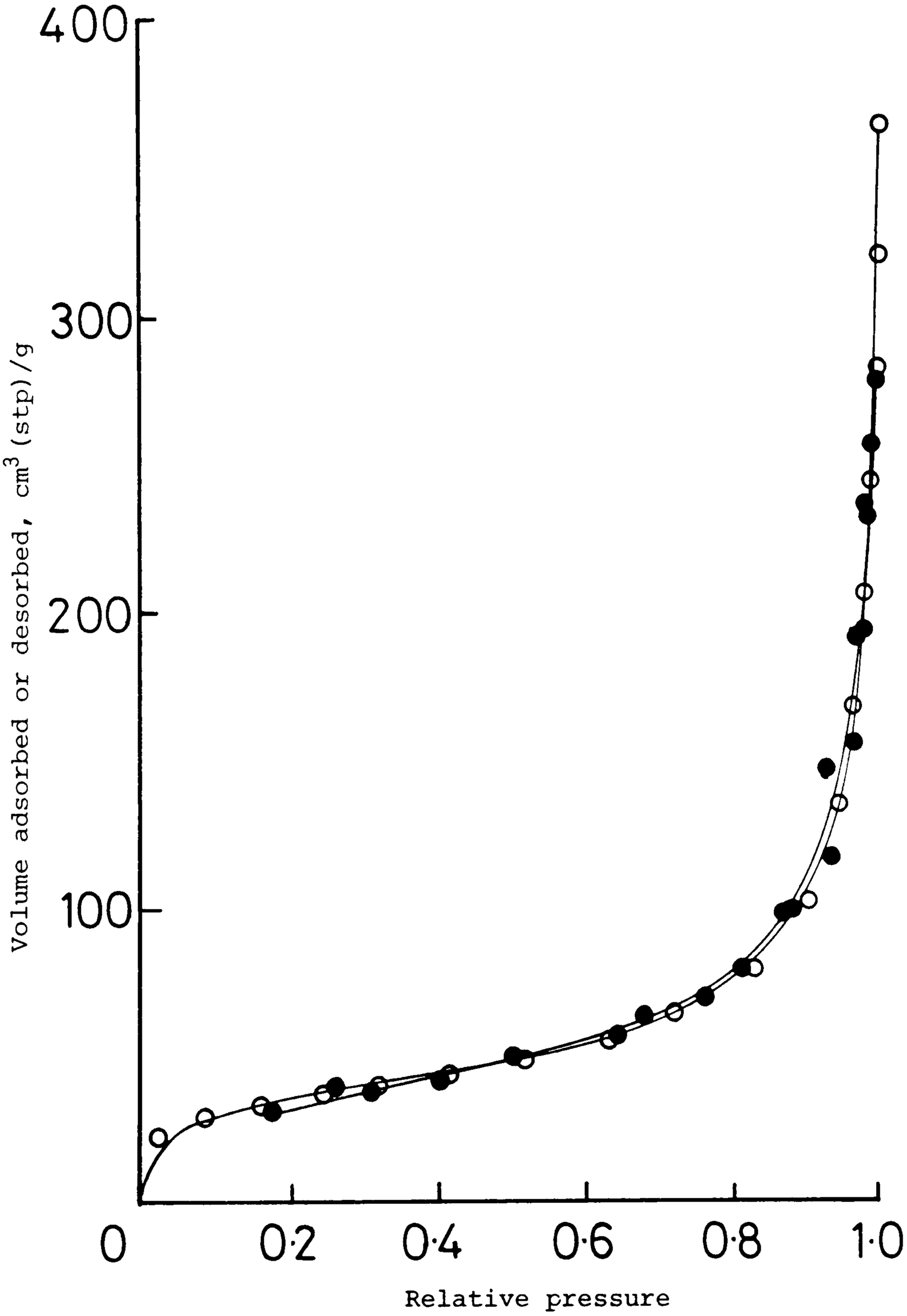

Figure 13: Adsorption (O)-Desorption (●) Isotherm for N_2 on silica (BDH) at 77.4 K.

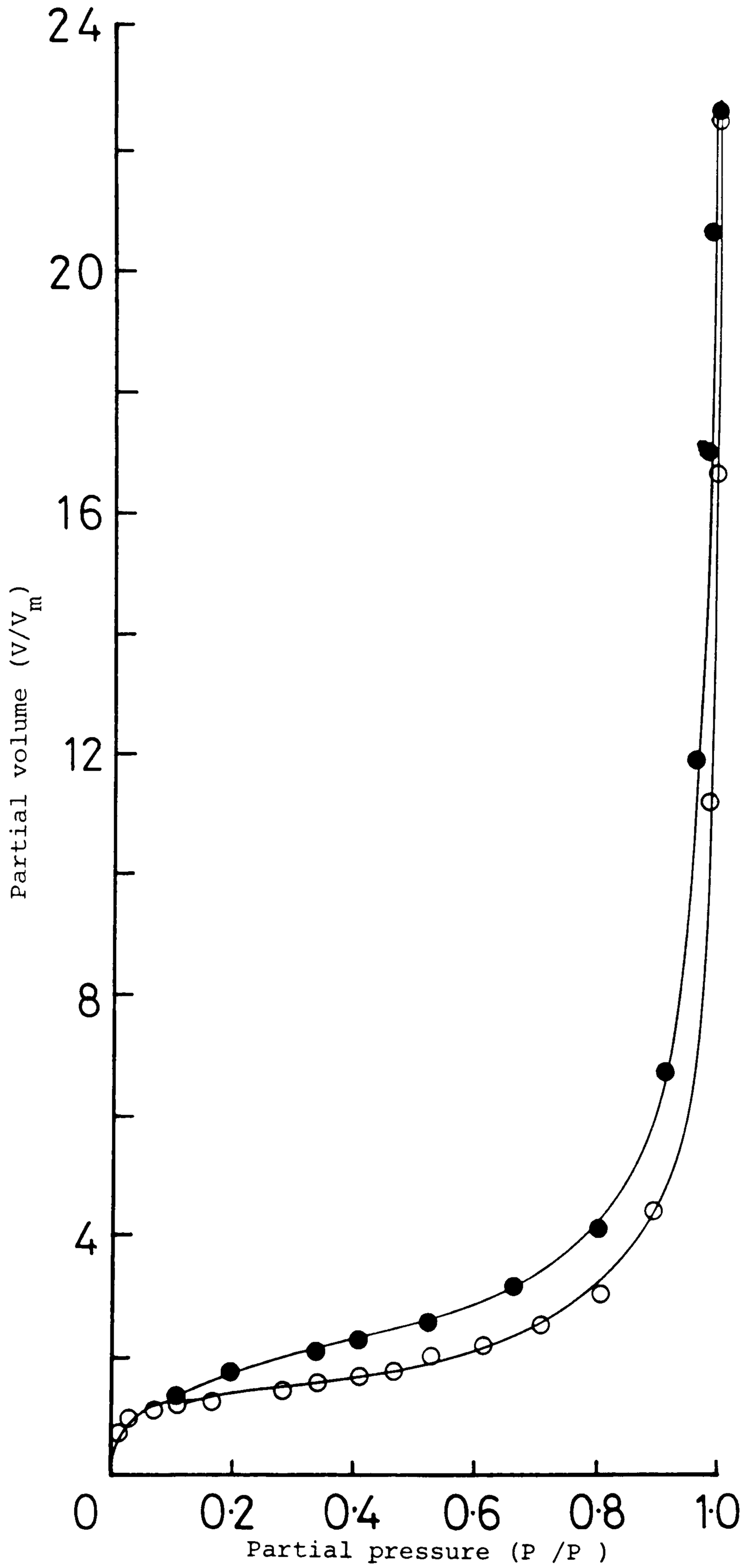

Figure 14: Adsorption (O)-desorption (●) isotherm for N_2 on kaolin at 77.7 K.

Figure 15: Scanning electron micrograph of kaolin particles.

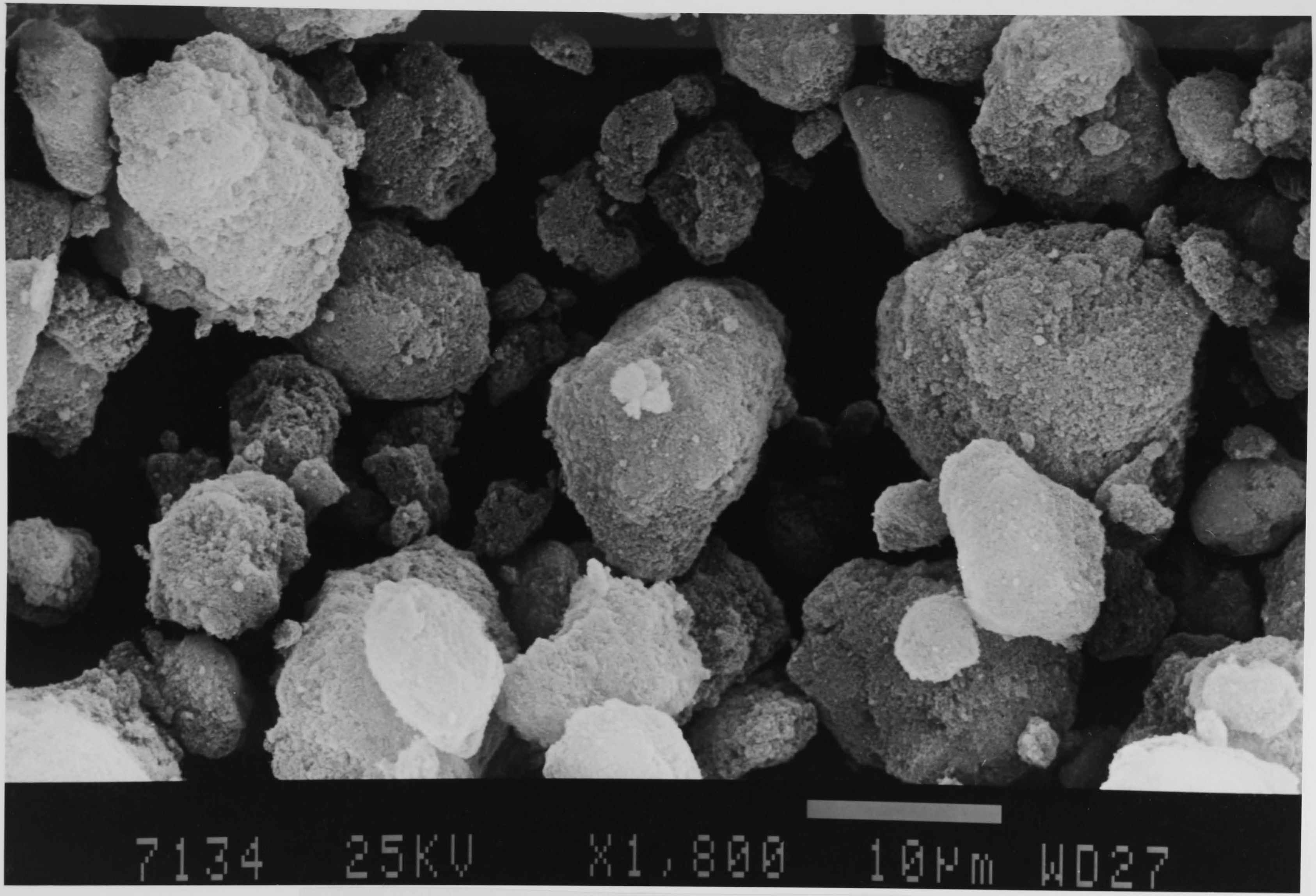

Figure 16: Scanning electron micrograph of silica particles.

Figure 17: Scanning electron micrograph of sandstone particles.

a brass support using silver (Dag) glue, and sputter-coated with gold by means of a Polaron SEM coating unit E5000.

2.4.3 Analysis of Alkylbenzenesulphonates

2.4.3.1 Infrared Spectroscopy

Infrared spectra of samples were obtained by IR transmittance spectroscopy using either a Perkin Elmer 598 I.R. spectrophotometer, with 3600 data station, or a Nicolet Digital FTS-IMX Fourier transform spectrometer.

Solid samples were prepared by grinding with dry KBr. This mixture was then pressed to form a transparent disc which was then mounted into the apparatus. This sample preparation is commonly used and is well documented in many standard texts (for example, B7). Liquid samples were prepared by compressing one drop between NaCl discs.

Spectra

The infrared spectrum of the 4-phenyldodecane hydrocarbon is shown in Figure 18. Spectra of the pure isomeric surfactants, 1-phenyl, 4-phenyl and 6-phenyl ABS are shown in Figures 19-21 respectively. Assignment of the absorption peaks is made in Table 2.

The most apparent difference between the hydrocarbon spectrum and that of the surfactant spectra is the presence of a very strong absorption at about 1180 cm^{-1} assigned the assymmetric stretching frequency of the S-O group in the sulphonated material. Comparison of this peak between the

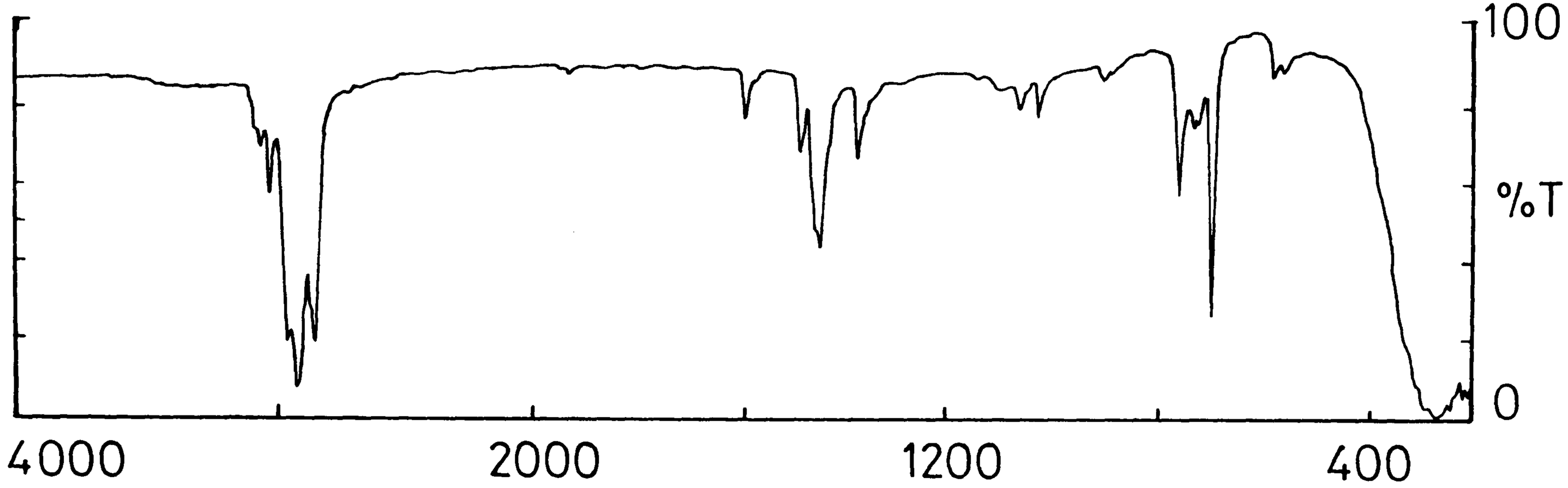

Figure 18: Infrared spectrum of 4-ϕ-dodecane.

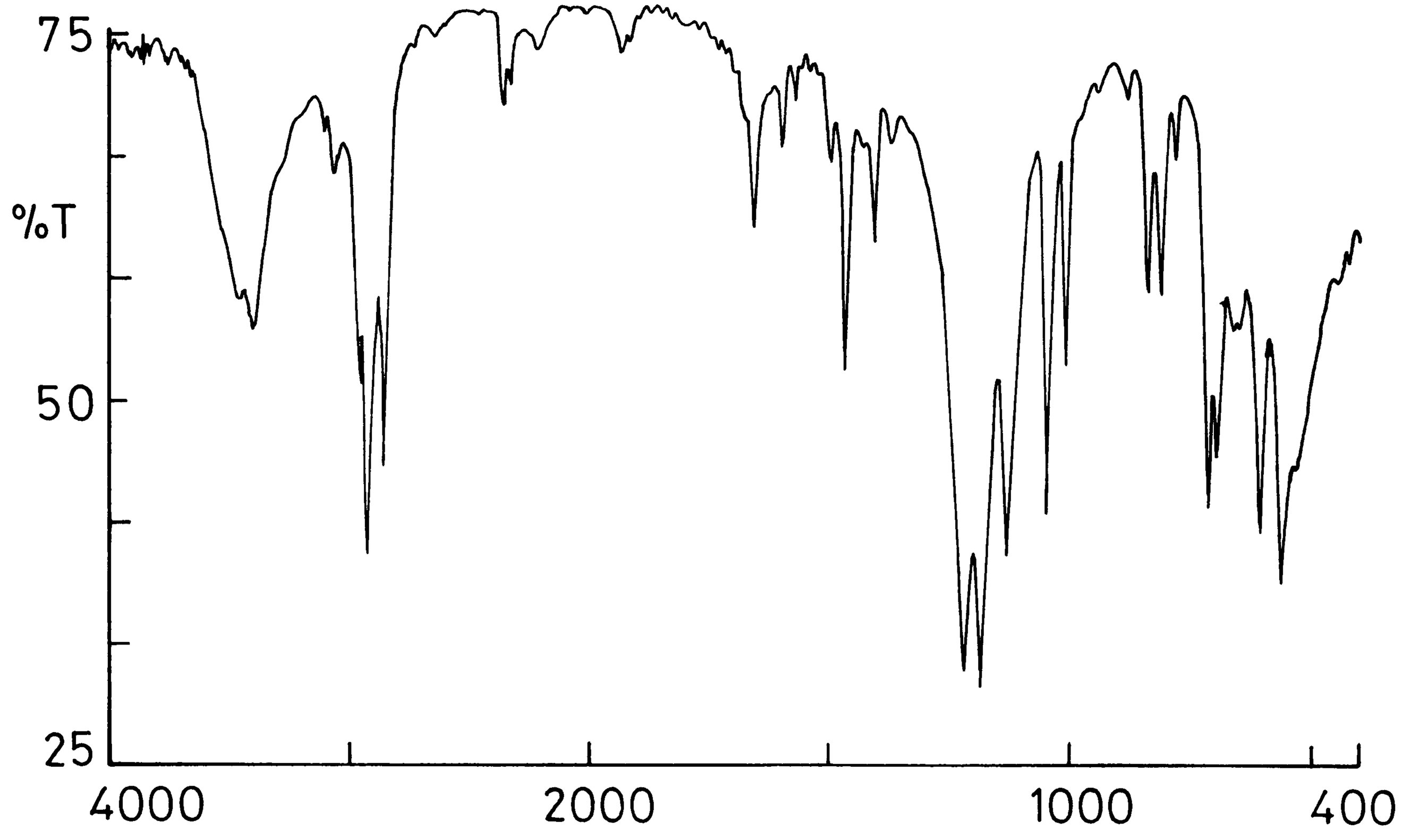

Figure 19: Infrared spectrum of 1-ϕ-C_{12} ABS.

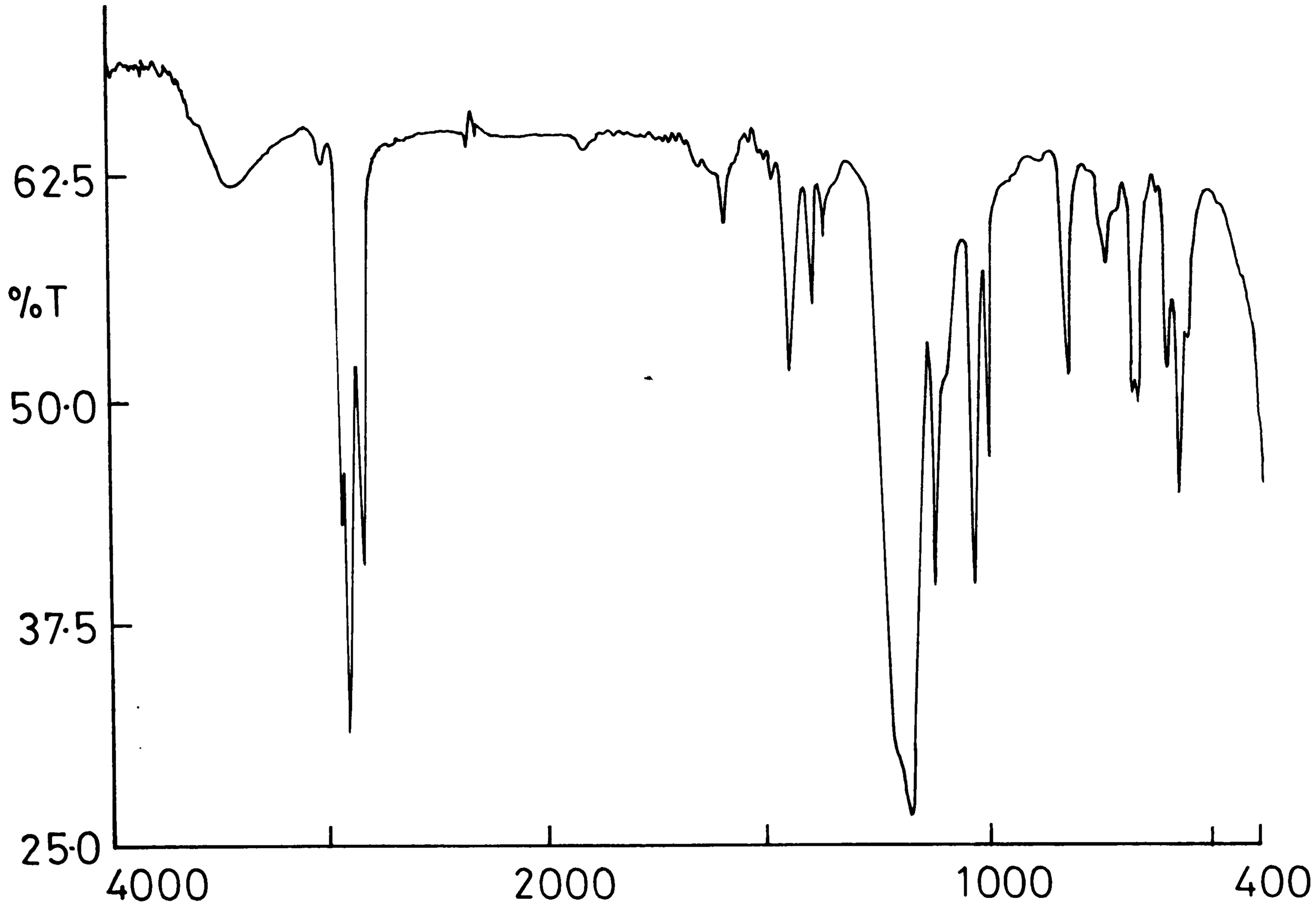

Figure 20: Infrared spectrum of 4-ϕ-C_{12} ABS.

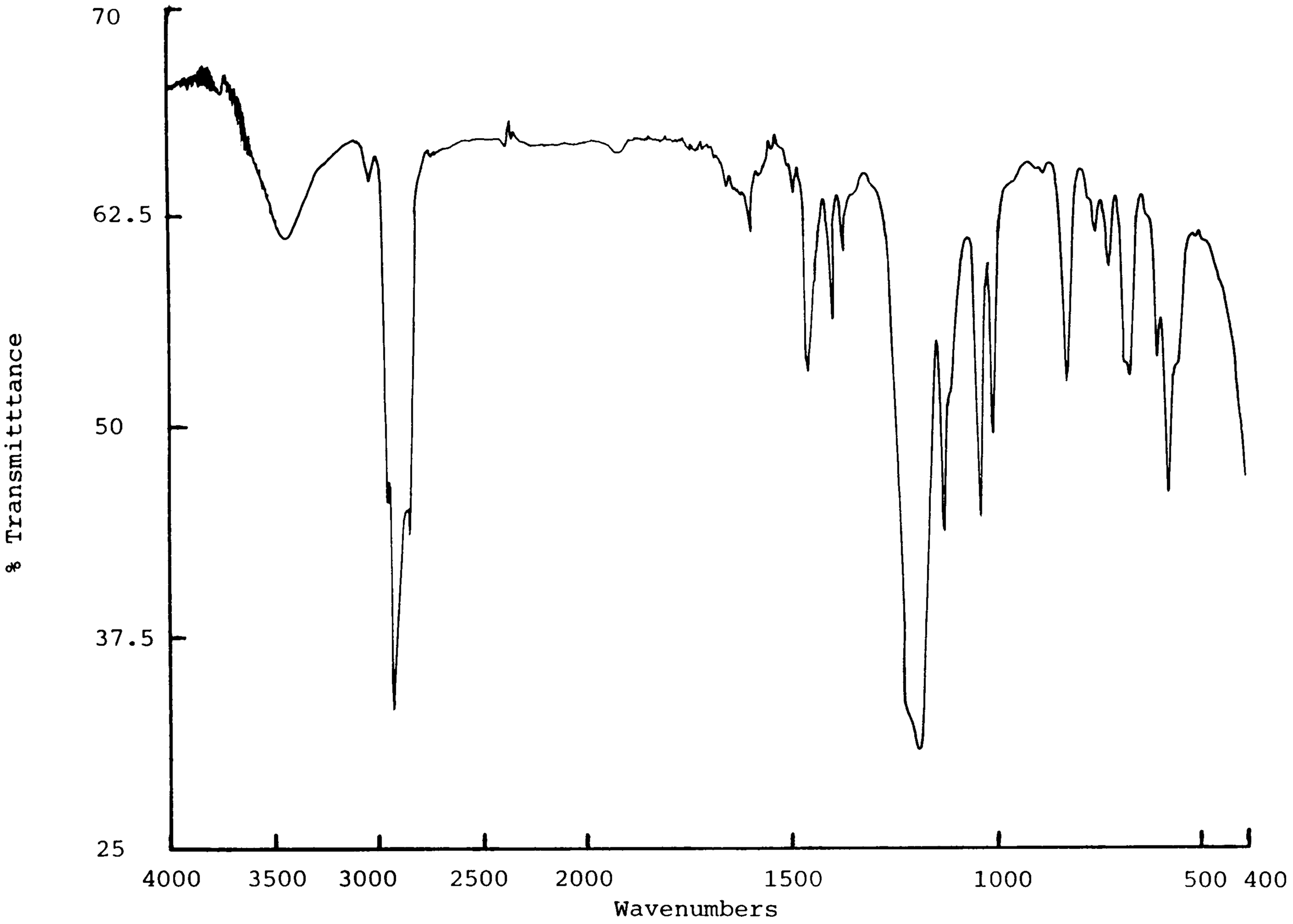

Figure 21: Infrared spectrum of 6-ϕ-C_{12} ABS.

Table 2. Main Absorption Peaks in the Infrared Spectra of the 1-, 4- and 6-ϕ-Surfactants (KBr Disc)

Wave Number cm^{-1}	Assignment [S8]
3700-3100	O-H stretch (damp disc)
3050	C-H aromatic stretch
2990-2740	C-H stretch
1900-1660	Combination bonds
1580	C⋯C aromatic ring stretch
1460	CH_2 bend
1400	CH_3 deformation mode
1370	CH_3 bend
1180	Asymmetric S-O stretch
1115	C-H aromatic bend
1040	Symmetric 2-O stretch
1010	C-H aromatic bend
845	C-H(p) o.o.p. deformation mode
680	$(CH_2)_{4+}$

surfactants shows that for the 1-phenyl isomer this is split into two, probably due to more effective packing of these molecules as compared to the tetrahedral carbon materials.

Further analysis of the spectra reveals an absorption peak at 680 cm^{-1} in the infrared spectra of both the 4-phenyl and 6-phenyl isomers (Figures 19 and 20 respectively). This absorbance has shifted to 700 cm^{-1} in the 1-phenyl ABS spectrum, possibly due to packing (Figure 19).

2.4.3.2 Nuclear Magnetic Resonance Spectroscopy (nmr)

Nuclear magnetic resonance spectra of the surfactants were run to assess the purity of the prepared samples.

A Jeol JNM GX27 ft nmr spectrometer (270 MHz ^{1}H, 67.8 MHz ^{13}C) was used to obtain the spectra, all of which were run in CD_3Cl.

Figures 22-24 show the resultant spectra, comparing the commercial material (Figure 22) to that of the pure materials (Figures 23 and 24), showing the purity of the latter. Note, the 1-ϕ-C_{12} ABS was not sufficiently soluble to yield an nmr spectrum.

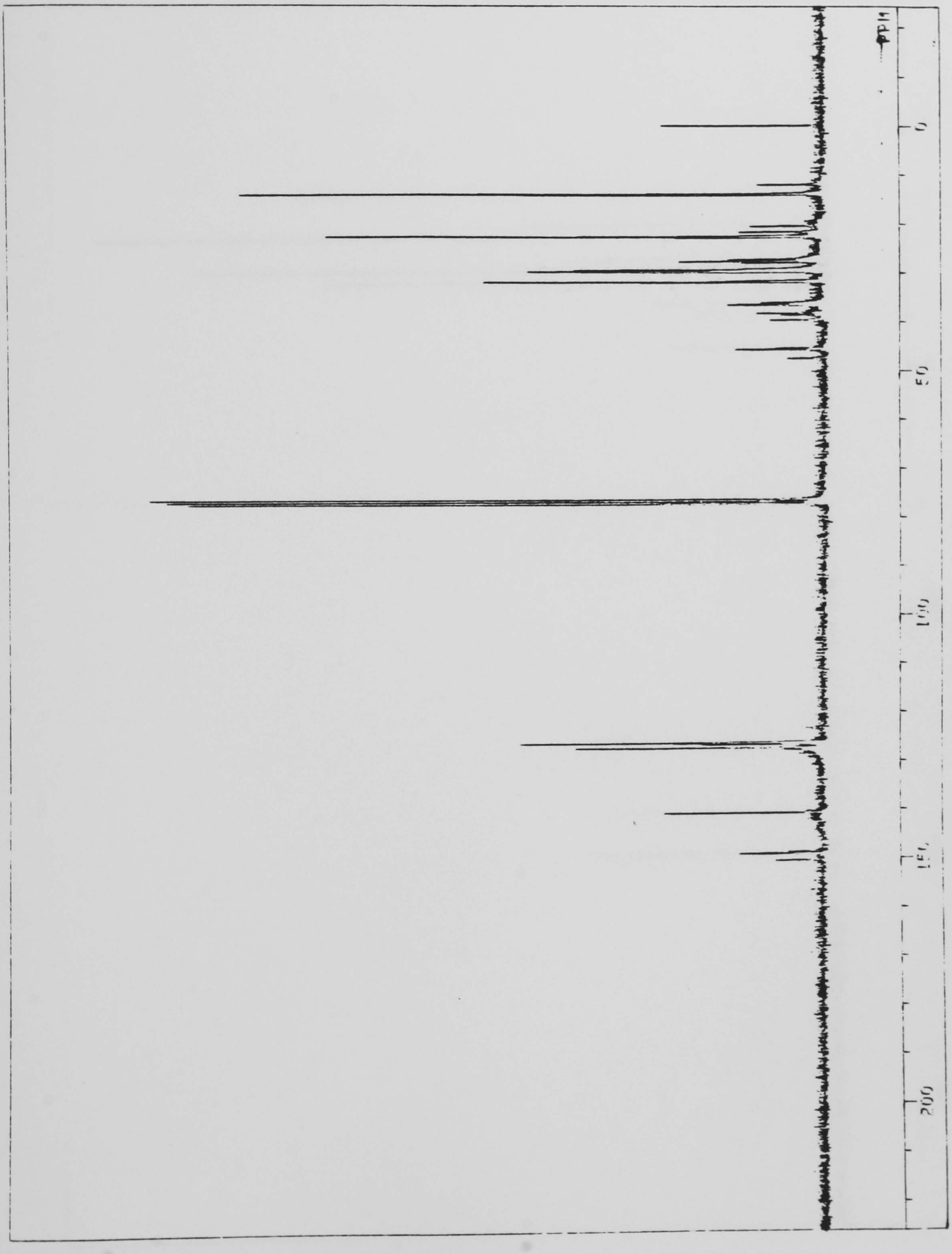

Figure 22: C-13 nmr of Commercial SDBS

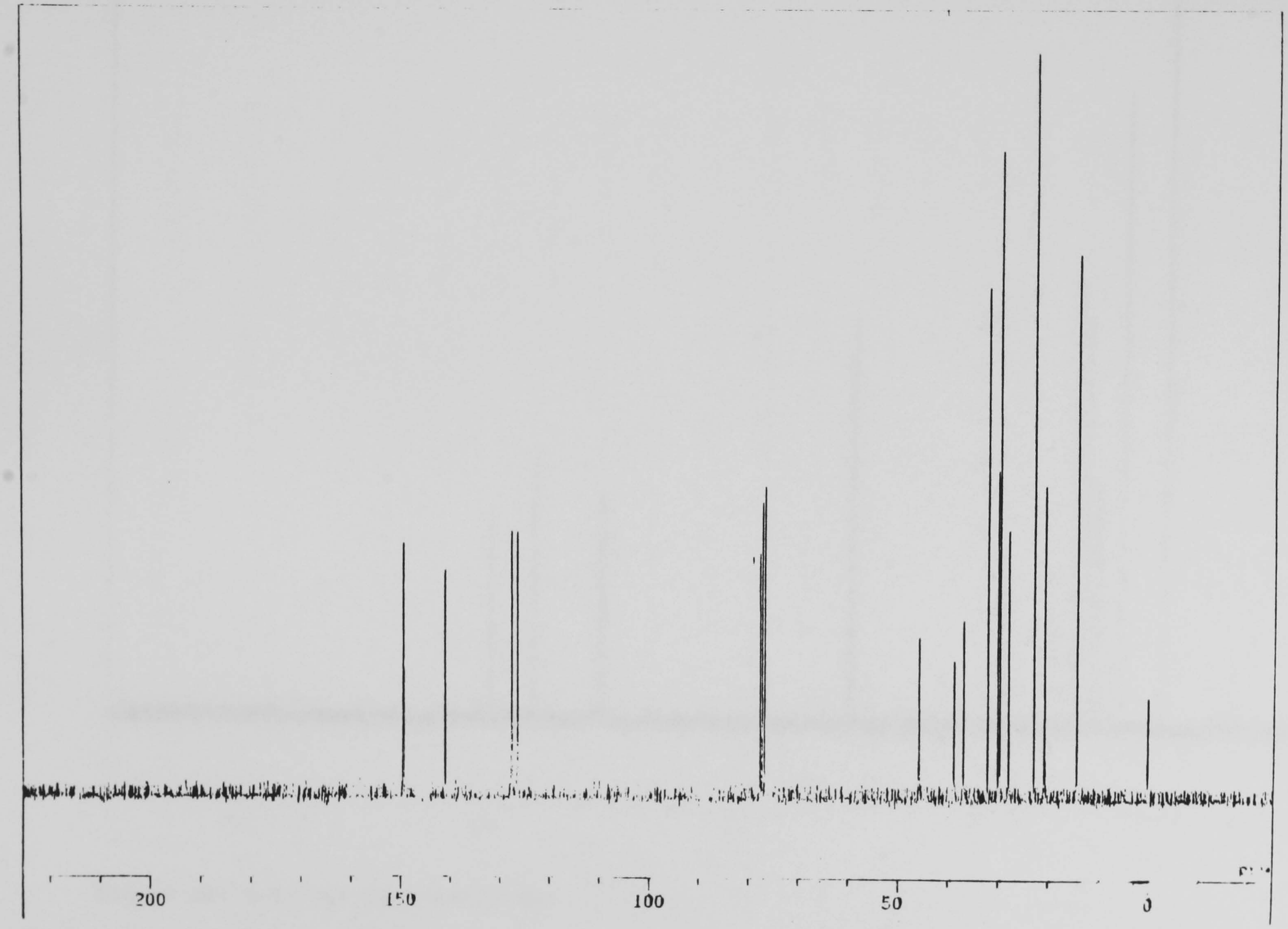

Figure 23: C-13 nmr of 4-ϕ-C_{12} ABS

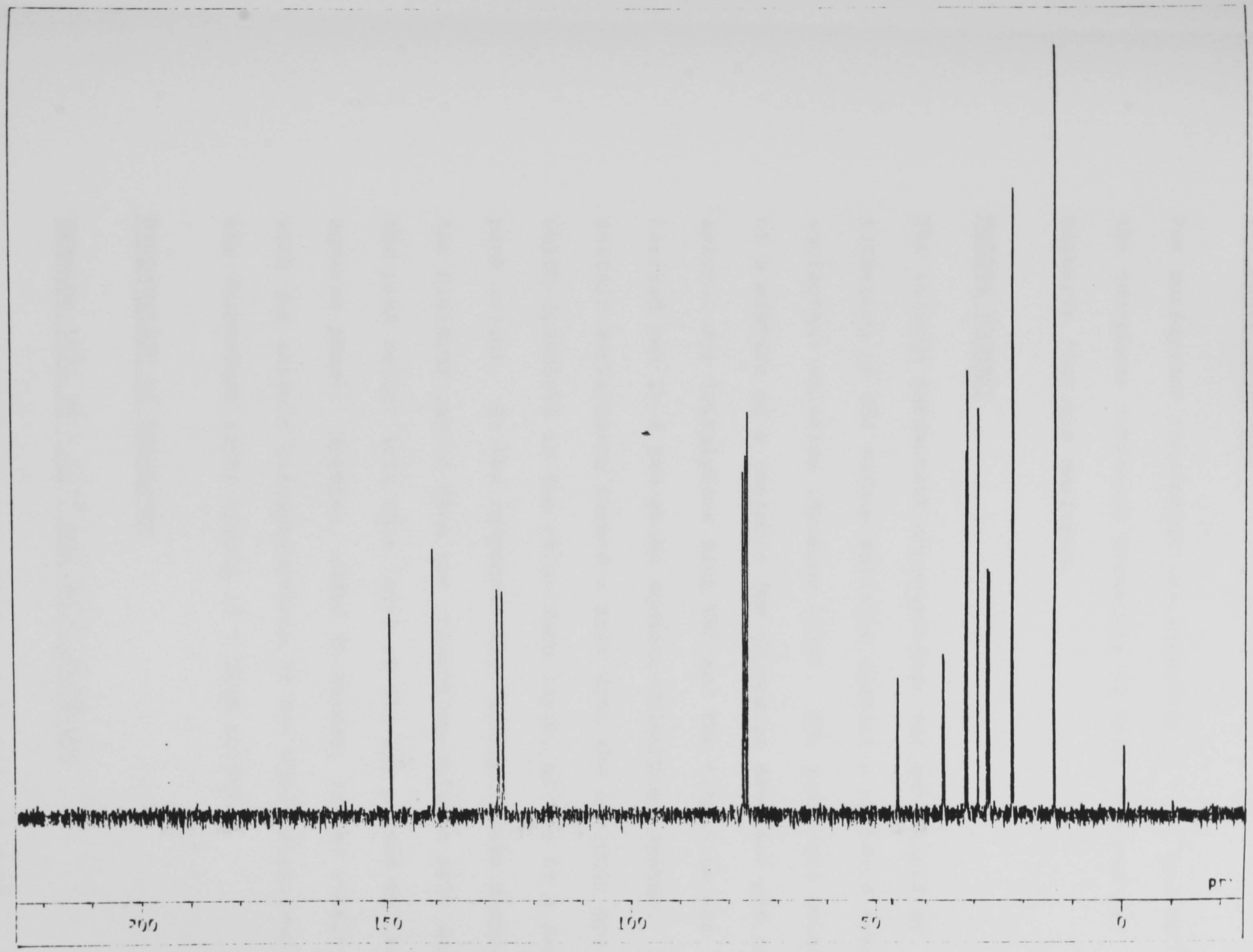

Figure 24: C-13 nmr of 6-ϕ-C_{12} ABS

2.4.4 Determination of Anionic Surfactants in Aqueous Solution

2.4.4.1 Two-phase titration

For surfactant concentrations exceeding 1×10^{-4} mol dm^{-3} the two-phase titration procedure of Reid, Longman and Heinerth [R4] was employed.

Method Summary

The anionic surfactant concentration was determined by titration of the sample solution against a standard cationic surfactant solution (Hyamine 1622). The indicator consisted of a mixture of a cationic dye (Dimidium Bromide) and an anionic dye (Disulphine Blue VN) and the titration was carried out in a two-phase aqueous-chloroform system. The anionic surfactants formed a salt with the cationic dye which dissolved in the chloroform layer, giving it a red-pink colour. At the endpoint, the Hyamine cation displaced the Dimidium cation from the chloroform-soluble salt and the pink colour left this layer as the dye passed to the aqueous phase. Hyamine, added in excess, formed a salt with the anionic Disulphine Blue VN dye which dissolved in the chloroform layer giving it a blue colour.

Preparation of Solutions

Hyamine 1622 (4×10^{-3} mol dm^{-3}) Solution

A prepared solution, specified to be 0.004 mol dm^{-3} Hyamine 1622 was purchased from BDH. This was standardised against a 0.004 mol dm^{-3} sodium dodecylsulphate solution [R4].

Preparation of Mixed Indicator Solution

This was prepared by diluting 20 cm^3 of a stock solution (BDH) with 200 cm^3 of distilled water. To this was added 20 cm^3 of 2.5 mol dm^{-3} H_2SO_4 solution and the whole was diluted to 500 cm^3 in a volumetric flask with distilled water. The solution was stored out of direct sunlight and prepared fresh every week.

Preparation of Sodium Dodecylsulphate (4×10^{-3} mol dm^{-3}) Solution (SDS)

The purity of SDS samples (BDH) was determined by accurately weighing approximately 5 g of the material into a 250 cm^3 round-bottomed flask and refluxing it, under a water condenser, with 25 cm^3 of a 0.5 mol dm^{-3} H_2SO_4 solution for about 90 minutes. After the reflux the sample was cooled and the condenser washed down with about 30 cm^3 of absolute ethanol followed by distilled water. The condenser was then removed and the lower point and neck washed with distilled water. A few drops of phenolphthalein solution (prepared by dissolving about 1 g of phenolphthalein in 50 cm^3 of ethanol and 50 cm^3 of water) were added and the solution was titrated with 1 mol dm^{-3} NaOH solution. A 25 cm^3 aliquot of the H_2SO_4 solution was also titrated against the standard alkaline solution. From the results, the purity of the SDS sample was calculated as follows:

$$\% \text{ purity of SDS} = \frac{28.84(A - B)S}{W_1}$$

where, A = volume of NaOH used for the sample, cm^3

B = volume of NaOH used for the blank, cm^3

W_1 = weight of the sample, g

S = the concentration of standard NaOH solution, mol dm^{-3}

For this sample, % purity = 98.8%.

A 0.004 mol dm^{-3} solution of SDS was then prepared by accurately weighting approximately 1.15 g (W_2) of the sample into a 500 cm^3 beaker, dissolving it with 200 cm^3 of distilled water and quantitatively transferring it to a 1 dm^3 volumetric flask and diluting to volume with distilled water. The molarity of the solution was then given by:

$$\text{Concentration of SDS} = \frac{W_2 \times \% \text{ Purity}}{288.4 \times 100} \text{ mol dm}^{-3}$$

where, W_2 = weight of SDS = 1.1402 g.

The prepared solution was then = $\underline{3.90 \times 10^{-3} \text{ mol dm}^{-3} \text{ SDS}}$

Preparation of Surfactant Solutions

Standard surfactant solutions, for preparation of a calibration graph were prepared by accurately weighing samples of the surfactant into beakers, transferring these to volumetric flasks and making up to volume with distilled water.

Titration Procedure

Standardisation of Hyamine 1622 (4×10^{-3} mol dm^{-3}) solution

To 20 cm^3 of a standardised SDS solution (3.90×10^{-3}mol dm^{-3}), in a 200 cm^3 glass stopped bottle were added 10 cm^3 of distilled water, 15 cm^3 of chloroform, and 10 cm^3 of acid indicator solution. The SDS solution was then titrated against the Hyamine 1622 solution, the vessel being vigorously shaken after each addition of titrant. At the start of the titration the lower chloroform layer was coloured pink. As the endpoint was approached emulsions, that had formed during shaking, tended to break more easily and the titration was continued with dropwise addition of titrant until the endpoint was reached, this being taken as the point at which the pink colour was completely discharged from the chloroform layer which then appeared as a faint greyish blue. The concentration of the Hyamine solution was then determined from:

$$\text{Concentration of Hyamine} = \frac{L \times 20}{V}$$

where, L = molarity of SDS solution = 3.90×10^{-3} mol dm^{-3}

V = titrant volume at the endpoint, cm^3, for a 20 cm^3 aliquot of SDS sample.

The concentration of Hyamine 1622 solutions were determined, in triplicate, for each batch of the surfactant purchased. The concentration range of four batches of the Hyamine solution was between 5 and 3×10^{-3} mol dm^{-3}.

All titrations were made using a 10 cm^3 burette having volume steps of 0.02 cm^3. The maximum error measured for the concentration determinations was ± 2% of the measured value. This maximum was used to assess the accuracy of the amount of surfactant lost from solution in the adsorption experiments.

Determination of Sodium Dodecylbenzenesulphonate

An accurately weighed quantity of the sample (∿ 0.3 g) was dissolved in distilled water (100 cm^3) and diluted to 250 cm^3 in a volumetric flask. 20 cm^3 of this solution was then pipetted into a 200 cm^3 glass-stoppered bottle and 10 cm^3 of distilled water, together with 15 cm^3 of chloroform and 10 cm^3 of acid indicator solution, added. The mixture was shaken vigorously and allowed to settle. The anionic-active matter in the sample was then determined by titration with standardised Hyamine 1622 solution. From the results, the percentage anionic-active matter in the sample was determined from:

$$\% \text{ wt. surface-active matter} = \frac{T \times f \times 250 \quad m}{20 \times 100 \times W_3} \times 100\%$$

in which, T = volume of titrant added (cm^3) to reach the end-point for a 20 cm^3 aliquot of sample solution,

m = molecular weight of anionic matter = 347.47

W_3 = weight of sample taken, g

f = concentration of Hyamine 1622 solution/ mol dm^{-3}.

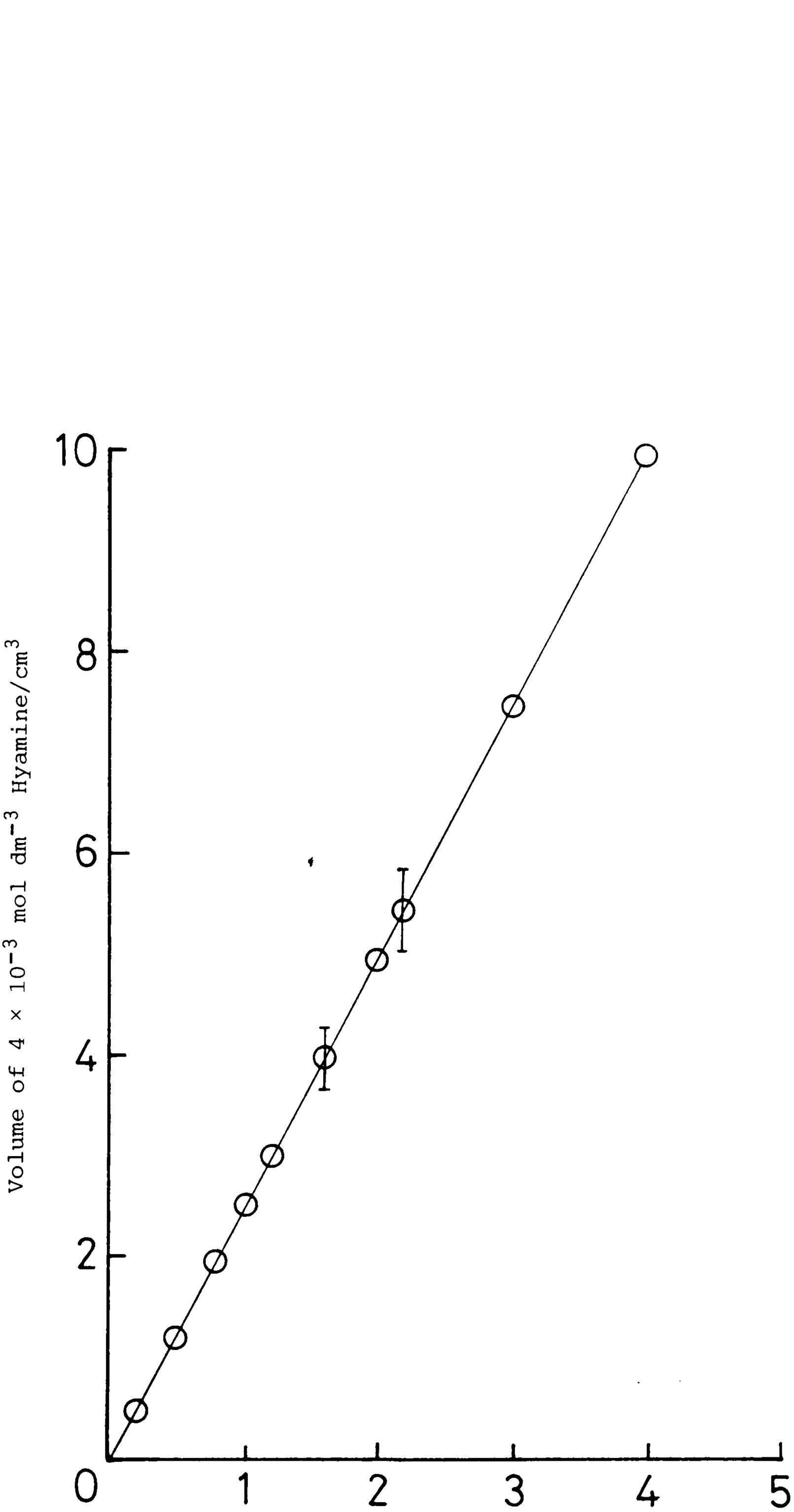

Figure 25: Calibration plot for titration of 10 cm^3 of 4-ϕ-C_{12} ABS solution with hyamine 1622 (4 × 10^{-3} mol dm^{-3})

From the results, the percentage weight of surface-active matter for the prepared surfactants was found to be: 84% for the Alfa sample and 97.7% for the pure 4-ϕ-C_{12} ABS surfactant.

Preparation of a calibration graph for 4-ϕ-C_{12} ABS in solution

To determine the concentration of anionic surfactant in aqueous solutions, a calibration plot was prepared by titrating surfactant standard solutions (of known concentration) against a standardised Hyamine 1622 solution. The titration procedure was that outlined above and Figure 25 shows the results of such a plot.

From the results of Figure 25, it can be seen that the titration was linear over the concentration range studied, that is, from zero to 40 μmols of surfactant. In order to keep the quantity of titrant within the same range (ca. 20 μmols), the volume of surfactant sample was varied according to its concentration. By confining the determination between these ranges suitable aliquots could be analysed from the constant-volume experiments, allowing duplicate determinations to be made with constant precision.

For acidic, or basic, samples the aliquot used for titration was neutralised against phenolphthalein, prior to the titration, with 1.0 mol dm^{-3} NaOH or 0.5 mol dm^{-3} H_2SO_4 as required.

Possible Interferences of Anionic Surfactant Analysis due to Components present in Adsorption Systems

Solution variables such as pH, ionic strength, and added alcohol, have been investigated during the surfactant adsorption studies (see below). As it was necessary to determine the anionic surfactant concentration under these varying conditions the influence of these on the titration of active matter has been examined.

The general method employed began with the preparation of a stock solution of the surfactant (4×10^{-3} mol dm^{-3}). For each variable examined a 10 cm^3 aliquot of this solution was transferred to a titration vessel and a measured quantity of the component under examination added. The titrant consumed was compared with that required for a 10 cm^3 aliquot of the alkylbenzene sulphonate solution in the absence of additive. In some cases (e.g. for NaCl effects) the addition of the component was made during the preparation of the anionic test solution in graduated flasks. The results are summarised in Table 4 below.

Effect of Changing Solution pH on the Determination of 4-ϕ-C_{12} ABS

As the mixed indicator titration is carried out in acid conditions (pH 2.0) low pH solutions would not be expected to interfere. However, when determining the surfactant in alkaline solutions, when there is partial or complete neutralisation of the acidity derived from the indicator

Table 4. Influence of additives on the determination of anionic surfactant concentration using two-phase Hyamine titration. Control surfactant concentration was 2.72 × 10^{-3} mol dm^{-3} . Percentage values in parentheses indicate the SD of the determination, from triplicate titrations

Solution Variable	Description	Concentration of surfactants determined 10^{-3} mol dm^{-3}	% deviation of concentration from control
None	Aqueous control pH = 6.9	2.72 (± 0.15%)	-
pH	Acidic, pH = 2.0	2.72 (± 0.16%)	-
	Basic, pH = 10.1	2.72 (± 0.15%)	-
0.1 mol dm^{-3} NaCl	Aqueous, pH = 6.7	2.70 (± 0.7%)	0.7
	Acidic, pH = 2.0	2.72 (± 0.3%)	-
	Basic, pH = 10.0	2.70 (± 0.15%)	0.7
1% (w/v) n-ButOH	Aqueous, pH = 6.9	2.69 (± 0.2%)	1.1
	Acidic, pH = 2.0	2.69 (± 0.2%)	1.1
	Basic, pH = 10.0	2.68 (± 0.15%)	1.5
+ NaCl	0.1 mol dm^{-3} NaCl		
	pH = 6.7	2.72 (± 0.15%)	-
	pH = 2.0	2.69 (± 0.5%)	1.1
	pH = 10.0	2.74 (± 0.15%)	0.7
10% (w/v) n-ButOH	Aqueous, pH = 6.9	2.67 (± 0.4%)	1.8
	Acidic, pH = 2.0	2.37 (± 0.3%)	12.9
	Basic, pH = 10.1	2.66 (± 0.15%)	2.2
+ NaCl	0.1 mol dm^{-3} NaCl	0.67 (± 1.3%)	75
	pH = 6.9	0.54 (± 1.0%)	80
	pH = 10.0	0.62 (± 0.5%)	77

solution, an adjustment of pH was required as indicated in the procedure (Table 4).

Effect of Sodium Chloride Addition on the Determination of 4-ϕ-C_{12} ABS

The influence of chloride ion was examined by titrating the surfactant solution in the presence of 0.10 mol dm^{-3} NaCl. As can be seen in Table 4, no influence on the titration was observed. However, the concentration of NaCl which could be used with the surfactant was limited by surfactant precipitation at high levels of salt (ca. 0.25 mol dm^{-3}).

2.4.4.2 Determination of Sulphate in 4-phenyl ABS Surfactant

To determine the amount of sulphate which may have been present in the prepared surfactant, after sulphonation and neutralisation, a lead nitrate titration was carried out [V4].

In the method, a weakly acidic sample solution (pH ≅ 5) in a water/acetone/isopropanol mixture is titrated against lead nitrate solution with dithizone as indicator. Sulphonate (surfactant) remains in solution but sulphate precipitates quantitatively as $PbSO_4$. The green colour of the indicator changes to purple in excess of Pb^{2+} ions. This colour change was taken as the titration endpoint.

Standardisation of 0.02M $Pb(NO_3)_2$ Solution

20 cm^3 of a standard sodium sulphate solution (9.92×10^{-3} mol dm^{-3} Na_2SO_4) was titrated against a lead nitrate

solution (∿ 0.02 mol dm^{-3} $Pb(NO_3)_2$) using dithizone as indicator. From triplicate titrations, the concentration of lead nitrate was determined:

$$Na_2SO_4 + Pb(NO_3)_2 \rightarrow PbSO_4 + 2NaNO_3$$

$$\underline{\text{Concentration } Pb(NO_3)_2 = 0.0196 \text{ mol } dm^{-3}} \quad .$$

Determination of Sulphate in Surfactant Sample

A solution of 4-phenyl ABS surfactant was prepared by weighing 16.41 g into a 250 cm^3 beaker and dissolving with about 200 cm^3 of distilled water. This was then quantitatively transferred to a 250 cm^3 volumetric flask and diluted to volume with distilled water.

A "blank" solution of distilled water (40 cm^3) was titrated with the standard $Pb(NO_3)_2$ solution, giving a titre of 0.1 cm^3. A 10 cm^3 aliquot of the surfactant solution was then titrated (in triplicate) with the nitrate solution to a purple endpoint. Titre was 0.15 ± 0.01 cm^3 of $Pb(NO_3)_2$. Then,

$$\% \ Na_2SO_4 = \frac{(0.15 - 0.10) \times 0.0196 \times 250 \times 71)}{10 \times 16.41 \times 1000} \times 100\%$$

giving $\underline{\% \ Na_2SO_4 = 0.01\%}$.

Determination of 4-ϕ-C_{12} ABS by Ultraviolet Spectroscopy

At concentrations below 10^{-3} mol dm^{-3}, 4-ϕ-C_{12} ABS cannot be measured accurately by titration in aqueous solution. Absorption of UV light, by the aromatic group of the

surfactant, is a more sensitive method and has been used for surfactant concentrations between 10^{-6} and 10^{-4} mol dm^{-3}. Absorbance maxima, shown in Figure 26, at 227 and 190 nm are independent of the chain to which the benzene group is attached.

Concentration measurements of the surfactant, in aqueous solution, have been made using the 227 nm absorbance. A linear Beer-Lambert relationship was found up to 1×10^{-4} mol dm^{-3} (absorbance 1.338), with a molar extinction coefficient of 1.317×10^5 dm^2 mol^{-1}, Figure 27.

Apparatus

The apparatus employed for the UV determinations was a Pye-Unicam UV/Visible spectrophotometer, using 1 cm quartz cells.

Calibration Plots

A series of aqueous surfactant solutions of varying concentration, ranging from zero to 1×10^{-4} mol dm^{-3}, were prepared and the absorbance of these, at 227 nm, was measured, Figure 27. From the results of Figure 27, it can be seen that the absorbances for the 6-ϕ- and 4-ϕ-C_{12} ABS isomers coincide over the concentration range, as illustrated earlier in Figure 26. Measurements were made against an aqueous reference.

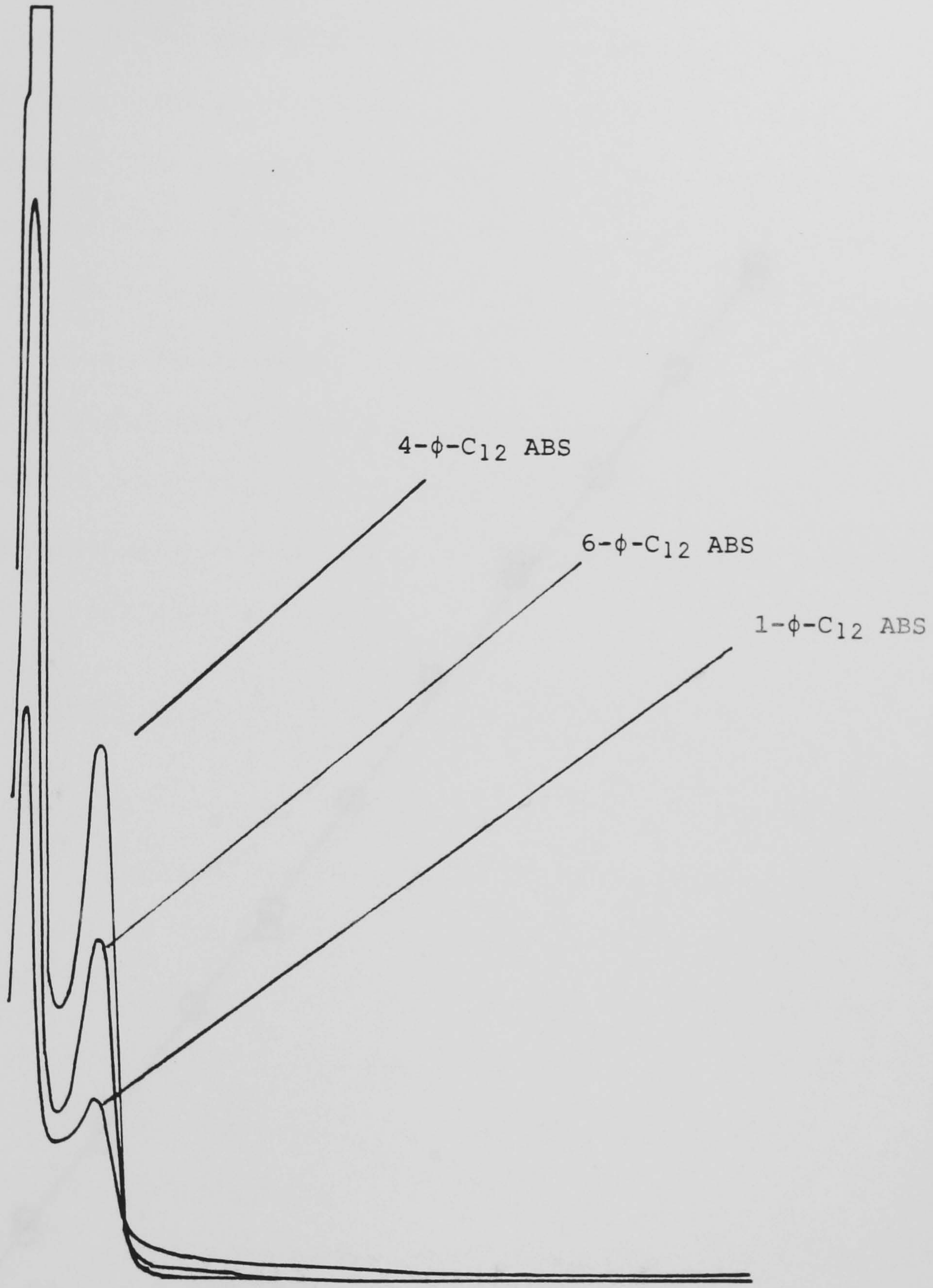

Figure 26: UV Absorbance of sodium dodecylbenzenesulphonate solutions.

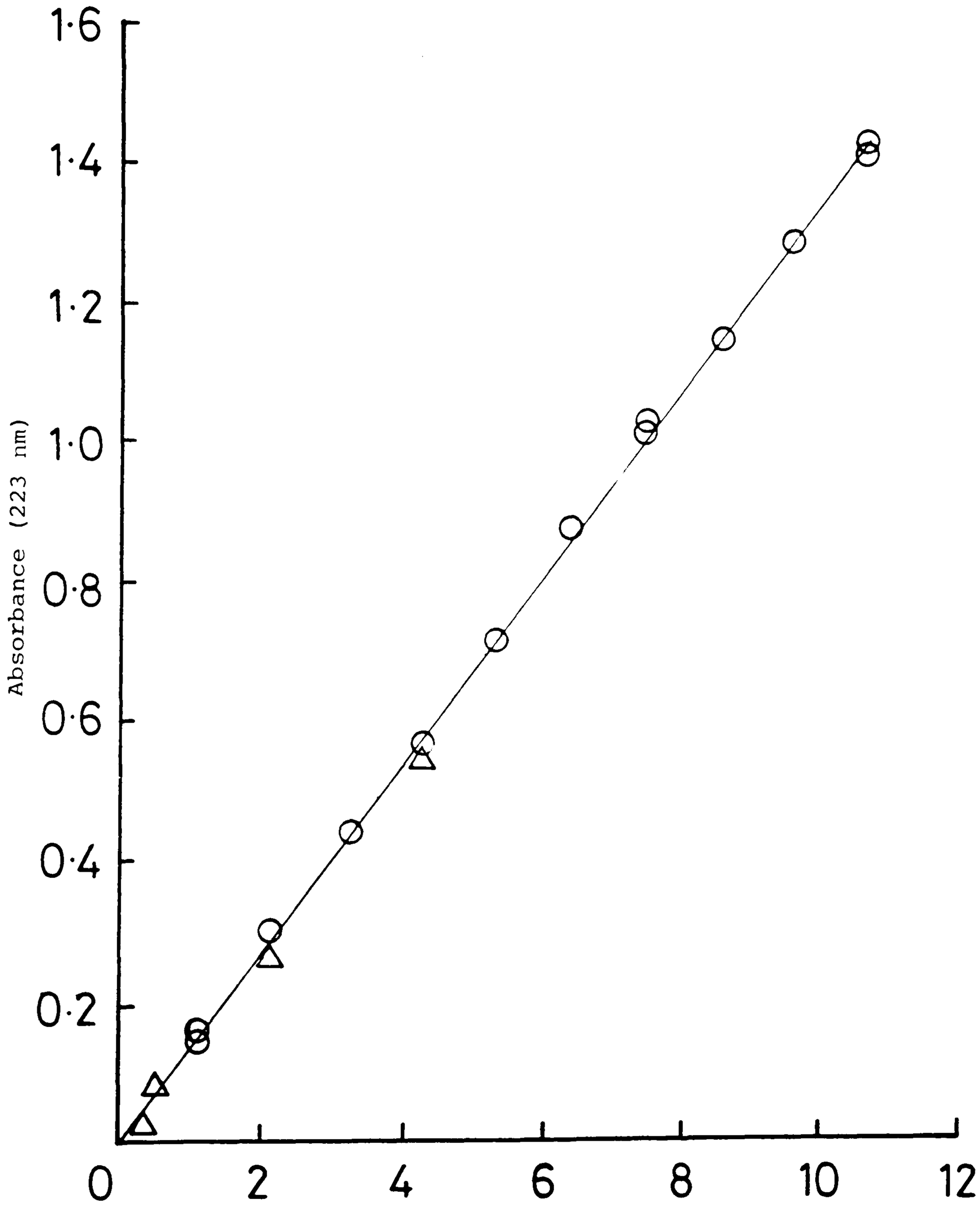

Figure 27: Calibration of 4-φ-C_{12} ABS (○) and 6-φ-C_{12} ABS (△) in aqueous solution, measured at 227 nm.

Slope = (1.317 ± 0.005) × 10^4 mol^{-1} dm^3

= (1.317 ± 0.005) × 10^5 mol^{-1} dm^2 (l = 0.1 dm)

Possible Interferences to UV Determination of 4-ϕ-C12 ABS

Variations in solution ionic strength (NaCl) or pH had no effect on the surfactant absorbance. However, the addition of small amounts of butanol (1 to 5% (v/v)) was found to increase the solution absorbance, due to a broad absorbance peak at about 220 nm from the butanol, Figure 28. Tests made using an aqueous alcohol solution as a reference for absorbance measurements however did allow compensation to be made for the alcohol absorbance, Figure 29. Thus, by careful preparation of solutions and standards, the determination of surfactant concentration could be made even in the presence of alcohol.

2.4.4.4 Liquid ScintillationCounting of 4-ϕ-C12 ABS [^{35}S]

Liquid scintillation counting was used to measure the loss of the radiolabelled anionic surfactant from the aqueous solution of radiolabelled sodium dodecylbenzenesulphonate [^{35}S]. The radioisotope used for labelling of the surfactant was sulphur-35 (section 2.2). This has a half-life of 87.5 days and emits beta (β^-) radiation with an $E_{\beta max}$ of 0.16 MeV (average energy = 53 keV).

Apparatus and Materials

The liquid scintillation counter was a Packard Tri-Carb 460C. This instrument incorporates coincidence counting (resolving time $\sim 2 \times 10^{-8}$ seconds) to reduce background and electronic noise, and an external calibration source (Radium-226) to correct for any loss of energy and light ("quenching").

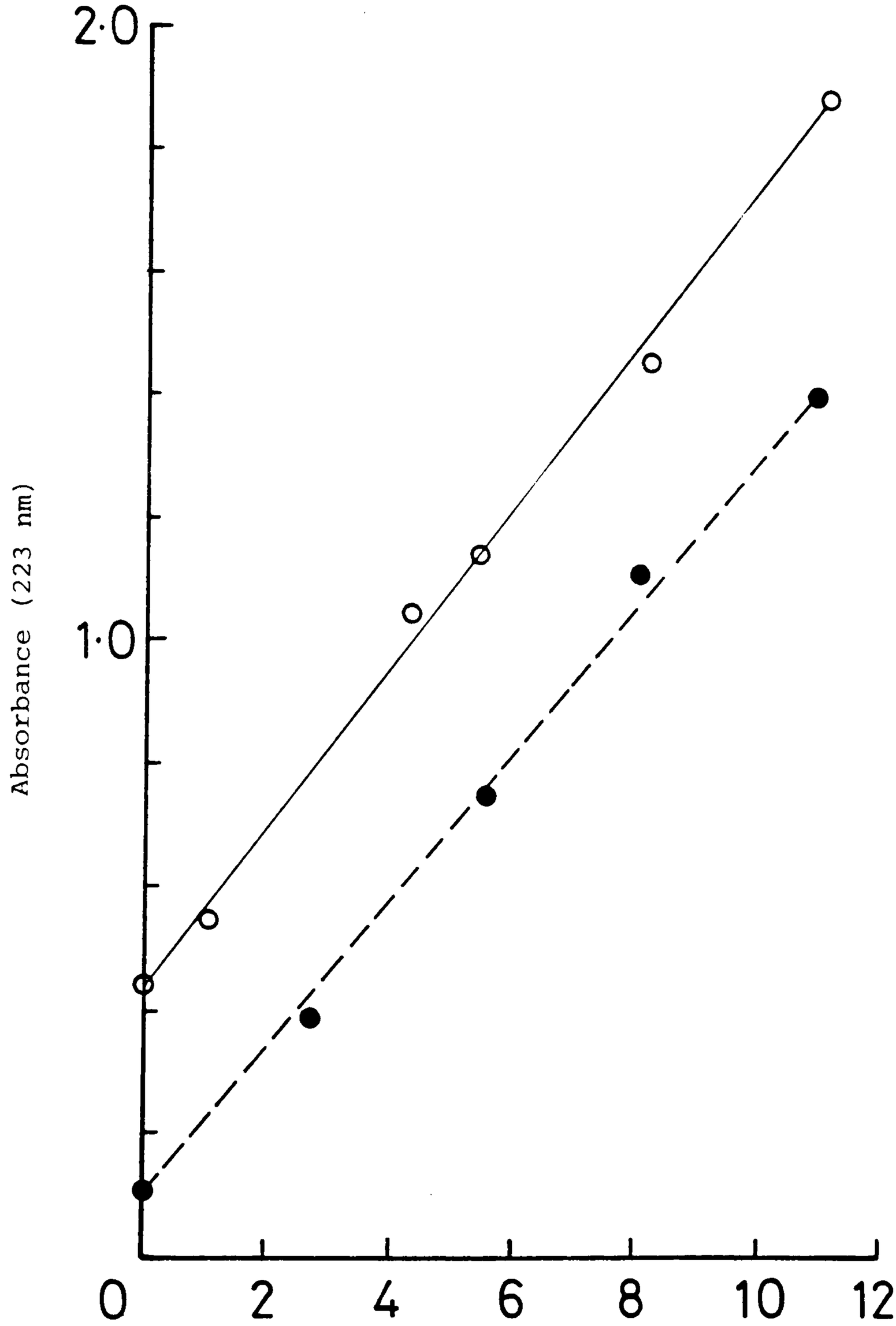

Figure 28: UV Absorbance of 4-ϕ-C_{12} ABS aqueous (broken line) and in 1% (●), 5% (○) n-butanol solution.

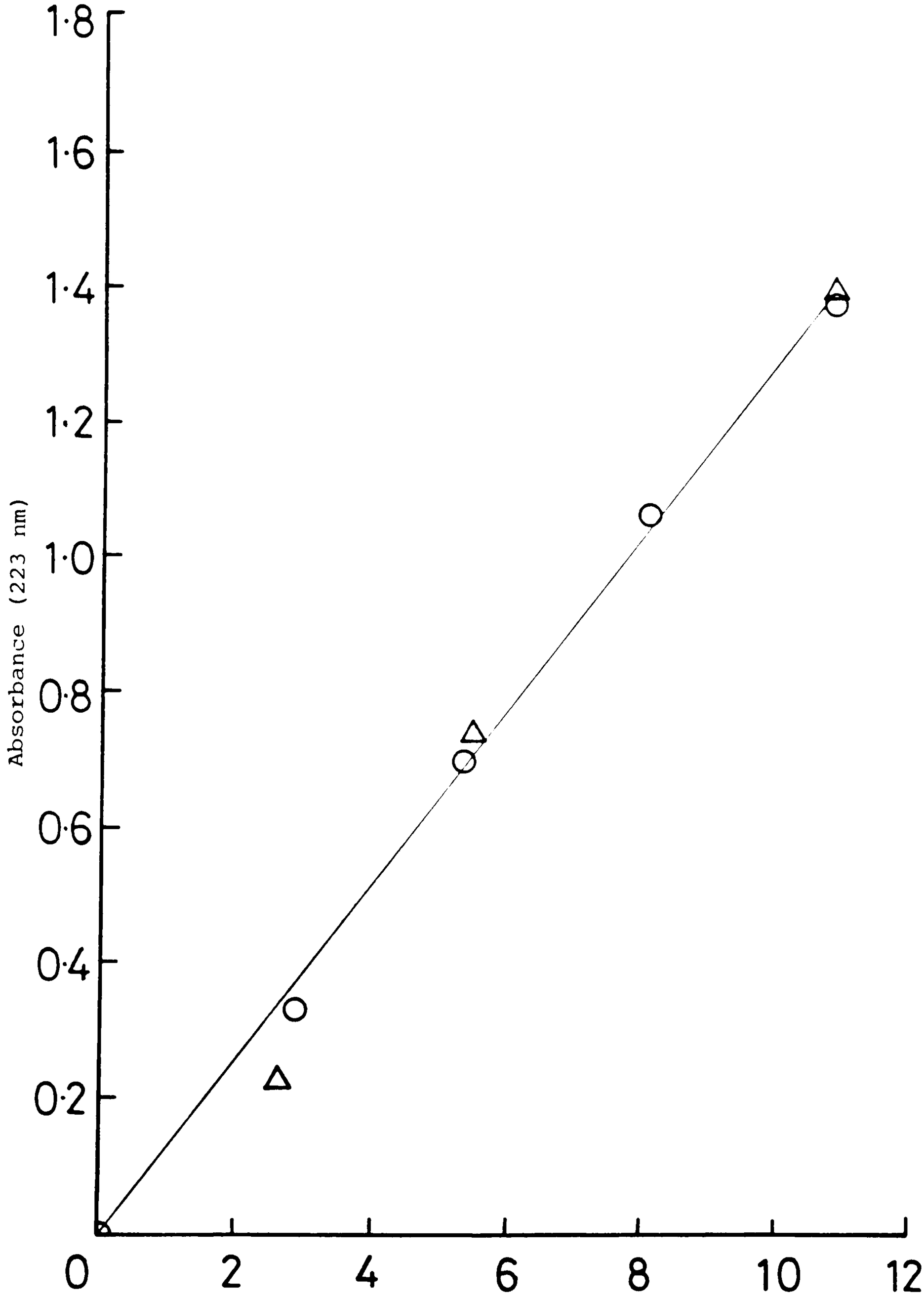

Figure 29: UV absorbance of 4-ϕ-C_{12} ABS solutions (0.1 mol dm^{-3} NaCl) in 1% (O) and 5% (Δ) n-butanol. Measurements obtained using a "blank" of n-butanol/water.

20 cm^3 Glass scintillation vials (low in potassium) were used to contain the final scintillation solutions and standards. These were thoroughly cleaned using chromic acid solution and distilled water to remove any residual radioactivity after counting.

A scintillation 'cocktail', NE260 (Nuclear Enterprises) was used as the scintillator solution. This cocktail is xylene based and contains 2,5-diphenyloxazole (PPO) as the scintillant.

1. Sample Preparation

For adsorption or distribution experiments, surfactant solutions of known concentration were prepared by dilution of a stock solution. These stock solutions were made by weighing the surfactant, determining its concentration by titration with standard Hyamine 1622 solution (see Section 2.4.5).

2. Determination of the Specific Radioactivity

0.1 ± 0.01 cm^3 of the aqueous solution, containing a known amount of surfactant were dissolved in 10 ± 0.1 cm^3 of the scintillation 'cocktail' in glass sample vials and counted in the liquid scintillation counter. Dilute samples (concentrations below 1×10^{-4} mol dm^{-3} surfactant) were counted for at least 10 minutes, while concentrated samples (i.e. those > 1×10^{-4} mol dm^{-3} surfactant) were counted for between 1 and 5 minutes. The cpm were then converted into Bq taking into account the percentage counting efficiency (see below).

Estimation of Counting Efficiency: External Standard Channels Ratio (ESCR)

In order to correct for quenching in counting radioactive samples, a measure was made of the counting efficiency of each solution. Using a set of calibration solutions (Carbon-14 labelled, of similar $E_{\beta max}$ to S-35) of known radioactive content (100,000 disintegrations per minute), and containing different amounts of quenching agent, a calibration plot relating the percentage counting efficiency to the "samples channel ratio" could be prepared. These calibration standards were counted for one minute. To relate the number of counts per minute (cpm) accumulated, for each sample, to the number of disintegrations per minute (dpm) of the sample the following equation was used:

$$\% \text{ efficiency of count} = \frac{\text{cpm}}{\text{dpm}} \times 100\% \ .$$

Figure 30 shows an example of a % efficiency versus sample channels ratio (SCR) plot. Such a calibration was carried out with every individual set of experiments because external variables such as background radiation and temperature can affect the calibration.

Measuring Radioactivity of Samples

Samples containing the radiolabelled surfactant were measured for radioactivity by counting for a fixed time in the liquid scintillation counter. The activity of the samples was recorded in counts per minute, together with

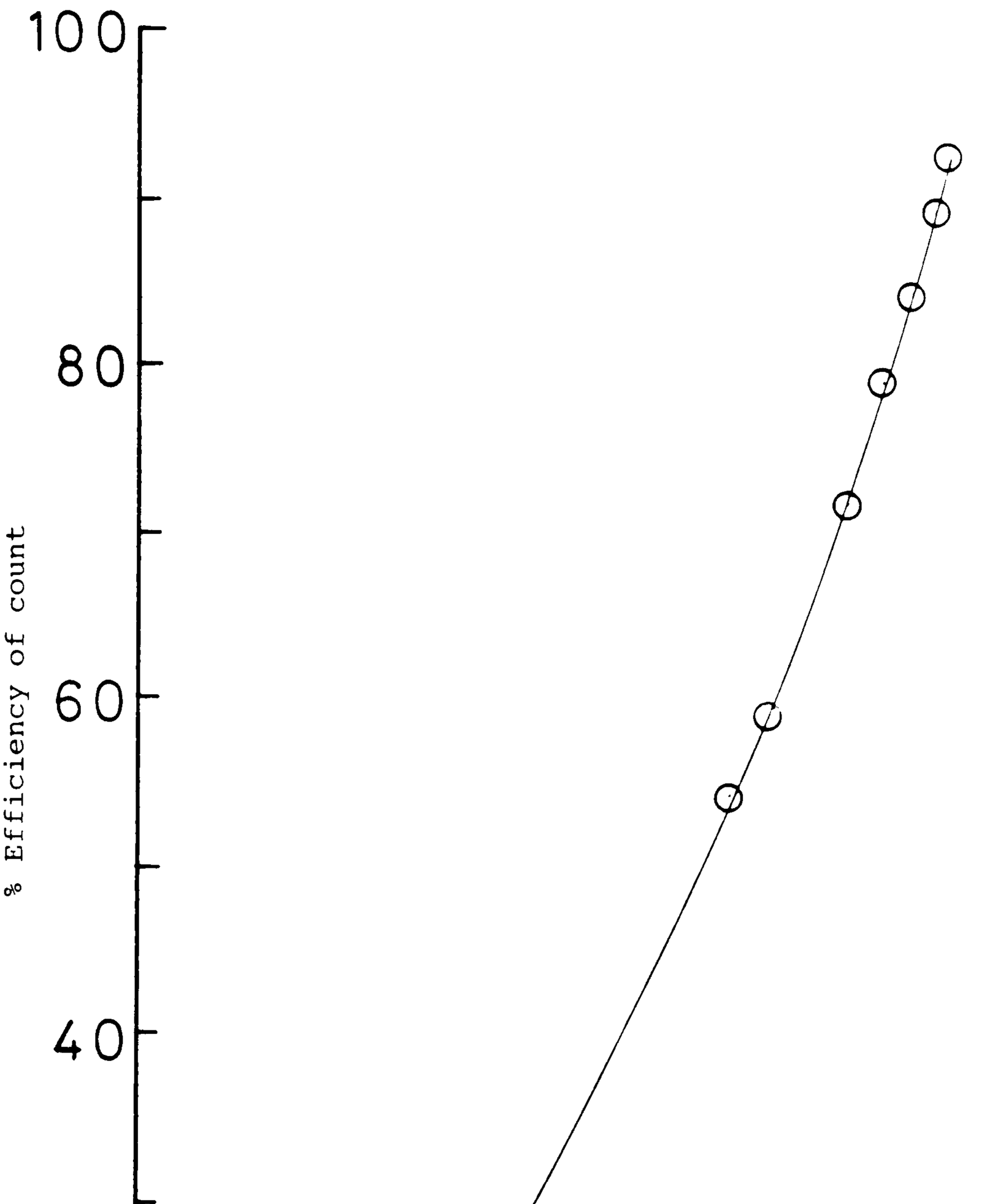

Figure 30: % Counting efficiency versus sample channels ratio for C-14.

the channels ratio (SCR). Using the SCR recorded for each sample, the % counting efficiency for the individual solutions was established, by reference to the prepared ESCR plot. The cpm of each sample was then converted to Becquerels (Bq) (disintegrations per second) by the equation:

$$\text{cpm} \times \frac{100}{\%\ \text{efficiency}} \times \frac{1}{60} = \text{Bq}$$

Knowing the specific radioactivity (MBq/mmol) the number of Bqs recorded for each sample could be converted to the concentration of surfactant in solution (mol dm^{-3}). A calibration plot relating the sample activity (Bq) to surfactant concentration is shown in Figure 31.

2.4.5 Surface and Interfacial Tension Measurements

Surface (air-water) and interfacial (oil-water) tension measurements have been made using the du Nouy method, the point of detachment of a platinum ring from the surface, or interface, being used as a measure of the tension.

Apparatus

The apparatus used was a Surface Tension and Interfacial Tension torsion Balance, Type 'OS', purchased from the White Electrical Instrument Co. Ltd. (Worcestershire).

The platinum ring, also from the White Electrical Co., was 1 cm in diameter. This was cleaned by immersion in a solution of chromic acid mixed with concentrated H_2SO_4, and

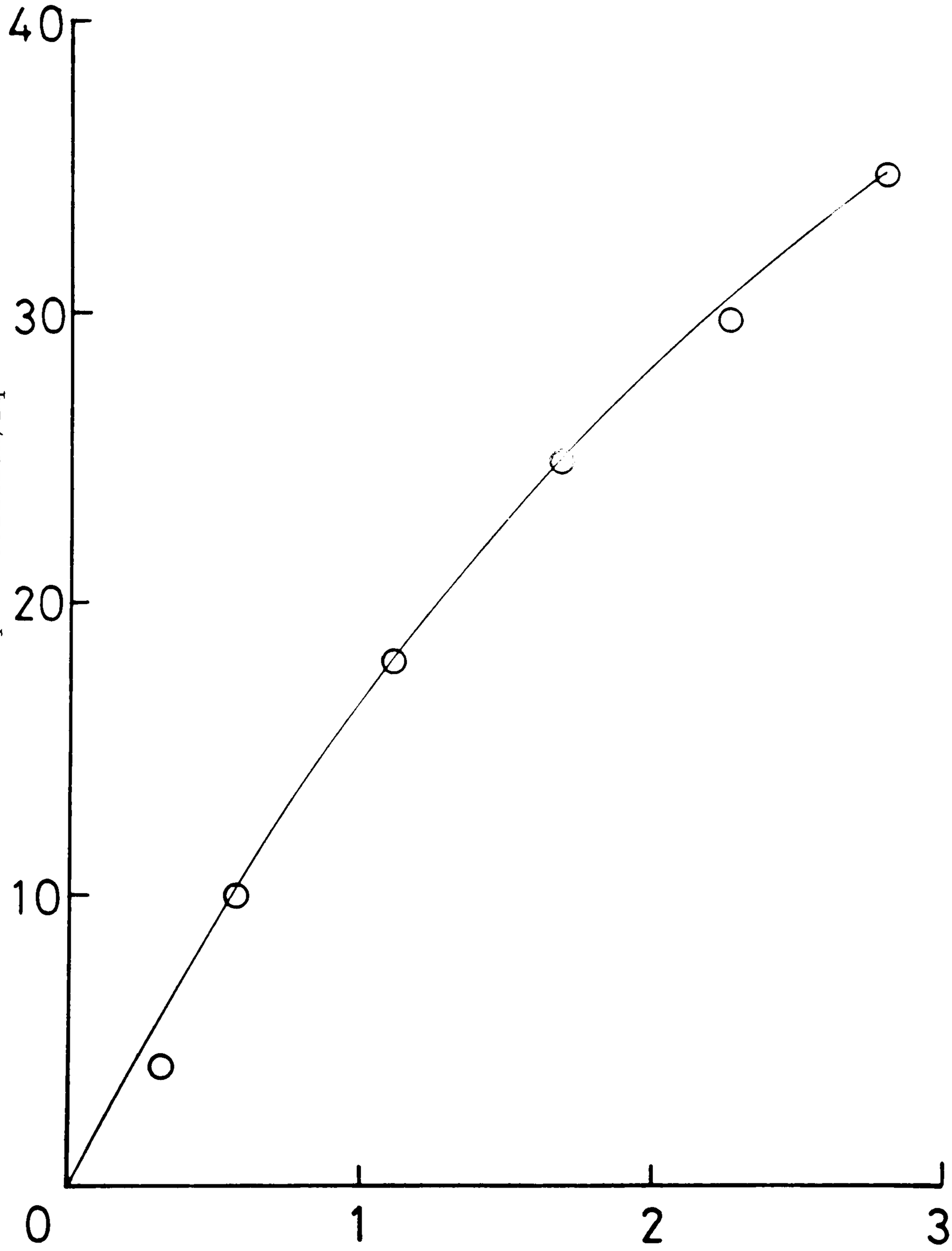

Figure 31: Calibration plot of Bq versus concentration for 4-ϕ-C_{12} ABS^{35} in aqueous solution.

thorough rinsing with distilled water. It was dried with the aid of filter paper after cleaning.

Surface Tension Measurements

These were made at the air-water interface by contacting the platinum ring with the surface and gently applying pressure to detach the ring from the surface. The surface tension was read directly from the instrument scale in mN m^{-1}.

Interfacial Tension Measurements

The procedure for measuring interfacial tensions was the same as for surface tensions except that the balance was zeroed with the platinum ring completely immersed in the upper of the two liquids and clear of both the interface and surface.

The ring was then completely immersed in the lower liquid before drawing it through the interface. Parting of the ring from the interface was less rapid and pronounced than it was when taking surface tension measurements due to the "plastic" nature of the interface.

2.4.6 Adsorption Studies

Surfactant Adsorption

Adsorption tests were conducted in Pyrex flasks by pre-equlibrating between 5 and 20 g of solid with water, or salt solution, of fixed pH for 2 hours (unless the effect of time was being studied). This equilibration was required for steady pH conditions to be reached in the presence of

kaolin. Below 2 hours, the solution pH was found to drift from that required. In the case of acid solutions, the pH increased with time toward 7, while for alkaline conditions, the pH was lowered, again towards neutral.

The solution volume, after pre-equilibration, was made up with surfactant solution to give a solid/solution ratio of between 10 and 40 per cent. The flasks were sealed and then agitated in a thermostat for a fixed time (nominally 24 hours).

At the end of a test, either the solution or the solid was analysed to determine the amount of surfactant adsorbed at the solid-liquid interface.

Two alternative procedures were employed to determine the amount adsorbed.

2.4.6.1 Direct Measurement of Surfactant on the Solid Surface (Silica)

Initial adsorption studies were conducted with radiolabelled sodium dodecylbenzenesulphonate [^{35}S] that had been prepared from dodecylbenzene purchased from Alfa Chemicals (see Section 2.3).

Upon completion of an adsorption experiment, the solution containing the solid was centrifuged at 3000 G for 30 minutes, after which the supernatant liquor was decanted and the moist silica dried between filter papers to dampness. A portion of this damp solid was weighed (x_1), taken

to complete dryness by heating under an infra-red lamp and then re-weighed (x_2). From the difference in weights, ($x_1 - x_2$), the amount of residual solution dried on the solid was calculated. An amount of the dried sample (> 0.2 g, Figure 32) was accurately weighed into a scintillator vial and 10 cm^3 of the scintillation cocktail (NE260) added to solubilise the surfactant off the solid. With corrections made for residual solution, losses during desorption and counting efficiency, the total amount of surfactant on the dried sample (adsorbed plus dried-on) was found directly. After correcting for the amount of surfactant in the solution dried onto the sample, the amount of surfactant truly adsorbed, in mols m^{-2}, was obtained.

2.4.6.2 Loss of Surfactant from Solution (Kaolin)

After centrifugation (at 3000 G for 30 minutes) the concentration of surfactant in the supernatant liquor was determined by two-phase titration (Section 2.4.5.1), ultra-violet absorbance (Section 2.4.5.2), or by liquid scintillation counting (Section 2.4.5.3). From the difference between the initial and final surfactant concentrations the amount adsorbed onto the solid, in mol m^{-2}, was calculated using the equation:

$$\Gamma = (C_i - C_f) \times \frac{V}{m \times s}$$

where, Γ = amount of surfactant adsorbed, mol m^{-2}

C_i, C_f = initial and final surfactant concentrations respectively, mol dm^{-3}

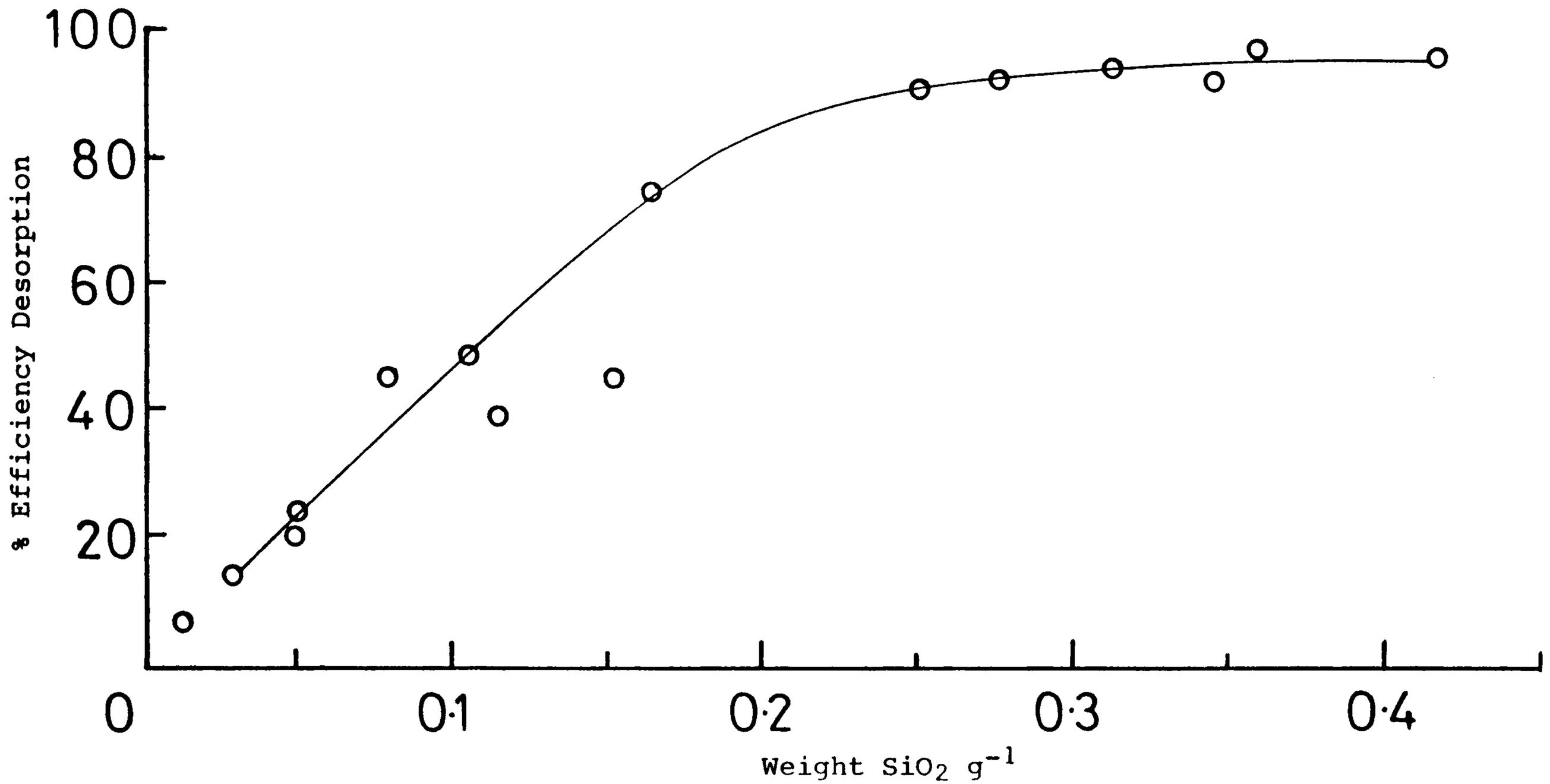

Figure 32: % Efficiency of desorbing SDBS from silica (into NE260) onto which known amounts of SDBS had been adsorbed and dried-on.

V = Volume of test solution, dm^3

m = mass of solid sample, g

s = specific surface area of the adsorbent, $m^2\ g^{-1}$

2.4.6.3 n-Butanol Adsorption

The adorption of n-butanol onto kaolin was determined using procedures similar to those for the surfactant adsorption measurements above, viz:

(a) surface tension measurements, or

(b) radiolabelled n-butanol (C-14).

(a) Surface Tension Measurements

Surface tension measurements of aqueous n-butanol solutions were made using the procedure outlined in Section 2.4.4.4.

Measurements of surface tensions were made before, and after, the solution has been in contact with the solid. An increase in surface tension indicated that adsorption at the solid surface had taken place and, using the difference in surface tension values, the residual concentration of the alcohol in the aqueous solution was determined. The number of moles of alcohol adsorbed per unit area of sample was calculated in the same way as for the surfactants.

(b) Radiolabelled n-butanol (C-14)

n-butanol, radiolabelled with C-14 and having a specific activity of 1.92×10^8 Bq $mmol^{-1}$, was "diluted" with 8 cm^3 of inactive n-butanol (AR). To determine the specific activity of this "stock solution", 0.1 cm^3 aliquots were

counted in 10 cm^3 of NE260 for one minute.

Determination of the specific activity of C-14 labelled n-butanol "stock solution".

CPMA/K	% Dev	SCR	% Efficiency	Activity / Bq
2,304,040	0.20	0.922	87.0	44139
2,326,525	0.20	0.922	87.0	44569

From the results, the specific activity of the n-butanol "stock solution" was found to be 4.07×10^4 Bq $mmol^{-1}$.

Adsorption measurements of the alcohol at the kaolin-solution interface were made using known volumes of this stock solution (see Section 3.3.4.1) and the same procedure as that for the surfactant adsorption tests (see above).

2.4.7 Electrophoretic Mobility Measurements

Apparatus

A single-particle microelectrophoresis apparatus (Rank Brothers MkII) (Figure 33) with auxillary water bath (receiving water from, and returning water to, a thermo-statted water reservoir) was used for all electrophoretic measurements. The length of one division of the eyepiece graticule within the observing microscope was 17.6 μm.

A thin-walled van Gils cylindrical cell, incorporating platinum electrodes, was used for mobility measurements

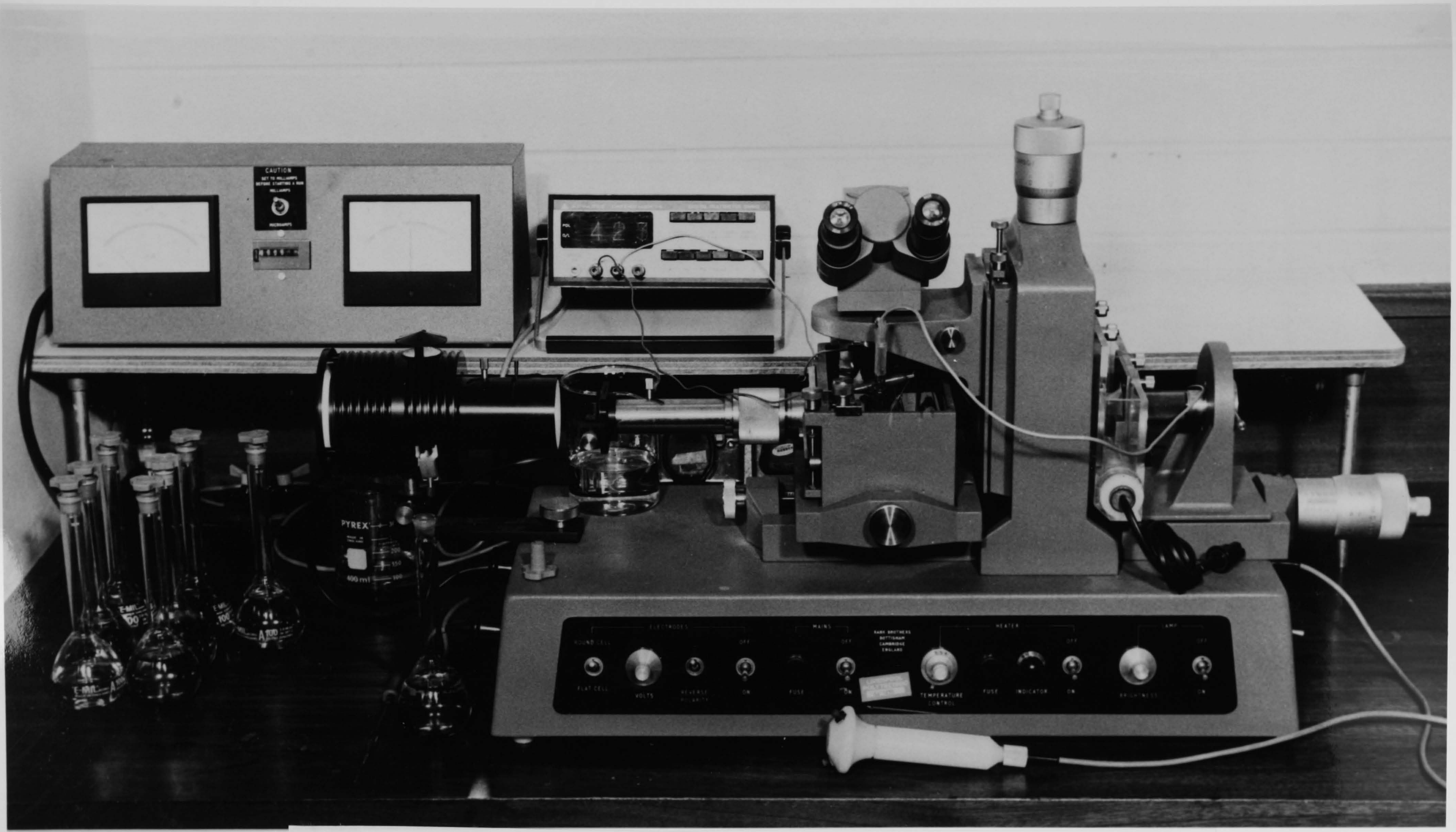

Figure 33: Rank Brothers, MkII, single-particle microelectrophoresis apparatus.

(Rank Brothers). The cell had an internal diameter of 1708 μm and a wall thickness of 80 μm. The apparatus was fitted with cylindrical platinum electrodes for use with the cylindrical cell.

Platinisation of Electrodes

The platinum metal electrodes (Rank Brothers) were thoroughly cleaned in soapy water using a small brush and rinsed with hot tap water. The electrodes were then immersed in hot chromic acid solution, prepared by carefully adding concentrated H_2SO_4 (SG 1.18) to $Na_2Cr_2O_7$ aq (5% w/w) [V5], for 30 minutes then rinsed with distilled water. The electrodes were then immersed in a platinising solution of K_2PtCl_6 (2% w/w) and $Pb(CH_3COO)_2$ (0.02% w/w) in aqueous HCl solution (25 mmol dm^{-3}) [F5] and connected to a 12 volt power supply, inducing electrodeposition from the solution onto the anodic electrode. The polarity of the electrodes was reversed every 30 seconds and within 30 minutes both electrodes were coated with a thin layer of black platinum.

Determination of Inter-electrode (Platinum Wires) Distance within the Particle Microelectrophoresis Cell

The interelectrode length of the cell, l_c, was determined by measuring the conductivity when filled with a 0.1 mol dm^{-3} aqueous KCl solution.

A universal conductance bridge (Wayne Kerr, model B224) was connected to the platinum wires of the cell and the conductance, G, of the electrolyte solution measured. From a

knowledge of the conductivity, K, of the KCl solution at 25°C, and the cross-sectional area, A, of the cell, l_c was determined using the expression:

$$l_c = \frac{K.A}{G}$$

where for a 0.1 mol dm^{-3} KCl solution at 25°C:

$$K = 1.28565\ m^{-1} \quad [A2]$$

and $$A = \frac{\pi d^2}{4}\ m^2$$

where, d = internal diameter of the cell = 1708×10^{-6} m

and G = 3.47×10^{-5}S.

Thus, l_c = 0.0848 m (8.48 cm)

Temperature Control

The temperature coefficient of particle mobilities is about 2% per degree C at room temperature. Efficient thermostatting is, therefore, necessary. Thermostatting is also necessary to avoid convectional disturbances.

Temperature control was maintained at 25 ± 0.2°C by continually circulating 22 dm^3 of tap-water through the microelectrophoresis cell water bath using a BTL CIRCON heater and pump.

Position of Stationary Levels within the Cell

Microelectrophoresis measurements are complicated by the simultaneous occurrence of both electrophoretic diffusion and electro-osmosis, which results in a parabolic

distribution of liquid speeds with distance from the cell wall [H7]. The true electrophoretic velocity is only observed at the so-called "stationary levels" in the cell where the electro-osmotic flow and return flow of liquid cancel. Theoretical considerations show that for a cylindrical cell, the stationary levels are located at 0.146d from the upper and lower walls, where d is the internal diameter of the cell [S2].

Preparation of Samples

A series of 50 cm^3 solutions spanning the pH range 1-12 were prepared. All the solutions were of ionic strengths ranging from 10^{-3} to 0.1 mol dm^{-3} NaCl. In addition to pH and salt effects, the influence of surfactant addition on the electrophoretic mobilities of kaolin particles has been investigated. The preparation of all solutions followed the same procedure, the adjustment of pH, ionic strength, or surfactant type, and concentrations being made as appropriate.

The solids concentration in suspensions used for single-particle microelectrophoresis must be high enough to allow quick location of particles in focus and yet low enough to avoid problems associated with sedimentation and inter-particle interaction. Street and Buchanan [S8] investigated the effect of solid concentration and found that there was no variation in measured mobility provided that the volume concentration lay between 2×10^{-5} and 2×10^{-4} (w/v). In the present study the optimum dilution was

quickly determined by dropwise addition of a stock suspension to a known volume of double distilled water and by observation under the ultramicroscope. To avoid concentration changes arising from mixing stock suspension and the electrolyte of interest, the solid concentration in the stock was adjusted such that no more than three drops (0.12 cm^3) were required to give a 50 cm^3 sample suspension having the required solids concentration for microelectrophoresis. The final amount of solid in the sample solutions never exceeded about 4 mg. The solution pH was adjusted by adding small volumes of 0.1 mol dm^{-3} HCl or NaOH solutions. The flasks were stoppered and the suspension shaken. Mobility measurements were made after leaving the suspension to stand for about 1 hour to allow sedimentation of particle aggregates.

Mobility Determinations

The previously cleaned cylindrical glass cell was flushed with two 4 cm^3 portions of the sample dispersion and finally completely filled with a third 4 cm^3 portion. With the microscope focussed at one of the stationary layers (see above), the platinum metal electrodes were inserted into the cell and a digital voltmeter (Advance Instruments,model DVM 4A) connected across the electrodes. The particles were illuminated using a quartz-iodine light source and the voltage across the cell was adjusted such that the time for an observed particle to move across two divisions of the

eyepiece graticule was approximately 10 (± 0.01) s.

The voltage polarity was then reversed and the time taken by the particle to travel the chosen distance recorded. This procedure was repeated for at least 20 particles moving in each direction at both the upper and lower stationary levels. The mean of the reciprocal times recorded was used to calculate the average particle electrophoretic mobility (see Section 1.6). Measurements were rejected if the 95% confidence interval for the mean time was more than 5% of this value.

It should be noted that velocity measurements made at both the upper and lower stationary levels of the cell, using kaolin at low pHs' (< 4) as the tracer suspension, resulted in a distorted profile in which particles in the lower half of the cell moved faster than those in the upper half. The distortion can be explained by particles settling on the lower cell wall and effectively shifting the position of the theoretical stationary level. Such an effect might be expected to be pH-dependent since as the pH is lowered particles become increasingly positive. This increases the tendency to adsorb at the lower cell wall, which is negatively charged. To avoid these problems, mobility measurements at low pHs were made only at the upper stationary level.

Accuracy of Electrophoretic Mobilities

In the determination of electrophoretic mobilities by the microscope method the main sources of error are inaccuracy in focussing on the stationary levels, and Brownian motion [S2].

The average error of a single velocity measurement due to focussing inaccuracy is of the order of 3%. Random Brownian motion, which is inevitably superimposed on the electrophoretic migration of the particles, can contribute an additional 3% error on a single velocity determination.

Those sources of error in addition to temperature fluctuations (an increase of 1°C increases mobilities by ∿ 2%), timing errors, and asymmetric flow, will generally lead to single velocity determinations with an average deviation of ca. 5 to 7 per cent from the mean. The probable error for an electrophoretic mobility calculated from the mean of 20 velocity determinations will (at best) be about 1½ to 2 per cent [S5]. Thus very careful attention to stable conditions was made.

2.4.8 Potentiometric Titrations

Potentiometric titrations to determine the surface charge density of kaolin particles have been made at different solution ionic strengths. The experimental set-up is shown in Figure 34.

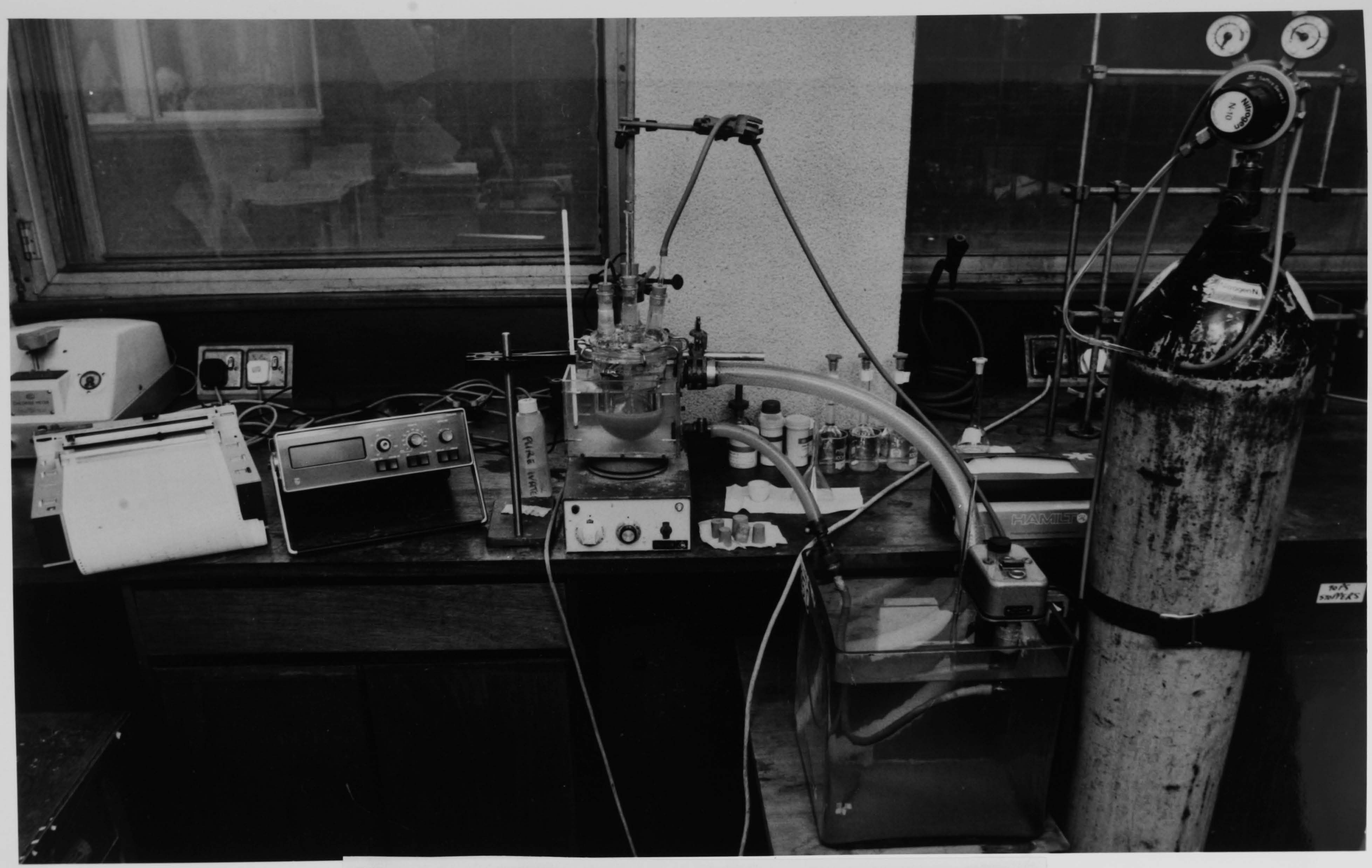

Figure 34: Experimental set-up for potentiometric titration of kaolin particles.

Apparatus

A cylindrical glass vessel of 700 cm^3 capacity, fitted with a multi-socket/flat flange lid was used as the reaction vessel (Fisons, reference numbers FR700F and MAF 2/32 respectively). To this were fitted a Pye Unicam pH glass electrode (type 201, membrane HA) and a Pye Unicam double junction reference electrode (type RE3/DJ/NS). In the latter electrode, a 0.1 mol dm^{-3} aq KNO_3 solution was used as the outflowing electrolyte. In compliance with the manufacturer's recommendation the outer-compartment of the electrode was drained of electrolyte at the end of each working day. pH measurements were made using a Pye Unicam pH meter (model PW9409) and recorded with a chart recorder set at 100 mV full-scale deflection (10 mV/pH unit) (Chessell Ltd.).

Method

200 cm^3 of double distilled water, or a NaCl(aq) solution, was pipetted into the reaction vessel and stirred using a Teflon-coated magnetic flea at an appropriate speed, avoiding excessive turbulence. The glass and reference electrodes were inserted through two inlet/outlet ports in the top of the reaction vessel, and their heights within the vessel adjusted so that their respective membrane and junction resided well within the stirred solution. The pH of the solution was displayed on the digital pH meter and recorded on the chart recorder. N_2 gas (BOC white spot grade) was bubbled (ca. 50 cm^{-3} min^{-1}) into the solution

via a Pasteur pipette inserted through an inlet/outlet port. As the solution pH approached 7 the N_2 gas bleed was slowed down. When the pH was 7.00 ± 0.01, 1.00 g ± 0.001 g of kaolin was quickly added to the stirred solution through a glass funnel positioned in the centre inlet/outlet port. At the same time the length of the Pasteur pipette, through which the N_2 gas flowed, inside the reaction vessel, was reduced so that its tip resided just above the surface of the suspension. In this way, the suspension was continuously blanketed by an inert atmosphere of nitrogen, so prohibiting the absorption by the suspension of CO_2.

The stirred suspension was left to stabilise until the pH was virtually (i.e. pH drift < 0.01 min^{-1}) constant. The suspension was then titrated in the reversible cell:

glass electrode	aqueous suspension of kaolin (electrolyte NaCl)	aq KNO_3 salt bridge (0.1 mol dm^{-3})	Saturated calomel electrode

The pH of the suspension being recorded before each addition of titrant and at the completion of a titration. Titrant addition was made using a microlitre syringe and was effected as soon as the pH reading was steady (i.e. drift < 0.01 min^{-1}). For the titrations the volume of titrant added was adjusted to give a pH change of about 0.2 units. In the vicinity of the equivalence point (pH 7) this titrant volume was ca 25 mm^3, while at extreme pH values progressively larger titrant volumes were required to effect the same pH change. At the extreme pH values, the time for

equilibrium to be reached was greater than that near the equivalence point, the times required ranging from about 2 hours to about 30 minutes respectively. The pH range covered was kept to less than 5 pH units. The titrant, HCl(aq), (0.1 mol dm^{-3}) was standardised with Na_2CO_3 (AR solution) using methyl orange as indicator, and the titrant NaOH(aq) (0.1 mol dm^{-3}) was standardised with potassium hydrogen phthalate using phenolphthalein as indicator [V4]. The standardisation procedure was repeated, for each stock solution, about every two weeks.

2.4.9 Atomic Absorption Spectrophotometry (AAS): Determination of Aluminium

Aluminium concentration in solution was determined using AAS. These studies were applied to aluminium-surfactant interactions and to clay dissolution.

Apparatus

The apparatus used was a Pye Unicam SP9-atomic absorption spectrophotometer fitted with an SP9-computer to process the results, these being printed directly in parts per million (ppm) aluminium.

A Pye Unicam aluminium hollow cathode lamp was used as a light source.

Instrumental conditions:

Flame	= N_2O/acetylene rich
N_2O flow rate	= 5.0 dm^3 min^{-1}
Acetylene flow rate	= 4.2-5.0 dm^3 m^{-1}
Wavelength	= 309.3 nm
Bandpass	= 0.4-0.5 nm
Lamp current	= 8 mA.

Adjusted to give maximum sensitivity.

Calibration of the Instrument

Aluminium solutions of known aluminium content (ppm) were prepared by dilution of a 100 ppm aluminium solution. These standards were matrix matched to that of the sample solutions. All solutions contained 1% (v/v) KCl as an ionisation buffer.

A plot of absorbance against aluminium concentration showed some curvature at high aluminium levels (Figure 35). Samples were therefore diluted when necessary to bring the measurements into the linear Beer-Lambert region, the aluminium content then being obtained directly in ppm.

The preparation of calibration plots for aluminium under differing solution conditions showed that the absorbance depended on the chemical species present in solution, Figure 36. Thus, appropriate calibrations were prepared for each set of experiments.

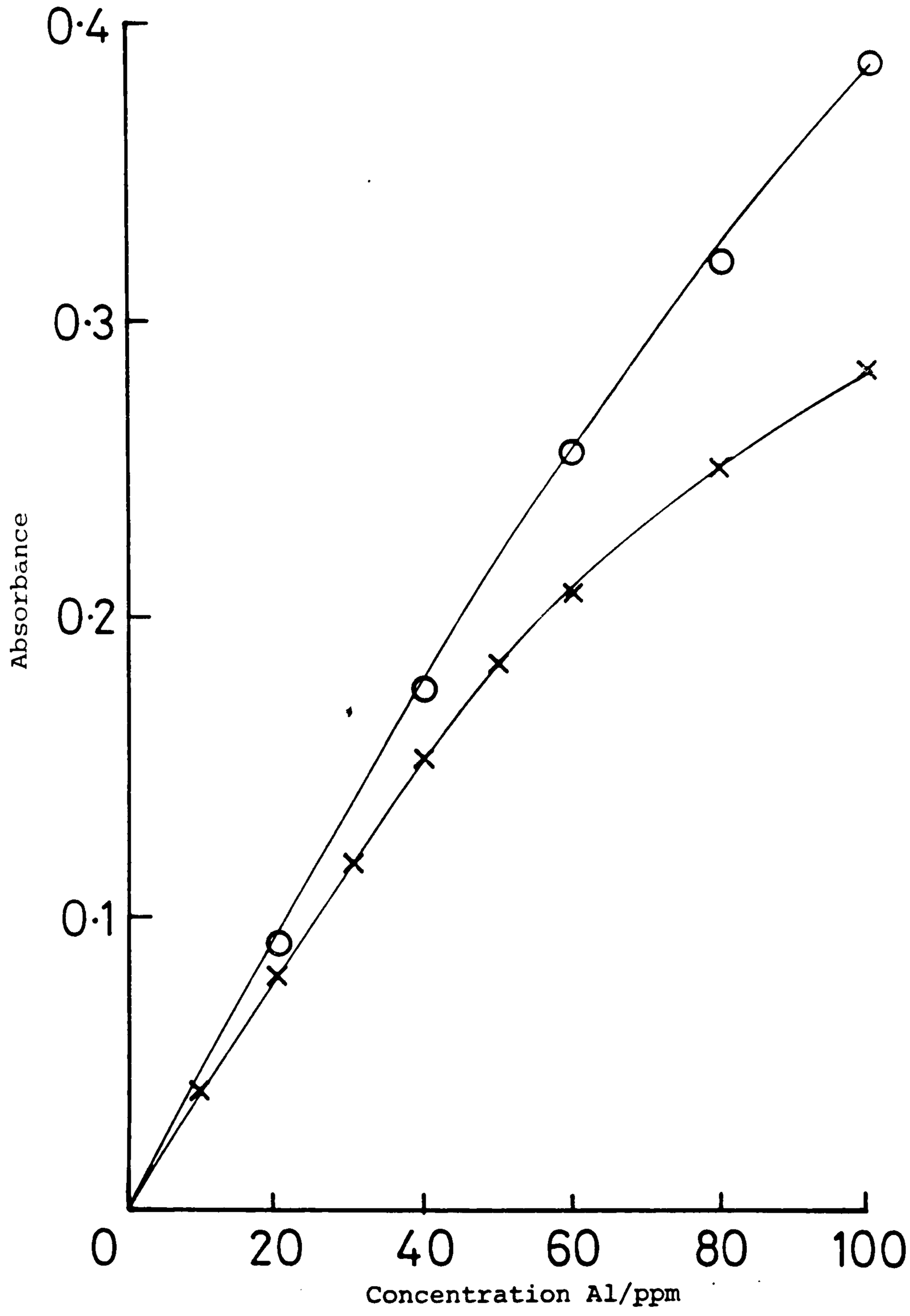

Figure 35: Determination of Al by AAS in solutions containing 1% (w/v) KCl (O) and no KCl, showing the improved response with added salt

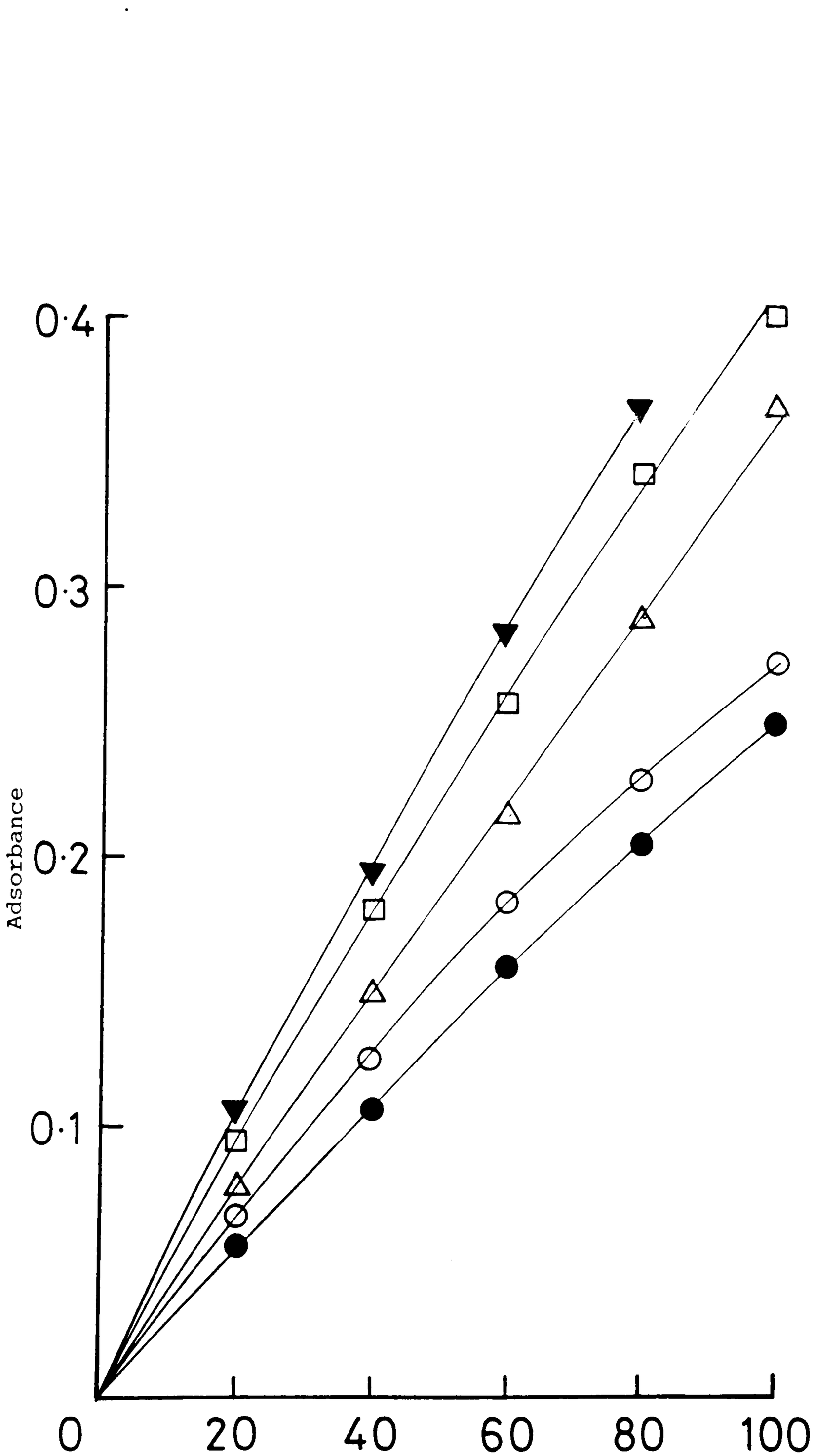

Figure 36: Determination of Al by AAS, in solutions containing 1% (w/w) KCl and, 0.1M, 0.5M NaCl (○,△); 1% (v/v), 5% (v/v) n-ButOH (●,□); 5% (w/v) n-ButOH + 0.5M NaCl (▼).

2.4.10 Gas Chromatographic Analysis: Determination of n-decane

Gas chromatography (GC) was used to measure the concentration of n-decane in various surfactant solutions. The procedure was adopted for its ability to separate the solution components and convenient estimation of the amount of oil present.

Apparatus

For the analyses, a Perkin Elmer Model 8400 Capillary Gas Chromatograph linked to a Perkin-Elmer GP-100 Graphics Printer was employed. A method for n-decane determination was set up, and stored in the memory of. the system computer. The following operational settings were used.

Parameter	Setting
Oven temperature (°C)	(1) 50
	(2) 100
Iso time (min)	(1) 3.0
	(2) 5.0
Ramp rate (°C/min)	16.0
FID sensitivity	High
Detector temperature (°C)	250
Pressure (psig)	22.5
Equilibration time (min)	1.0
Total run time (min)	17.3

Calibration of the Instrument

Retention times were recorded for injected samples of chloroform, and n-butanol, or n-decane in chloroform. Upon establishing the retention time for n-decane, a number of integrated areas were recorded of acceptable n-decane peaks generated by injection of fixed volumes, 0.1 microlitres, of n-decane solutions in chloroform. A linear relationship was found to occur between the areas and sample concentrations and was used to determine the concentrations of oil in sample solutions, Figure 37.

Preparation of Samples

To prevent interference arising from the presence of non-volatile components (NaCl and surfactant) in sample solutions, aliquots of these solutions (5.0 ± 0.1 cm^3) were extracted with an equal volume of chloroform (5.0 cm ± 0.1 cm^3, Analar). Chloroform was added to the sample aliquot by pipette and the mixture shaken thoroughly in sealed tubes at 25°C overnight. A fixed volume of the organic phase, 0.1 µl, was then injected onto the capillary column and the quantity of decane determined using the aforementioned calibration plot.

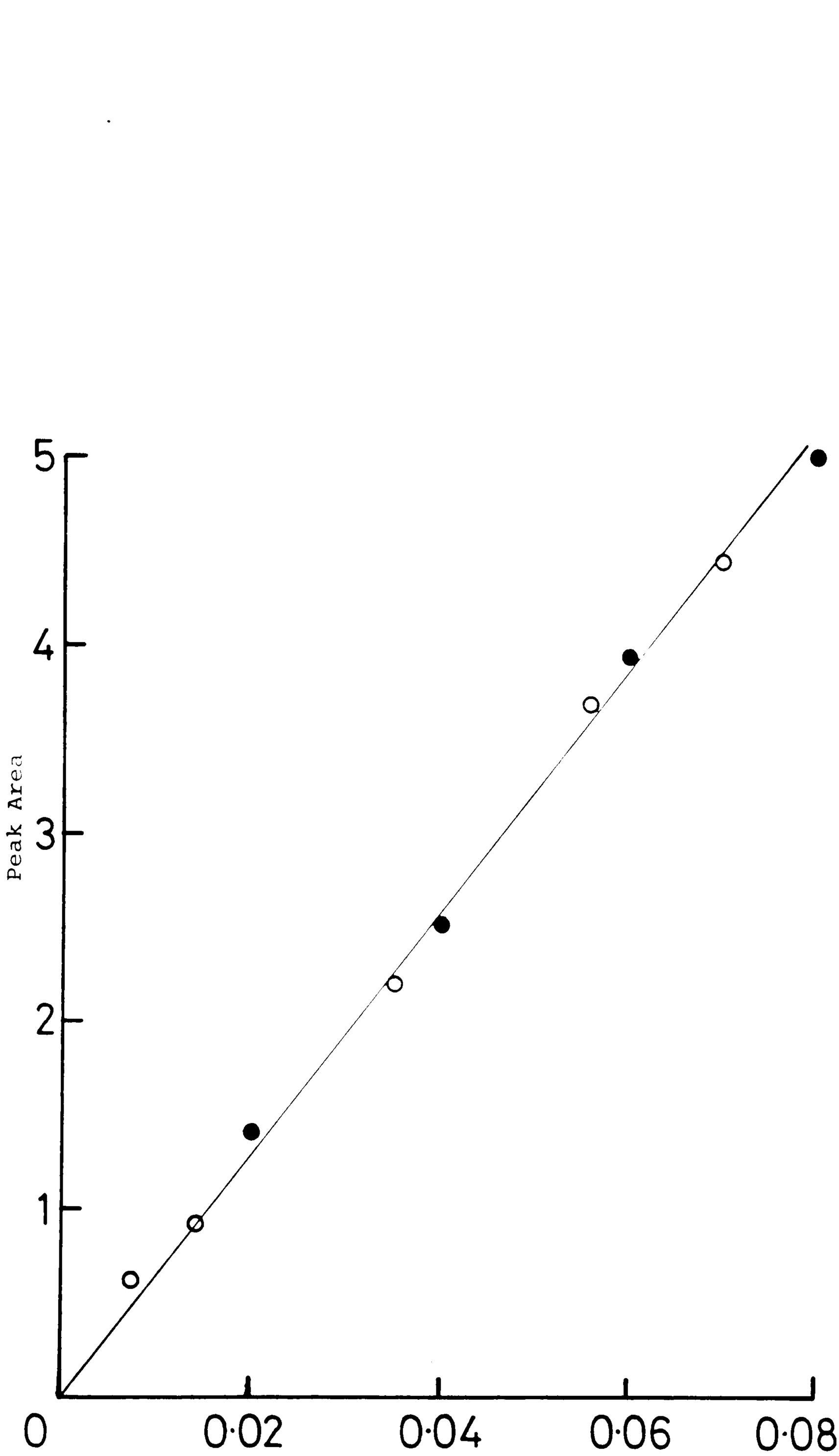

Figure 37: Calibration plot for GC analysis of n-decane in chloroform solution (O), in chloroform-extracted solution (●), 0.1 µl sample.

Chapter Three

Results

3.1 The Adsorption of Sodium Dodecylbenzenesulphonate Isomers, and CTAB, at the Air-Solution Interface

In order to distinguish which of the alkylbenzenesulphonate isomers would be most suited for application to the present work, the adsorption tendencies of the different isomers has been measured, together with that of CTAB for comparison.

The reduction of aqueous surface tension, γ, with increasing surfactant concentration, m_D, for p-1, 4- and 6-phenyl C_{12} ABS surfactants, together with CTAB, is shown in Figure 38.

The change in surface tension is related to the bulk concentration of surfactant by the Gibbs equation:

$$-d\gamma = 2.303y\ RT\ \Gamma_D\ d(\log m_D) \qquad (3.1)$$

in which, $y = 1 + \dfrac{m_D}{m_D + C_{m_S}}$

where, C_{m_S} = the concentration of NaCl/mol dm^{-3},

Γ_D = the surface excess concentration of surfactant ion relative to a Gibbs dividing surface, such that Γ_{H_2O} = 0/mol m^{-2}

The quantity, Γ_D, is effectively equal to $\dfrac{1}{A_s N_A}$

where, A_s = area occupied/surfactant molecule at the interface/ m^2 molecule^{-1}

Values of Γ_D, A_s, and the surfactant critical micelle concentrations, obtained from the data of Figure 38, are given in Table 5(a) from which it can be seen that these quantities vary according to the surfactant structure, thus allowing

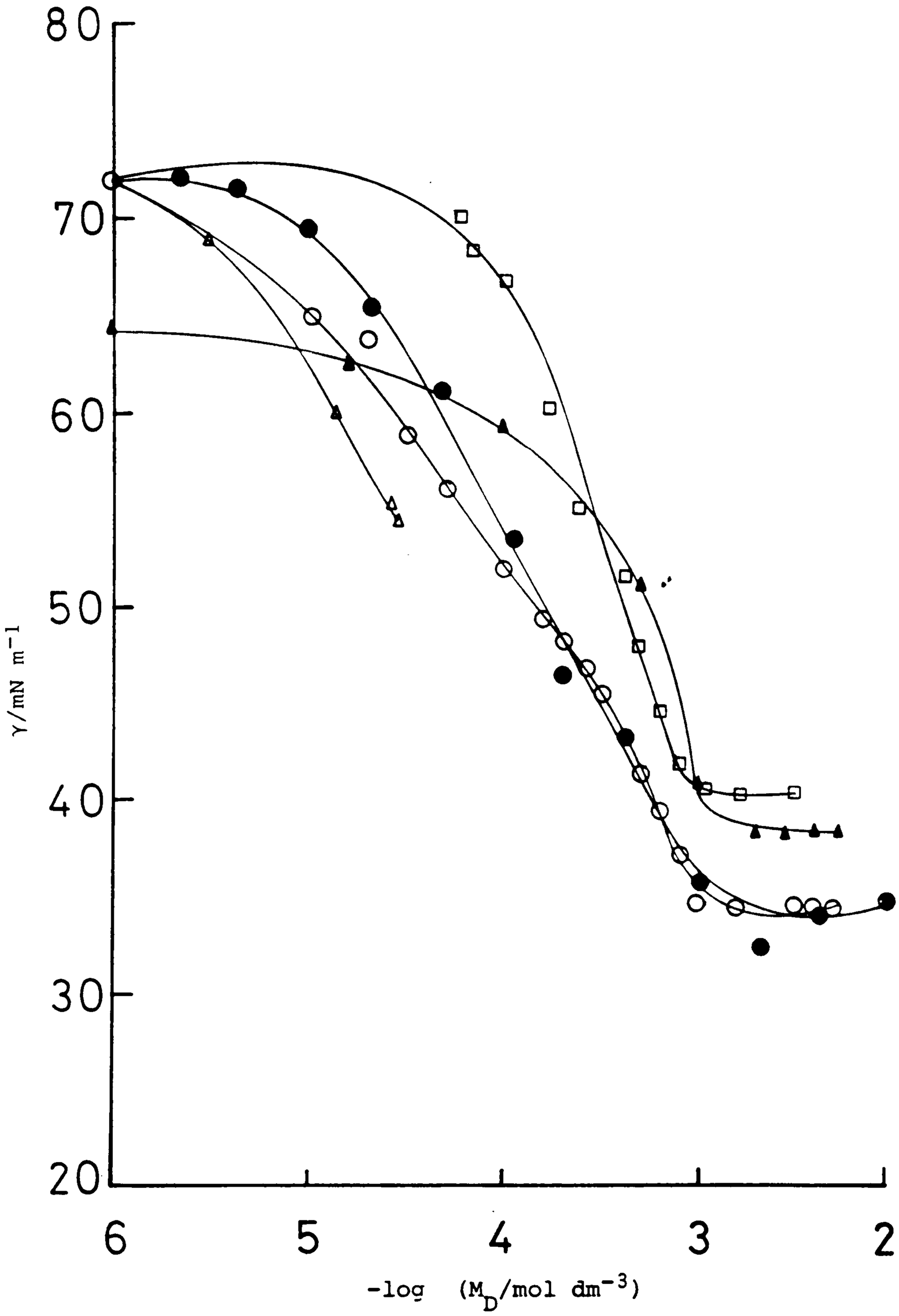

Figure 38: Surface tension (γ) for the air-aqueous solution interface, at 25°C, as a function of 1-ϕ-C_{12} ABS (Δ), 4-ϕ-C_{12} ABS (O), 6-ϕ-C_{12} ABS (●), and CTAB (□) concentrations; and of 1-ϕ-C_{12} ABS at 70°C (▲)

Table 5(a). Effectiveness of adsorption, Γ_D, area/molecule at surface saturation, A_s, and critical micelle concentrations of surfactants at the air/aqueous solution interface.

Surfactant	Temperature / °C	Γ_D / 10^{-6} mol m^{-2}	A_s / nm^2	CMC / 10^{-3} mol dm^{-3}	Ref
p-1-ϕ-C_{12} ABS	25	2.0	0.83	-	This work
p-1-ϕ-C_{12} ABS	70	2.33	0.71	1.26	This work
p-1-ϕ-C_{12} ABS	70	3.7	0.45	1.23	L1
p-4-ϕ-C_{12} ABS	25	1.9	0.87	1.00	This work
p-6-ϕ-C_{12} ABS	25	1.58	1.05	1.06	This work
CTAB	25	2.78	0.60	0.94	This work
CTAB	25	-	-	0.92	M3

quantitative estimates to be made of the surfactant behaviour.

Comparisons of the surfactant behaviour have been made by consideration of their effectiveness of adsorption (π_{cmc}) and their efficiency of adsorption ($pM_D(20)$ [R2]. These terms are fully defined in the discussion. Section 4.1 (p.210) Table 5(b) shows the determined values of these parameters, as obtained from the data of Figure 38.

3.1.1 The Effect of Sodium Chloride on the Adsorption of 4-ϕ-C_{12} ABS and CTAB at the Air/Water Interface

Surface tensions, γ, measured at 25°C, as a function of 4-ϕ-C_{12} ABS concentration, m_D, at various salt concentrations, m_s, are shown in Figure 39. The surfactant critical micelle concentration, its surface excess concentration, and the area per molecule at the interface, calculated from the data of Figure 39, are given in Table 6.

The variation of γ with CTAB, under differing conditions of salt concentration, is shown in Figure 40, and the calculated parameters from these data are given in Table 7.

Comparison of the results of Figures 39 and 40 show that for a given surfactant concentration, under the same conditions of sodium chloride, the anionic surfactant, 4-ϕ-C_{12} ABS, causes a greater reduction in the surface tension than the cationic material, a result which reflects the differences in structure of these surfactants (see discussion, Section 4.1).

Table 5(b). Effectiveness, π_{CMC} and efficiency, $pM_D(20)$ of surface tension reduction of surfactants at the air/aqueous solution interface.

Surfactant	Temperature / °C	π_{CMC} / mN m^{-1}		$pM_D(20)$ / mol dm^{-3}	Ref.
		Experimental	Calculated		
p-1-ϕ-C_{12} ABS	25	17.9	-	4.55	This work
p-1-ϕ-C_{12} ABS	70	26.0	26.1	3.1	This work
p-1-ϕ-C_{12} ABS	70	25.8	25.5	3.1	L1
p-4-ϕ-C_{12} ABS	25	37.5	39.5	4.0	This work
p-6-ϕ-C_{12} ABS	25	37.0	38.0	3.9	This work
CTAB	25	31.5	31.8	3.4	This work

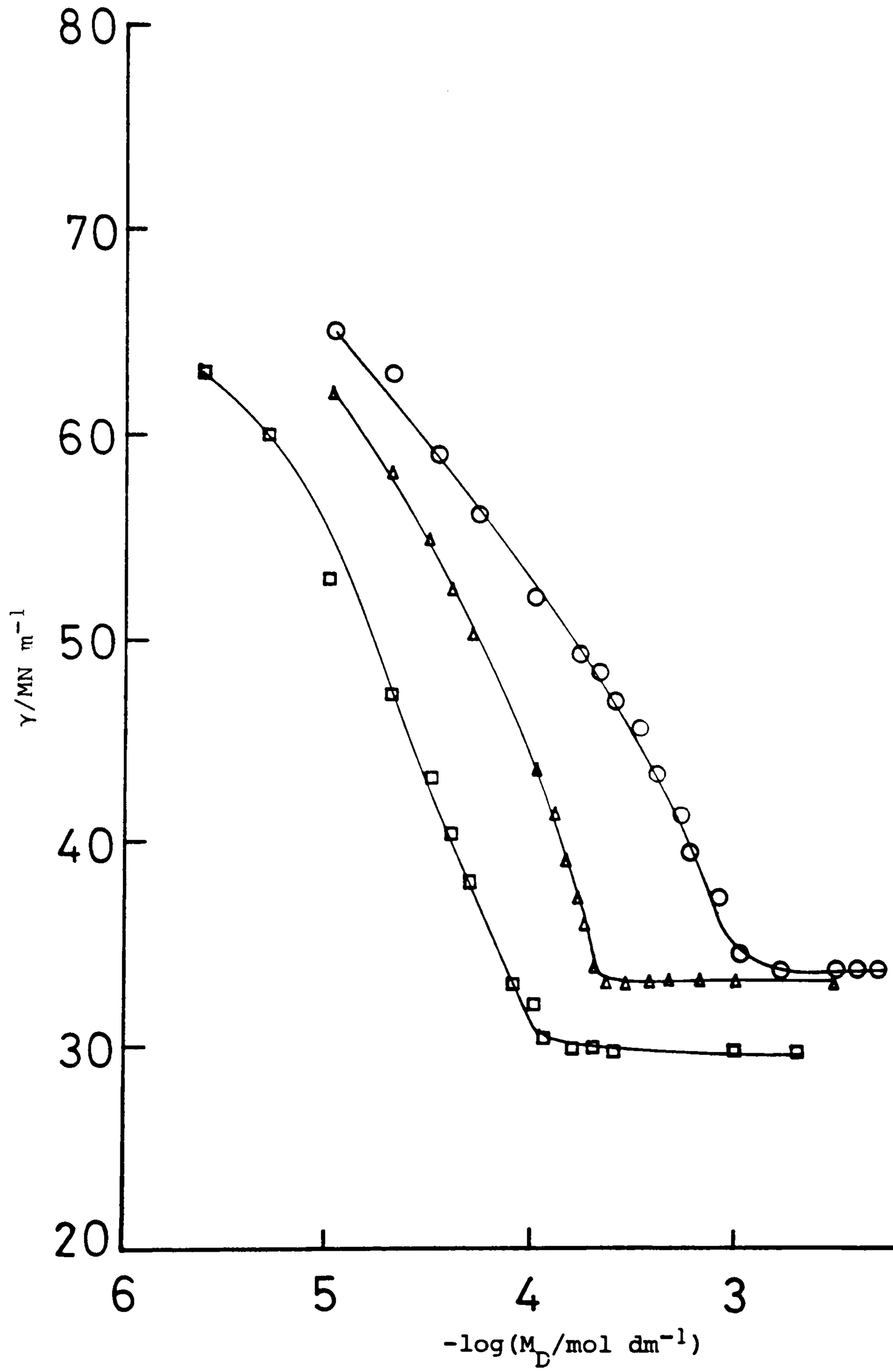

Figure 39: Surface tensions for the air-aqueous NaCl interface at 25°C as a function of 4-ϕ-C_{12} ABS concentration. NaCl concentrations of 0.00 (○), 0.01 (△), and 0.10 (□) mol dm^{-1}

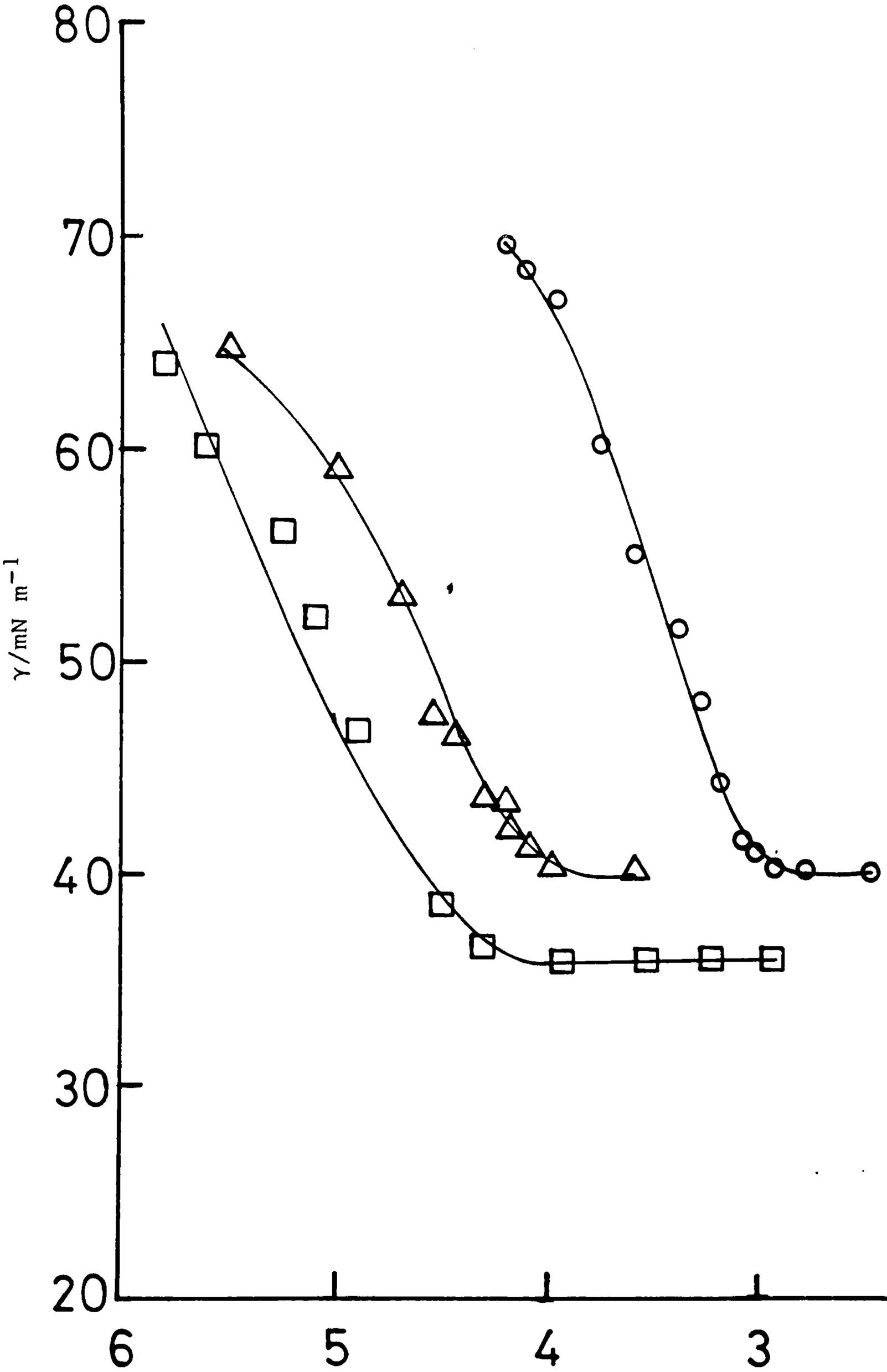

Figure 40: Surface tensions for the air-aqueous NaCl interface at 25°C as a function of CTAB concentration. NaCl concentrations of 0.00 (○), 0.10 (△), and 0.50 (□) mol dm^{-3}

Table 6. Values of Γ_D, A_s, CMC, $pM_D(20)$ and π_{CMC}, in saturated films of 4-ϕ-C_{12} ABS at the air-aqueous NaCl interface at 25°C.

M_s / mol dm^{-1}	Γ_D / 10^{-6} mol m^{-2}	A_s / nm^2	CMC / 10^{-3} mol dm^{-3}	$pM_D(20)$ / mol dm^{-3}	π_{CMC} / mN m^{-1}	
					Exptl.	Solid
0.00	1.9	0.87	1.0	4.0	37.5	39.5
0.01	4.77	0.35	0.22	4.35	38.5	38.8
0.10	5.03	0.33	0.11	4.95	42.0	48.4

Table 7. Values of Γ_D, A_s, CMC, $pM_D(20)$, and π_{CMC}, in saturated films of CTAB at the air-aqueous NaCl interface at 25°C.

M_s / mol dm^{-1}	Γ_D / 10^{-6} mol m^{-2}	A_s / nm	CMC / 10^{-4} mol dm^{-3}	$pM_D(20)$ / mol dm^{-3}	π_{CMC} / mN m^{-1}	
					Exptl.	Solid
0.00	2.78	0.60	9.4	3.42	31.6	32.0
0.10	3.5	0.47	0.73	4.7	32.0	31.9
0.50	3.86	0.43	0.40	5.2	37.8	37.7

3.1.2 The Effect of pH on 4-ϕ-C_{12} ABS and CTAB Adsorption at the Air/Aqueous Solution Interface

The reduction in surface tension of 0.1 mol dm^{-3} NaCl solutions, produced at 25°C, with increasing concentration of 4-ϕ-C_{12} ABS and CTAB, are shown in Figures 41 and 42 respectively.

Tables 8 and 9 give the determined CMC's, Γ_D, π_{CMC}, and $pM_D(20)$ derived from the data in these figures.

Figure 43 and Table 10 show results for the reduction in surface tension produced by CTAB in the absence of added salt.

From the results it can be seen that varying the solution pH has little effect on the surfactant adsorption, or surface tension reduction. A slight decrease in the CMC, and increase in Γ_D, for 4-ϕ-C_{12} ABS can be seen in Table 8 with an increase in pH to 12.0. This is probably a consequence of a high concentration of Na^+ in solution, produced through the addition of NaOH.

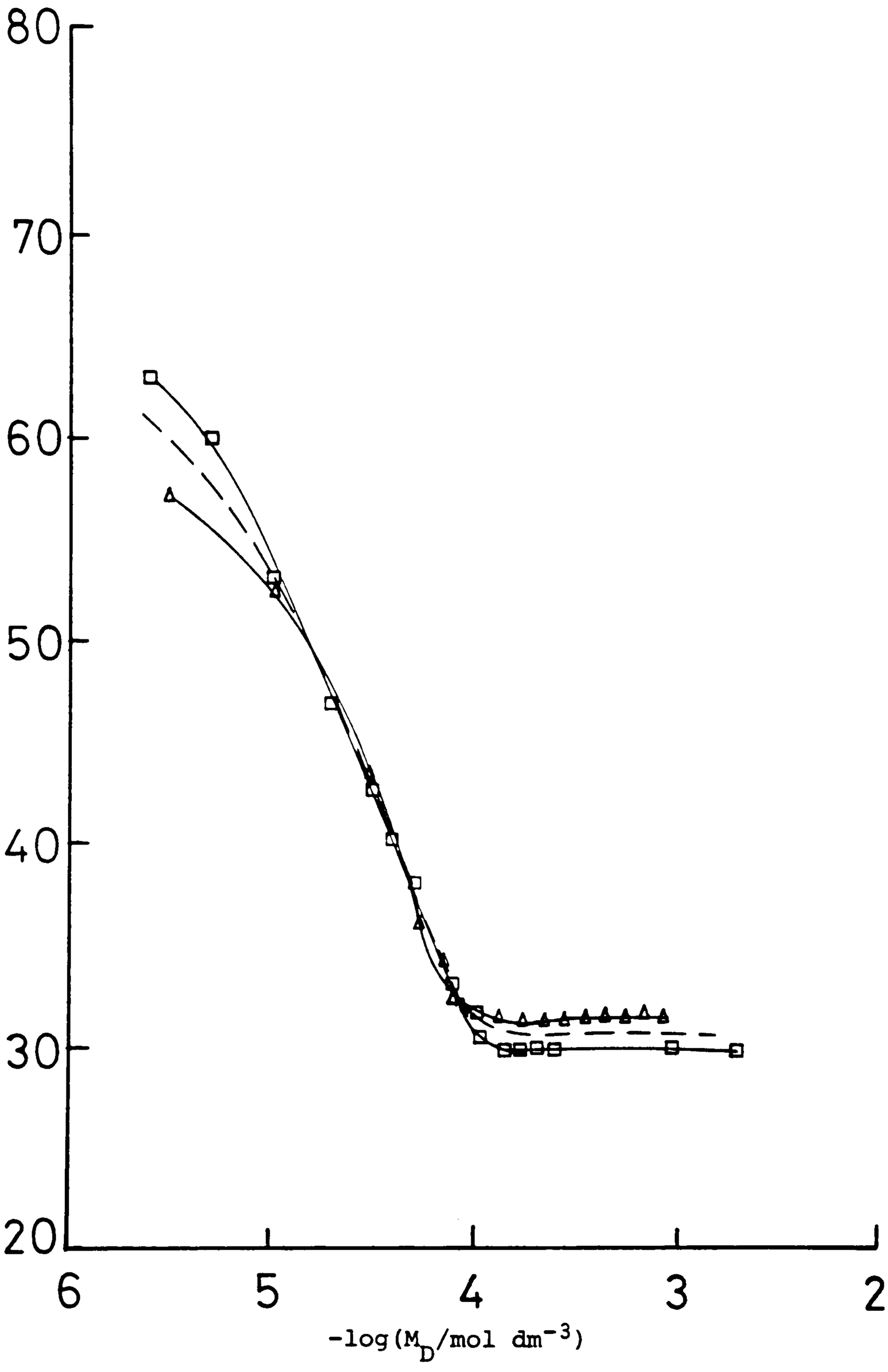

Figure 41: Surface tensions for the air-aqueous NaCl interface (0.10 mol dm^{-3} NaCl), at 25°C, as a function of 4-ϕ-C_{12} ABS concentration, at solution pHs of 1.8 (Δ), 6.0 (□), and 12.0 (-).

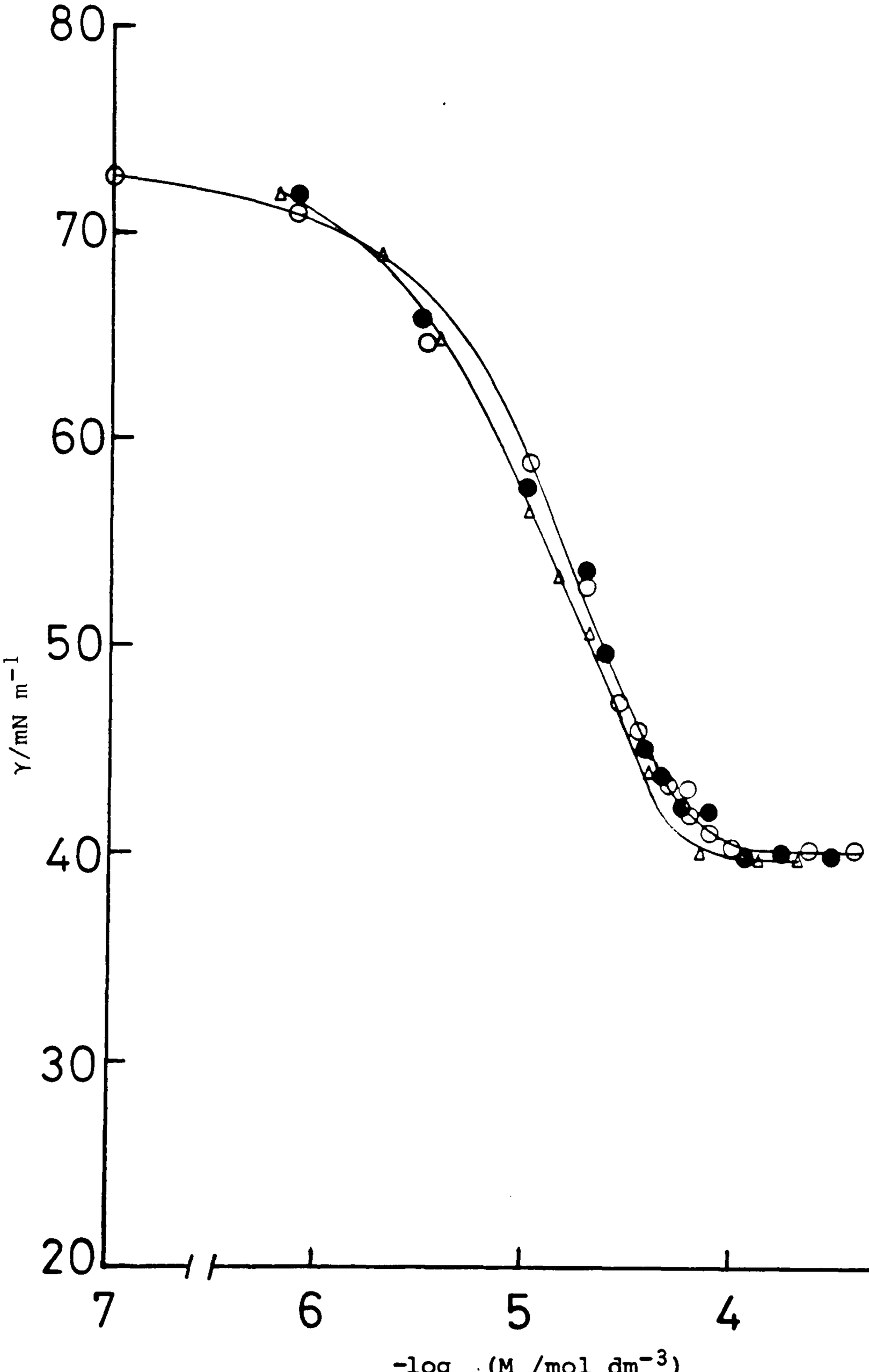

Figure 42: Surface tensions for the air-aqueous NaCl interface (0.10 mol dm^{-3} NaCl), at 25°C, as a function of CTAB concentration, at solution pHs of 3.0 (Δ), 6.0 (O) and 11.0 (●).

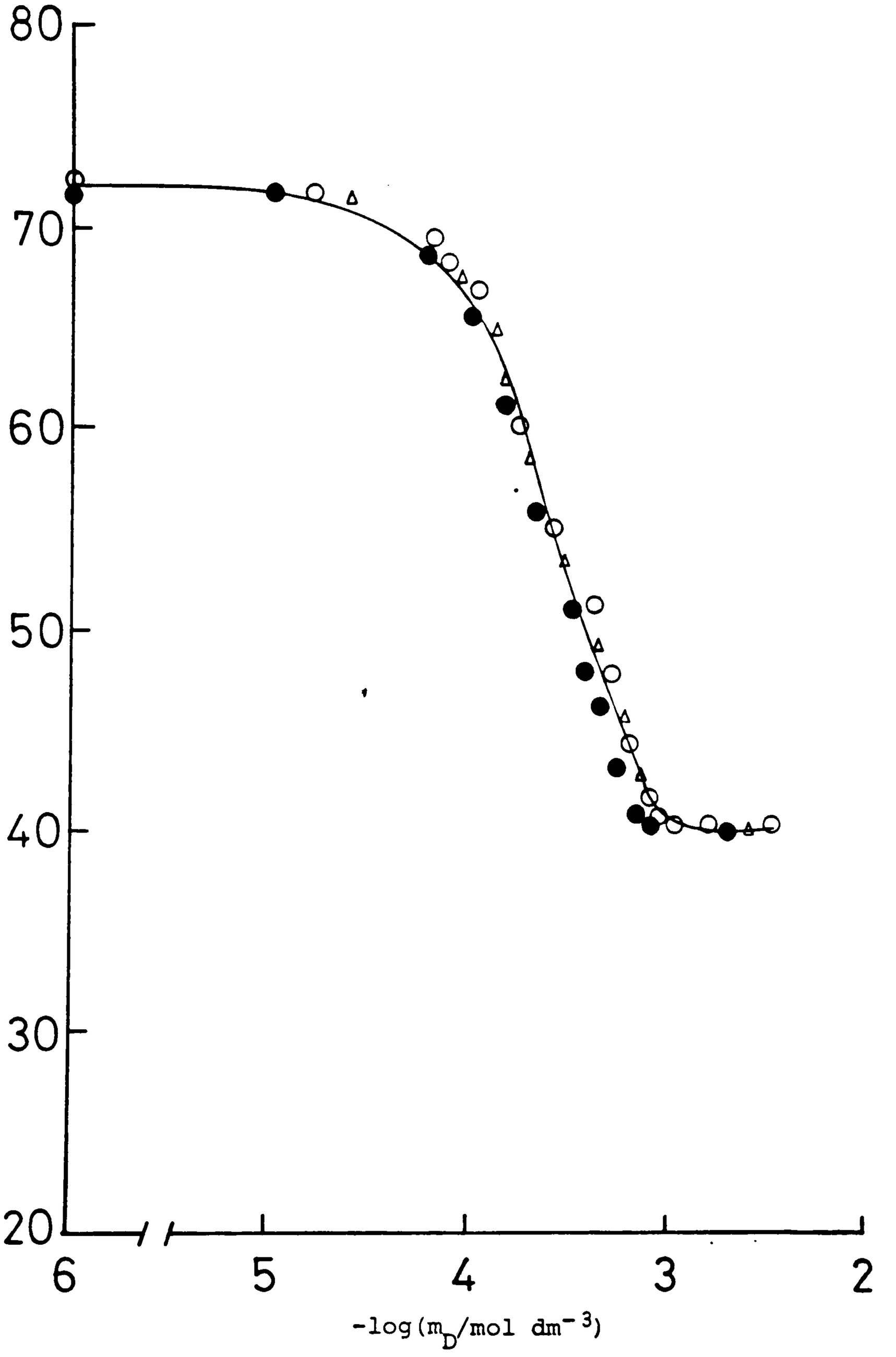

Figure 43: Surface tensions for the air-aqueous solution interface, at 25°C, as a function of CTAB concentration, at solution pHs of 2.0 (Δ), 6.0 (O) and 11.0 (●).

Table 8. Effect of solution pH on values of Γ_D, A_s, CMC, $pM_D(20)$ and π_{CMC}, at 25°C, in saturated films of 4-ϕ-C_{12}ABS at the air-aqueous NaCl (0.1 mol dm^{-3}) interface.

pH	Γ_D / 10^{-6} mol m^{-2}	A_s / nm^2	CMC / 10^{-3} mol dm^{-3}	$pM_D(20)$ / mol dm^{-3}	π_{CMC} / mN m^{-1}	
					Exptl.	Cal'd
1.8	4.63	0.36	0.11	5.0	40.5	45.2
6.0	5.03	0.33	0.11	4.95	42.0	48.4
12.0	5.24	0.32	0.09	5.00	41.0	48.5

Tables 9 and 10. Effect of solution pH on values of Γ_D, A_s, CMC, $pM_D(20)$ and π_{CMC}, at 25°C, in saturated films of CTAB at (9) the air-aqueous NaCl (0.10 mol dm^{-1}) interface, and (10) at the air-aqueous solution interface.

pH	Γ_D / 10^{-6} mol m^{-2}	A_s / nm^2	CMC / 10^{-4} mol dm^{-3}	$pM_D(20)$ / mol dm^{-3}	π_{CMC} / mN m^{-1}	
					Exptl.	Cal'd
3.61	3.61	0.46	0.71	4.78	31.9	32.9
6.0	3.5	0.47	0.73	4.7	32.0	31.9
11.0	3.51	0.47	0.73	4.7	32.0	31.3

Table 10.

pH	Γ_D / 10^{-6} mol m^{-2}	A_s / nm^2	CMC / 10^{-4} mol dm^{-3}	$pM_D(20)$ / mol dm^{-3}	π_{CMC} / mN m^{-1}	
					Exptl.	Cal'd
3.0	2.72	0.81	7.3	3.5	31.7	31.3
6.0	2.78	0.60	9.4	3.42	31.6	32.0
11.0	2.78	0.60	9.2	3.48	31.6	34.1

3.1.3 The Effect of n-Butanol on the Adsorption of 4-ϕ-C_{12} ABS at the Air-Aqueous Interface

The reduction in aqueous (0.10 mol dm^{-3} NaCl) surface tensions with concentration of 4-ϕ-C_{12} ABS, at 25°C, for various n-butanol concentrations, and that for butanol alone, are shown in Figure 44 and 45 respectively. Tables 11 and 12 show the calculated adsorption parameters, and Figure 46 shows the depression in the surfactant CMC produced by alcohol addition.

From the results of surfactant adsorption (Figure 44 and Table 11) it can be seen that both Γ_D, and the CMC, are reduced as alcohol is added to the solution. Table 11 also shows that alcohol has little effect on the surface pressure, π_{CMC}, produced by the surfactant. Values of $pM_D(20)$ for the alcohol/surfactant system have not been calculated, since the addition of alcohol alone is sufficient to lower the aqueous tension by 20 mN m^{-1} (Figure 45).

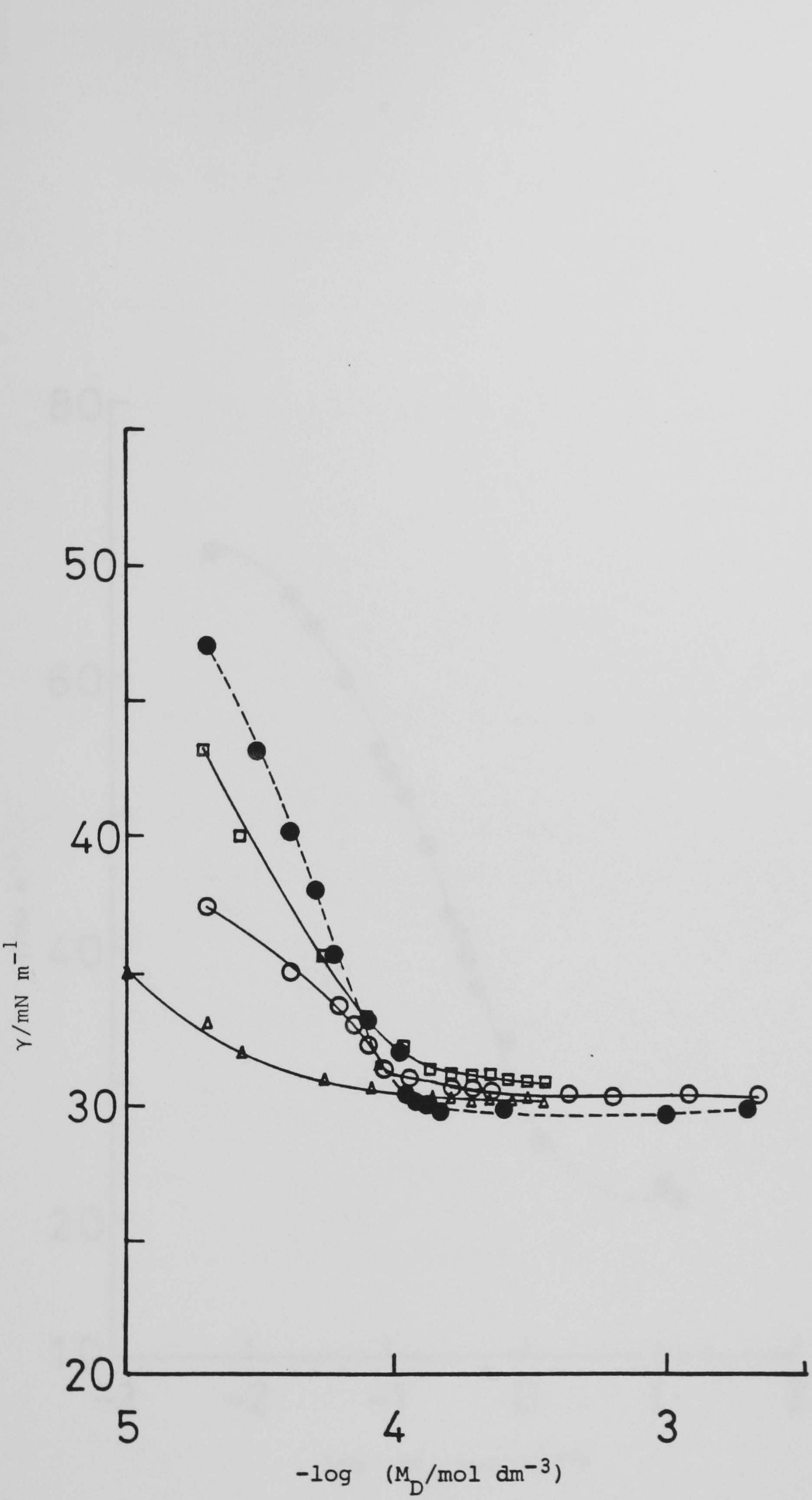

Figure 44: Effect of added n-butanol on the surface tension, at 25°C, of 4-ϕ-C_{12} ABS aqueous NaCl (0.1 mol dm^{-3}) solutions. n-butanol = 0 (●), 0.11 (□), 0.33 (○), 0.55 (▲) mol dm^{-3}.

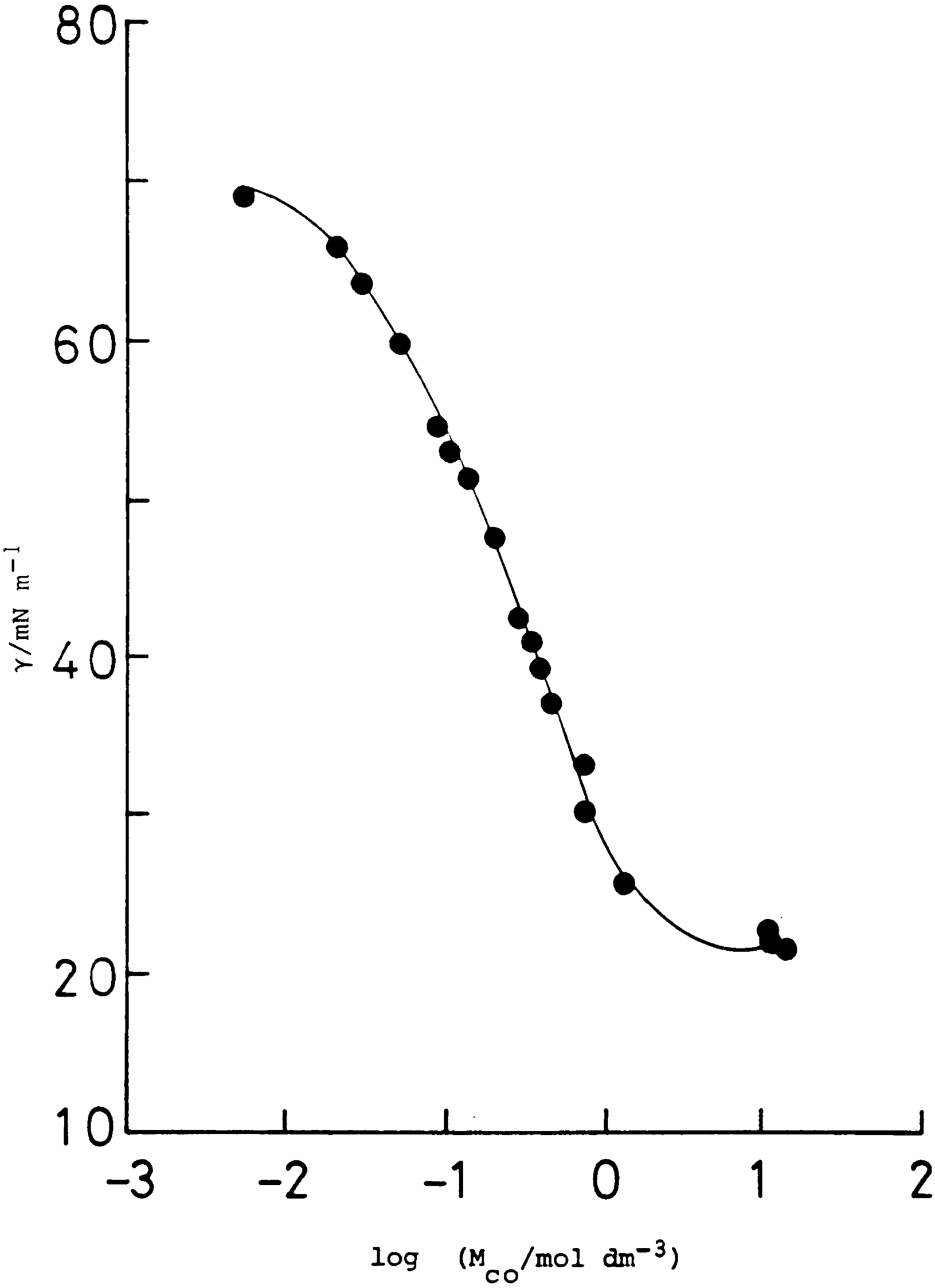

Figure 45: Variation of surface tension of 0.1 mol dm^{-3} NaCl solution with added n-butanol. T = 25°C.

Table 11. Values of Γ_D, A_s, CMC, $pM_D(20)$, and π_{CMC}, in saturated films of 4-ϕ-C_{12} ABS at the air-aqueous (0.1 mol dm^{-3} NaCl) butanol interface, at 25°C.

M_{co} / mol dm^{-3}	Γ_D / 10^{-6} mol m^{-2}	A_s / nm^2	CMC / 10^{-4} mol dm^{-3}	$pM_D(20)$ / mol dm^{-3}	π_{CMC} / mN m^{-1}	
					Exptl.	Cal'd
0.00	5.03	0.33	1.12	4.95	42.0	42.4
0.11	2.44	0.68	1.12	4.1	40.0	40.4
0.33	2.1	0.79	0.99	-	41.0	-
0.55	1.08	1.53	0.55	-	41.5	-

Table 12. Values of Γ_{co}, $pM_D(20)$ and π_{CMC}, in saturated films of n-butanol at the air-aqueous NaCl (0.1 mol dm^{-3}) interface, at 25°C.

Γ_{co} / 10^{-6} mol m^{-2}	A_s / nm^2	$pM_D(20)$ / mol dm^{-3}	π_{CMC} / mN m^{-1}	
			Exptl.	Cal'd
6.39	0.26	0.8	44.2	45.5

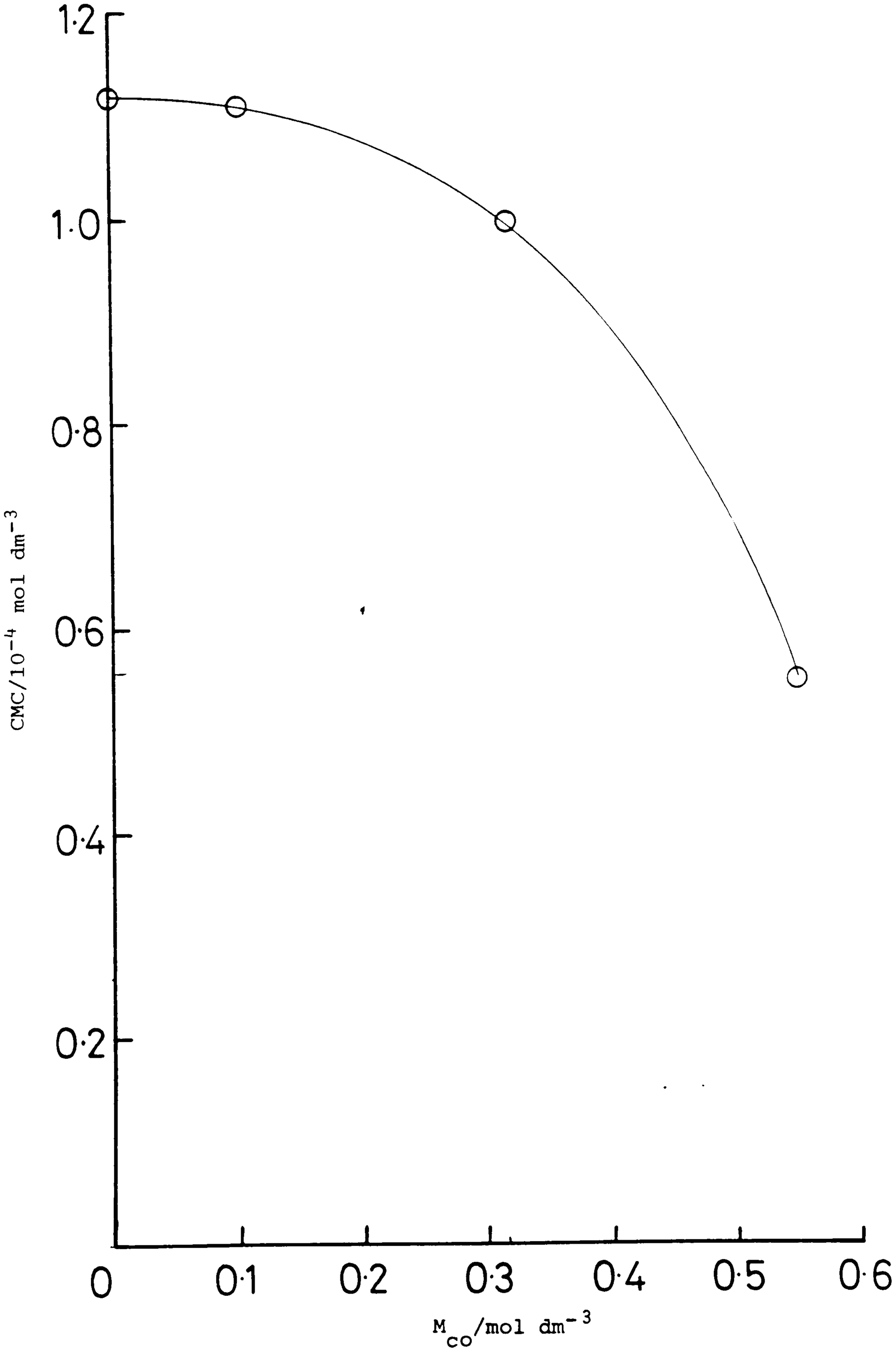

Figure 46: Effect of added n-butanol on the Critical Micelle Concentration of 4-ϕ-C_{12} ABS in 0.1 mol dm^{-3} NaCl solution. T = 25°C.

3.1.4 Determination of n-Butanol Solubility in Aqueous 4-ϕ-C_{12} ABS Solutions

In view of the effects of n-butanol addition on 4-ϕ-C_{12} ABS adsorption at the air-aqueous interface, an investigation was carried out to explain further why this behaviour should occur. The amount of n-butanol which could be solubilised, by 4-ϕ-C_{12} ABS, in water was determined visually by titrating the sample solution with the alcohol.

The solubility limit was taken as the point at which the solution became turbid.

The results are shown in Figure 47 by the solubility of n-butanol (mol dm^{-3}), in the aqueous system, as a function of the concentration of 4-ϕ-C_{12} ABS micelles, M_D^m, in solution, determined using:

$$\text{Concentration of 4-}\phi\text{-}C_{12}\text{ ABS micelles, } M_D^m = (M_D^t - \text{CMC}) \text{ in mol dm}^{-3}$$

where, M_D^t = the total surfactant concentration/mol dm^{-3}

CMC = the surfactant critical micelle concentration/ mol dm^{-3}.

The results show that as the concentration of surfactant micelles in solution increases, the amount of alcohol dissolved increases linearly. Thus, n-butanol-surfactant micelle interactions are apparent.

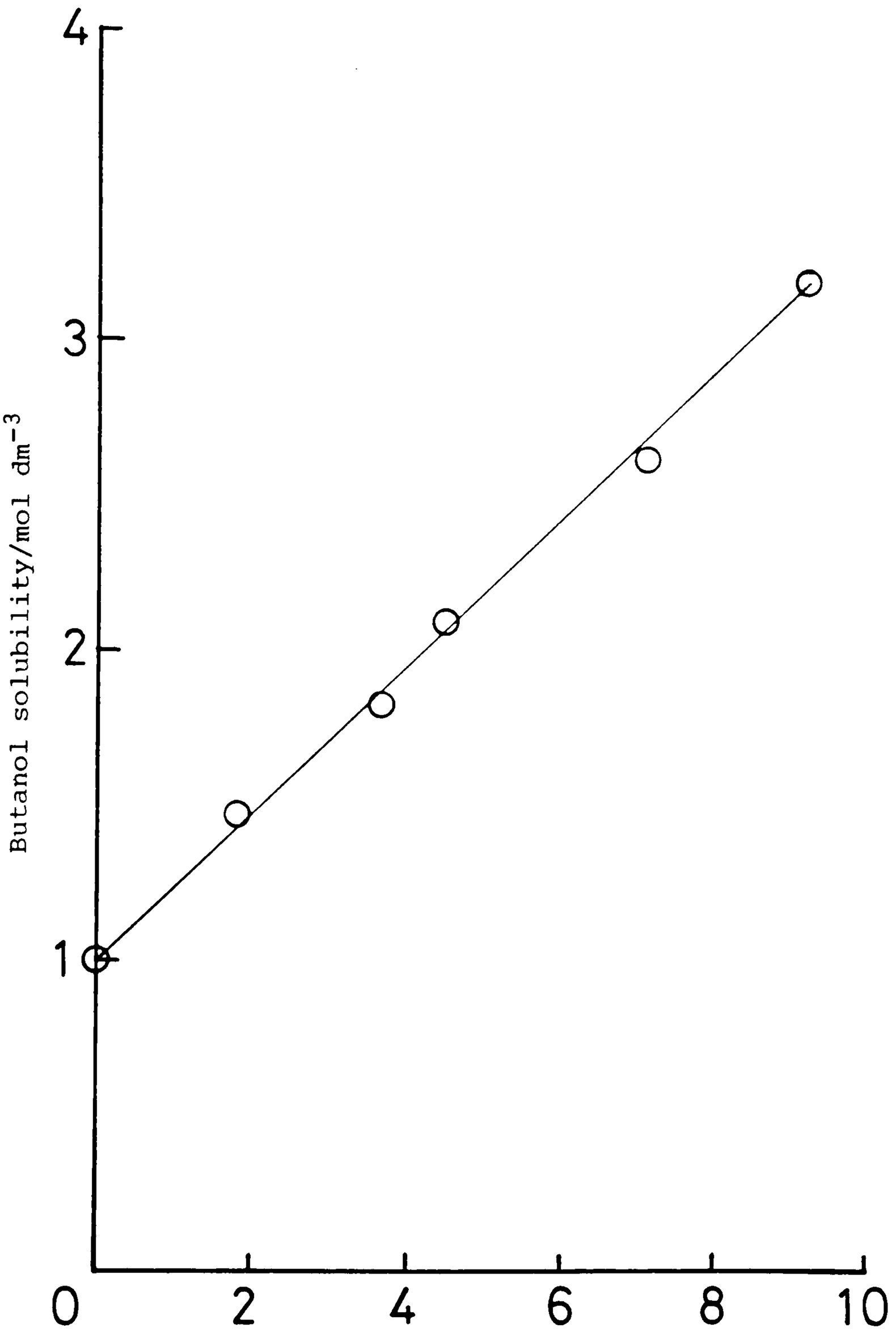

Figure 47: Partition coefficient determination, K_{eq} for n-butanol between 4-ϕ-C_{12} ABS micelles and aqueous solution

3.2 Adsorption of 4-ϕ-C_{12} ABS at the n-decane-aqueous Solution Interface

3.2.1 Effect of Sodium Chloride on 4-ϕ-C_{12} ABS Adsorption at the n-decane-aqueous Solution Interface

In order that the surfactant (4-ϕ-C_{12} ABS) behaviour in the three-phase flooding system be completely understood [L1], it was necessary to determine its adsorption at the oil-water interface under various solution conditions. Interfacial tensions, γ_i, obtained at 25°C as a function of 4-ϕ-C_{12} ABS concentration, M_D, for various salt concentrations, M_s, in the n-decane/water system are shown in Figure 48.

The tensions are not ultralow, ranging from 5 mN m^{-1} in the absence of salt, to 1 mM m^{-1} for salt concentrations up to 0.2 mol dm^{-3}. They do not pass through a minimum (Figure 49). Values of A_s obtained from the data of Figure 49, by use of the Gibbs equation (3.1), are given in Table 13.

Table 13. Values of the area per molecule, A_s, and CMC, in saturated films of 4-phenyl-C_{12} ABS at the decane-aqueous NaCl interface at 25°C

A_s/nm^2 molecule^{-1}	1.14	0.82	0.70	0.71
M_s (NaCl)/mol dm^{-3}	0.00	0.05	0.10	0.20
$\Gamma_D/10^{-6}$ mol m^{-2}	1.46	2.03	2.37	2.34
CMC/10^{-4} mol dm^{-3}	6.31	5.01	2.51	1.26

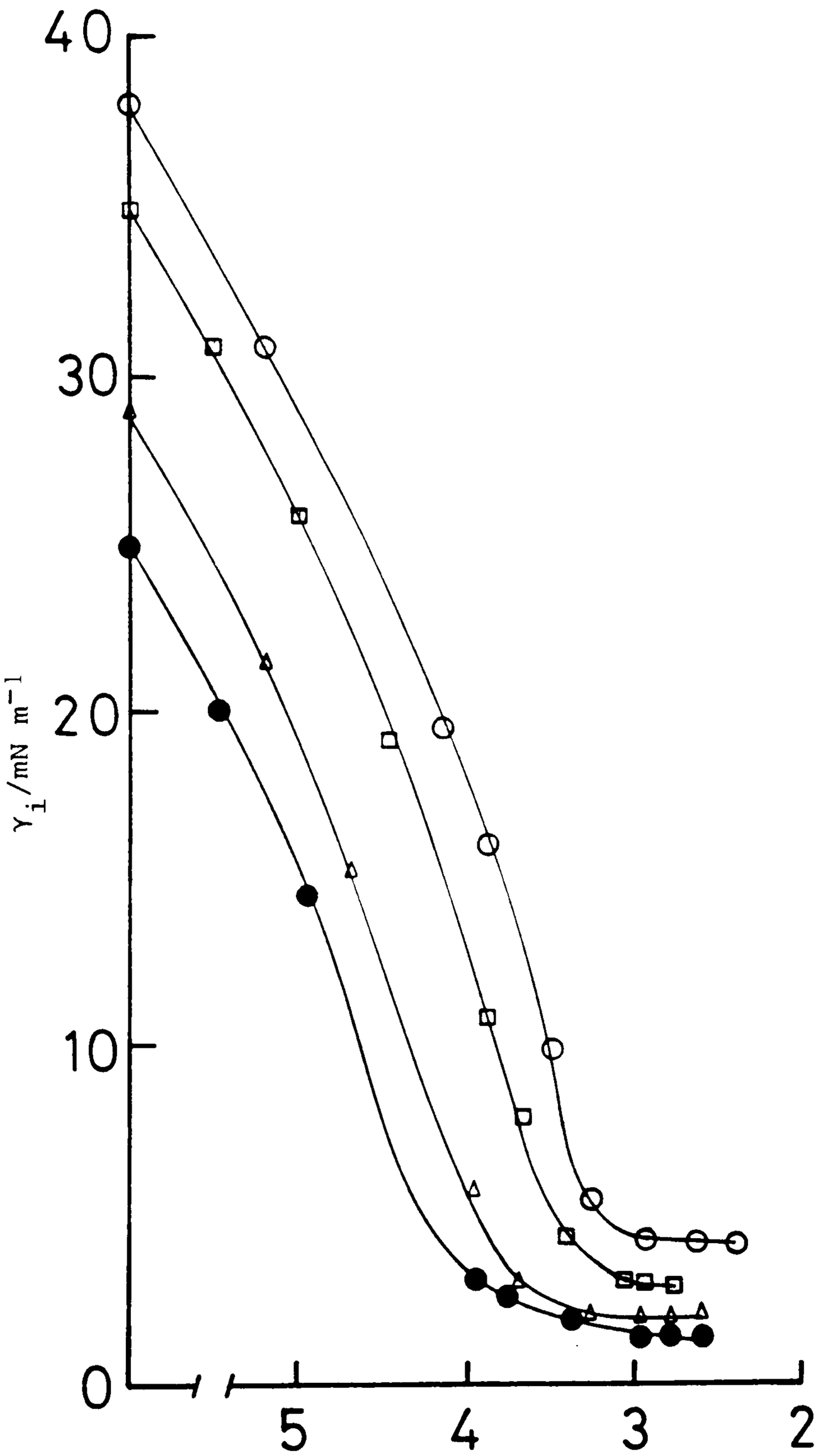

Figure 48: Interfacial tensions, γ_i, for the decane-aqueous NaCl interface at 25°C as a function of 4-ϕ-C_{12} ABS concentration, M_D. Curves are for NaCl concentrations of 0.00 (○), 0.05 (□), 0.10 (△), and 0.20 (●) mol dm^{-3}, respectively.

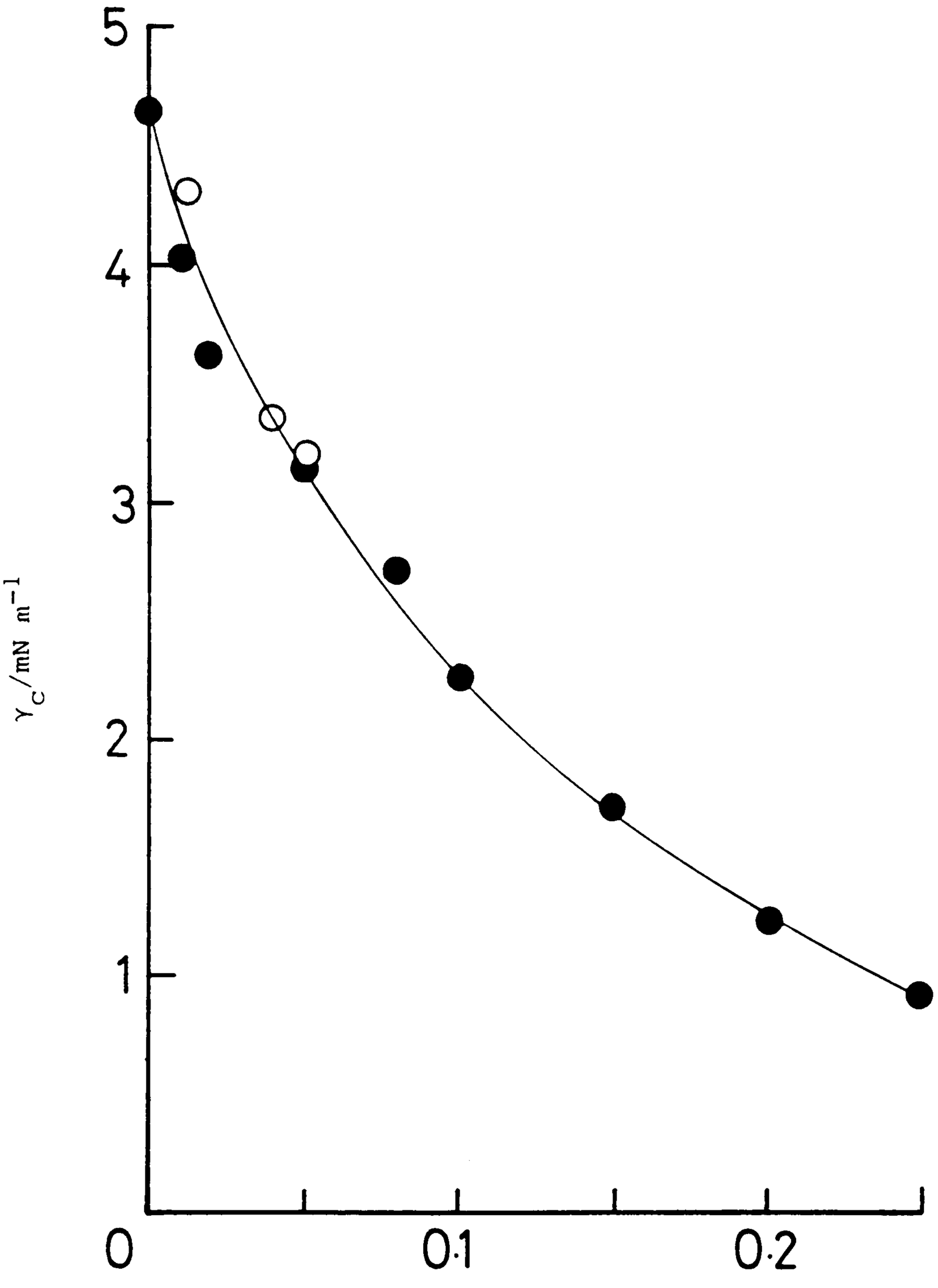

Figure 49: Variation of γ_c with M_{Na} for 4-ϕ-C_{12} ABS in decane-aqueous NaCl systems at 25°C (O), from Figure 48; (●), individual values from separate experiments in which the surfactant concentration was 2.16×10^{-3} mol dm^{-3}.

3.2.2 Effect of n-butanol on 4-ϕ-C_{12} ABS adsorption at the n-decane/aqueous Solution Interface

Figure 50 shows the effect on γ_i, and surfactant distribution, of progressive addition of n-butanol to the n-decane/aqueous system, containing 4-ϕ-C_{12} ABS above its CMC. A minimum in interfacial tension is apparent from these results, occurring at a point where there is marked transfer of the surfactant from the aqueous to the oil-phase.

Figure 51 shows a photograph of the solutions, indicated in Figure 50 by numbering from 1 to 12, from which it is apparent that over a range of alcohol concentrations, ca. 0.1 to 1.1 mol dm^{-3} n-butanol, a stable middle (opaque) phase is formed. The solutions shown in the plate are over three weeks old.

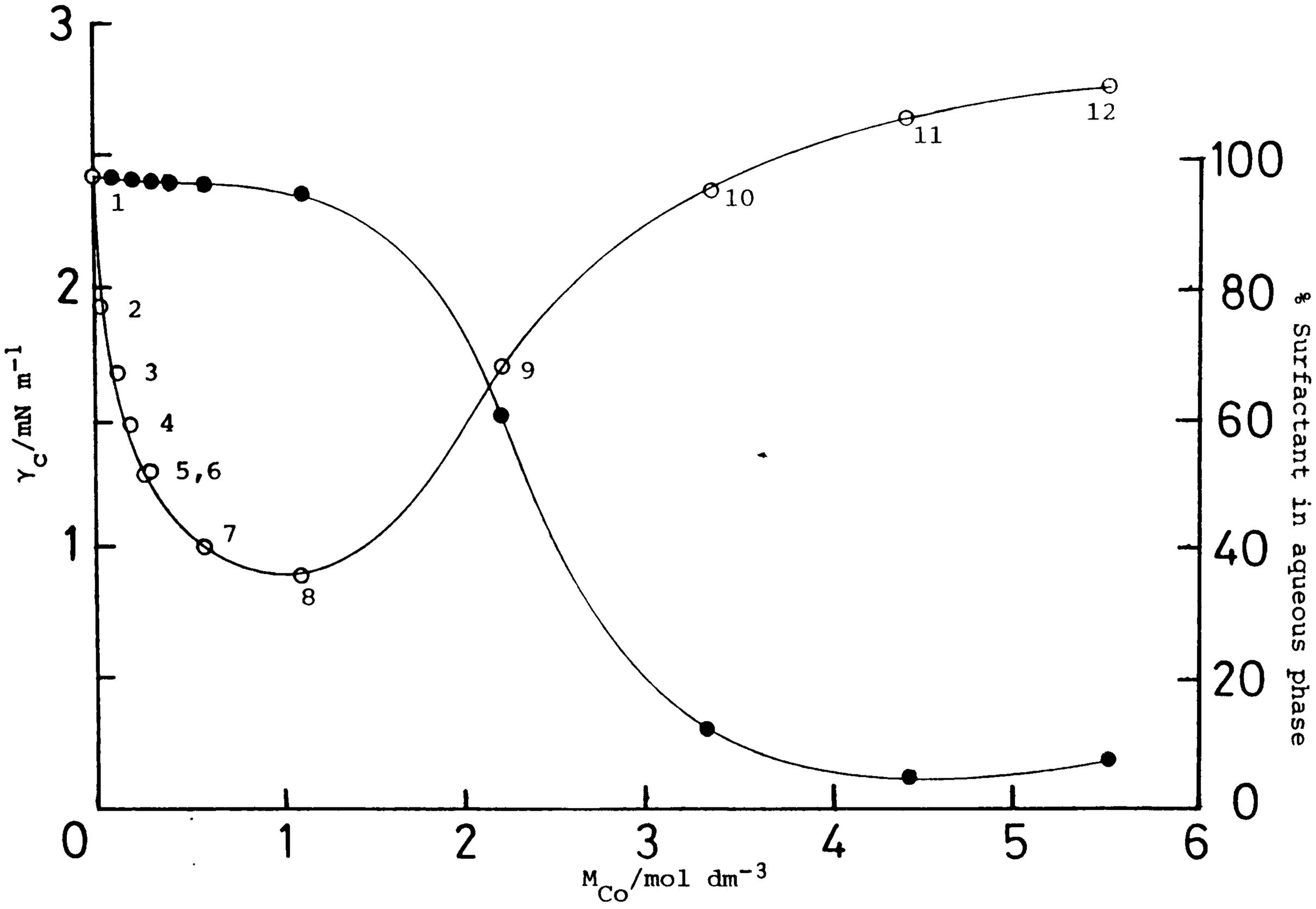

Figure 50: Variation of γ_c with co-surfactant concentration in the system 4-ϕ-C_{12} ABS-decane-aqueous (0.1 mol dm^{-3}) NaCl solution, at 25°C (O), and variation of 4-ϕ-C_{12} ABS aqueous concentration (●). Solution numbers (1-12) refer to plate 51. The initial aqueous-phase concentrations of 4-ϕ-C_{12} ABS was 2.23×10^{-3} mol dm^{-3}.

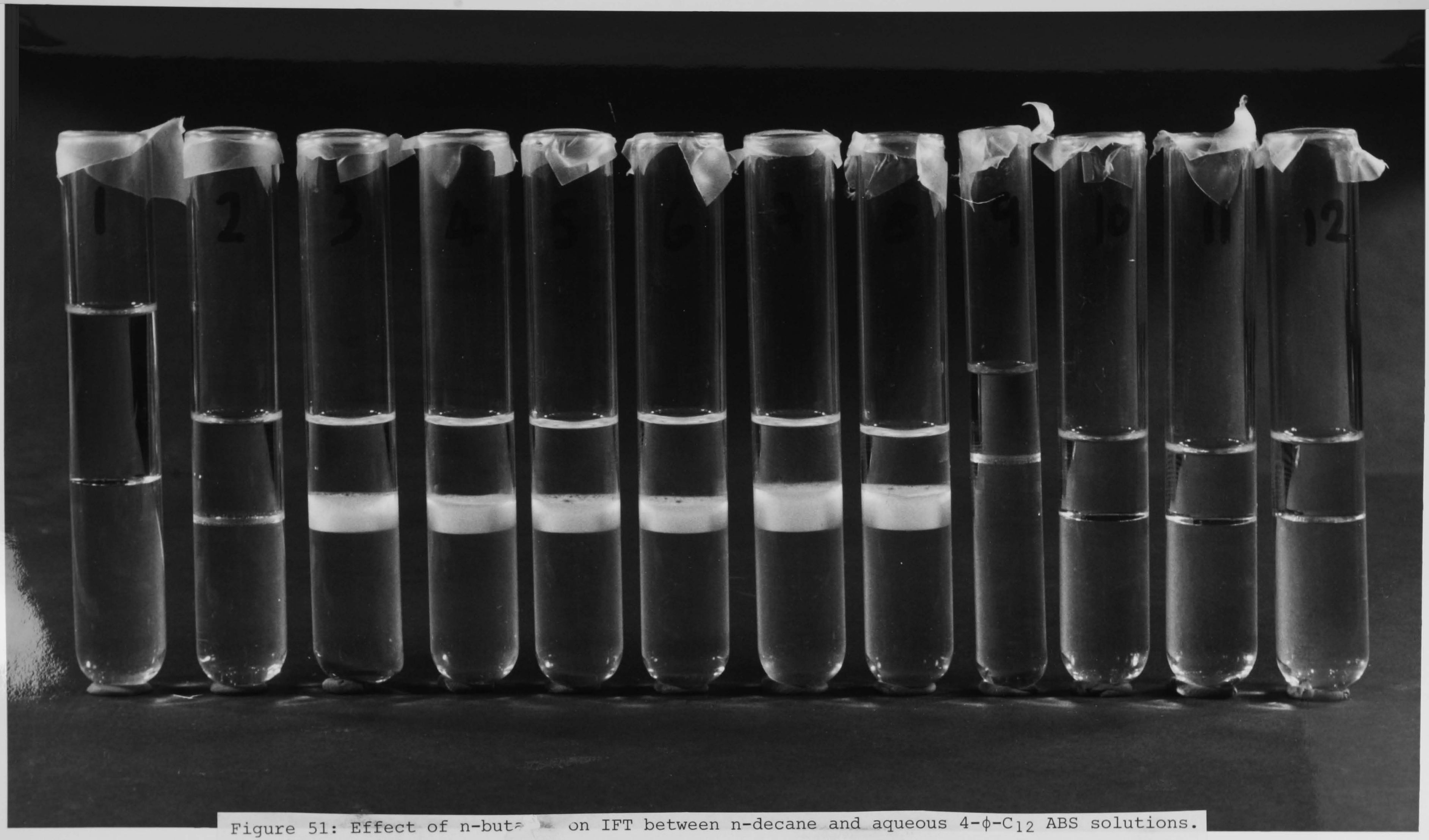

Figure 51: Effect of n-butanol on IFT between n-decane and aqueous 4-ϕ-C_{12} ABS solutions.

Numbers correspond to those of Figure 50.

3.3 Adsorption at the Kaolin-Aqueous Solution Interface

3.3.1 Adsorption of 4-ϕ-C12 ABS

The adsorption, at 25°C, of 4-ϕ-C_{12} ABS onto kaolin from aqueous NaCl solution, with respect to contact time, is shown in Figure 52. From the results, which were obtained at surfactant concentrations above the CMC (viz. 1×10^{-3} mol dm^{-3}) it can be seen that equilibrium is rapid (ca. 1 hour) and that the amount of surfactant adsorbed per unit area decreases from about 0.9×10^{-6} mol m^{-2}, at 10% solids, to about 0.3×10^{-6} mol m^{-2} at 40% solids (w/v). At surfactant concentrations above the CMC, loss from solution (ΔM_D) appears to be independent of the surface area of the adsorbent, Table 14 and Figure 53. It is, however, dependent on surfactant concentration.

Table 14. Effect of increasing solids on change in surfactant concentration/mol dm^{-3} in aqueous solution

% Solids (w/v)	10	20	40
$\Delta M_D/10^{-4}$ mol dm^{-3}	7.43	8.26	8.59

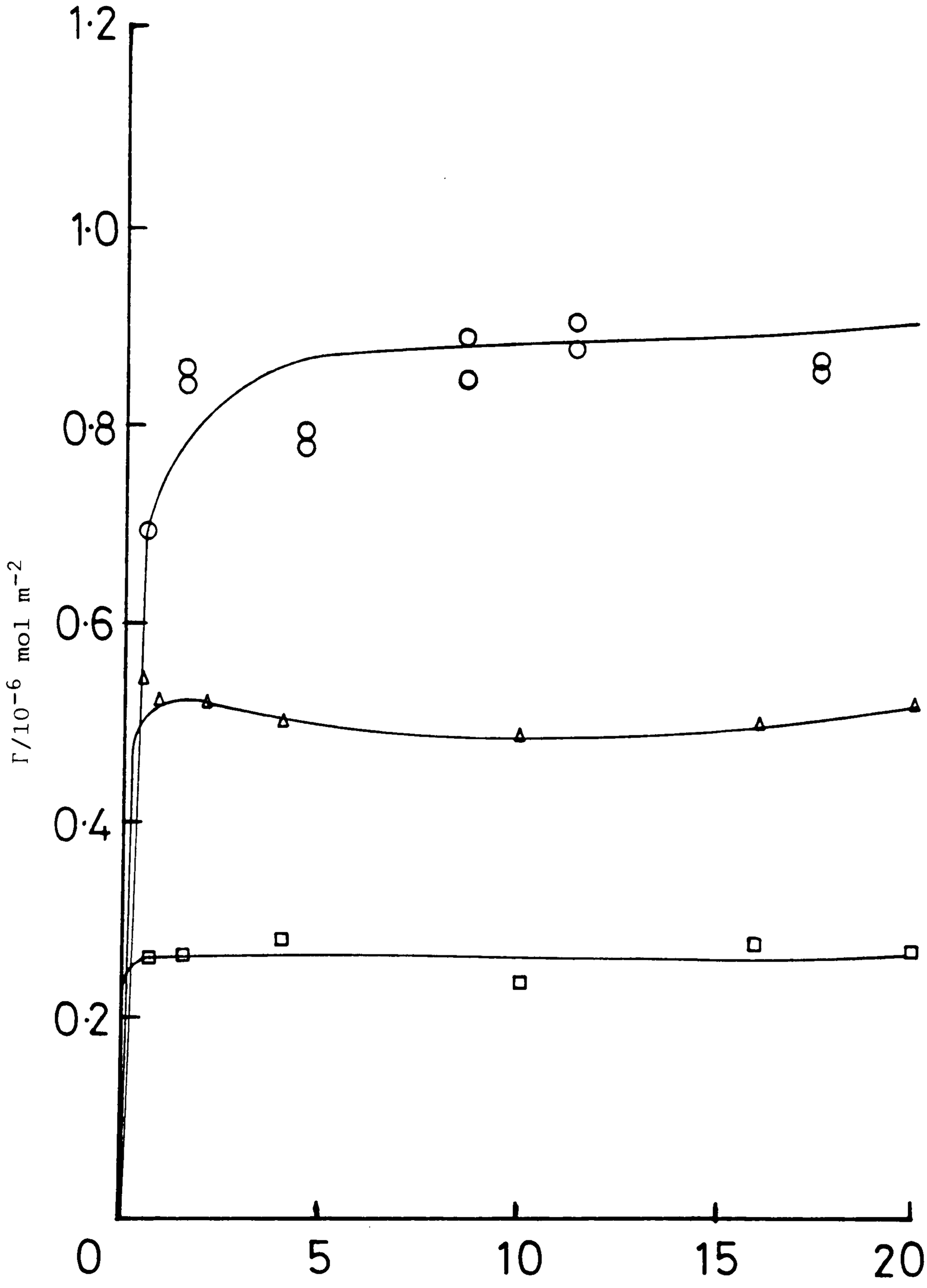

Figure 52: Adsorption of 4-ϕ-C_{12} ABS onto kaolin, at 25°C, from 0.10 mol dm^{-3} NaCl, as a function of time and solid-solution ratio. % solids = 10% (O), 20% (Δ), and 40% (□). Initial concentration of surfactant = 1×10^{-3} mol dm^{-3}. Solution pH = 5.2.

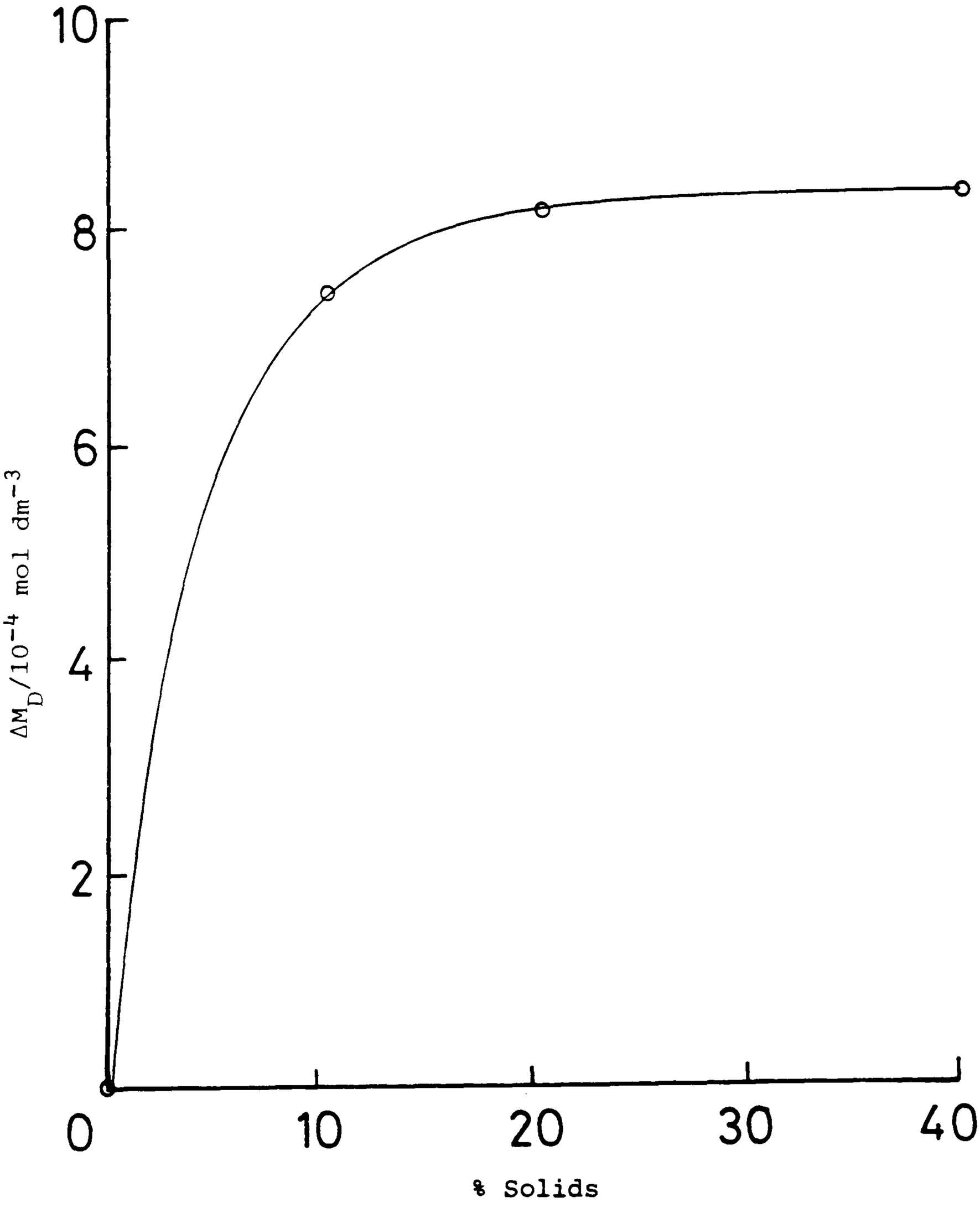

Figure 53: Effect of solid-solution ratio (% solids) on the change in concentration, ΔM_D, of 4-ϕ-C_{12} ABS in 0.10 mol dm^{-3} NaCl solution. Data from Table 14.

3.3.2 The Effect of Sodium Chloride on 4-ϕ-C_{12} ABS Adsorption at the Kaolin/Water Interface

The adsorption of 4-ϕ-C_{12} ABS onto kaolin has been measured, at 25°C, as a function of surfactant concentration, M_D, at various salt concentrations (Figure 54). Values of Γ_{max}, the area/molecule at the interface (A_s), and the percentage of solid surface covered, are shown in Table 15, as a function of NaCl concentration.

Table 15. Effect of NaCl addition on the adsorption parameters of 4-ϕ-C_{12} ABS at the air-solution interface

$\frac{[NaCl]}{mol\ dm^{-3}}$	$\frac{\Gamma_{max}}{10^{-6}\ mol\ m^{-2}}$	$\frac{A_s}{nm^2}$	$\frac{\theta}{\%}$
0.00	0.49	3.39	10.6
0.01	0.61	2.72	13.2
0.10	1.02	1.63	22.1

The isotherms of Figure 54 show the general shape expected of charged surfactant adsorption at a charged interface (see Discussion, Section 4.3), and it can be seen that the addition of NaCl displaces the isotherms to lower equilibrium concentrations, enhancing the adsorption maxima.

The results of Figure 54 show the magnitude of error in determining the amount of surfactant lost from solution. From here, it is clear that at the highest residual surfactant concentrations, the errors involved are very large indeed, although the reduction in surfactant loss at these concentrations

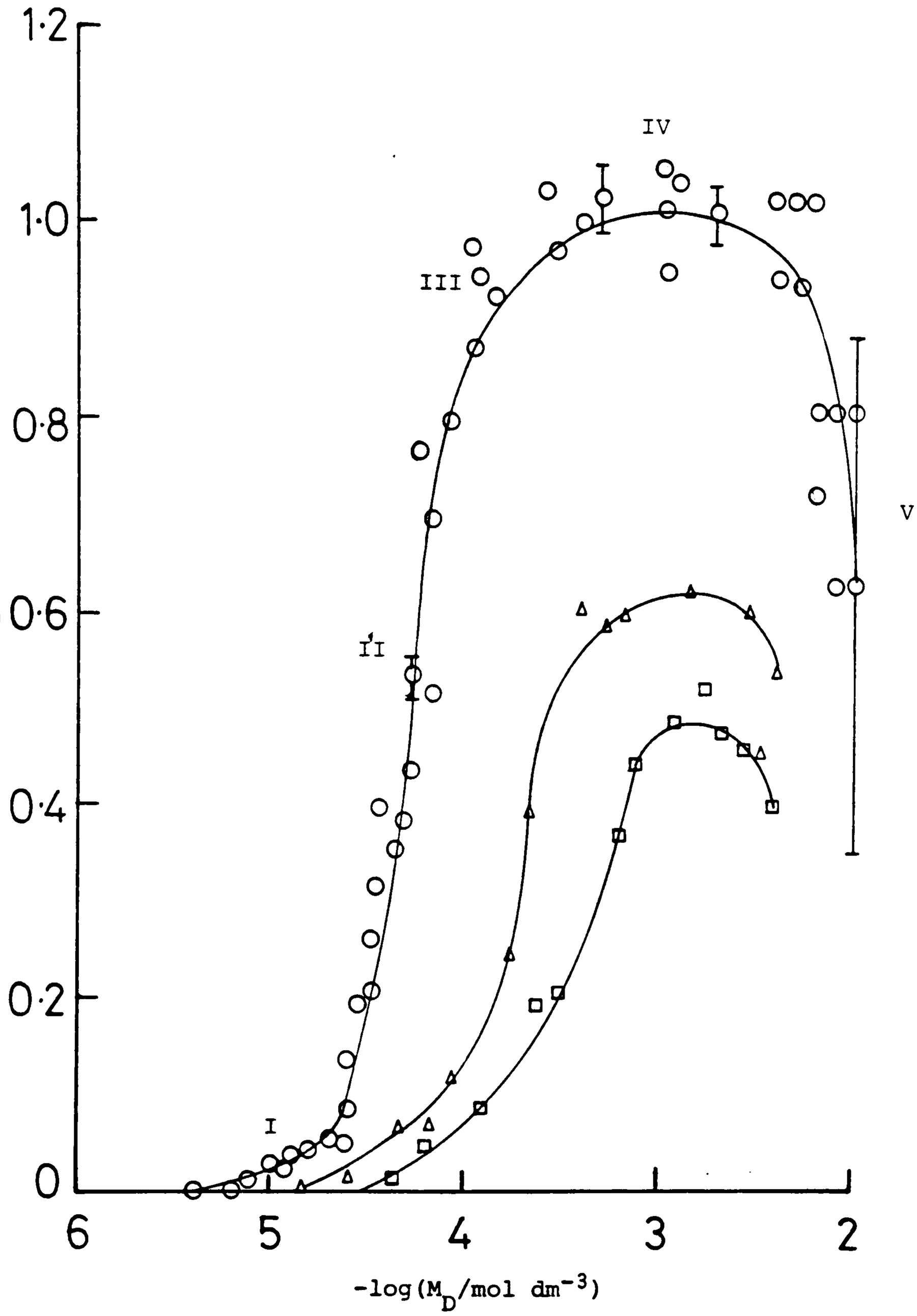

Figure 54: Adsorption of 4-ϕ-C_{12} ABS at the kaolin-aqueous solution interface, at 25°C, as a function of surfactant concentration. NaCl concentrations = 0.00 (□), 0.01 (Δ) and 0.10 (O) mol dm^{-3}. pH = 6.3, % solids = 10.

does appear to be consistent. These results are discussed further in Section 4.

3.3.3 The Effect of pH on 4-ϕ-C_{12} ABS Adsorption at the Kaolin-Aqueous Solution Interface

The adsorption of 4-ϕ-C_{12} ABS onto kaolin at 25°C from 0.1 mol dm^{-3} NaCl solution, has been measured, as a function of surfactant concentration, M_D, under different conditions of pH. The complete isotherms are shown in Figures 55 and 56.

The isotherms have the same shape as those obtained earlier (Section 3.3.2), having a low initial adsorption, followed by a marked increase, up to a plateau in the region of the surfactant CMC.

The results of Figure 55, for pH values above 4.0, show that the surfactant adsorption increases as the pH is reduced. Figure 56 gives results for the adsorption of pH 1.8, 4.0, a very large increase in adsorption being apparent for pH 1.8, relative to 4.0, the adsorption continuing above the CMC at this very low pH.

Figure 57 gives a summary of the plateau adsorption values shown in Figures 55 and 56, together with some indication of the amount of surfactant needed to give a complete bilayer coverage of the surface.

Table 16 gives values of Γ_{max}, from Figures 55 and 56, together with the area occupied per molecule, and the percentage of surface covered at each pH. From here it is apparent that the very low pH (1.8) has large influence on the surfactant

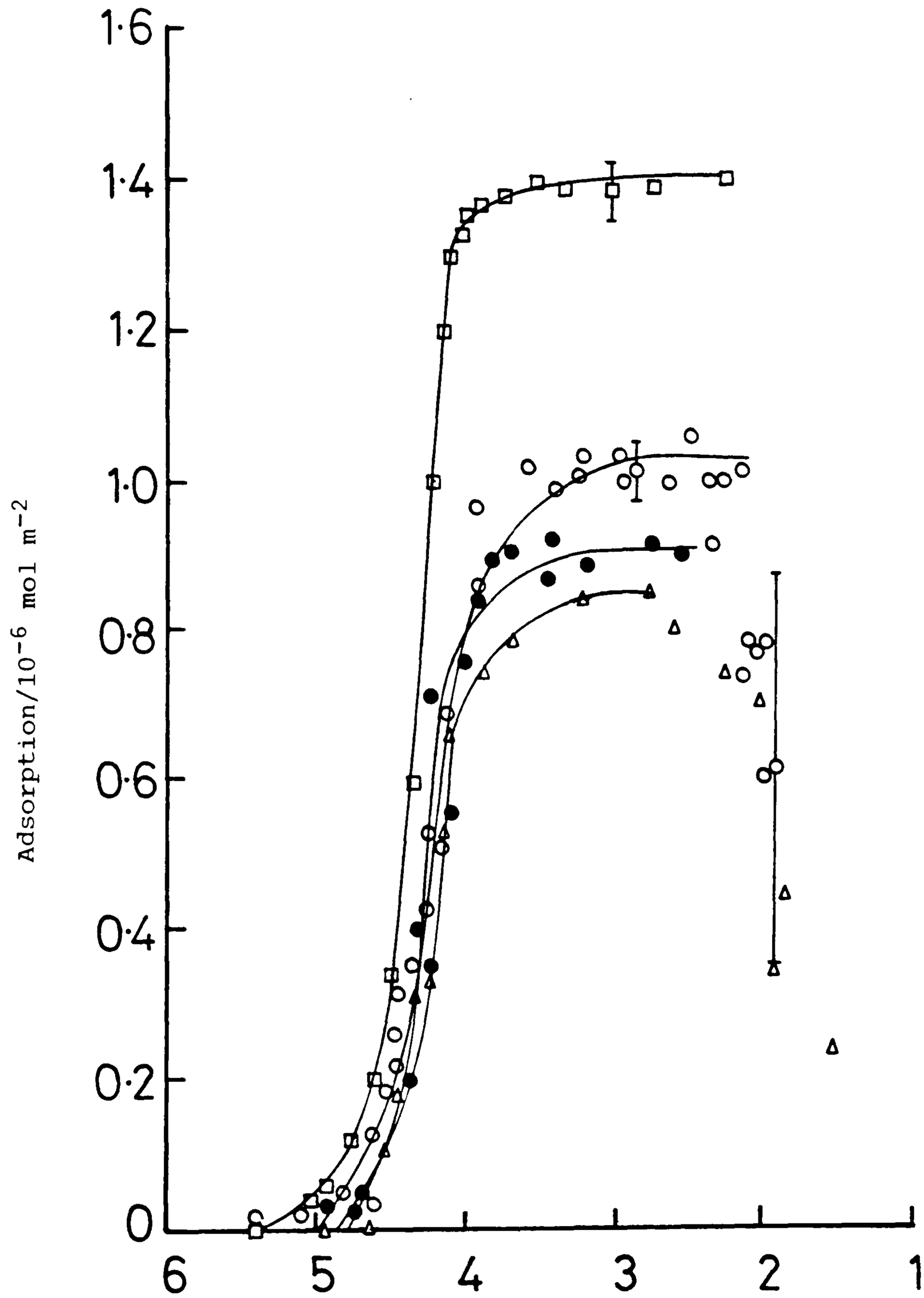

Figure 55: Effect of pH on adsorption of 4-ϕ-C_{12} ABS onto kaolin, 0.1 mol dm^{-3} NaCl. T = 25°C, time = 24 hours.

pH = 4.0 (□), 6.3 (○), 8.0 (●), 12.3 (△)

S/L = 10%.

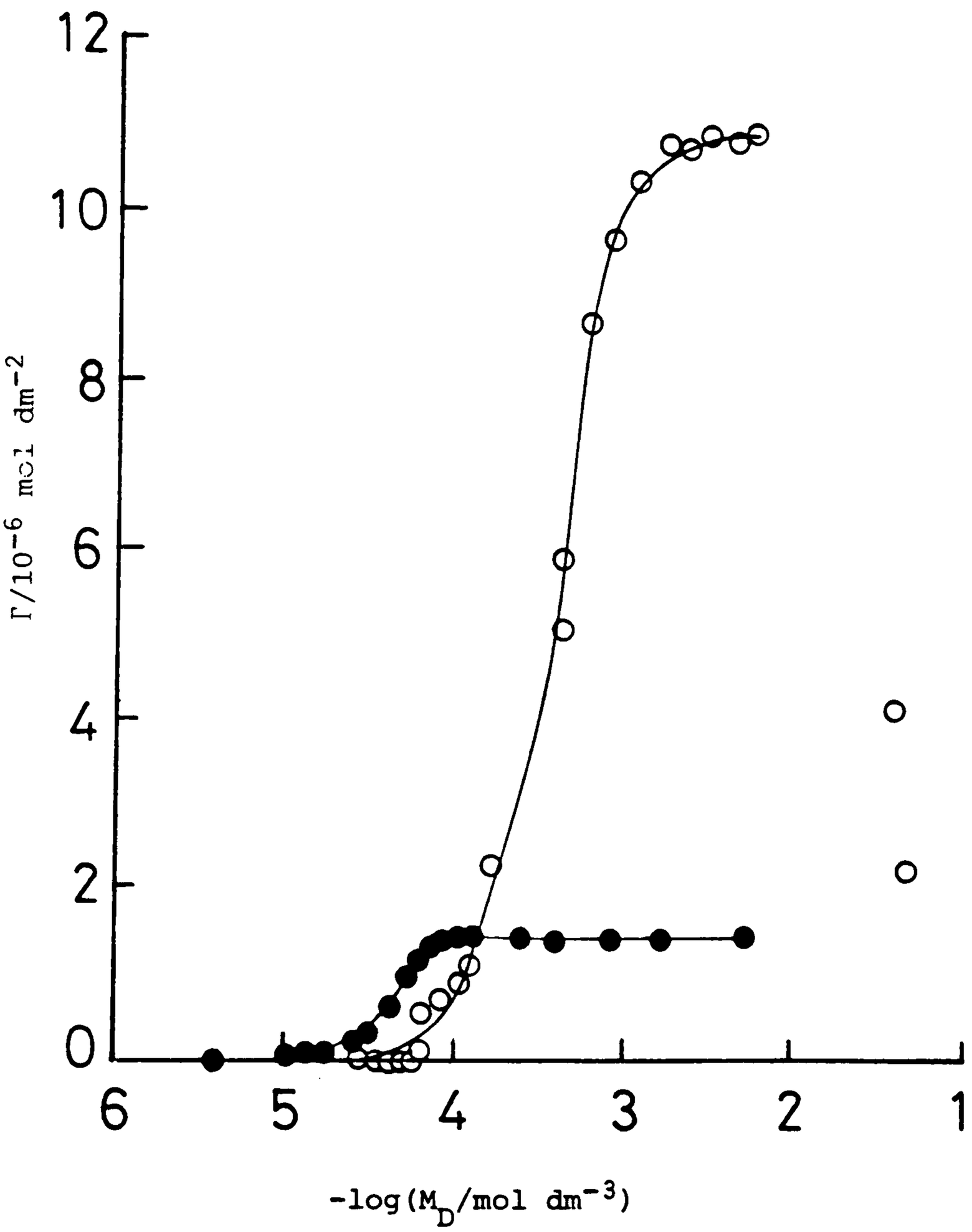

Figure 56: Effect of pH on 4-ϕ-C_{12} ABS adsorption, at 25°C, onto kaolin from aqueous NaCl (0.1 mol dm^{-3}) solution.

Solution pH = 4.0 (●), 1.8 (O). Solid/Liquid = 10%.

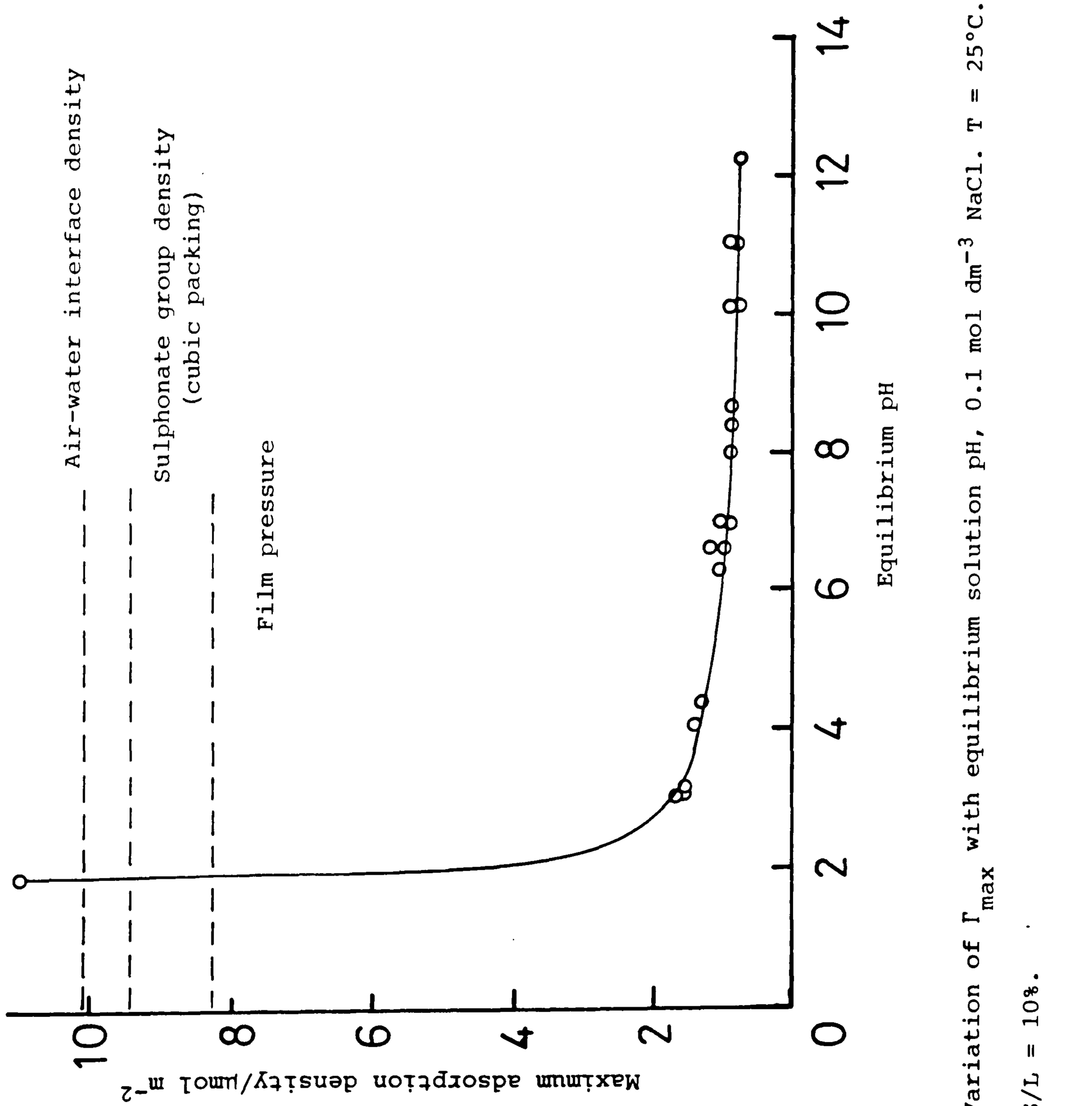

Figure 57: Variation of Γ_{max} with equilibrium solution pH, 0.1 mol dm^{-3} NaCl. T = 25°C

adsorption, indicating:

(i) the adsorption increases dramatically and/or,

(ii) the loss from solution may be due to precipitation.

Table 16. Effect of solution pH on the adsorption of 4-ϕ-C_{12} ABS at the kaolin-solution interface, from 0.10 mol dm^{-3} NaCl

pH	$\frac{\Gamma_{max}}{10^{-6}\ mol\ m^{-2}}$	$\frac{A_s}{nm^2}$	$\frac{\theta}{\%}$
1.8	11.2	0.15	243.0
4.0	1.4	1.19	30.4
6.3	1.02	1.63	22.1
8.0	0.91	1.83	19.7
12.3	0.84	1.98	18.2

3.3.4 The Effect of n-Butanol on 4-ϕ-C_{12} ABS Adsorption at the Kaolin/Aqueous Interface

The effect of n-butanol addition on the adsorption of 4-ϕ-C_{12} ABS, at 25°C, from 0.1 mol dm^{-3} NaCl solution, onto kaolin is shown as a function of surfactant concentration, M_D, in Figure 58. From here it can be seen that at concentrations below the CMC, alcohol addition (below 8% v/v) increases the surfactant adsorption, while above the CMC, adsorption is reduced.

Addition of the alcohol can also be seen to affect the shape of the isotherm, introducing two plateaux of adsorption at low (0.11 mol dm^{-3}) and high (0.47 mol dm^{-3}) alcohol concentrations.

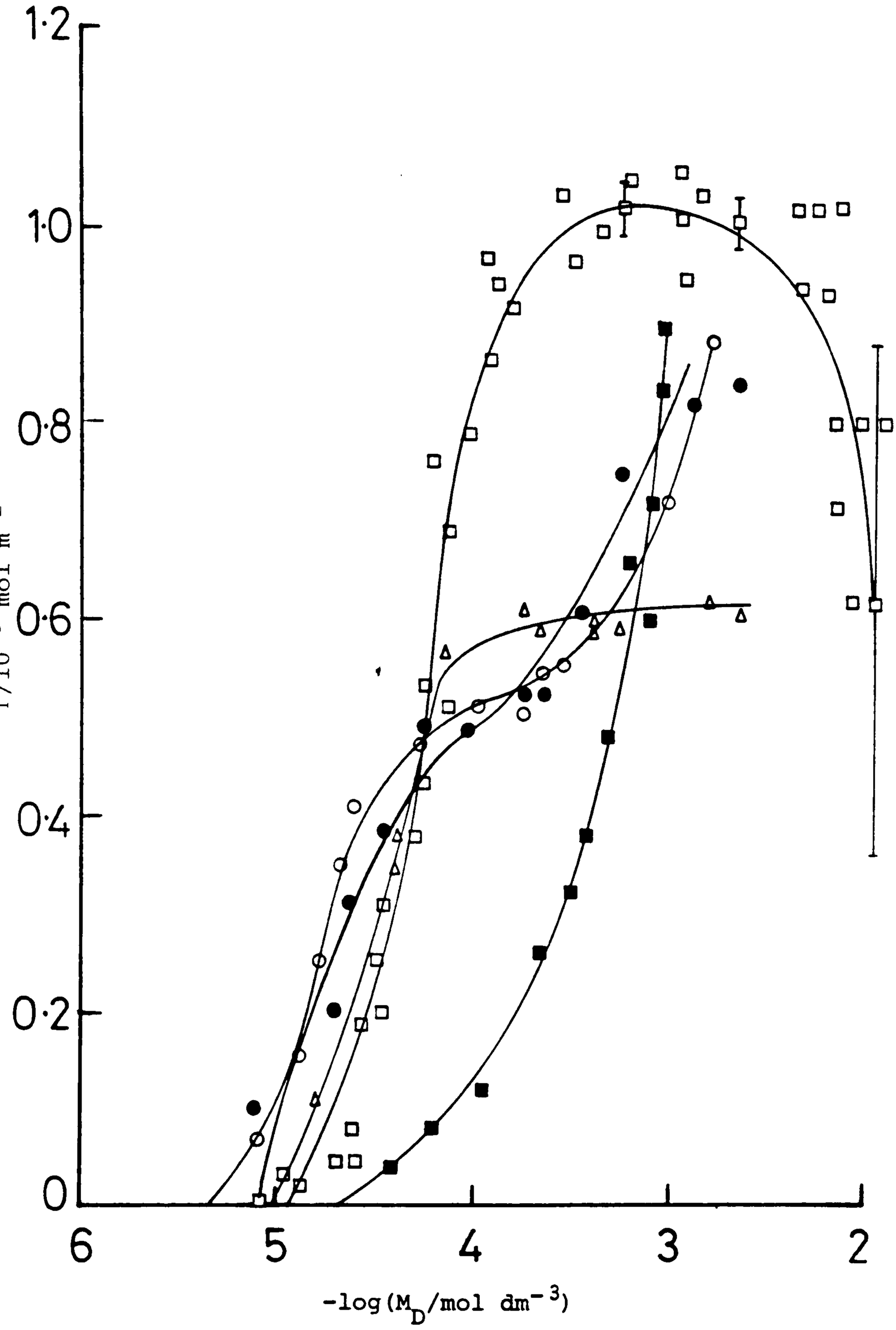

Figure 58: Effect of n-butanol addition on 4-ϕ-C_{12} ABS adsorption onto kaolin from 0.1 mol dm^{-3} NaCl solution, at 25°C and pH 6.3. S/L = 10%.
[n-butanol] = 0 (□), 0.11 (●), 0.33 (Δ), 0.47 (○), and 1.1 mol dm^{-3} (■).

In contrast, however, at the intermediate concentration of 0.33 mol dm^{-3}, the isotherm is less complex.

At the highest concentration of alcohol (1.1 mol dm^{-3}), the loss of surfactant increases rapidly with increasing surfactant concentration. However at this n-butanol concentration, a separate alcohol phase was apparent and investigation of the relative solubility of 4-ϕ-C_{12} ABS in the alcohol-water system has shown the surfactant to dissolve preferentially in the organic phase (see Section 3.3.4.2).

3.3.4.1 Adsorption of n-Butanol at the Kaolin-Aqueous Solution Interface

Measurements of n-butanol adsorption were made using both surface tension (Section 2.4.4) and radiolabelling (C-14) techniques (Section 2.4.6).

The results of Figure 59 show the amount of alcohol adsorbed (mol m^{-2}), at the kaolin-solution interface, as determined by surface tension measurements. The results indicate that above about 0.03 mol dm^{-3}, the adsorption increases with concentration up to a maximum of about 5×10^{-5} mol m^{-2}, at an n-butanol concentration of 0.10 mol dm^{-3}, beyond which the adsorption becomes constant.

Measurements of the alcohol adsorption at low initial concentrations ($< 10^{-2}$ mol dm^{-3}) in the presence, and absence, of surfactant (4-ϕ-C_{12} ABS) have been made using radiolabelled (C-14) material.

The results of Tables 17 and 18, obtained using 0.1 cm^3 of the "stock" n-butanol solution (specific activity 4.07×10^4 Bq $mmol^{-1}$,

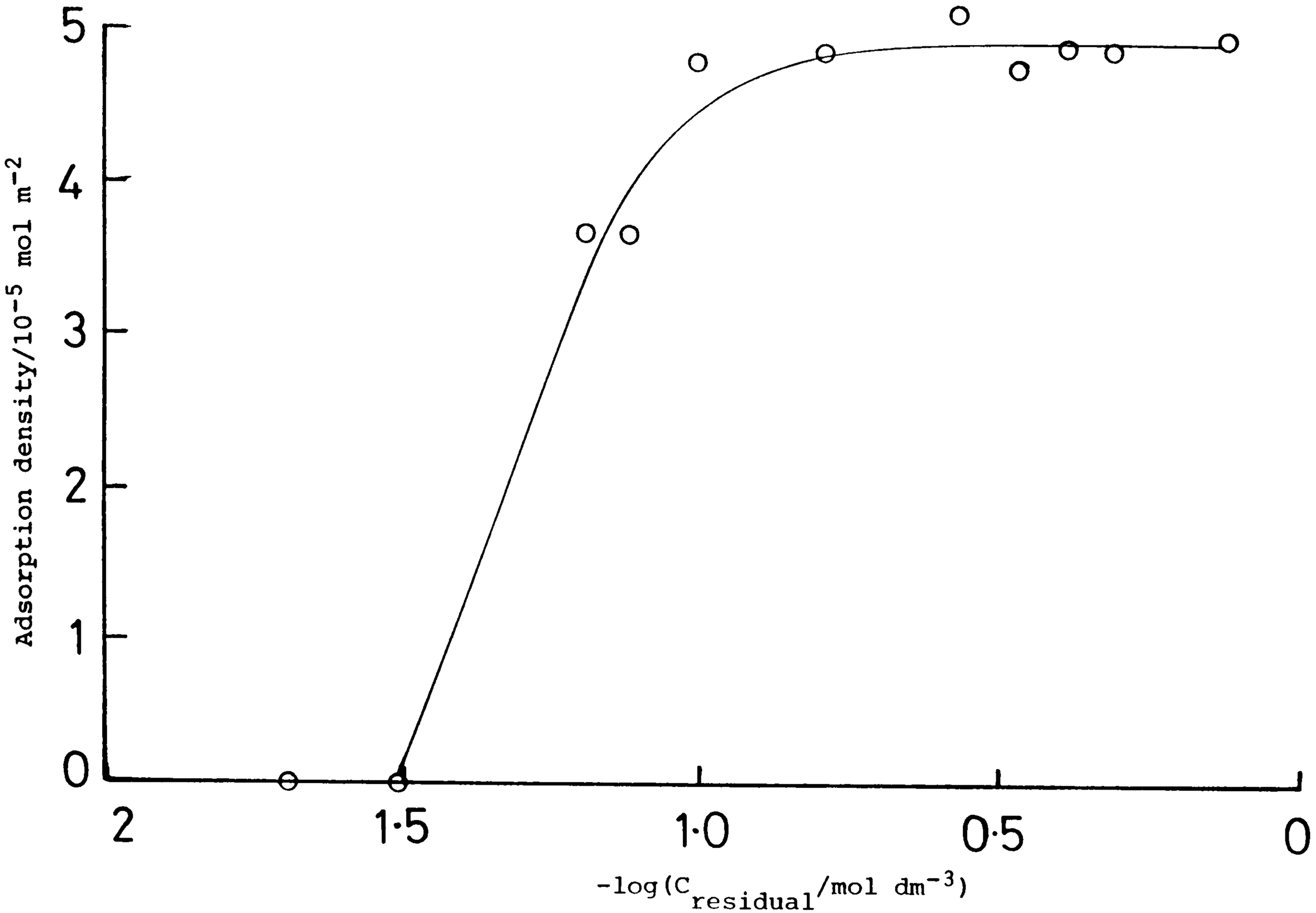

Figure 59: Adsorption of n-ButOH onto kaolin from 0.1 mol dm^{-3} NaCl solution. pH = 6.3, S/L = 10%. T = 25°C, measured by surface tension.

Table 17. Activity of n-butanol solutions with, and without, kaolin, in solutions of varying 4-ϕ-C_{12} ABS concentrations, at 25°C. S/L = 10%.

Wt. kaolin / g	[4-ϕ-C_{12} ABS] / mol dm^{-3}	Activity / Bq	No. mol n-butanol / 10^{-6} mol	
-	-	364.4	8.95	9.00 ± 0.5%
		367.8	9.04	
1.0645	-	343.1	8.43	8.35 ± 1%
		336.0	8.26	
-	1.06×10^{-4}	359.1	8.82	8.53 ± 3%
		355.5	8.24	
0.8822	1.06×10^{-4}	386.1	9.49	9.35 1.5%
		375.0	9.21	
-	1.06×10^{-3}	389.7	9.57	9.35 ± 0.5%
		385.9	0.48	
0.9667	1.06×10^{-3}	345.5	8.49	8.76 ± 3%
		367.6	9.03	
-	1.31×10^{-2}	389.4	9.57	9.62 ± 0.5%
		393.3	9.66	
0.8921	1.31×10^{-2}	405.6	9.97	9.84 ± 1.3%
		395.0	9.71	

Table 18. Adsorption of C-14 n-butanol onto kaolin from aqueous solution, at 25°C, S/L = 10%

Wt. kaolin / g	[4-ϕ-C_{12} ABS] / mol dm^{-3}	[ButOH]i / 10^{-4} mol dm^{-3}	[ButOH]f / 10^{-4} mol dm^{-3}	ButOH / 10^{-8} mol dm^{-3}
1.0645	zero	9.00	8.35	7.38
0.8822	1.06×10^{-4}	8.53	9.35	-
0.9667	1.06×10^{-3}	9.53	8.76	9.63
0.8921	1.31×10^{-2}	9.62	9.84	-

Section 2.4.6), show that there is very little (circa 10^{-8} mol m^{-2}) loss of alcohol from the solution. However, consideration of the measured radioactivity of the solutions, in the absence of kaolin, shows some dependence of the results on the concentration of surfactant, Table 17 and Figure 60, the solution activity increasing as the surfactant concentration is increased, although a maximum is reached.

To extend these studies, 1 cm^3 of the "stock" n-butanol (C-14) solution was added to 9 cm^3 of inactive n-butanol (AR) as shown below.

CPMA/K	% Dev	% Efficiency of Count	Activity / Bq
228519	0.20	90.7	4199
228515	0.20	90.7	4199

0.5 cm^3 of this solution was then added to 10 cm^3 of 1.08×10^{-3} mol dm^{-3} 4-ϕ-C_{12} ABS solution (c.f. Figure 60), and used for adsorption measurements as shown below,

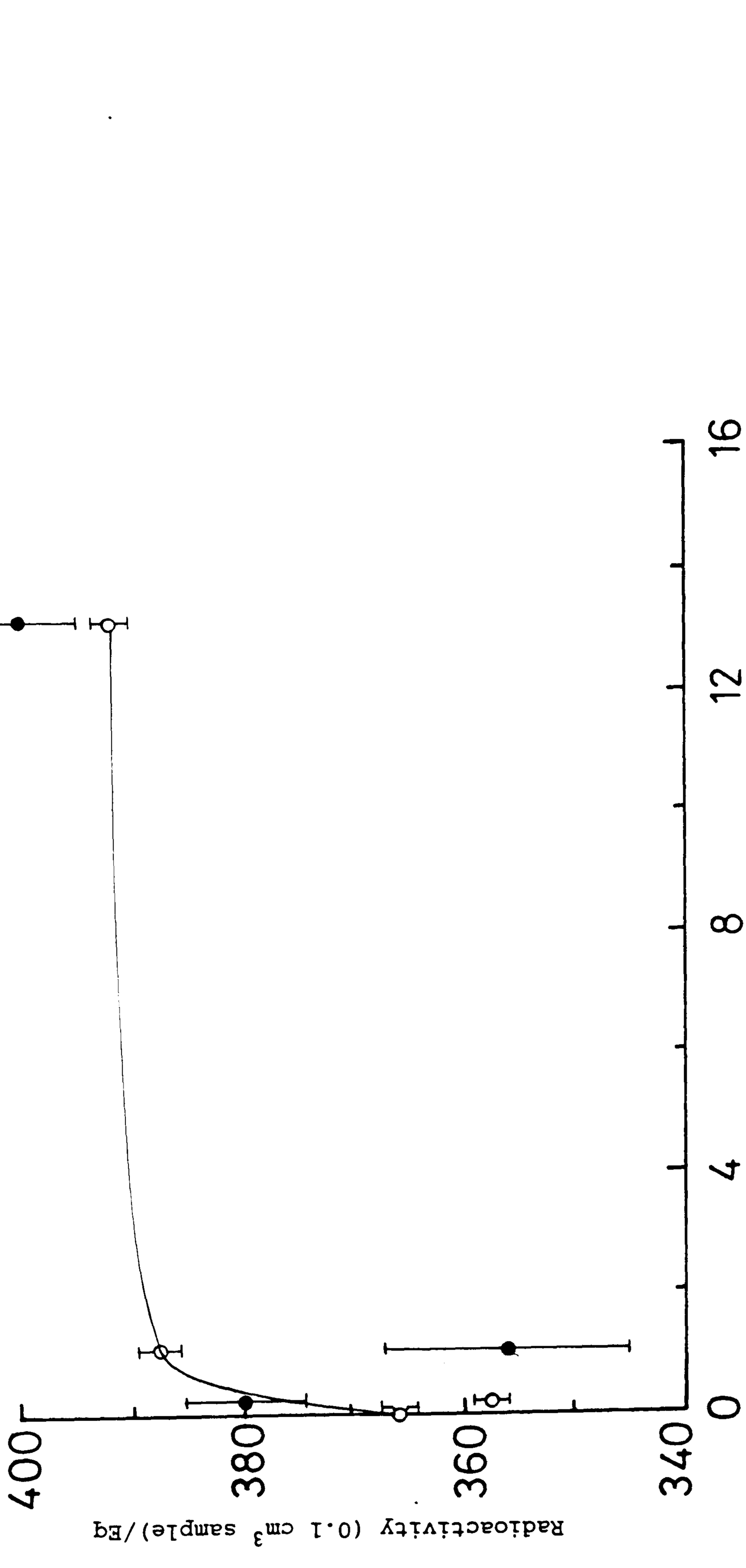

Figure 60: Variation of n-butanol (C-14) activity in NE260 solution with surfactant concentration (O). with added kaolin (●).

Kaolin g	[4-ϕ-C_{12} ABS] 10^{-3} mol dm^{-3}	Activity Bq	Mol of n-butanol 10^{-6} mol
-	1.08	197 193	4.84 4.74 — 4.79 ± 1%
0.8221	1.08	191 194	4.69 4.77 — 4.73 ± 0.8%

giving the amount of n-butanol adsorbed = 0.88×10^{-10} mol m^{-2} which is negligible.

Increasing the weight of kaolin had little effect on the adsorption (see below),

Kaolin g	[4-ϕ-C_{12} ABS] 10^{-3} mol dm^{-3}	Activity Bq	Mol. of n-butanol 10^{-6} mol
1.5314	1.08	181.4 176.7	4.46 4.34 — 4.4 ± 1.4%

giving the number of mol of n-butanol adsorbed = 3.08×10^{-10} mol m^{-2}; and showing it is still negligible.

Measurements of n-butanol Adsorption in the Absence of Surfactant

0.5 cm^3 of C-14 labelled n-butanol (prepared as above) were added to 10 cm^3 of water, and the adsorption onto increasing weights of kaolin measured, as shown below:

Kaolin g	Activity of solution Bq	[n-butanol] 10^{-4} mol dm^{-3}	Γ_{ButOH} 10^{-7} mol m^{-2}
-	187.0 175.5	4.59 4.45 ± 3% 4.31	-
0.5325	180.5 176.6	4.43 4.39 ± 1% 4.34	0.14
0.4996	184.2 173.7	4.53 4.4 ± 3% 4.27	0.12
-	178.9 165.9	4.40 4.23 ± 4% 4.06	0.27

These results show adsorption of the alcohol, the amount adsorbed increasing as the weight of kaolin was increased. Thus, the presence of surfactant appears to inhibit the alcohol adsorption.

3.3.4.2 The Distribution of 4-ϕ-C_{12} ABS between n-butanol and Aqueous Phases

The relative solubility, measured as distribution, of 4-ϕ-C_{12} ABS in n-butanol, and water, was determined using radiolabelled (^{35}S) surfactant.

Figure 61 shows the partition coefficient, K_{eq}. defined by equation (3.2), for the surfactant as a function of butanol, at 25°C:

$$K_{eq} = \frac{\text{No. mol of surfactant in n-ButOH phase}}{\text{No. mol of surfactant in water phase}} \qquad (3.2)$$

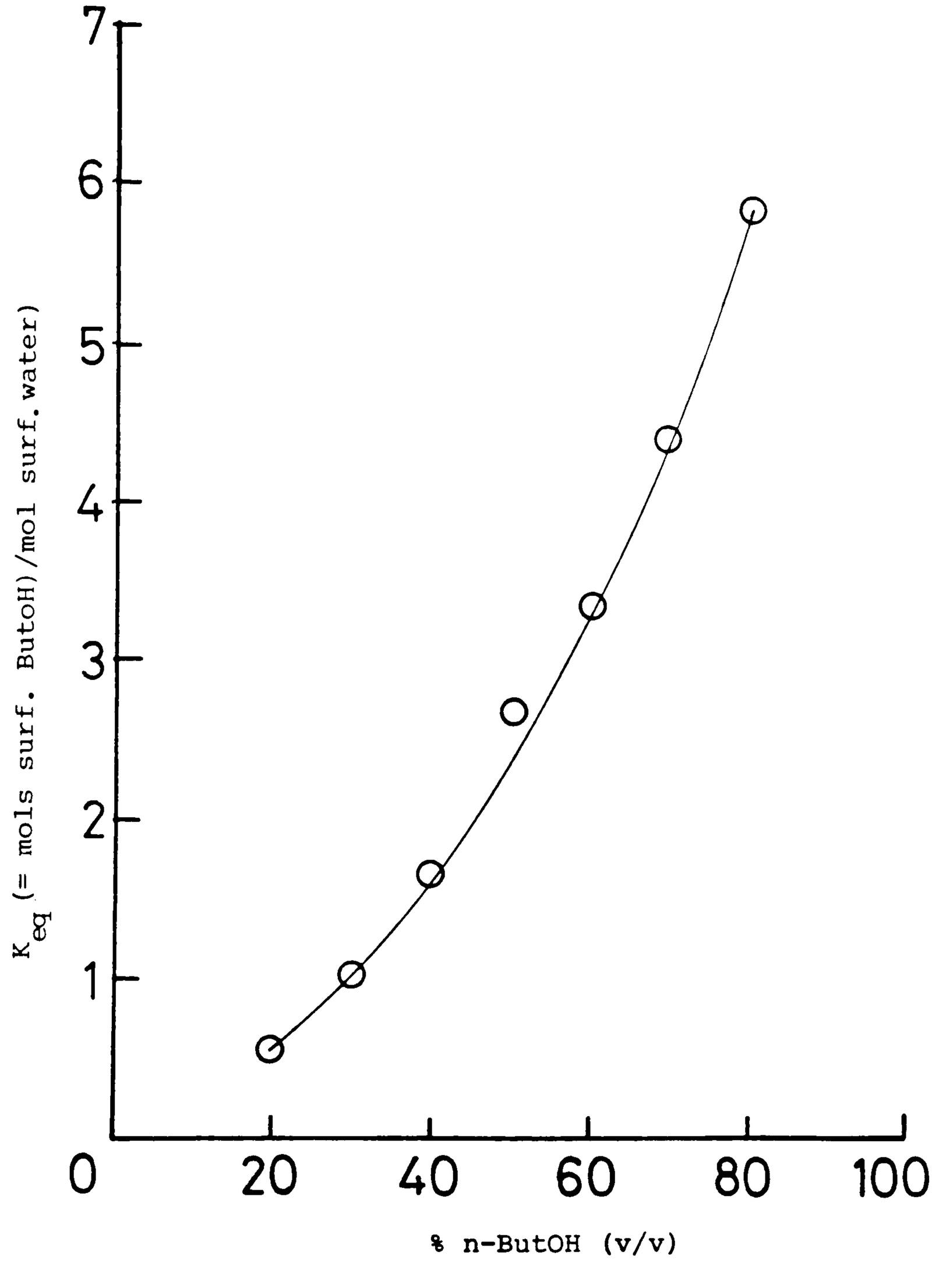

Figure 61: Distribution of 4-ϕ-C_{12} ABS^{35} between n-butanol and aqueous phases, at 25°C.

From the results of Figure 61 it can be seen that the value of K_{eq} increases rapidly as the percentage volume of alcohol is increased. From equation (3.2) it can be seen that this indicates that the number of mols of anionic surfactant in the alcohol phase is increasing, showing the surfactant to be more soluble in the organic phase.

3.3.5 The Effect of Temperature on 4-ϕ-C_{12} ABS Adsorption at the Kaolin-Aqueous Solution Interface

In order that possible temperature variations in application may be accounted for, the adsorption of 4-ϕ-C_{12} ABS onto kaolin from aqueous (0.1 mol dm^{-3} NaCl) solution at 25, 60 and 80°C, is shown in Figure 62 as a function of residual surfactant concentration.

From the results it can be seen that increasing the solution temperature, from 25 to 60°C, reduces the surfactant adsorption. However, an additional increase in temperature, from 60 to 80°C, failed to reduce the adsorption further, indicating some plateau of adsorption as a function of temperature.

3.3.6 The Effect of n-decane on 4-ϕ-C_{12} ABS Adsorption at the Kaolin/Aqueous Solution Interface

Emulsions, containing surfactant, n-decane, n-butanol, and sodium chloride, were prepared by weight. The oil-in-water (o/w) emulsions were opaque, with a milky-white appearance, while the water-in-oil (w/o) systems were grey and only slightly opaque.

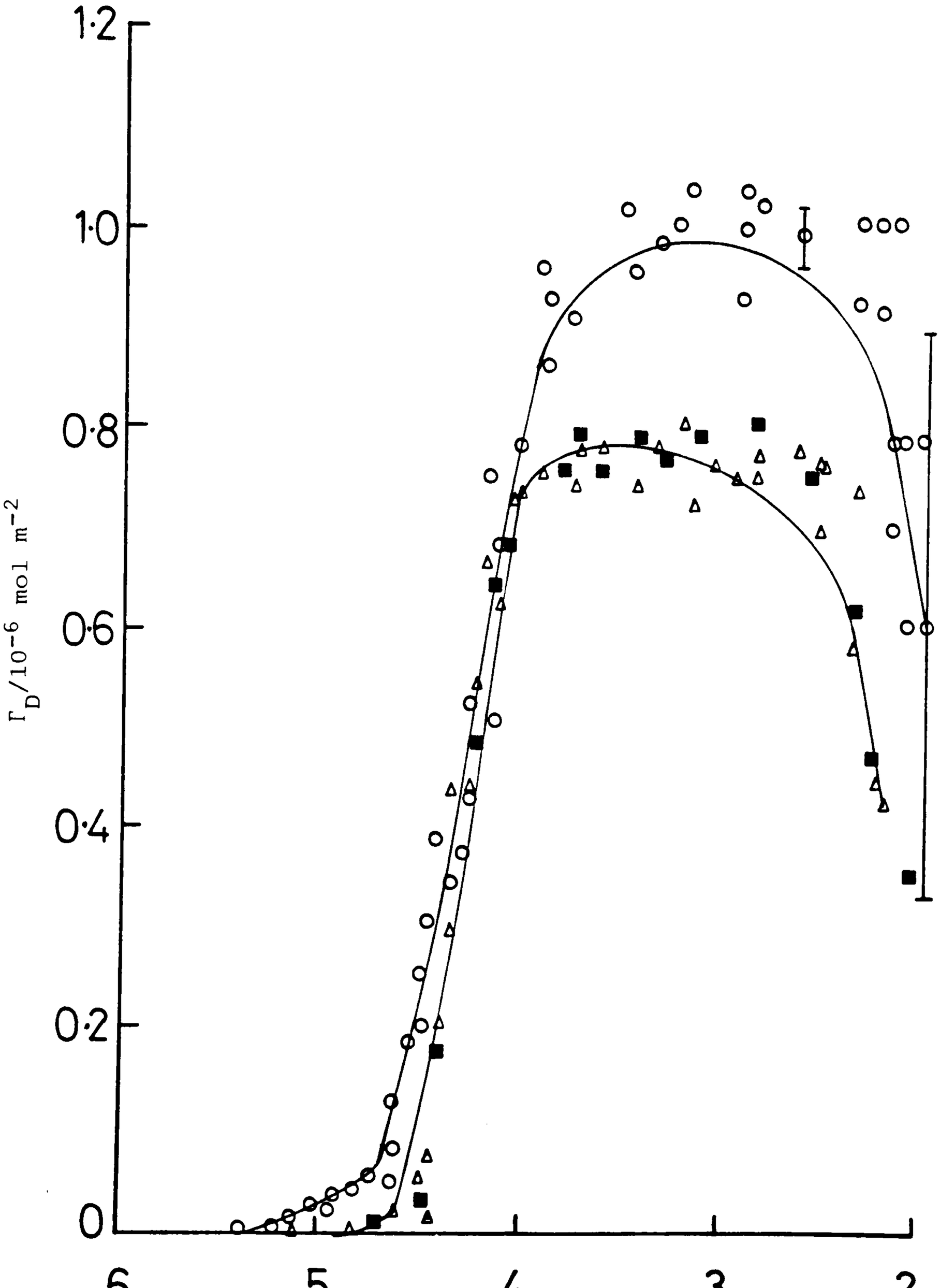

Figure 62: Effect of temperature on 4-ϕ-C_{12} ABS adsorption from 0.1 mol dm^{-3} NaCl, at pH 6.3, onto kaolin. S/L = 10%. Temperature = 25 (O), 60 (Δ), and 80 (■) °C.

The loss of 4-ϕ-C_{12} ABS, initially above its CMC, from 0.1 mol dm^{-3} NaCl solutions of varying oil fraction, onto kaolin, at 25°C, is show in Figure 63. The results show that as the weight fraction of oil is increased, and the system moves from an oil-in-water emulsion to a water-in-oil emulsion, the amount of surfactant lost at first decreases, then increases, up to a maximum of about 1×10^{-6} mol m^{-2}, then appears to fall.

3.3.6.1 The Adsorption of 4-ϕ-C_{12} ABS onto Kaolin, from n-decane Solutions, in the Presence of n-Butanol

The adsorption of 4-ϕ-C_{12} ABS, and n-decane, from 0.1 mol dm^{-3} NaCl solution, in the presence of 0.5 mol dm^{-3} of n-butanol, at 25°C, is shown as a function of residual surfactant concentration in Figure 64.

The isotherm of surfactant adsorption (open circles of Figure 64) is of the same form as those found earlier (Sections 3.2 onwards), although displaced to the higher surfactant equilibrium concentration (5×10^{-5} to 5×10^{-3} mol dm^{-3}).

The adsorption measurements of the decane oil show that the loss at first decreases, at low surfactant concentrations, and constant surfactant adsorption, then increases rapidly as the surfactant adsorption increases. At the plateau of surfactant adsorption, the amount of oil lost from solution falls rapidly.

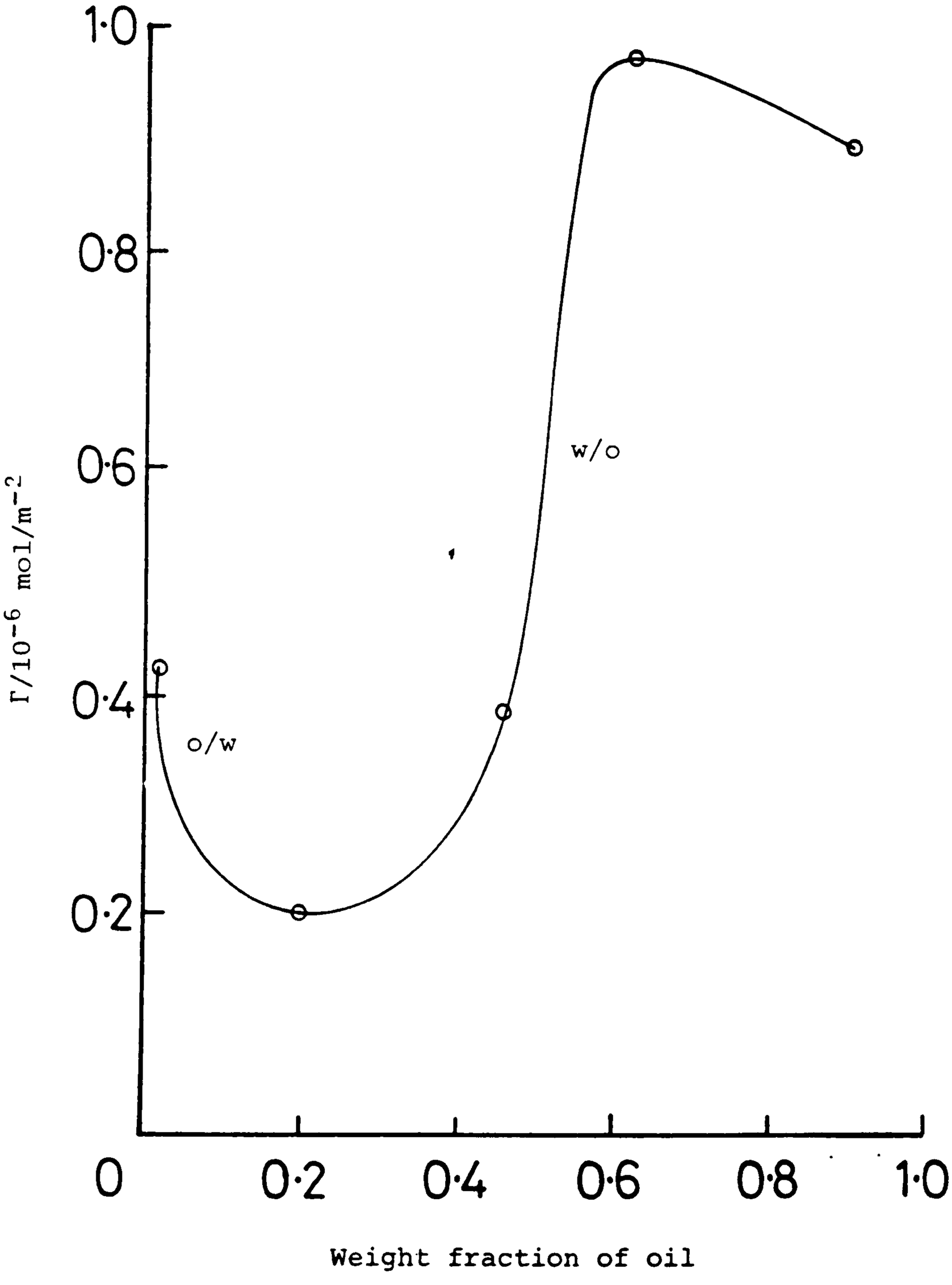

Figure 63: Adsorption of 4-ϕ-C_{12} ABS onto kaolin from 0.1 mol dm^{-3} NaCl, at 25°C, and pH 6.0, in the presence of varying amounts of n-decane (S/L = 10%). Initial surfactant = 2.16×10^{-3} mol dm^{-3}.

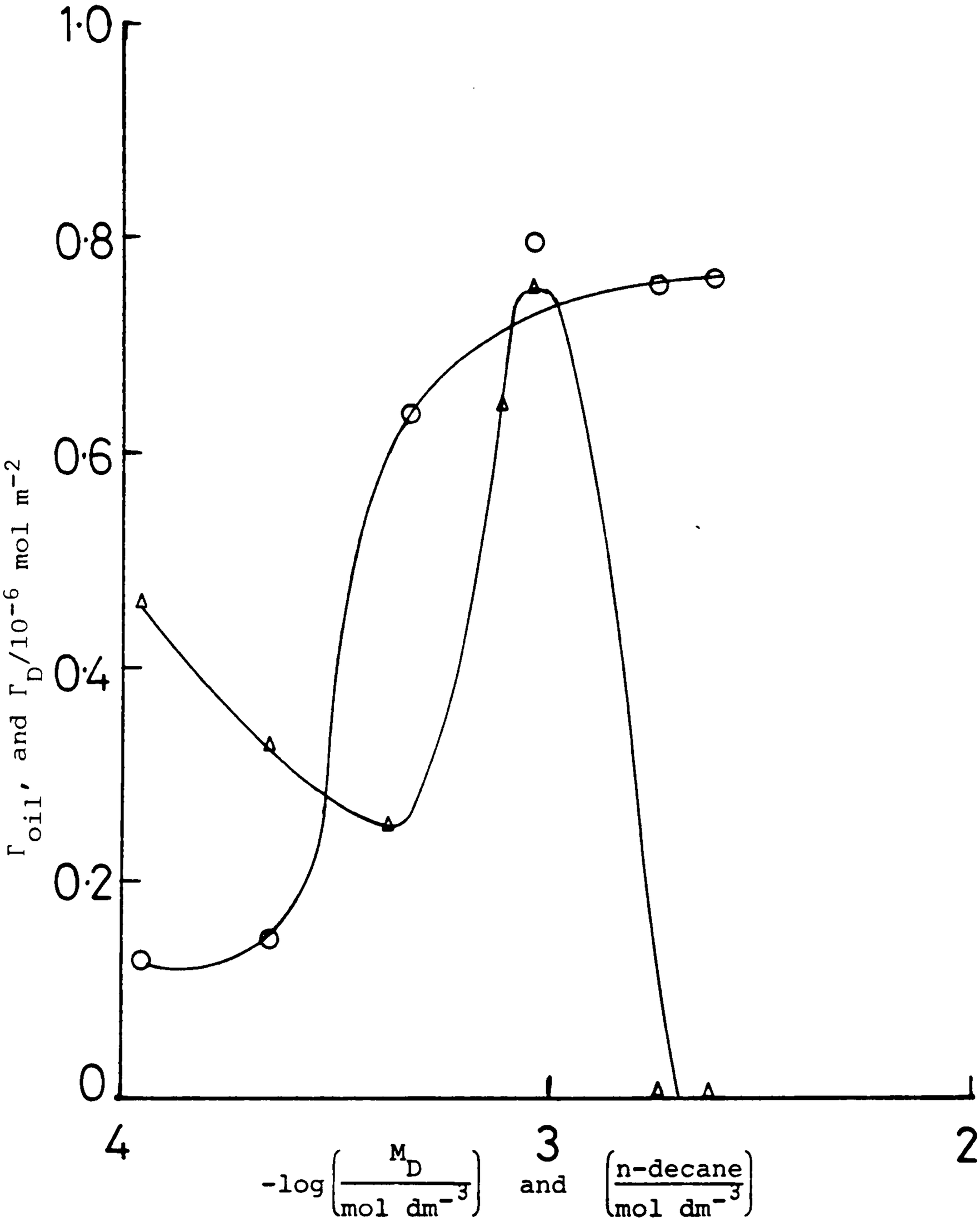

Figure 64: Adsorption of 4-ϕ-C_{12} ABS (O) onto kaolin, at 25°C, from 0.1 mol dm^{-3} NaCl solution, containing 0.5 mol dm^{-3} n-butanol and 0.04 mol dm^{-3} n-decane. Included are losses of n-decane from solution, (Δ).

3.3.6.2 The Effect of n-butanol on 4-ϕ-C_{12} ABS Adsorption at the Kaolin/Aqueous Solution Interface in the Presence of n-decane

The loss of surfactant from emulsions of n-decane prepared both, through n-decane removal from clay by a surfactant formulation, and by addition of n-decane to the surfactant formulation prior to contact with clay, has been measured as a function of n-butanol concentration, Figure 65. The results here show the same trend, whether the oil originates from the clay, or is originally present in solution. At low concentrations of alcohol (ca. < 0.4 mol dm^{-3} for oil-on-clay, and < 0.2 mol dm^{-3} for oil-in-solution) the surfactant loss from solution is highest. At 0.5 mol dm^{-3} n-butanol a minimum of surfactant adsorption is reached, and above this the loss increases, although at the highest concentration of alcohol (1.0 mol dm^{-3} n-butanol) the loss is lower than in the absence of alcohol.

Results for surfactant loss onto kaolin, in the absence of n-decane, taken from Figure 58, at 1.00×10^{-3} mol dm^{-3} 4-ϕ-C_{12} ABS, are also included for comparison in Figure 65. The results indicate that surfactant loss is lower in the absence of the oil, and all three curves show a minimum in adsorption, although in the absence of decane this is shifted to lower alcohol concentration.

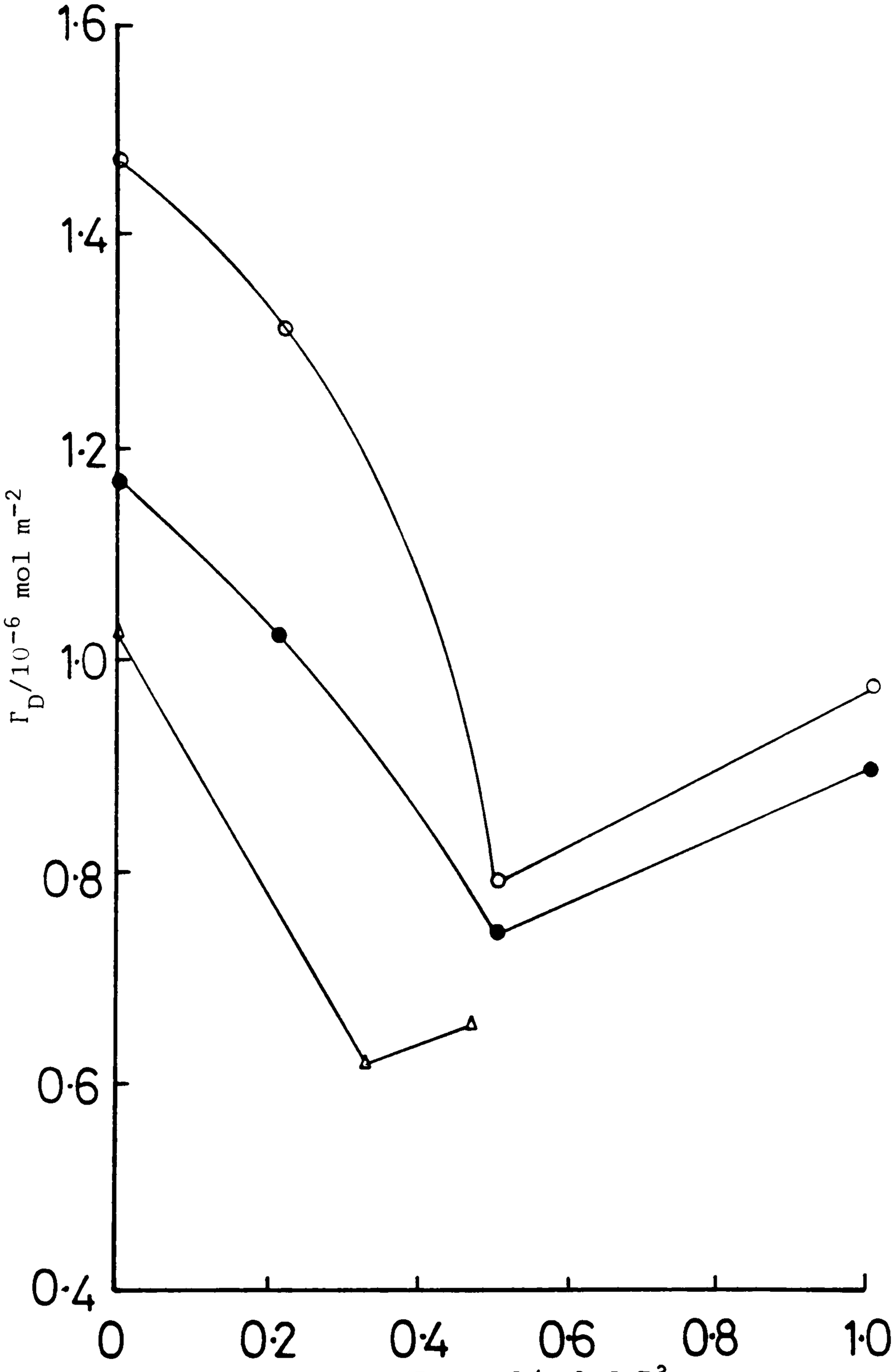

Figure 65: Effect of n-butanol on 4-ϕ-C_{12} ABS adsorption, at 25°C, onto kaolin from aqueous NaCl (0.1 mol dm^{-3}) solution, with n-decane (0.04 mol dm^{-3}), on the clay (o), and, in solution (●). In the absence of n-decane (Δ). C_i = 1.56 × 10^{-3} mol dm^{-3} 4-ϕ-C_{12} ABS.

3.4 The Adsorption of CTAB at the Kaolin/Aqueous Solution Interface

3.4.1 The effect of NaCl on CTAB Adsorption onto Kaolin

By way of comparison of anionic surfactant adsorption (viz. 4-ϕ-C_{12} ABS) at the clay surface, the adsorption of the cationic surfactant, CTAB, has been measured.

The adsorption isotherms of CTAB, at 25°C, onto kaolin, as a function of surfactant concentration, M_D, from water, and 0.10 mol dm^{-3} NaCl solution, can be seen to be of the same form as those of 4-ϕ-C_{12} ABS under similar solution conditions, Figures 6.6 and 54 respectively.

However, in contrast to the anionic surfactant, sodium chloride addition slightly reduces the adsorption maximum of the CTAB surfactant.

The values of $\Gamma_{D,max}$, the area per molecule at the solid-liquid interface (A_s), and the percentage of solid surface covered, based on an ion size of 0.47 nm^2 obtained from surface tension measurements (Table 7) are given in Table 19,

Table 19. The effect of NaCl on $\Gamma_{D,max}$, A_s, and θ%, for CTAB adsorption at the kaolin/solution interface.

[NaCl] / mol dm^{-3}	$\Gamma_{D,max}$ / 10^{-6} mol m^{-2}	A_s / nm^2	θ / %
-	16.7	0.10	470
0.10	15.4	0.11	427

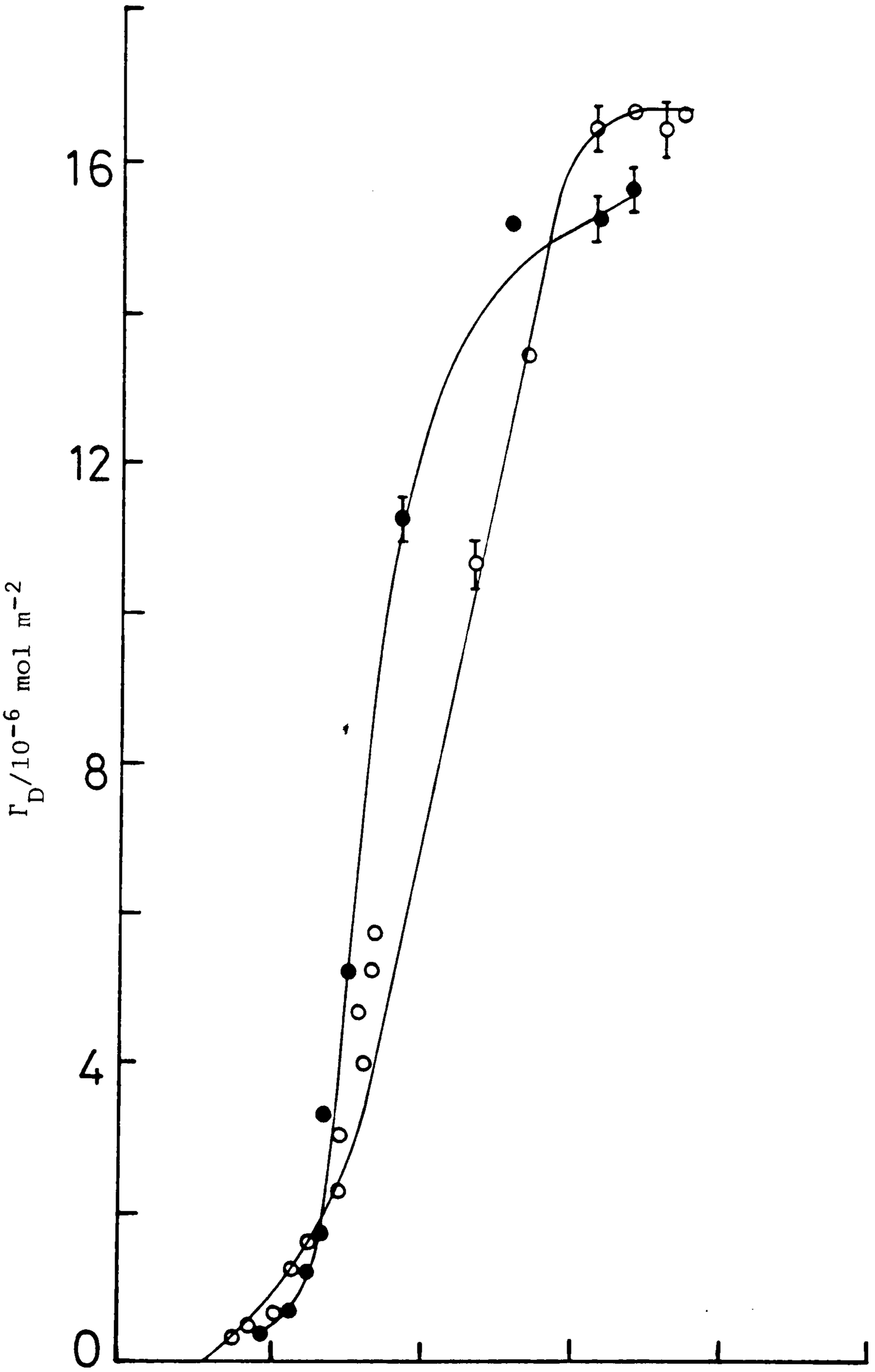

Figure 66: CTAB adsorption onto kaolin, at 25°C and pH 6.0, from aqueous (O) and 0.1 mol dm^{-3} NaCl solution. S/L = 10% with increasing cationic surfactant concentrations.

3.4.2 The Effect of Solution pH on The Adsorption of CTAB at the Kaolin/Solution Interface

The adsorption of CTAB (initially above the CMC), at 25°C, from 0.10 mol dm^{-3} NaCl solution onto kaolin, is shown as a function of solution pH in Figure 67. It can be seen that, in contrast to the previously considered anionic surfactant (Figure 55), the adsorption of CTAB increases as the solution pH is increased. However, comparing Figures 55 and 67, the adsorption of cationic surfactant exceeds that of the anionic even at low pH ($\sim$ 2). The increase in adsorption is attributed to the large negative charge density of the clay particles at low pH, which dominates the surface properties of the clay. At all pHs, the CTAB surface coverage exceeds 400% (Table 20).

Table 20. The effect of solution pH on $\Gamma_{D,max}$, A_s, and θ%, for CTAB adsorption at the kaolin/aqueous solution interface

pH	$\frac{\Gamma_{D,max}}{10^{-6}\ mol\ m^{-2}}$	$\frac{A_s}{nm^2}$	$\frac{\theta}{\%}$
2	14.5	0.11	427
6	15.5	0.11	427
12	16.7	0.10	470

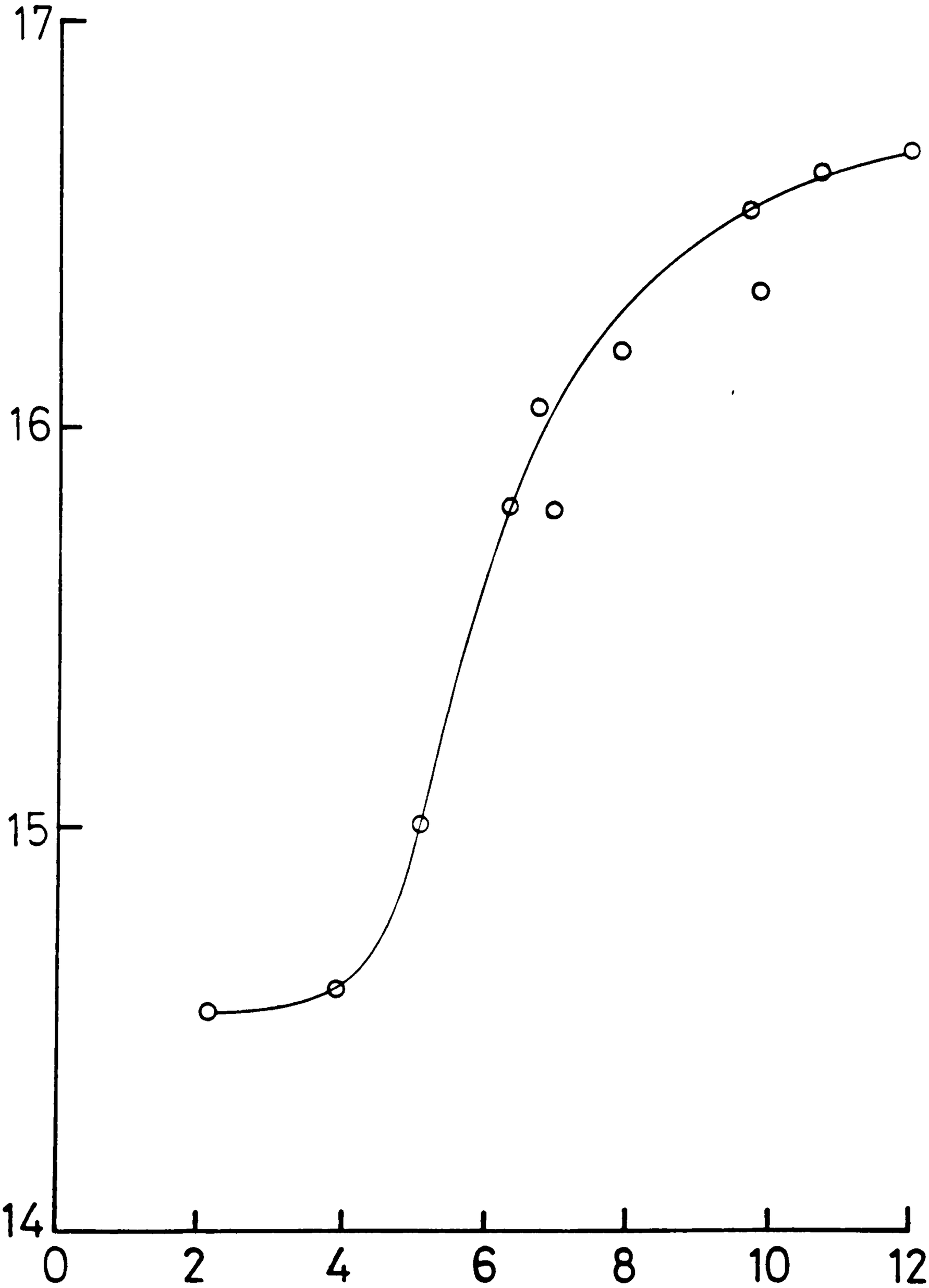

Figure 67: Effect of solution pH on the maximum adsorption of CTAB, at 25°C, at the kaolin-aqueous NaCl (0.1 mol dm^{-3}) interface.
Initial surfactant concentration = 4 × 10^{-3} mol dm^{-3}.
S/L = 10%.

3.5 Adsorption of 4-ϕ-C_{12} ABS onto Clashach Sandstone, BDH Precipitated Silica, and Crosfield's Gasil-35

The adsorption, at 25°C and pH 6.0, of 4-ϕ-C_{12} ABS[35] onto Clashach sandstone, and BDH precipitated silica, is shown in Figure 68 as a function of surfactant concentration.

The adsorption measurements of the sandstone were made after thorough washing of the material with water, to remove any adhering clay particles. Measurements made after washing with hydrochloric acid (0.1 mol dm^{-3}) showed no adsorption.

The results of adsorption measurements for 4-ϕ-C_{12} ABS[35] onto Gasil-35, at pH 2.4, are shown in Figure 69. The measurements were made by determining the amount of surfactant lost from solution, in contrast to the sandstone, and BDH silica results in which measurements were made by direct counting of the solids (see Section 2.4.6).

Figure 68 illustrates the variation of surface excess concentration, Γ_D, with concentration of 4-ϕ-C_{12} ABS on Clashach sandstone and precipitated silica (BDH). The adsorption isotherm for 4-ϕ-C_{12} ABS on Gasil-35 (Figure 69) is of the "normal" shape, however, the extent of adsorption on silica, which was greater than that on sandstone, was several orders of magnitude less than the corresponding values for kaolin.

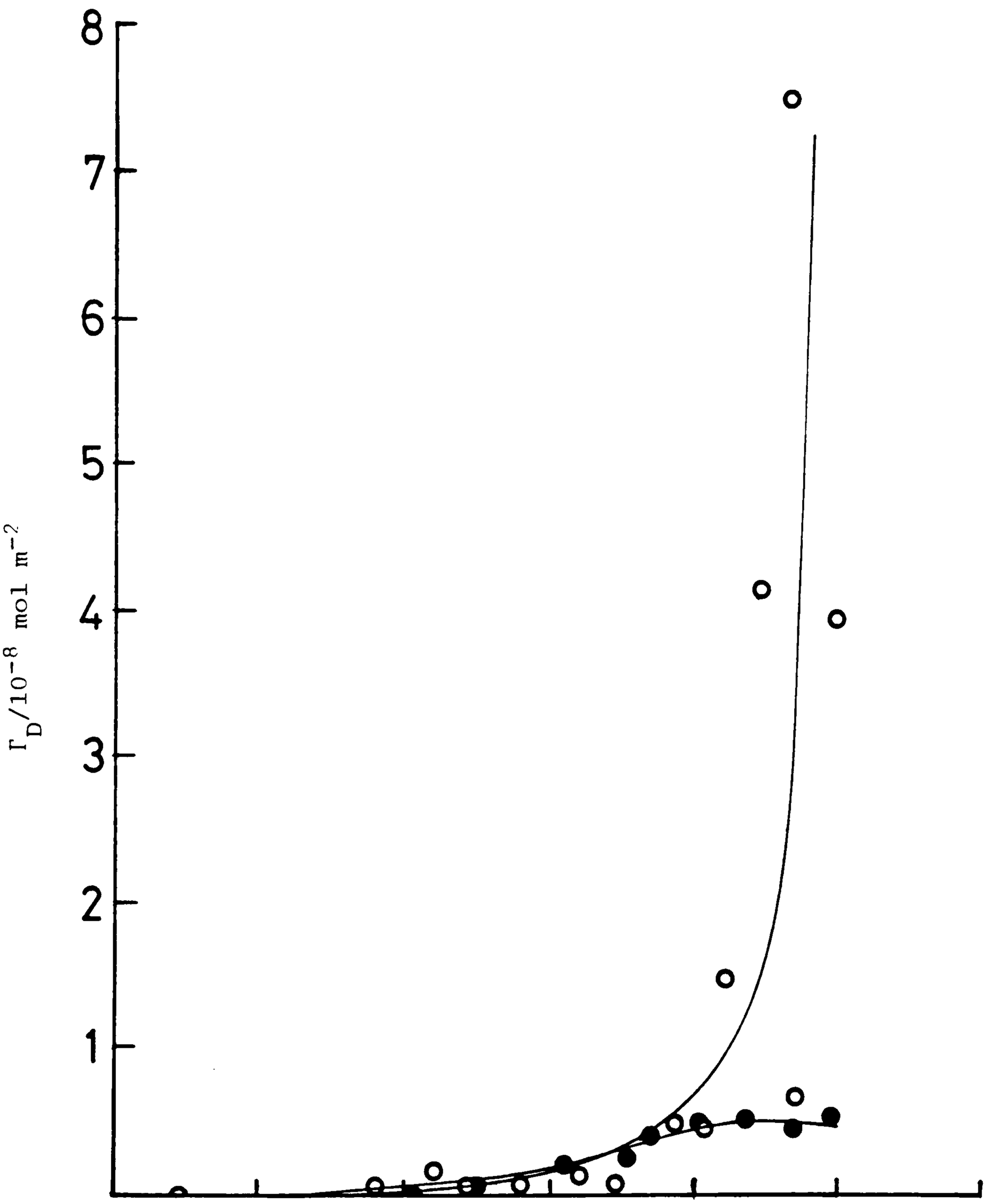

Figure 68: Adsorption of 4-ϕ-C_{12} ABS onto Clashach sandstone (●), and BDH precipitatedsilica (O), from aqueous solution, at pH 6.0 and 25°C. S/L = 10%.

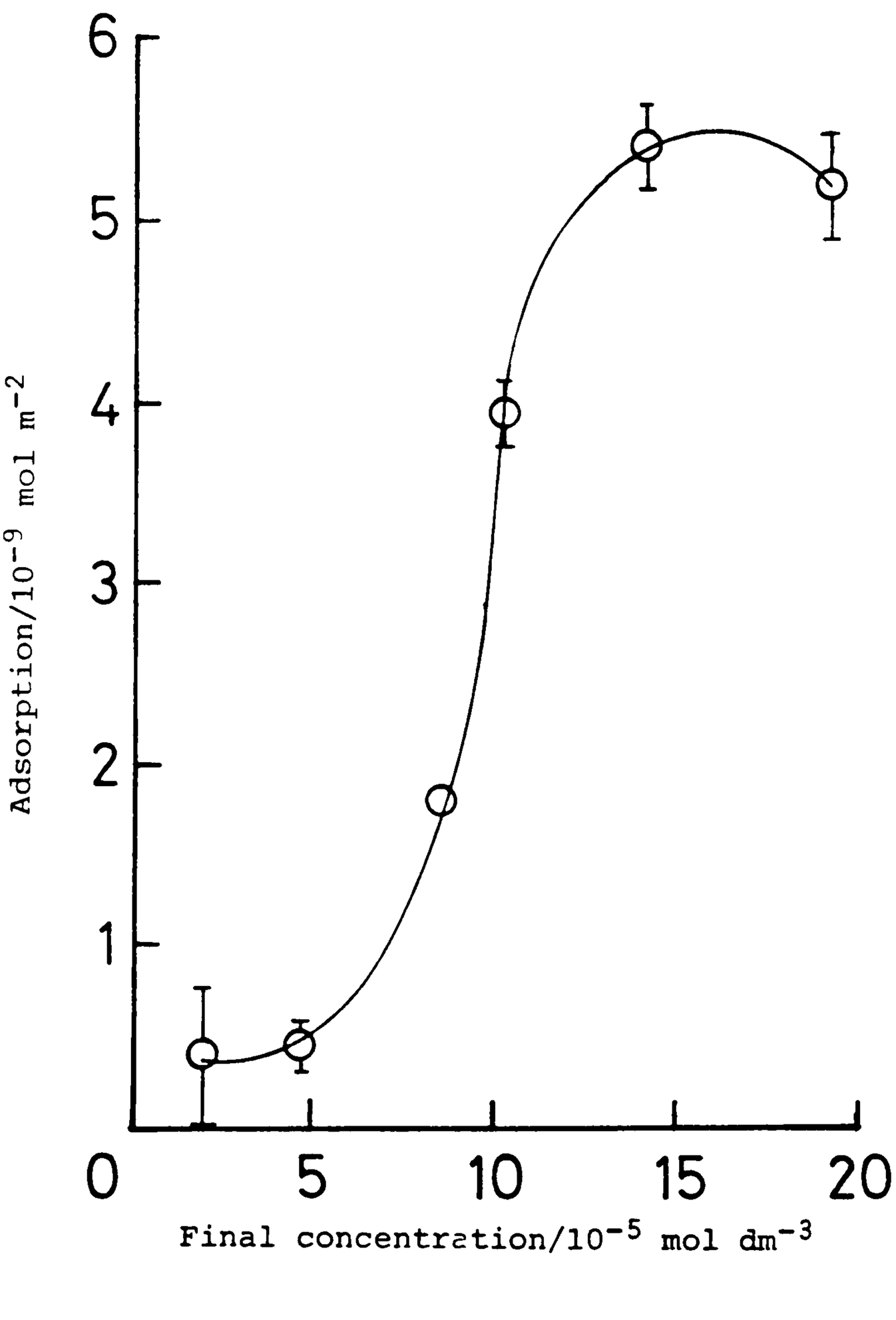

Figure 69: Adsorption of 4-ϕ-C_{12} ABS^{35} onto Gasil-35 from aqueous solution. pH = 2.4, T = 25°C, time = 24 hours. S/L = 10%.

3.6 Microelectrophoretic Studies

3.6.1 The Effect of Solution pH and NaCl Concentration on the Electrophoretic Mobility of Kaolin Particles

Variation of the electrophoretic mobility, U_E, of kaolin particles with solution pH, and at different NaCl concentrations, is shown in Figure 70. From the results it can be seen that as the solution pH is increased, the particles become increasingly negatively charged. At high solution pH (c.a. 10) a plateau is apparent in the mobilities, the value of which can be seen to depend on the ionic strength (as a function of NaCl concentration) of the solution, the highest mobility occurring at the lowest (ca. 10^{-3} mol dm^{-3} NaCl) salt concentration. At low pH ($\sim$ 2) lower mobilities are found, although a point of zero charge (pzc) is not reached.

3.6.2 The Effect of 4-ϕ-C_{12} ABS Adsorption on the Electrophoretic Mobility of Kaolin Particles

The electrophoretic mobility of kaolin particles, at 25°C, in 0.1 mol dm^{-3} NaCl solution, as a function of 4-ϕ-C_{12} ABS concentration, for three different solution pHs is shown in Figure 71. The results indicate that addition of the anionic surfactant, at a given pH, increases the negative charge of the particles (as shown by the increased negative mobility), up to a plateau value at a surfactant concentration of about 10^{-4} mol dm^{-3} (i.e. approximately the CMC under the salt conditions, Section 3.11). For a fixed surfactant concentration, above 10^{-4} mol dm^{-3} say, an increase in solution pH resulted in an increase (in a negative sense) of the mobility of the particles.

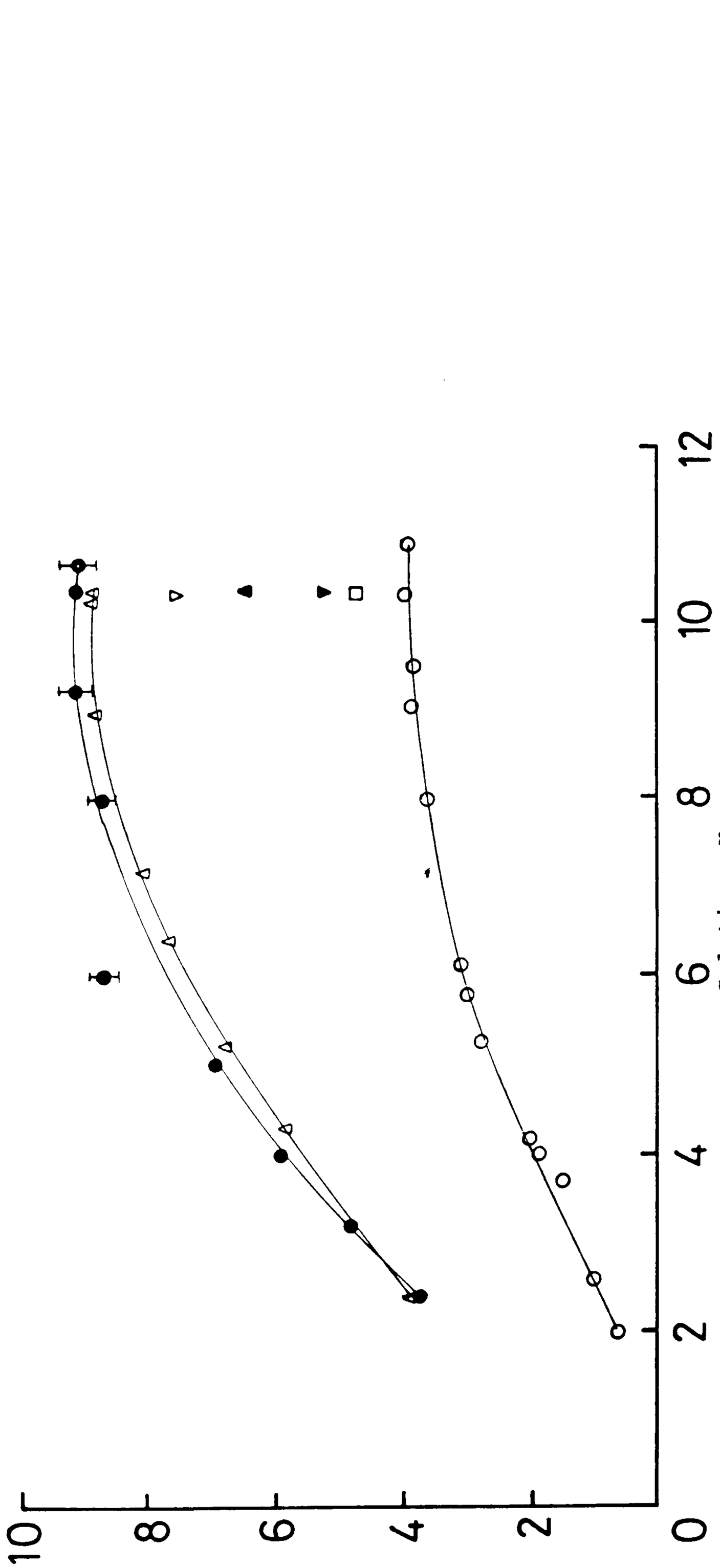

Figure 70: Effect of pH on the electrophoretic mobility of kaolin particles at differing NaCl concentrations and 25°C.

NaCl = 10^{-3} (Δ), 10^{-2} (●), 2×10^{-2} (▽), 4×10^{-2} (▲), 6×10^{-2} (▼), 8×10^{-2} (□), and 0.1 (O) mol dm^{-3}.

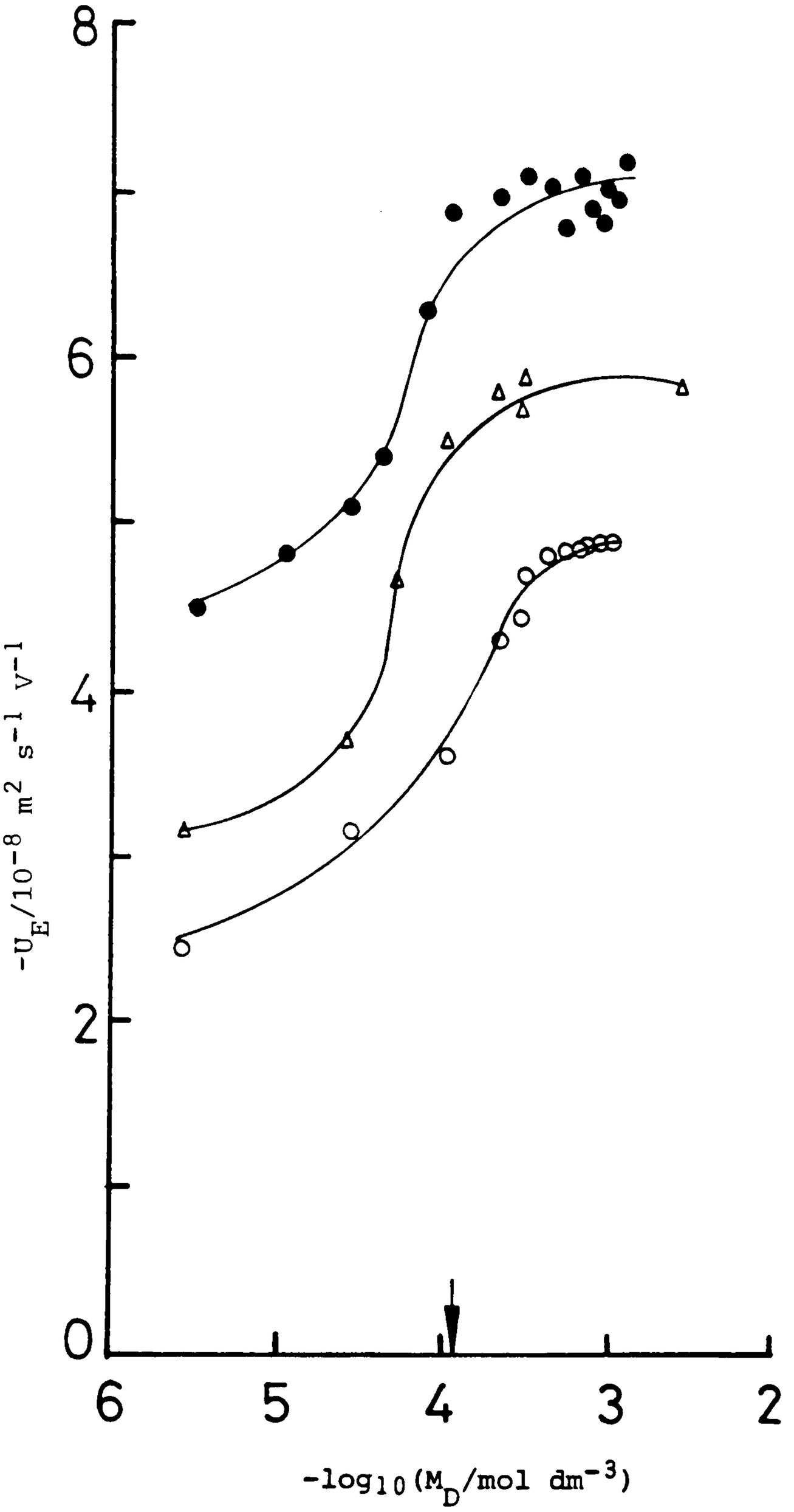

Figure 71: Effect of 4-ϕ-C_{12} ABS on the electrophoretic mobility of kaolin particles in 0.1 mol dm^{-3} NaCl, at 25°C, and pH 2.3 (O), 8.3 (Δ), 11.0 (●).

3.6.3 The Effect of CTAB Adsorption on the Electrophoretic Mobility of Kaolin Particles

The effect of CTAB addition on the electrophoretic mobility of kaolin particles, at 25°C in 0.1 mol dm^{-3} NaCl solution, as a function of surfactant concentration, at four different solution pHs, is shown in Figure 72.

From the results it is immediately apparent that the addition of cationic surfactant to the system reduces the (negative) electrophoretic mobility of the particles to zero and ultimately reverses the charge on the particle, a result which could not be achieved through pH adjustment alone (Figure 70).

3.7 Electrophoretic Mobility Measurements of Gasil-35 Silica

By way of comparison to kaolin, variation of the electrophoretic mobility of silica particles, with pH and salt concentration, has been measured, Figure 73.

Comparison of the results with those for kaolin, Figure 70, shows that the silica particles behave in the same manner as those of kaolin, that is, increasing pH causes an increase in the negative electrophoretic mobility, whereas increasing additions of NaCl reduce the mobility.

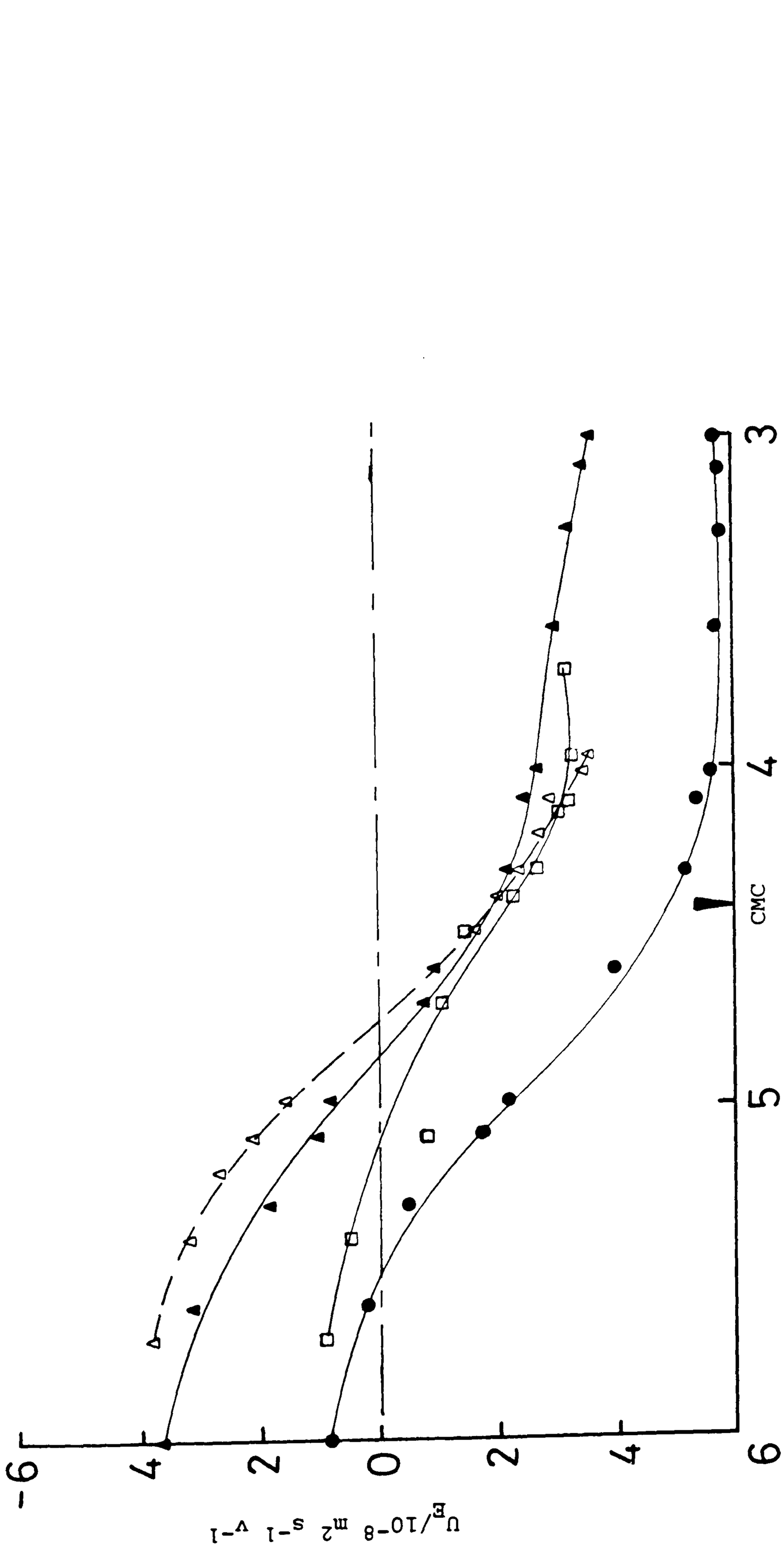

Figure 72: Effect of CTAB on the electrophoretic mobility of kaolin in 0.1 mol dm^{-3} NaCl, at 25°C, and pH 2.7 (●), 6.0 (□), 8.3 (▲) and 11.0 (Δ).

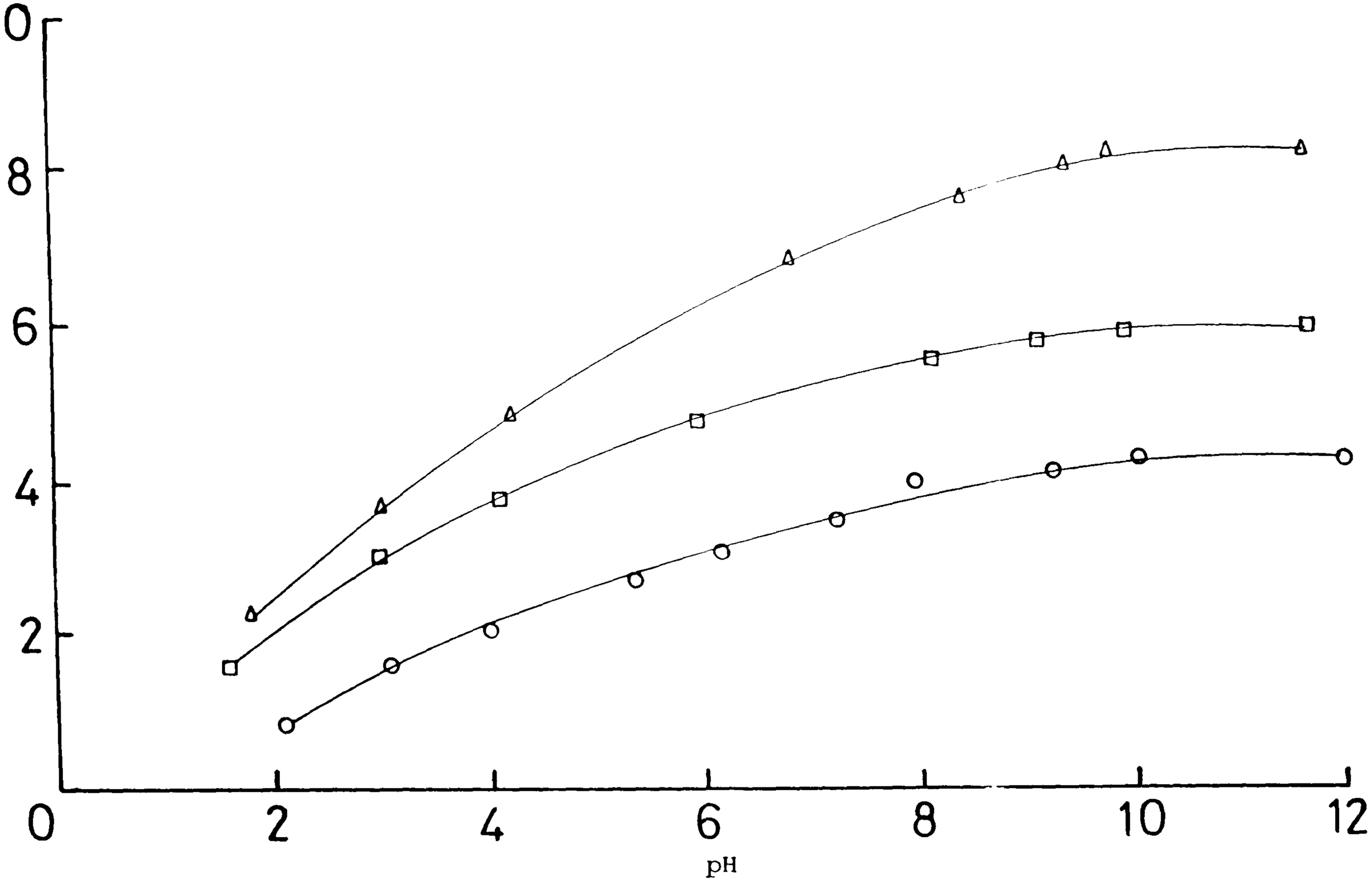

Figure 73: Effect of pH on the electrophoretic mobility of silica (Gasil-35) particles at differing NaCl concentrations, at 25°C. NaCl = 0.1 (○), 0.01 (□), and 0.001 (Δ) mol dm^{-3}.

3.8 Potentiometric Titration of the Kaolin Surface

To evaluate the surface charge (σ_o) of kaolin, as opposed to the diffuse layer charge (σ_d), from electrophoresis, a potentiometric titration of the surface was made.

The results of measurements made by titration of the clay surface, at 25°C, in solutions of differing ionic strength (adjusted with NaCl), as a function of surface charge density against equilibrium solution pH are shown in Figure 74.

The results are quite complex, showing, in contrast to the electrophoretic mobility measurements, a point of zero charge at a pH of about 6.0. However, in addition to this, a second charge reversal appears to have occurred, yielding a second point-of-zero charge at about pH 3.0. The results obtained are very consistent, making these observations all the more surprising.

3.9 Interactions between Aluminium Ions and 4-ϕ-C_{12} ABS

In order to obviate the possibility of surfactant loss to the kaolin surface by precipitation, interactions between aluminium ions and alkylbenzenesulphonate ions in aqueous solutions of varying pH, salt concentration, and co-surfactant concentration (n-butanol) have been investigated, both qualitatively, using light transmission, and quantitatively, using atomic absorption spectroscopy to determine aluminium concentrations in solution.

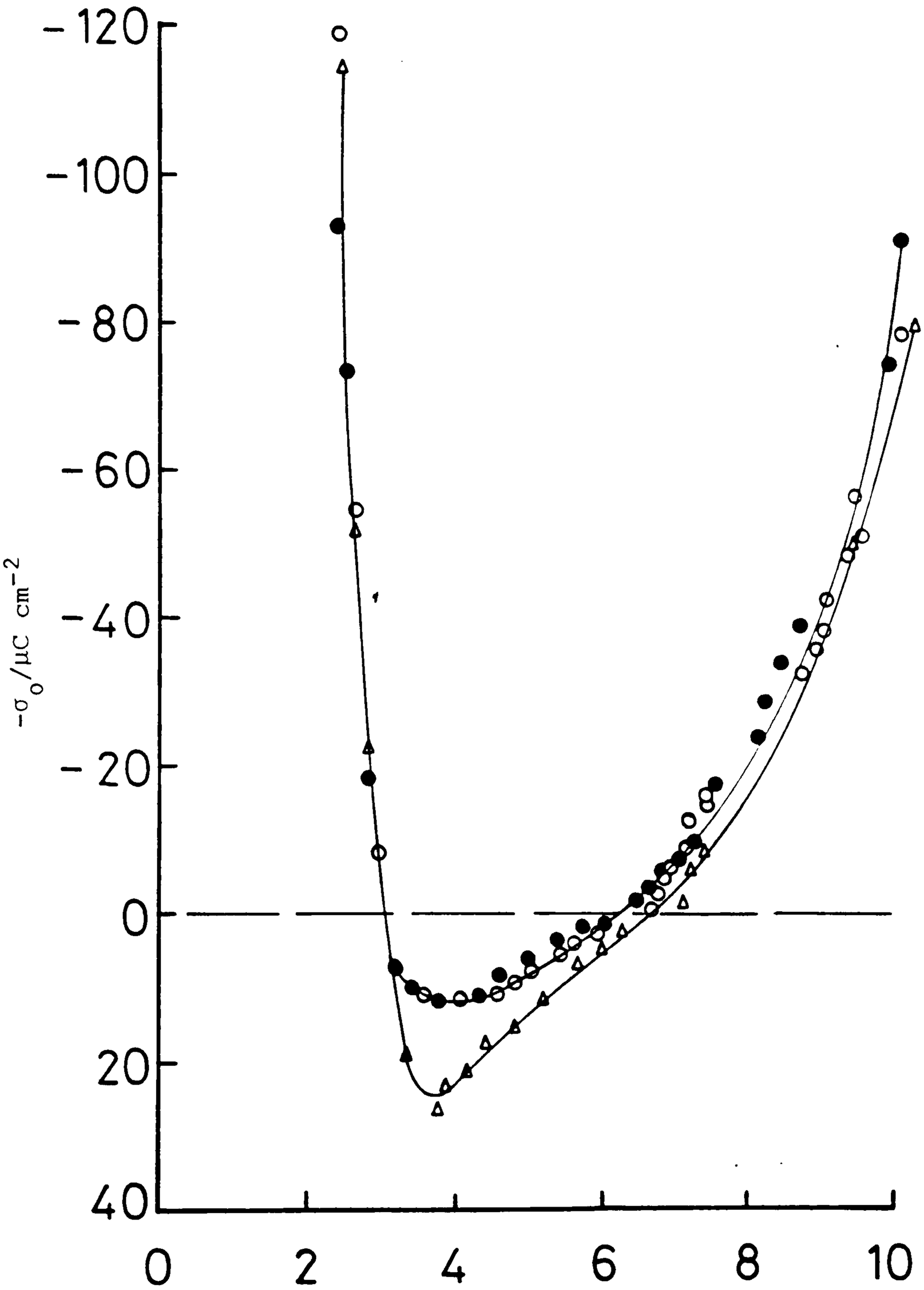

Figure 74: Effect of pH on the surface charge density of kaolin (from potentiometric titration) in NaCl solution = 0.1 (O), 0.05 (●), 0.01 (Δ) mol dm^{-3}, at 25°C.

3.9.1 Qualitative Measurements

Results obtained for the light transmission at 700 and 400 nm, of 4-ϕ-C_{12} ABS solutions, at 25°C and pH 3.7, as a function of aluminium concentration, are given in Figure 75. From here it can be seen that, for surfactant concentrations greater than 5.4×10^{-5} mol dm^{-3}, addition of aluminium (at concentrations above 10 ppm (3.7×10^{-4} mol dm^{-3})) causes a significant decrease in light transmission, due to increased turbidity of the solution. This is taken to be precipitate formation between aluminium and surfactant ions.

Figure 76 shows the results for the interactions at aluminium concentrations of 20 and 50 ppm, taken from the data of Figure 75.

Figure 77 shows the results of surfactant-aluminium interactions at 700 nm over a broader range of aluminium concentrations, and includes measurements at 100 ppm Al solutions,

3.9.1.1 Effect of Solution pH on Al-4-ϕ-C_{12} ABS Interactions

The effect of pH on the aluminium-surfactant interactions has been investigated for an initial aluminium concentration of 30 ppm. The results are shown, as a function of percent transmission, and log surfactant concentration, in Figure 78. From the results it can be seen that an increase in pH reduces the precipitation, the percentage transmission increasing from about 15% at pH 3.7, to 61% at pH 9.5, indicating that precipitate has either re-dissolved, or not formed readily at the higher pHs.

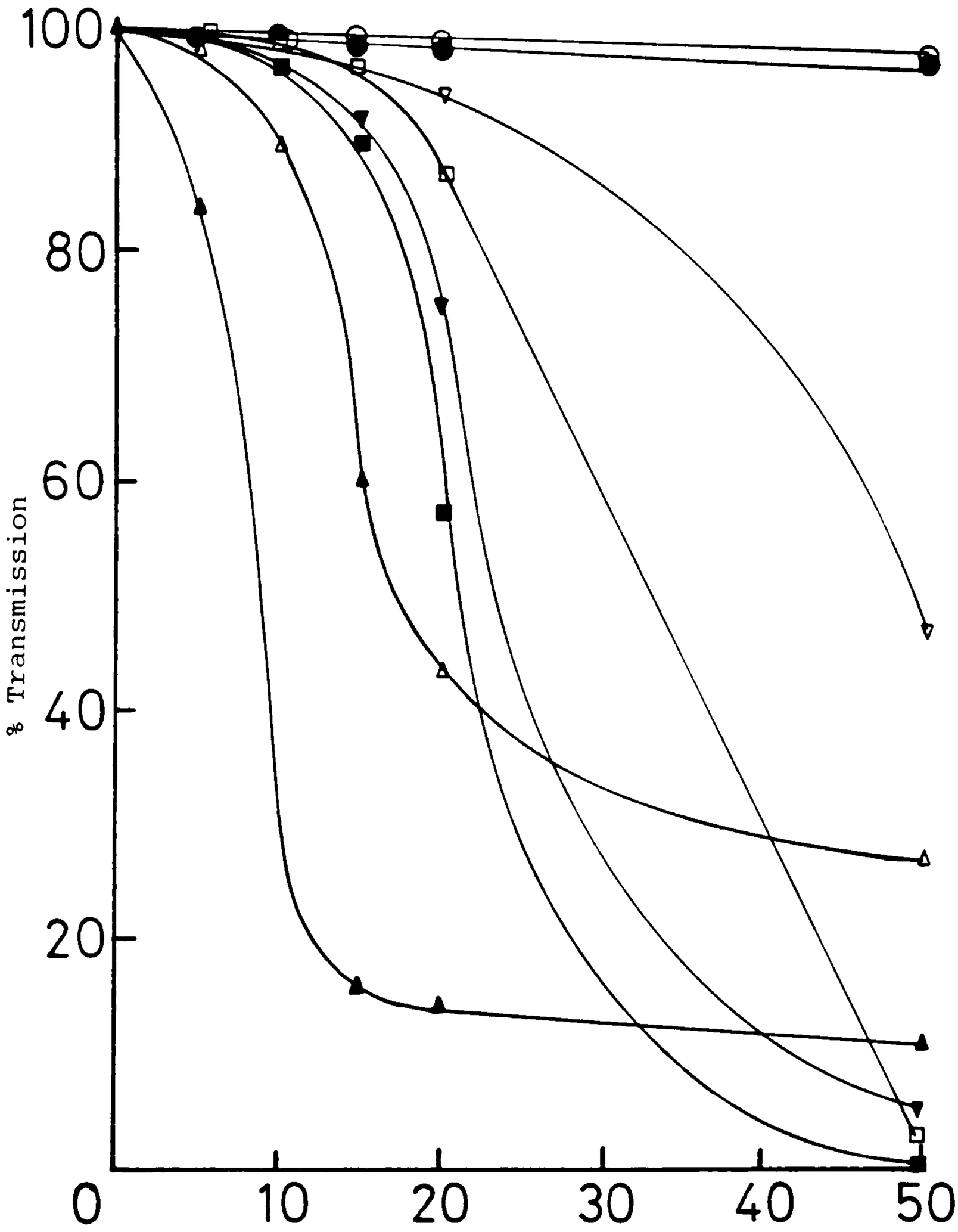

Figure 75: Percentage solution transmission, at 700 nm (open symbols) and 400 nm (closed symbols); versus aluminium concentration, at 4-ϕ-C_{12} ABS concentrations of 5.4×10^{-5} (○,●); 5.4×10^{-4} (△,▲); 5.4×10^{-3} (□,■); and 1.06×10^{-2} (▽,▼) mol dm^{-3}.

Solution pH = 3.7.

Temperature = 25°C.

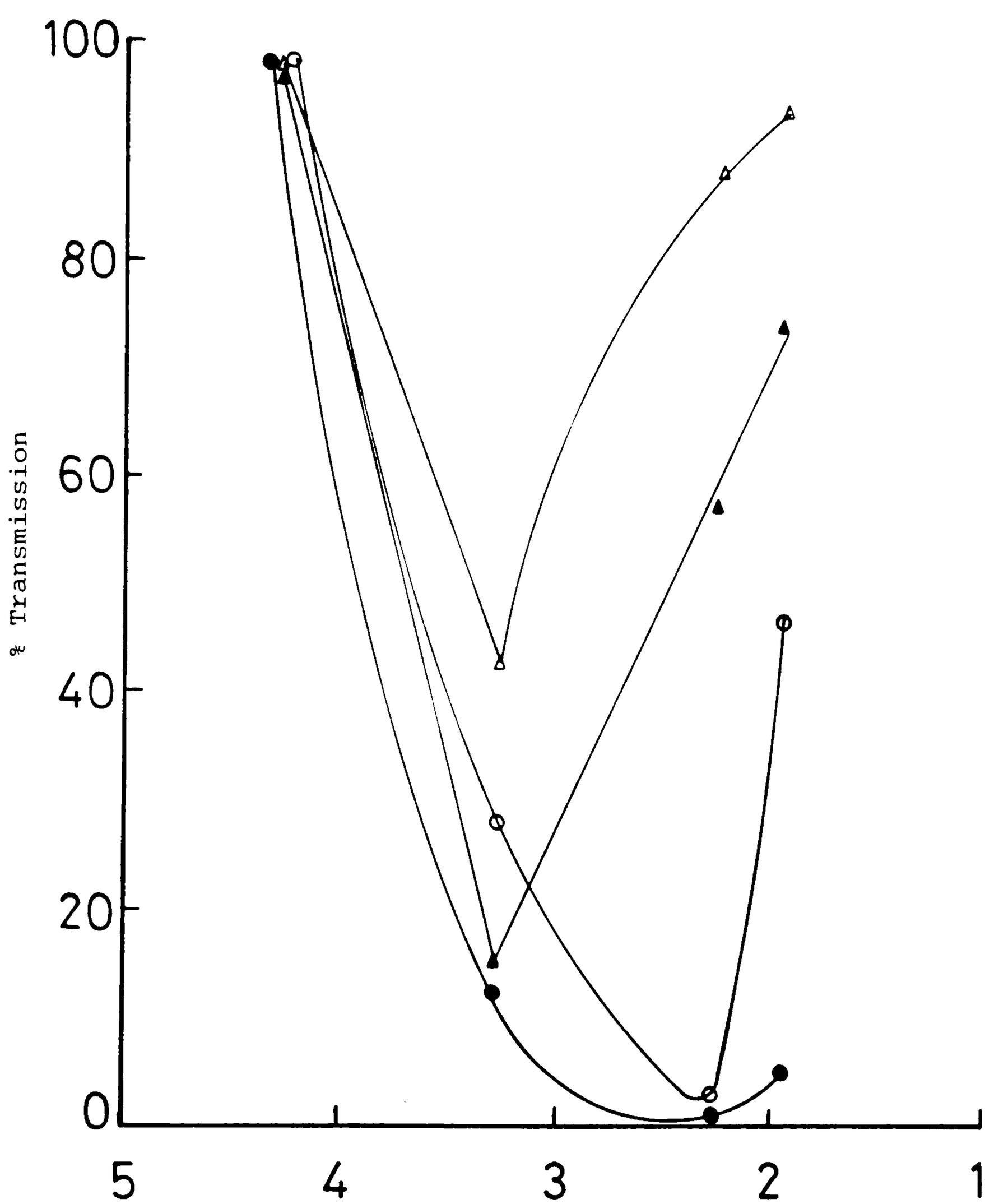

Figure 76: Percentage solution transmission, at 700 nm (open symbols) and 400 nm (closed symbols), versus surfactant concentration, at aluminium concentrations of 20 (Δ,▲) and 50 (O,●) ppm, from Figure 75. Solution pH = 3.7, Temperature = 25°C.

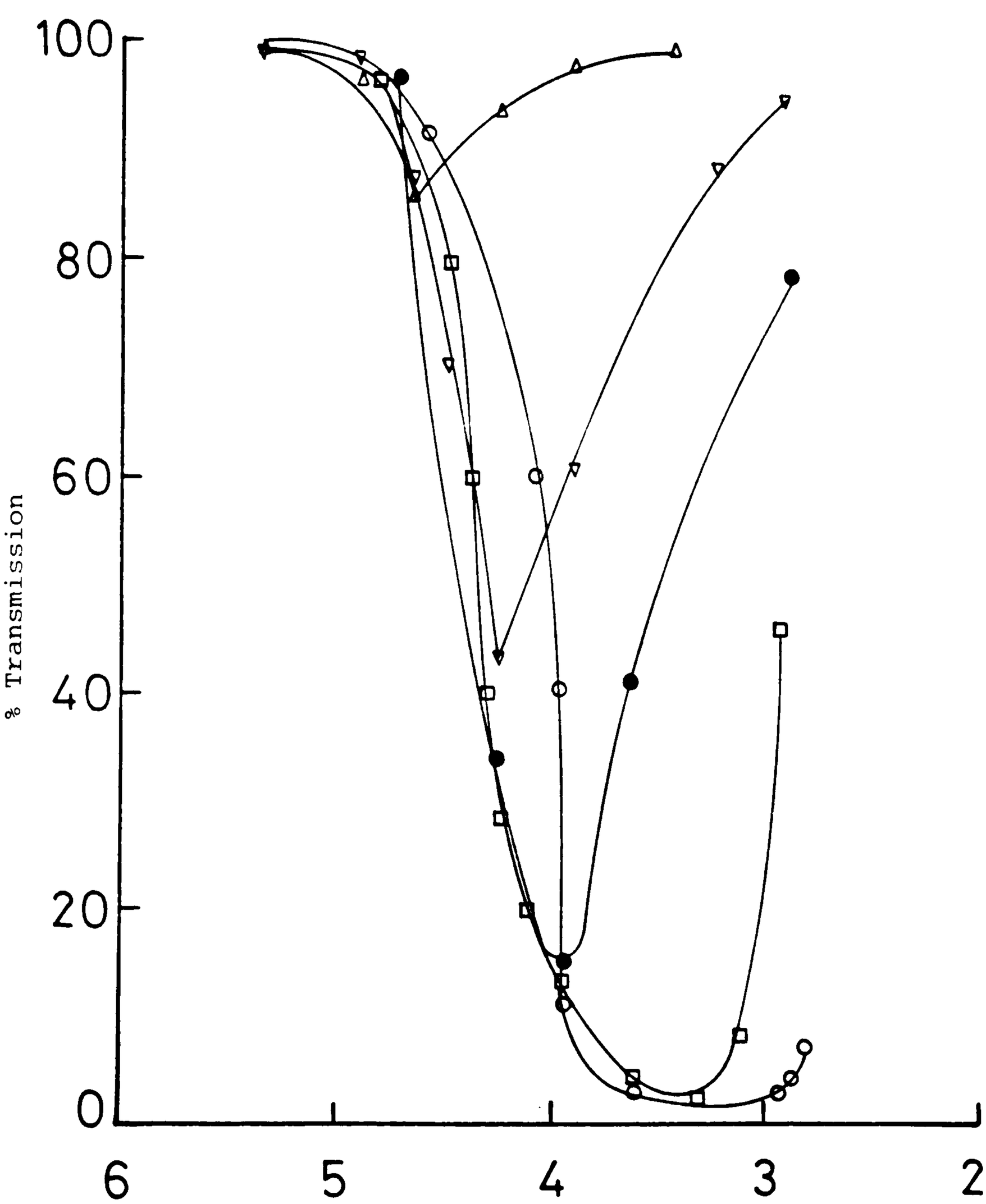

Figure 77: Percentage solution transmission, at 700 nm, versus 4-ϕ-C_{12} ABS concentration, for aluminium concentrations of 10 (Δ), 20 (∇), 30 ($\bullet$), 50 ($\square$), and 100 (O) ppm, at pH 3.7 and 25°C.

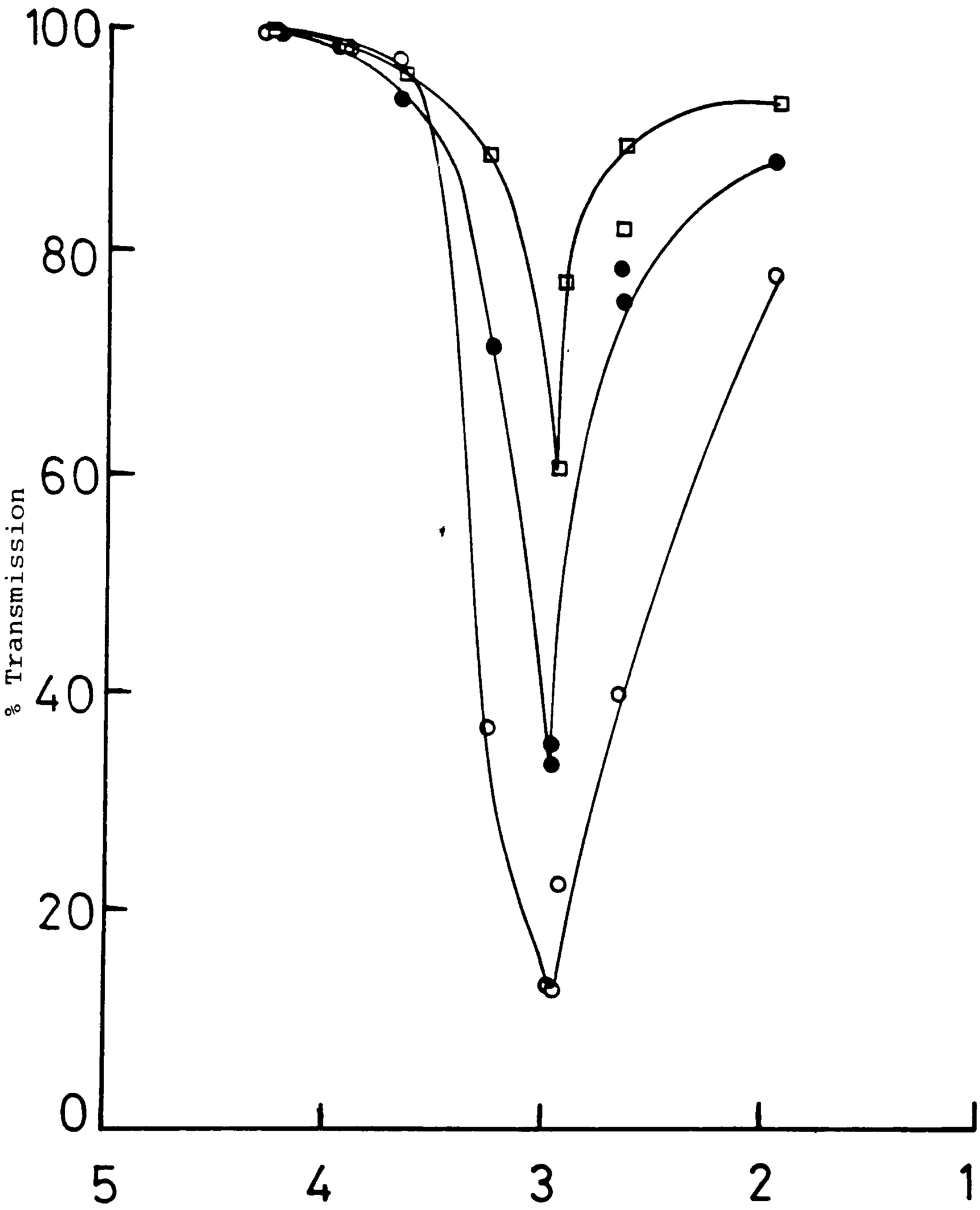

Figure 78: Percentage solution transmission, at 700 nm, versus 4-ϕ-C_{12} ABS concentration, for 30 ppm aluminium, at pH = 3.7 (○), 7.5 (●), and 9.5 (□).

To elucidate the mechanism of interaction between the aluminium and surfactant species in solution, quantitative measurements, utilising atomic absorption spectroscopy to determine aluminium, have also been made.

3.9.2 Quantitative Measurements of Aluminium-4-ϕ-C_{12} ABS Interactions

3.9.2.1 The Effect of Solution pH on the Aluminium-4-ϕ-C_{12} ABS Interactions

Figure 79 shows the residual concentration of aluminium (initially at 100 ppm, 3.7×10^{-3} mol dm^{-3}), as a function of log surfactant concentration, in solutions of aluminium and surfactant, at 25°C, and at different solution pHs. The results indicate that the precipitate formation is pH-dependent, with increasing pH reducing the amount of precipitation, in agreement with the earlier qualitative observations (Section 3.6.1.1).

Figure 80 shows the results for an aluminium-surfactant system in which the initial concentration of aluminium was 50 ppm (1.85×10^{-3} mol dm^{-3}). At this lower concentration of aluminium, and pH 4.38, almost complete re-dissolution of the precipitate is achieved, the residual concentration of aluminium, at about 10^{-2} mol dm^{-3} 4-ϕ-C_{12} ABS, being almost the same as that at zero surfactant concentration.

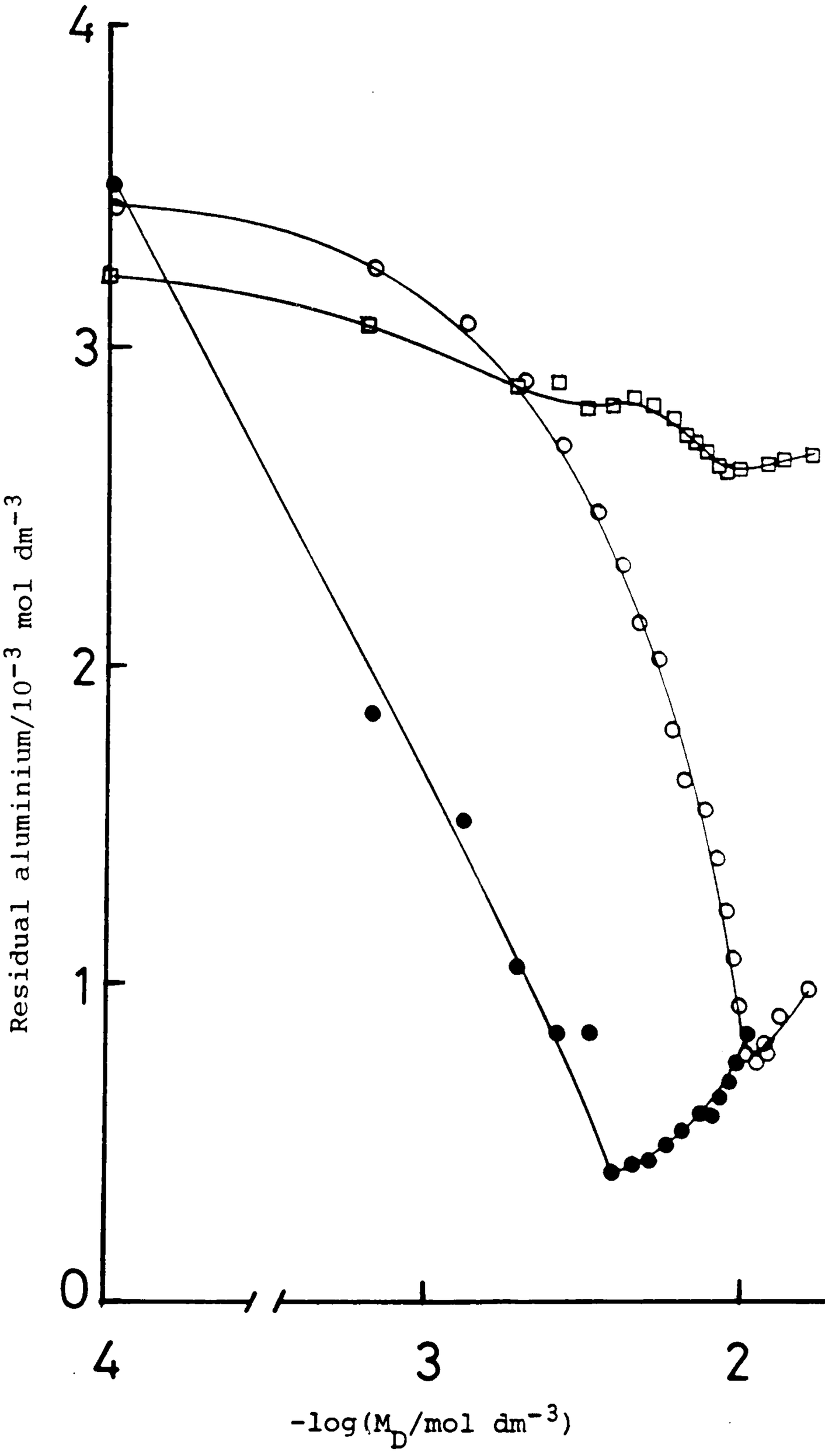

Figure 79: Effect of 4-ϕ-C_{12} ABS concentration on the amount of aluminium (initially at 100 ppm, 3.7×10^{-3} mol dm^{-3}) remaining in solution, at pH 1.57 (○), 4.24 (●), 11.0 (□). T = 25°C.

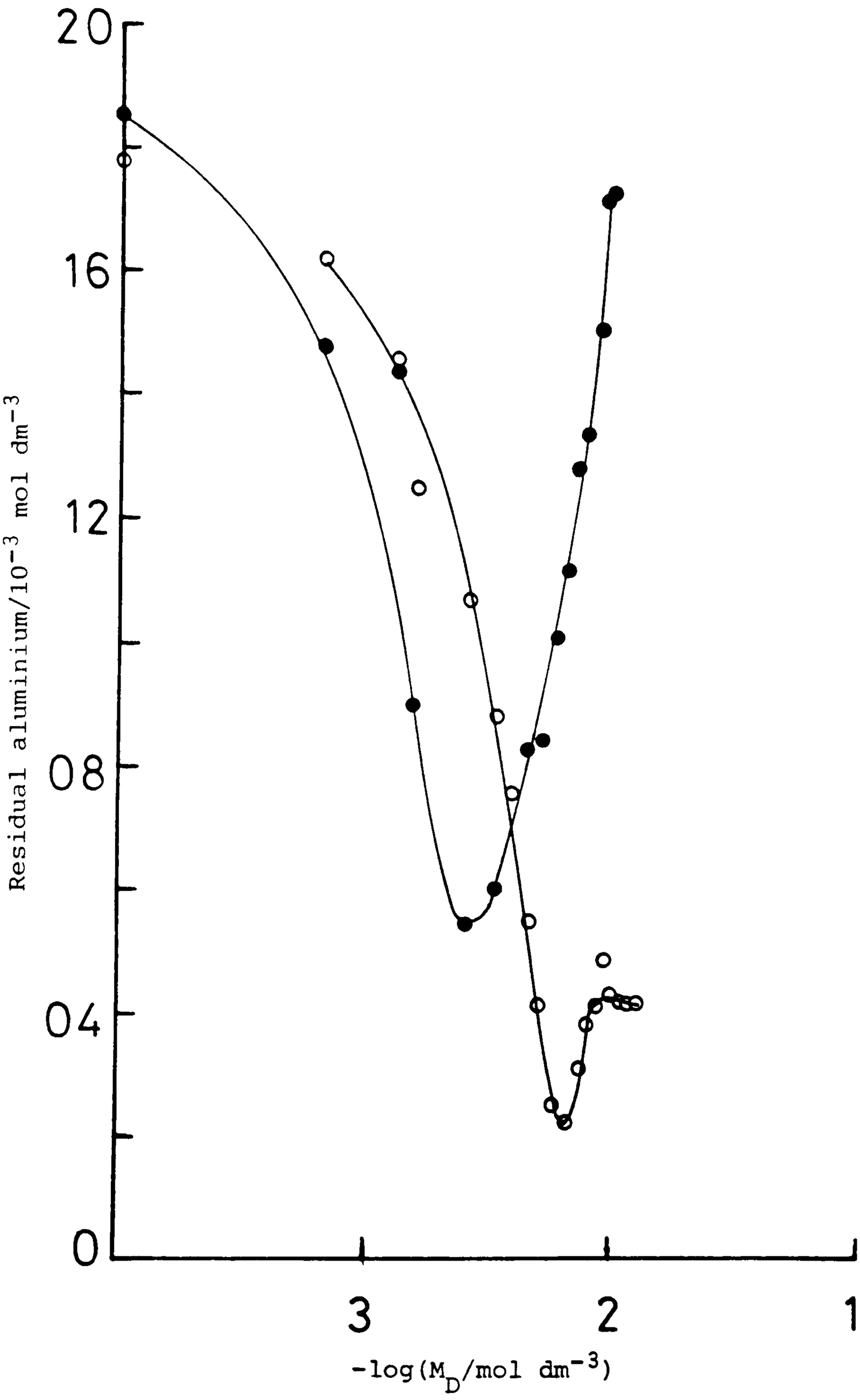

Figure 80: Effect of 4-ϕ-C_{12} ABS concentration on the amount of aluminium (initially at 50 ppm, 1.85×10^{-3} mol dm^{-3}) remaining in solution, at pH 1.8 (O) and 4.38 (●). T = 25°C.

3.9.2.2 The Effect of Sodium Chloride on Aluminium-4-ϕ-C_{12} ABS Interactions

The formation, and re-dissolution, of aluminium-surfactant complexes, as a function of surfactant concentration, at pH 1.57, and varying NaCl concentrations, is shown in Figure 81, for an initial aluminium concentration of 100 ppm. The results show that increasing concentrations of NaCl reduce the precipitate formation, although the position of the minima remains approximately the same. The effect of 0.5 mol dm^{-3} NaCl on the precipitation-redissolution process is interesting because, in other studies, the surfactant has been found to precipitate at such salt concentrations, and to re-dissolve. This suggests that a competition is taking place between alumina and sodium ions for the anionic surfactant, and probably the greater concentration of Na^{+}, over Al^{3+}, dominates the system, thus the observations may arise from [Na^{+}-4-ϕ-C_{12} ABS^{-}] precipitation and re-dissolution.

3.9.2.3 The Effect of n-butanol on Aluminium-4-ϕ-C12 ABS Interactions

The effect of n-butanol on aluminium-4-ϕ-C_{12} ABS solution interactions at pH 1.57, and 25°C, is shown in Figure 82, as a function of 4-ϕ-C_{12} ABS concentration. From the results, it can be seen that at low surfactant concentrations (ca. 10^{-3} mol dm^{-3}) butanol addition reduces precipitation, however at higher concentrations (ca. 10^{-2} mol dm^{-3}) this is reversed, although the minima are very close together.

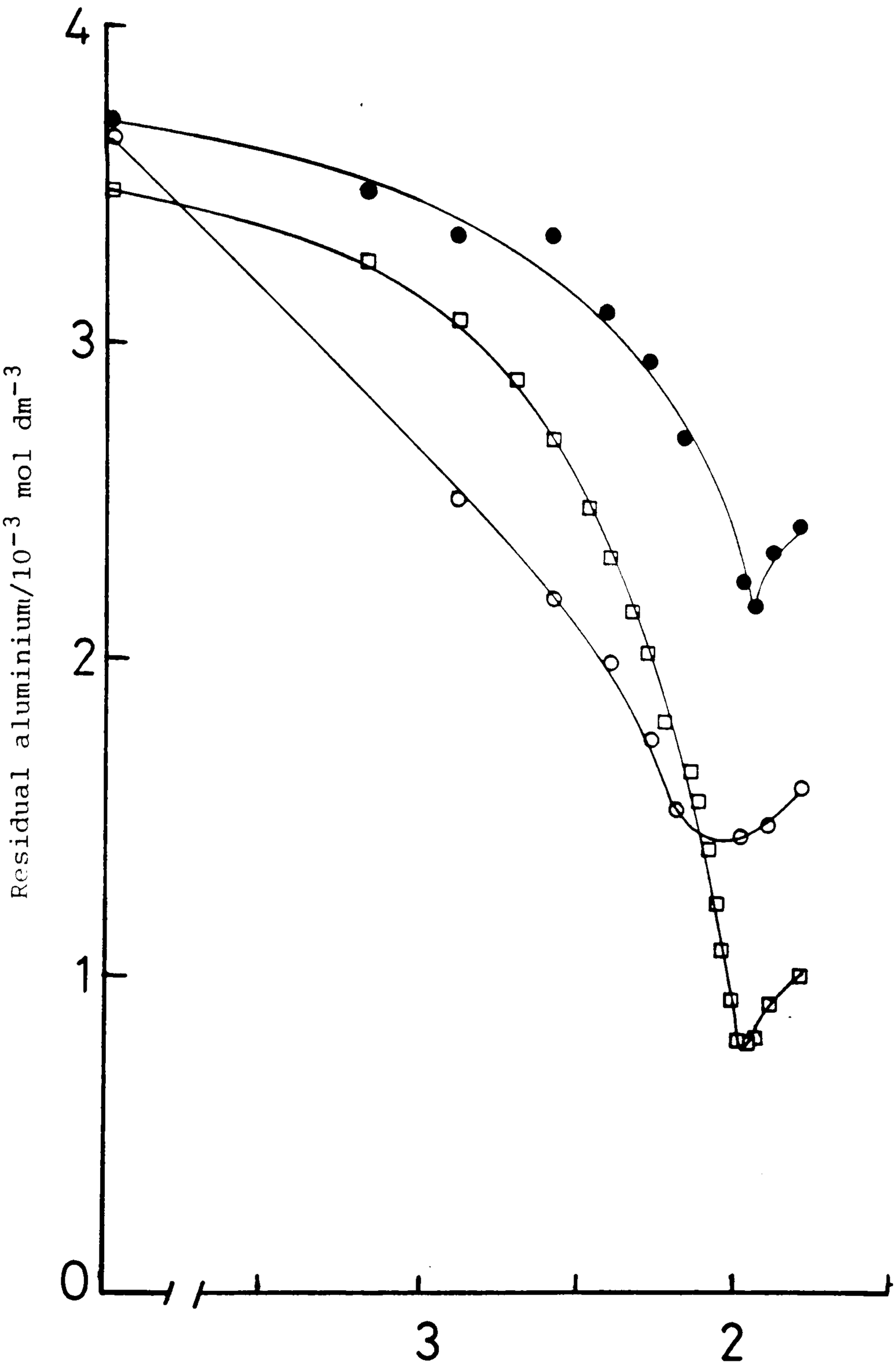

Figure 81: Effect of 4-ϕ-C_{12} ABS concentration on residual aluminium concentration, at pH 1.6 and initial aluminium of 100 ppm (3.7×10^{-3} mol dm^{-3}); for NaCl concentrations of 0 (□), 0.1 (○), and 0.5 (●) mol dm^{-3}; T = 25°C.

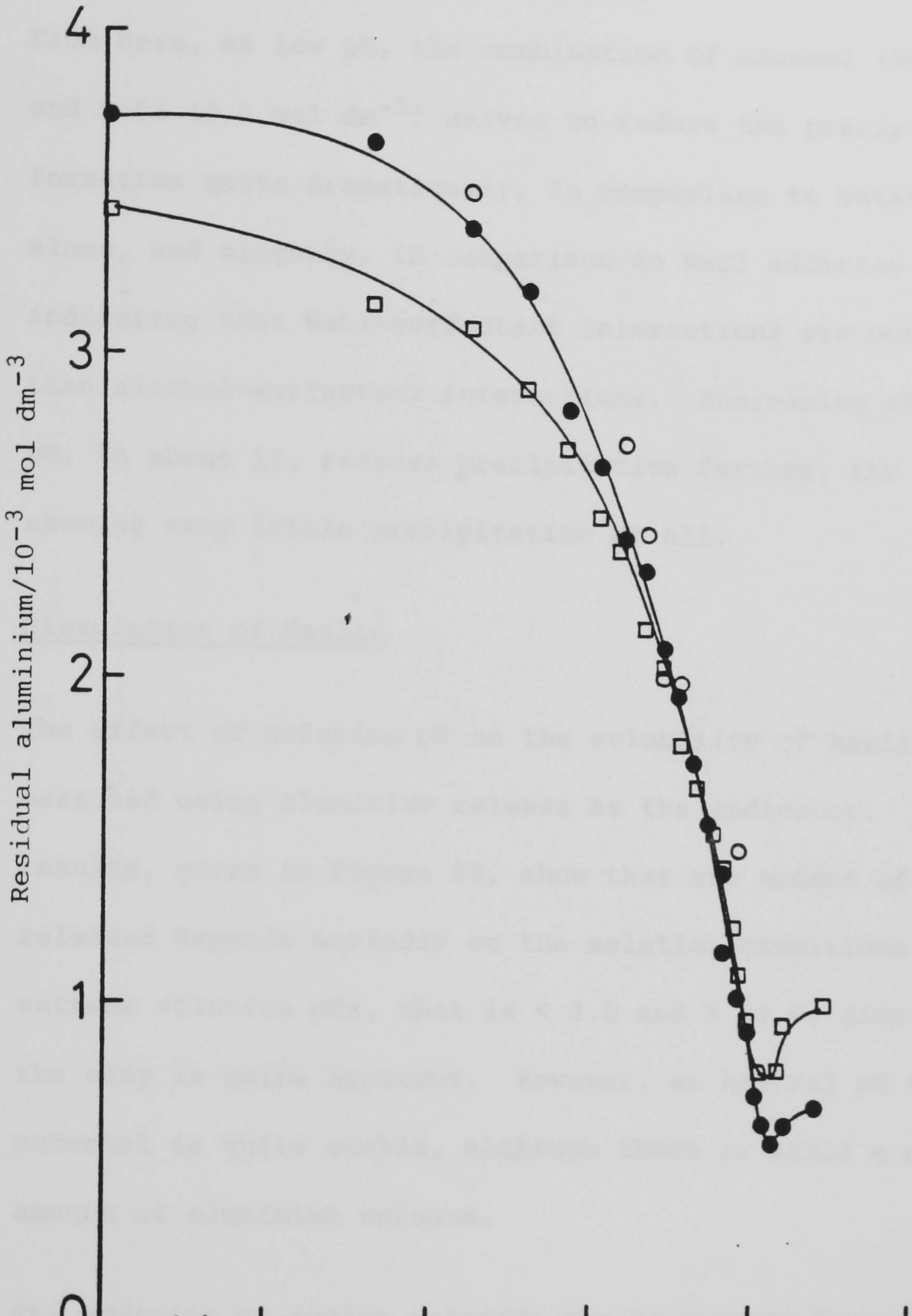

Figure 82: Effect of butanol on aluminium/4-ϕ-C_{12} ABS interactions at pH1.6.

Butanol = 1% (v/v) (O), 5% (v/v) (●), 0% (v/v) (□).

Initial Al = 100 ppm = 3.7×10^{-3} mol dm^{-3}.

T = 25°C.

3.9.2.4 The Combined Effect of Sodium Chloride and n-butanol on Aluminium-4-ϕ-C_{12} ABS Interactions

The combined effects of NaCl, and n-butanol, addition on the precipitation of aluminium as a function of 4-ϕ-C_{12} ABS concentration, in acidic and basic pHs, is shown in Figure 83. From here, at low pH, the combination of alcohol (5% (v/v)) and NaCl (0.5 mol dm^{-3}) serves to reduce the precipitate formation quite dramatically, in comparison to butanol addition alone, and slightly, in comparison to NaCl addition alone, indicating that NaCl-surfactant interactions are more effective than alcohol-surfactant interactions. Increasing the solution pH, to about 12, reduces precipitation further, the results showing very little precipitation at all.

3.9.3 Dissolution of Kaolin

The effect of solution pH on the solubility of kaolin has been measured using aluminium release as the indicator. The results, given in Figure 84, show that the amount of aluminium released depends markedly on the solution conditions. At extreme solution pHs, that is < 2.0 and > 12.0, dissolution of the clay is quite apparent. However, at neutral pH the material is quite stable, although there is still a measurable amount of aluminium release.

The addition of sodium chloride can be seen to have an influence on the solid's stability, an increase in added salt reducing aluminium release even in the extreme pH regions.

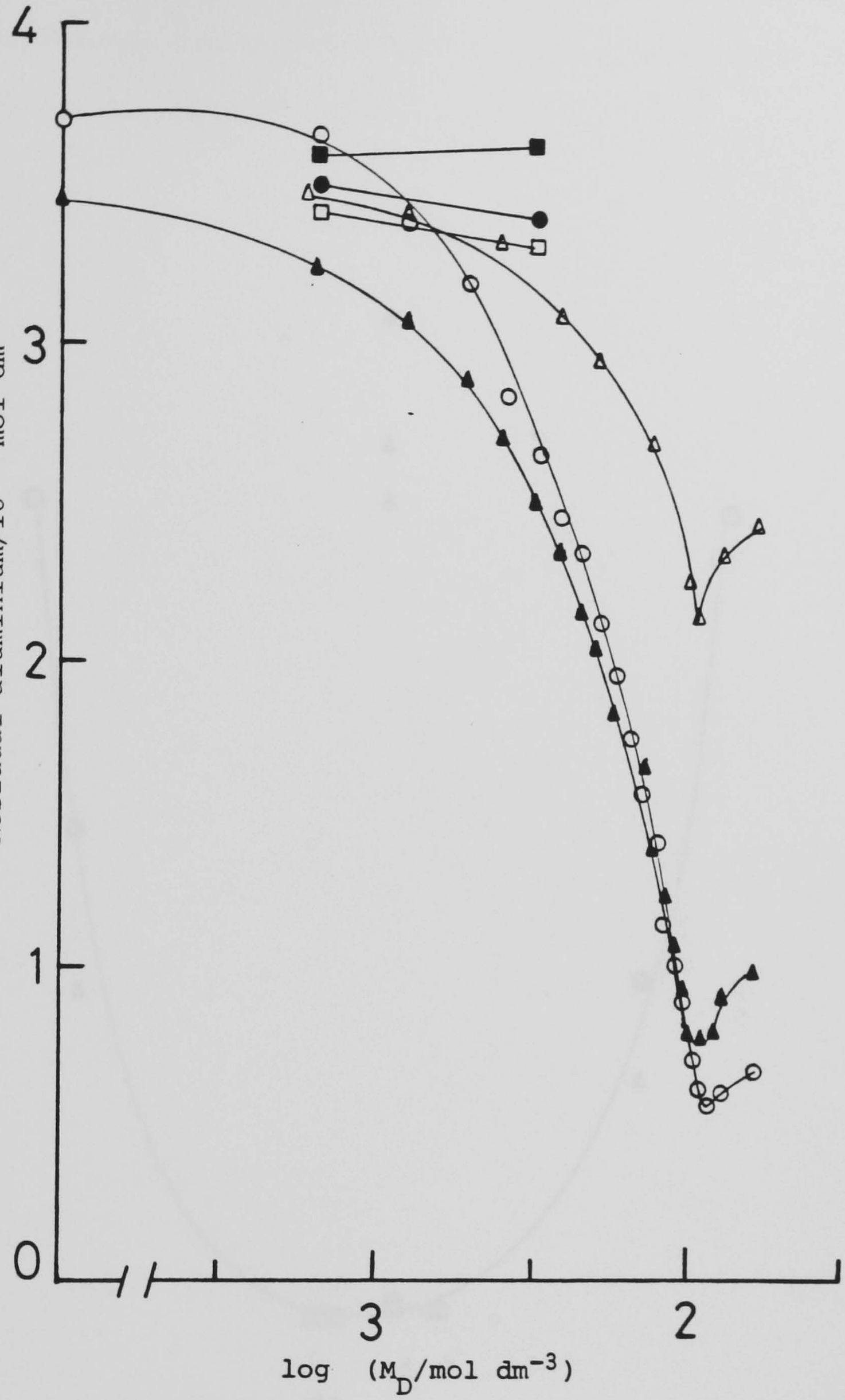

Figure 83: Effect of 4-ϕ-C_{12} ABS on residual aluminium concentration (initially 100 ppm, 3.7×10^{-3} mol dm^{-3}), at 25°C and various solution pHs, in the presence of NaCl and n-butanol.

(▲) 0 mol dm^{-3} n-ButOH, 0 mol dm^{-3} NaCl, pH 1.6.
(△) 0 mol dm^{-3} n-ButOH, 0.5 mol dm^{-3} NaCl, pH 1.0.
(○) 0.55 mol dm^{-3} n-ButOH, 0 mol dm^{-3} NaCl, pH 1.6
(●) 0.55 mol dm^{-3} n-ButOH, 0.5 mol dm^{-3} NaCl, pH 0.9.
(□) 0.55 mol dm^{-3} n-ButOH, 0.5 mol dm^{-3} NaCl, pH 2.3.
(■) 0.55 mol dm^{-3} n-ButOH, 0.5 mol dm^{-3} NaCl, pH 12.3.

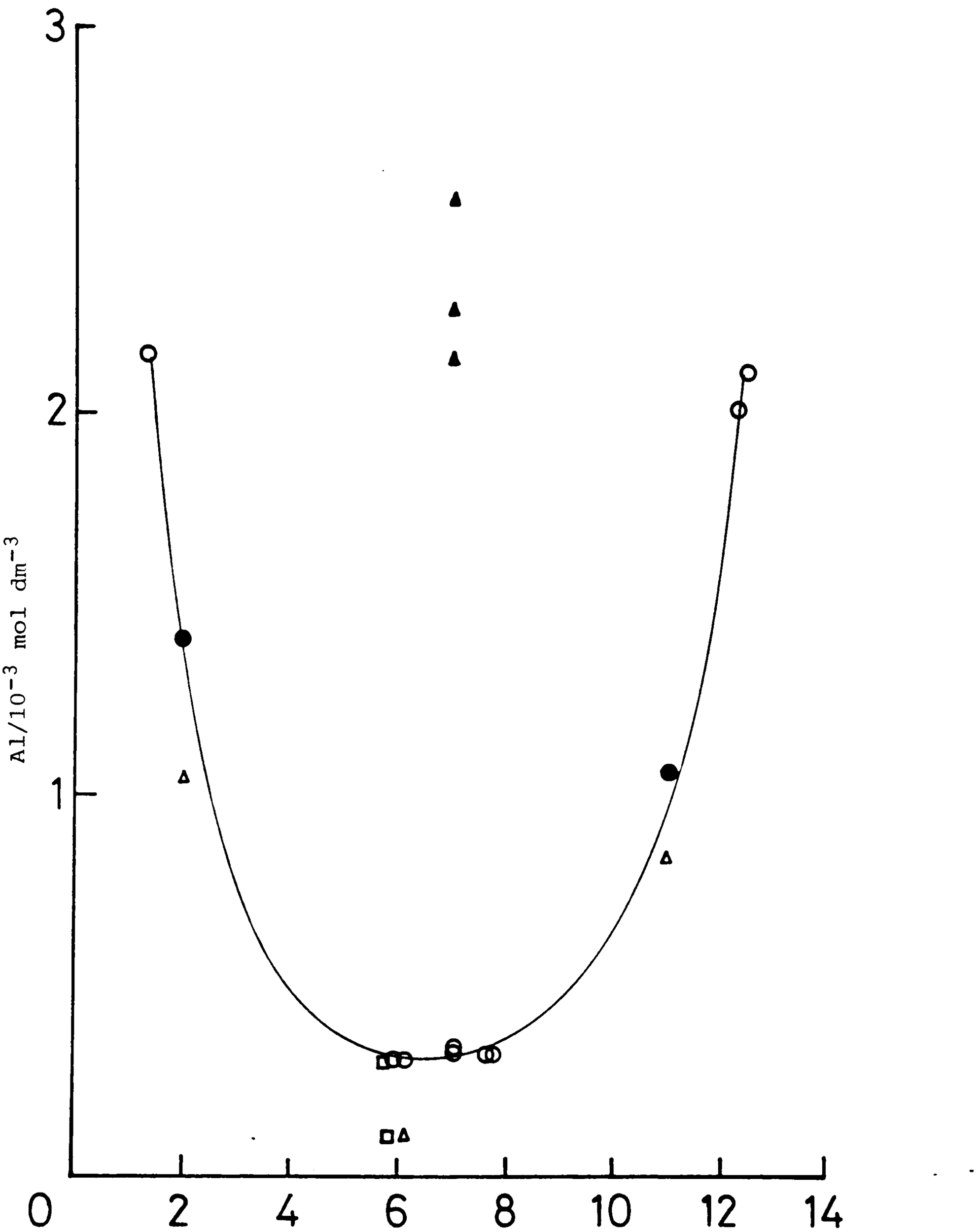

Figure 84: Effect of solution conditions on aluminium release from kaolin, at 25°C

(O) Aluminium in aqueous solution, (●) 0.1 mol dm^{-3} NaCl
(Δ) 0.5 mol dm^{-3} NaCl, (▲) 0.55 mol dm^{-3} n-butanol
(□) 0.55 mol dm^{-3} n-butanol + 0.5 mol dm^{-3} NaCl

The effect of n-butanol addition on the aluminium release is surprising; addition of this organic compound causing the release to increase greatly at neutral pH.

Chapter Four

Discussion

4.1 Adsorption of Sodium Dodecylbenzenesulphonate Isomers, and CTAB, at the Air/Aqueous Solution Interface (Section 3.1)

At surface saturation, the surface excess concentration of a surfactant, Γ_D, is a useful measure of the "effectiveness" of surfactant adsorption, since it is the maximum adsorption that can be attained [R5]. From the data in Table 5(a) (Section 3.1), it can be seen that, at 25°C, CTAB is most effectively adsorbed at the air-water interface. This behaviour can be attributed to the longer hydrophobic chain, and lower aqueous solubility, of this surfactant.

The effect of chain-length on the adsorption of alkylbenzene-sulphonate isomers is also apparent from the results in Table 5(a). With the phenyl group, at a terminal position on the hydrophobic chain, the surfactant, at 25°C, is below its Krafft point [R2] and the solubility limits the adsorption at the interface. Movement of the phenyl sulphonate group away from the terminal position, as in the 4-, or 6-phenyl isomers, effectively reduces the hydrophobic chain length, by introducing branching at the phenyl position, increasing the aqueous solubility of the surfactant and thus the CMC. Adsorption at the air-water interface is therefore reduced by the increased solubility and the effective area/molecule, A_s, is increased.

Packing of surfactant at an interface is an important parameter in surfactant adsorption because it can affect the reduction in surface tension produced by adsorption. Comparison of the area /molecule for the 1-phenyl-C_{12} ABS isomer at 70°C, and CTAB at 25°C, with those of the branched isomers reveals that the

straight-chain molecules pack better, and reduce the area/molecule at the interface (Table 5(a)). However, since the cross-sectional area of an aliphatic chain oriented perpendicularly to an interface is about 20 $Å^2$ [R2] and that of a benzene ring about 25 $Å^2$, it is apparent from the values of A_s, in Table 5(a) that the hydrophobic chain of the adsorbed molecules are not in close-packed arrangement normal to the interface at saturation adsorption. At the other extreme, the cross-sectional area of a $-CH_2-$ group lying flat is about 7 $Å^2$ and so the molecules are not flat in the interface either. Thus, from the data, the molecules must be tilted with respect to the interface, and branching, which is present in the 4- and 6-phenyl isomers, enhances this effect.

While Γ_D measures the "effectiveness of surfactant adsorption" at an interface, the surface pressure, π_{CMC}, measures the "effectiveness of a surfactant at reducing surface, or interfacial tension" through determination of the maximum amount by which the surfactant can lower the solvent surface tension, from its initial value, γ_0, to some value, γ_1, at the CMC [R6]. π_{CMC} is related to the bulk concentration of surfactant by [R2]:

$$\pi_{CMC} = (\gamma_0 - \gamma_1) + 2.303y\, RT\, \Gamma_D \log\left(\frac{M_{D(CMC)}}{M_{D_1}}\right) \qquad (4.1)$$

where $M_{D(CMC)}$ is the surfactant CMC.

From the Frumkin equation [F6]:

$$\pi_{CMC} = -2.303RT\, \Gamma_D \log\left(1 - \frac{\Gamma_1}{\Gamma_D}\right),$$

where Γ_1 is the surface excess concentration of surfactant at M_{D_1}, it can be shown that a reduction of γ_0, by 20 mN m^{-1},

results from an increase of surfactant surface excess concentration of 0.84 to 0.999Γ_D [R2]. Therefore, the surface concentration at π = 20 mN m^{-1} is 84-99.9% saturated. Substitution, for M_{D_1}, in equation (4.1) under these conditions gives:

$$\pi_{CMC} = 20 + 2.303y\ RT\ \Gamma_D \log\left(\frac{M_{D(CMC)}}{M_{D(\gamma=20)}}\right) \qquad (4.2)$$

and using this equation, gives a quantitative measure of the effectiveness of surface tension reduction (π_{CMC}) can be obtained. Table 5(b) gives experimental, and calculated, values of π_{CMC} obtained from the data in Figure 38. From the results it can be seen that agreement between the experimental and calculated values is good, and that the most effective reduction in surface tension (highest π_{CMC}), at 25°C, is given by the branched chain alkylbenzenesulphonates. The maximum reduction in tension for the 1-phenyl isomer, at this temperature, is limited by the concentration of monomer at solution saturation. That branched molecules should be more effective in surface tension reduction than their straight-chain counterparts is a consequence of their greater area/molecule at the interface, which indicates that these molecules "spread-out" over the interfacial area more so than do their straight-chain equivalents (e.g. 1-phenyl-C_{12} ABS at 70°C, and CTAB at 25°C).

An additional parameter, with which the adsorption of these surfactants may be compared, is their "adsorption efficiency" [R6]. This quantity, defined as $-\log\left(M_{D(CMC)}\right)$, or $pM_D(20)$, indicates the bulk concentration of surfactant needed to produce a 20 mN m^{-1} reduction in the solvent tension. It is therefore related to π_{CMC} by equation (4.2). Table 5(b) shows

values of $pM_D(20)$ obtained from data in Figure 38. It is noteworthy that $pM_D(20)$ is a log scale and so covers a large concentration range.

From Table 5(b), the 1-phenyl-C_{12} ABS isomer, at 25°C, shows the greatest efficiency of adsorption at the aqueous surface. In terms of concentration, the amount of this surfactant, needed to reduce the tension by 20 mN m^{-1}, is, respectively, some 28 to 22% less than that required of the 4- and 6-phenyl isomers. This large difference is due to the low aqueous solubility of the 1-phenyl isomer at this temperature. CTAB shows the least efficiency of adsorption, and this may be due to 'coiling' of the long hydrophobic chain at the interface, with a consequent decrease in its ability to reduce the tension [M3]. The concentration (mol dm^{-3}) of CTAB needed to effect the 20 mN m^{-1} reduction in tension is about 25% greater than that of the 1-phenyl-C_{12} ABS isomer, and 16% greater than that of the 4- and 6-phenyl-C_{12} ABS isomers.

The results found above, of Γ_D, π_{CMC}, and $pM_D(20)$, show that while a surfactant may be efficient at adsorbing at an interface, for example, Γ_D (CTAB) > Γ_D (alkylbenzenesulphonate), at 25°C, it is not necessarily effective, nor efficient, at reducing the tension.

4.1.1 The Effect of Sodium Chloride on 4-ϕ-C_{12} ABS and CTAB Adsorption at the Air-Aqueous Solution Interace (Section 3.1.1)

From the results, given in Tables 6 and 7, it is apparent that the effectiveness of surfactant adsorption at the air-water interface, increases with increased concentration of NaCl, and that

both A_s (area/molecule) and the surfactant CMC, decrease with the addition. The efficiency of adsorption at the interface increases markedly with increasing NaCl concentration, and effectiveness of surface tension reduction is also increased.

The increase in surface activity, and the decrease in CMC, arise from reduced repulsion between oriented ionic head-groups. The Gouy-Chapman-Stern model, derived for spherical colloidal particles [W6,H7,O4], represents the electrical double layer (edl) at the ionic head-group-water interface, and the thickness of this layer, $\frac{1}{\kappa}$, can be related to the solution ionic strength by equation (1.12) [A4]:

$$\kappa = \left(\frac{2e^2 N_A . C Z^2}{\varepsilon\ kT}\right)^{\frac{1}{2}}$$

in which $\varepsilon_r = (\varepsilon/\varepsilon_0)$ = the relative static permittivity, or dielectric constant, of the solution. (ε = static permittivity of the solution, and ε_0 = permittivity of a vacuum).

Using this equation, the effect of adding NaCl, to the aqueous system, on $\frac{1}{\kappa}$ can be evaluated. Figure 85 shows the variation of $\frac{1}{\kappa}$ with added NaCl, at 298 K. From the results (Figure 85), it can be seen that the electrolyte compresses the edl and therefore will allow closer approach of the ionic head-groups. As a result of the reduction in $\frac{1}{\kappa}$, increased surface activity and lower CMCs are found. In terms of bulk concentrations, the addition of NaCl to the surfactant system improves the effectiveness of surface tension reduction; for 0.01 mol dm^{-3} NaCl about 55% less surfactant is needed to effect the same change in surface tension than in aqueous solution alone. For 0.1 mol dm^{-3} NaCl this difference is 89%. These are significant

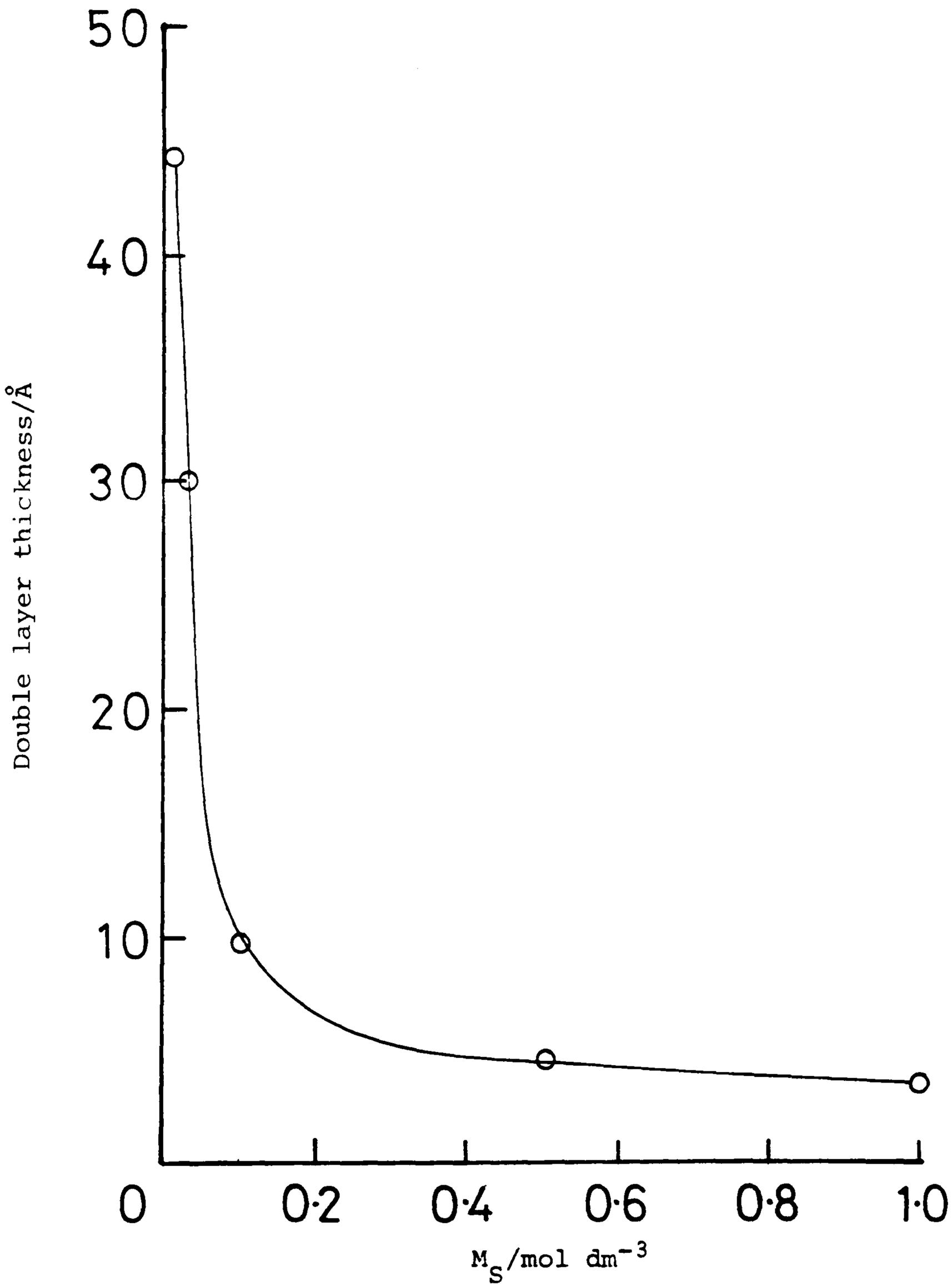

Figure 85: Variation of double layer thickness, $\frac{1}{\kappa}$, with concentration of added 1:1 electrolyte, NaCl, at 25°C.

results with respect to the amount of material that may be needed for an EOR application, therefore 0.4 mol dm^{-3} sea water will have a significant beneficial effect, however, this improvement does have a limit, and this limit is defined by the minimum to which $\frac{1}{\kappa}$ can be reduced. From Figure 85, it can be seen that the minimum is reached at relatively low concentrations of electrolytes.

4.1.2 The Effect of pH on 4-ϕ-C_{12} ABS and CTAB Adsorption at the Air-Aqueous Solution Interface (Section 3.1.2)

The results of Figures 41, 42 and 43, for 4-ϕ-C_{12} ABS and CTAB adsorption respectively, show that variations in the solution pH, over a wide range (1.8-12.0), has little effect on the surfactant's surface activity.

Tables 8, 9 and 10 show the calculated "adsorption parameters" (Γ_D, A_s, CMC, $pM_D(20)$, π_{CMC}) for the surfactants, obtained from Figures 41, 42 and 43).

Comparison of the results here to those of the sodium chloride addition, Tables 9 and 10, show that the salt addition has a very great influence on the surfactant properties, due, as outlined above (Section 4.1.1) its marked effect on the value of κ.

The anionic surfactant (4-ϕ-C_{12} ABS) continues to show the greater surface activity (relative to CTAB), and the reasons for this have been discussed in Section 4.1.1.

4.1.3 The Effect of n-butanol Addition on the Adsorption of 4-ϕ-C_{12} ABS at the Air/Aqueous Solution Interface (Section 3.1.3)

Considering the behaviour of n-butanol in aqueous solution, reference will be made to the results of Figure 46 and Table 12 (Section 3.1.3). Butanol adsorbs at the air/water interface because of its hydrophobic nature. This adsorption results in a reduction of surface tension, and from the results of Table 12, this reduction appears to indicate that the amount of alcohol adsorption is greater than that for the 4-ϕ-C_{12} ABS surfactant, that is Γ_D, and π_{CMC} are greater for the alcohol than the surfactant (see Table 11).

These results must be put into perspective. Comparing the values of $pM_D(20)$ for the alcohol and surfactant, Tables 12 and 11 respectively, show that to effect the same surface tension reduction (ca. 20 mN m^{-1}), the concentration of alcohol needed is some 14,000 × that of 4-ϕ-C_{12} ABS. Thus, the surfactant is far more surface-active, and efficient at reducing tensions, than the alcohol.

Alcohol adsorption at the interface, while being less efficient than 4-ϕ-C_{12} ABS, does influence the surfactant adsorption however, as is evident from Figure 46, and Table 11. From these, Γ_D can be seen to fall as alcohol addition is increased. This can be explained by a step-wise process. With the solution (0.1 mol dm^{-3} NaCl) initially containing alcohol, a surface tension of less than 72 mN m^{-1} is found (Figure 44). This lowering of tension is, as explained above, due to alcohol adsorption at the air/water interface. Addition of surfactant

to the system will continue to reduce the tension until the critical micelle concentration has been reached. The results of Figure 46 show that the critical micelle concentration for the surfactant is lowered in the presence of n-butanol, thus the maximum reduction in surface tension will be achieved at lower bulk surfactant concentrations, in a manner analogous to the effect of electrolyte on surfactant behaviour. Micelles are in a dynamic equilibrium between the bulk aqueous phase and the micellar phase, with both alcohol and surfactant monomer exchanging between phases [G5].

A large amount of work has been carried out on the effect of medium chain-length alcohols (propanol to heptanol) on the properites of surfactants, above the CMC, with the objective of determining the role of these alcohols as co-surfactants in microemulsion systems [H8-H11]. These alcohols, as mentioned above, are partitioned between the micellar and aqueous phases and several papers dealing with their distribution in SDS, or CTAB/water systems have been published in recent years [A5,A6, G5,S11,R7].

In the present study, with 4-ϕ-C_{12} ABS, the partitioning of n-butanol between 4-ϕ-C_{12} ABS micelles and the aqueous phase has been followed through solubility measurements (3.1.4). From the data (Figure 47) the partition coefficient, K_{eq}, defined [G5] as the molar ratio of alcohol in micellar phase to that in the aqueous phase, was determined from the equation:

$$K_{eq} = \frac{M_{Co}^{t} - M_{Co}^{w}}{[M_{co}^{w}]\,(M_{D}^{m} + M_{Co}^{t} - M_{Co}^{w})} \qquad (4.3)$$

where M_{Co}^{w} is the aqueous solubility of the alcohol, M_{D}^{m} is the concentration of surfactant in the form of micelles (= M_{D}^{t} - CMC), M_{Co}^{t} is the total alcohol, and M_{D}^{t} is the total surfactant concentration respectively. Rearrangement of equation (4.3) gives:

$$M_{Co}^{t} = \frac{[M_{Co}^{w}]K_{eq}}{1 - [M_{Co}^{w}]K_{eq}} \cdot M_{D}^{m} + [M_{Co}^{w}]$$

which means that a plot of M_{Co}^{t} against M_{D}^{m} should be linear with a slope of:

$$\frac{[M_{Co}^{w}]K_{eq}}{1 - [M_{Co}^{w}]K_{eq}}$$

and intercept $[M_{Co}^{w}]$. This is found in Figure 47, and values of K_{eq} and $[M_{Co}^{w}]$ are listed in Table 20 (overleaf), together with the literature [S12] values of $[M_{Co}^{w}]$.

From Table 20, the partition coefficient, K_{eq} for the alcohol exchange process increases in going from propan-1-ol through to hexan-1-ol which clearly agrees with the trend in the solubilities of these compounds. The value of K_{eq}, close to 1.0, for n-butanol indicates the equal distribution of the alcohol molecules between aqueous and micellar phases.

The effect of alcohols on the micellar properties of surfactants has been extensively studied (H8-H11 for example). Calculations of micellar aggregation numbers from fluorescence quenching studies [A7] indicate that as alcohol is added to a surfactant system, the

Table 20. Values of $[M^{w}_{Co}]$ and K_{eq} determined from each alcohol from solubility measurements

Alcohol	Surfactant	$\frac{[M^{w}_{Co}]}{mol\ dm^{-3}}$	$\frac{[M^{w}_{Co}]\ [S12]}{mol\ dm^{-3}}$	$\frac{K_{eq}}{dm^{3}\ mol^{-1}}$	Reference
Butan-1-ol	4-ϕ-C_{12} ABS	1.00	1.01	0.96	This work
Butan-1-ol	CTAB	0.92	1.01	1.00	G5
Pentan-1-ol	CTAB	0.23	0.25	3.7	G5
Hexan-1-ol	CTAB	0.08	0.06	10.2	G5

molecules penetrate the micelle (as concluded above). As more alcohol is added, however, a decrease in the micellar aggregation numbers has been shown to occur [A7,Z3]. This will reduce the surface charge of the micelle, since less monomer will be present in the structure. In addition to this, intercalation of alcohol molecules between surfactant head-groups will open up the surface region and, from geometric considerations, will also reduce the surface charge density [A8]. Thus, micelles will be formed which have a relatively low surfactant aggregation number, but, being easily formed (lower head-head repulsion) will be numerous. Such a process will therefore lower the surface-activity of surfactant molecules and limit, once again, surface tension reduction.

4.2 Adsorption of 4-ϕ-C_{12} ABS at the n-decane/aqueous Solution Interface (Section 3.2)

In a system consisting of a non-polar oil (n-decane) in contact with a solution of NaCl, addition of the anionic surfactant 4-phenyl-C_{12} ABS reduces the oil-water interfacial tension (γ_i) until the aggregation point (CMC) is reached and thereafter the tension remains constant (at γ_c) with increasing surfactant concentration (Figure 48 and [O5]). The value of γ_i depends on the salt concentration, M_s, and the concentration M_{Co}, of cosurfactant, n-butanol, if present. For the twin-tailed anionic surfactant Aerosol OT (AOT), addition of NaCl can produce very (ultra) low oil-water tensions (ca. 10^{-3} mN m^{-1}) and γ_c can be made to pass through a minimum [A1,A9,A10). For single-chain anionic surfactants (e.g. SDS, or 4-phenyl-C_{12} ABS),

however, salt alone cannot produce a minimum in γ_c, nor is γ_c very low. Addition of cosurfactant (n-butanol) to the aqueous system, containing 4-phenyl-C_{12} ABS above its CMC can, however, result in low values of γ_c and also a minimum as M_{co} is varied (Figure 50).

Figure 49 shows the variation of interfacial tension, between n-decane and water, with surfactant addition, and illustrates that the minimum in interfacial tension cannot be achieved through the salt addition.

The interfacial tension can be related to M_{Na}, the total sodium ion concentration, by [A9]:

$$\frac{-d\gamma}{d \log M_{Na}} = 2.30RT\left\{1 + 2\left(\frac{\partial \log f_{\pm}^{NaCl}}{\partial \log M_{Na}}\right) + \frac{d \log(CMC)}{d \log M_{Na}} + \frac{2\Gamma_{Cl}}{\Gamma_D}\left[1 + \left(\frac{\partial \log f_{\pm}^{NaCl}}{\partial \log M_{Na}}\right)_{D,T}\right]\right\} \qquad (4.4)$$

in which $f_{\pm}^{NaCl}$ is the mean ionic activity coefficient of the salt and Γ_{Cl} is the surface excess of Cl^- anion. For a surface containing a monolayer of anionic surfactant, Γ_{Cl} is expected to be small and negative [A9,T6] and the term Γ_{Cl} can be neglected in equation (4.4). The CMC has been obtained as a function of salt concentration from the data in Figure 49 and a plot of log(CMC) vs log(M_{Na}) is given in Figure 86 (overleaf). It is linear and of slope -1.13. In the range of M_s studied, $2(\partial \log f_{\pm}^{NaCl}/\partial \log M_{Na})$ is in the region of -0.12 to -0.18, and it can therefore be seen from equation (4.4) (assuming $\Gamma_{Cl} = 0$) that $d\gamma_c/d \log M_{Na}$ will not be zero, and hence γ_c is not

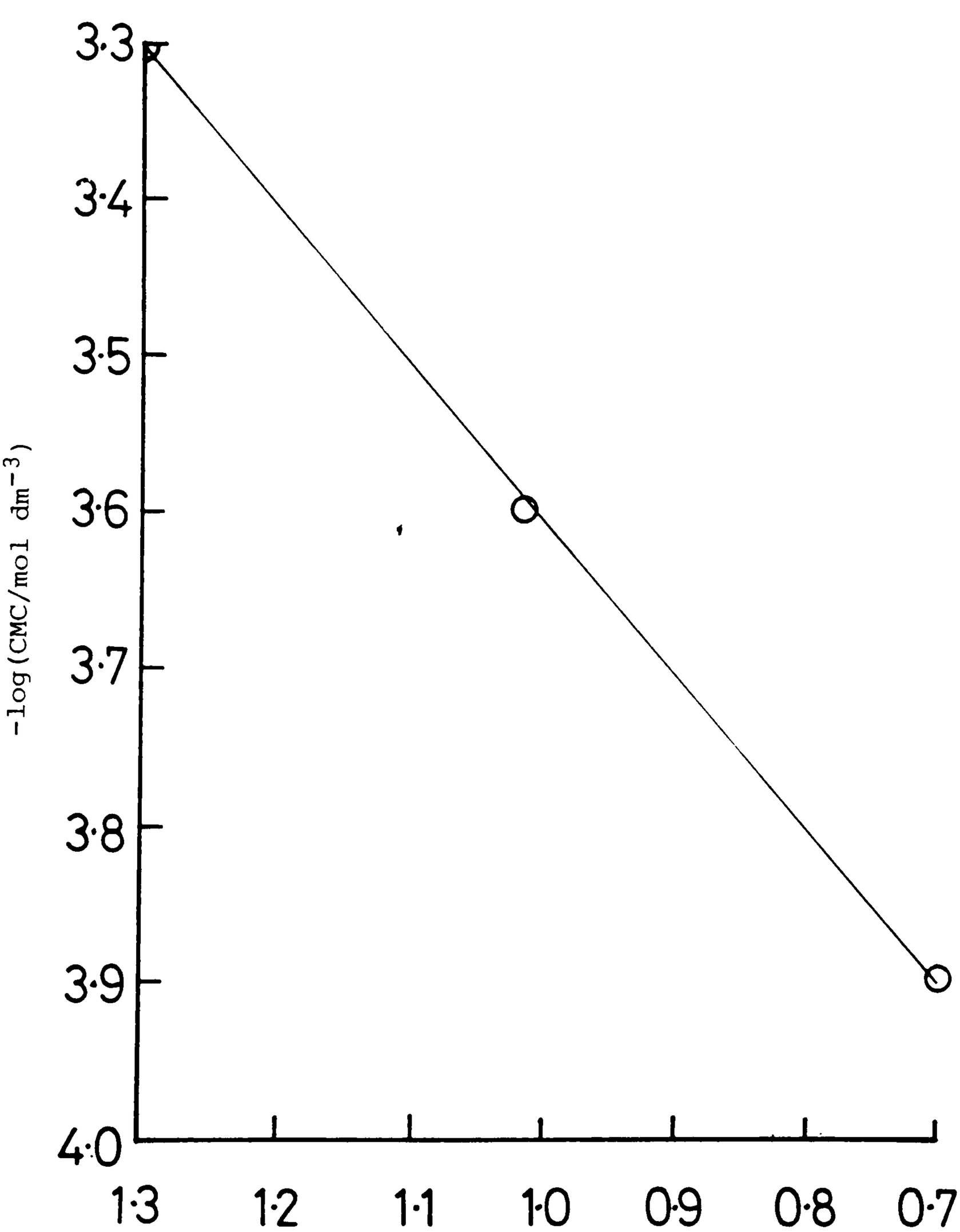

Figure 86: Variation of CMC of 4-ϕ-C_{12} ABS with sodium ion concentration M_{Na} in systems containing NaCl.

expected to pass through a minimum. This is as observed in Figure 49.

In terms of the molecular geometry of 4-ϕ-C_{12} ABS the absence of a minimum in γ_c is a result of the different cross-sectional areas of the anionic head group (a_h) and the hydrophobic chain (a_c) [A3]. In the absence of salt a_h is greater than a_c. Although addition of salt compresses a_h (as is seen from the values of A_s in Table 13), apparently a_h is not reduced below a_c. In order to achieving matching of (mean) a_h and a_c it is necessary to introduce into the monolayer a surfactant for which $a_c < a_h$ [A3].

From the results of Figure 50, it can be seen that progressive addition of n-butanol to systems containing 4-ϕ-C_{12} ABS, above its CMC, gives a minimum in γ_c. The presence of a minimum is ascribable to the surfactant distribution between the aqueous and organic phases, the minimum occurring where there is a marked transfer of the surfactant from the aqueous to the oil-phase, Figure 51. This behaviour has been observed by other workers in systems containing SDS and pentanol [O5], and SDS with octanol [A3].

It is noteworthy that 4-ϕ-C_{12} ABS transfers to some extent to the butanol solution in decane, even below its aggregation point, where in a system without alkanol it would reside entirely in the aqueous phase. This has meant that in measuring tensions (including those below the CMC) all systems had to be pre-equilibrated, and equilibrium 4-ϕ-C_{12} ABS concentrations in the aqueous phase determined. In the (broad) region

(3 to 9 in Figure 50), a third phase forms. Figure 51 shows the effect of increasing n-butanol concentration, from solution 1 12 (corresponding to Figure 51), on the solution phase changes, an optimum middle region being apparent, where a stable, third phase forms (the solutions are > three weeks old).

The minimum in γ_c occurs when there is no tendency of the adsorbed monolayer to bend and this situation arises when the effective cross-sectional areas of a_h and a_c are equal [A3]. When cosurfactant is present the operative a_h and a_c are mean values for the mixed film. For alkanols $a_h < a_c$ while for 4-ϕ-C_{12} ABS (at all concentrations of NaCl), $a_h > a_c$.

The results show that upon the addition of alkanol (n-butanol), a concentration is reached where the mean $a_h = a_c$, therefore γ_c has a minimum. The addition of NaCl to the aqueous solution of surfactant reduces a_h by electrostatic interaction and thus, if the concentration of NaCl was increased the concentration of alcohol needed to achieve γ_c minimum would be reduced [A3]. Thus, if sufficient alcohol was present then the salt addition can achieve γ_c minimum.

4.3 Surfactant Adsorption at the Kaolin Surface

The influence of sodium chloride on the 4-ϕ-C_{12} ABS surfactant adsorption (Figures 53 and 54) can be explained by the effect of salt on the electrical double layers of both the surfactant molecules, and charged sites at the solid surface. In solution,

surfactant-surfactant interactions are enhanced with salt addition, lowering the CMC (Section 3.1), thus adsorption equilibria are reached at lower bulk surfactant concentrations, displacing the adsorption isotherm plateau to lower equilibrium surfactant concentrations. The electrolyte will similarly affect the electrical double layer at the charged sites on the solid surface, so reducing surfactant-solid interactions whether attractive, or repulsive. The adsorption of surfactant at the liquid-solid interface is therefore controlled by a balance between these forces. The adsorption results (Figure 54) indicate that this "salt effect" is greatest at sites carrying a similar sign of charge to the surfactant than on those of opposite charge.

From the isotherms, and an estimate of the size of the surfactant ions, the adsorption density for a monolayer can be determined. Estimates of the surfactant ion size have been obtained from three sources; air-water interfacial density, as determined from surface tension data (this work, Section 3.1) (33 $Å^2$), film pressure studies on sodium dodecylsulphonate [M5] (40 $Å^2$), and sulphonate head groups (widest portion of the ion) density for cubic packing, based on a diameter of 5.9 Å (27 $Å^2$) [S13]. The air-water interfacial density is typical of values compiled by Rosen [R2] for a large number of sulphonates. From the data and adsorption isotherms the average fractional surface covering, θ, has been determined (Table 15, shown here). These results show that complete surface covering does not take place.

There may be two reasons for this:

(1) the surfactant CMC limits adsorption at the interface,

and/or

(2) not all of the particle surface is available for surfactant adsorption.

Considering the first possibility; it is true that micellisation inhibits surfactant adsorption at interfaces, as is shown by adsorption at gas-liquid, and liquid-liquid interfaces (Sections 3.1 and 3.2 respectively). However, that this should be the main limiting factor to adsorption at the solid-liquid interface is questionable, since an increase in salt concentration, through lowering the CMC, would reduce, rather than enhance, the adsorption.

Considering the second point, that of surface availability; the surface area of the kaolin sample, by BET N_2 adsorption, was found to be 8.27 $m^2\ g^{-1}$ (Section 2.4.1, Figure 25). Access to the surface by the small, neutral N_2 molecules can be expected to be greater than that of the large, charged, surfactant ions being measured here. Thus, limited surface coverage could well be explained by limited surface access.

Turning now to the "adsorption regions" of the isotherms (I→ III) (Figure 54). In region I only first-layer unassociated surfactant anions are adsorbing on a surface where the surface concentration of the ion is low enough for adsorbate-adsorbate interactions to be negligible. Adsorption in this region occurs because of electrostatic interactions between surface charge and the ionic head group, and is thus determined mainly

by surface charge. In region II, hemimicelles [G9] are present, and second-layer adsorption becomes significant through cohesive chain-chain interactions. At region III, a plateau of adsorption is reached, occurring at concentrations at, and above, the surfactant CMC. The pseudo-phase-separation model of micellisation [S16] predicts that the monomer concentrations in solution above the CMC are constants and that the concentrations of micelles increase with increasing total surfactant concentration. Thus the observed invariance of adsorption above the CMC is consistent with both the pseudo-phase-separation model and the assumptions that only monomers, and not micelles, are adsorbed [C6].

Based on the Stern-Grahame treatment of the electrical double layer (Section 1.6), an expression for the adsorption of surfactant ions at the Stern plane, δ, can be modified into the following form to take into account the interaction of surfactant ions at the interface:

$$\Gamma_\delta = 2 \times 10^{-3} \; r \; C \exp\left(\frac{-Z \; F \; \Psi_\delta - n \; \psi}{RT}\right) \qquad (4.5)$$

where Γ_δ = the adsorption density in the Stern plane, mol m^{-2},

r = the effective radius of the adsorbed ion, m^2

C = the bulk concentration of ions, mol dm^{-3}

Z = the valence of the surfactant ion, including sign

F = the Faraday constant, 96,487 C

Ψ_δ = the potential in the Stern plane, V

n = the average number of associating CH_2 groups per hydrocarbon chain

ψ = the cohesive energy per mole of CH_2 groups

R = the gas constant, 8.31 J K^{-1} mol^{-1}

T = the absolute temperature, K.

At low surface coverage, region I, the $n\psi$ term is negligible, as $ZF\Psi_\delta$ will be the dominating term in adsorption energy, thus:

$$\Gamma_\delta \approx 2 \times 10^{-3} \; r \; C \exp\left(\frac{-Z \; F \; \Psi_\delta}{RT}\right),$$

and an estimate of the free energy of adsorption, due to electrical interactions as surface coverage takes place can be made. For the results of surfactant adsorption from 0.1 mol dm^{-3} NaCl solution, values of $\exp\left(\frac{-Z \; F \; \Psi_\delta}{RT}\right)$ have been evaluated, Figure 87, in which ΔG_{elec} $(-Z \; F \; \Psi_\delta)$, using a value of r = 2.95 Å (from head group packing value earlier).

The results from these calculations (Figure 87) show that the free energy of adsorption reaches a maximum at 0.045 mol m^{-2} and then appears to fall as the surface sites are filled.

At concentrations where hemimicelles form (i.e. the end of region I), surfactant adsorption takes place via cohesive chain-chain interactions and the free energy of adsorption, due to these non-electrical, Van der Waals, interactions governs the adsorption process. Thus, equation (4.4) becomes:

$$\Gamma_\delta = 2 \times 10^{-3} \; r \; C \exp\left(-\frac{n \; \Psi}{RT}\right)$$

$$\text{so that,} \qquad n\,\psi = -RT \ln\left(\frac{\Gamma_\delta}{2 \times 10^{-3} \; r \; C}\right)$$

Now, let $\Delta G_{coh} = n \; \Psi$, where ΔG_{coh} = cohesive free energy.

Values of ΔG_{coh} have been evaluated for Γ_s, Figure 88. These

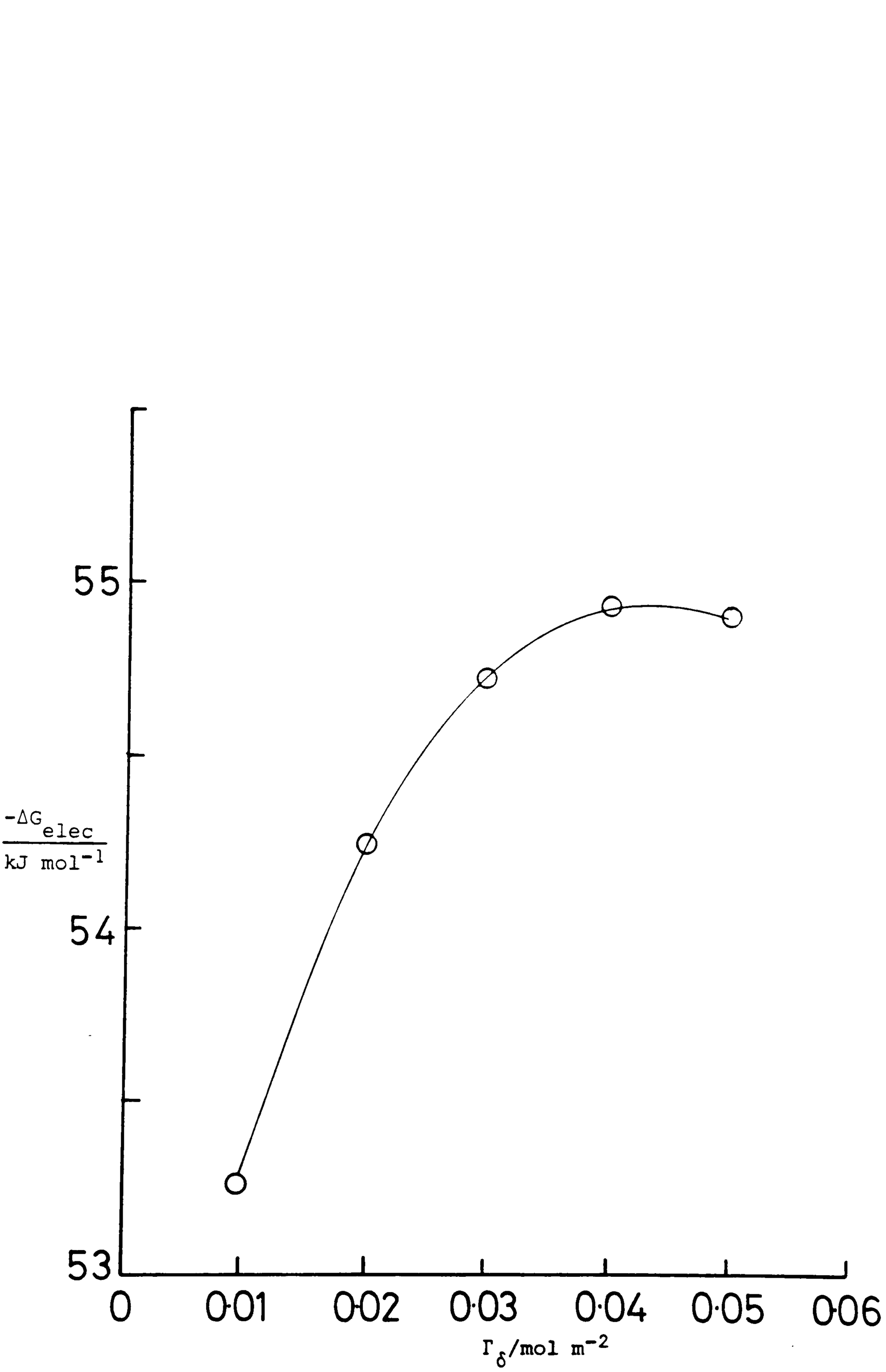

Figure 87: Variation of electrostatic free energy of adsorption of 4-ϕ-C_{12} ABS, at 25°C, from aqueous, 0.10 mol dm^{-3} NaCl, solution onto kaolin, with number of moles of surfactant adsorbed per unit area.

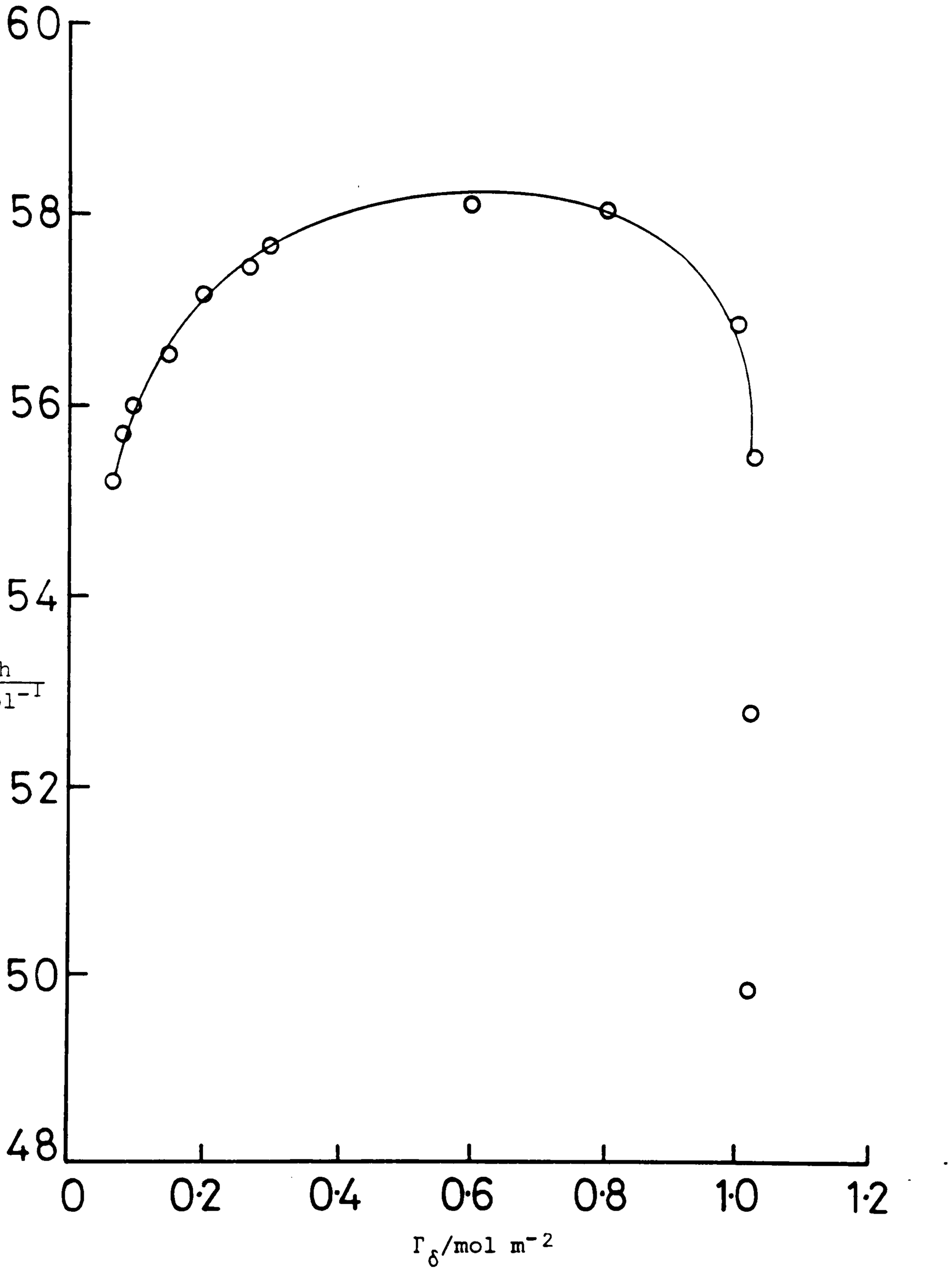

Figure 88: Variation in cohesive free energy of adsorption for 4-ϕ-C_{12} ABS onto kaolin from aqueous, 0.1 mol dm^{-1} NaCl, solution, at 25°C, with moles of surfactant adsorbed per unit area.

results show that the free energy term here is constant over a wide range of Γ_δ values (see range of ΔG_{el}), and only falls at high surface coverage, reflecting the reduction in hydrocarbon-chain interactions as the second layer of surfactant is formed.

4.3.1 The Effect of pH on 4-ϕ-C_{12} ABS Adsorption at the Kaolin-Aqueous Solution Interface (Section 3.3.3); and Aluminium-Surfactant Interactions (Section 3.9)

Upon varying the solution pH, 4-ϕ-C_{12} ABS surfactant adsorption increased from about 0.84 µmol m^{-2} at pH 12.3, to approximately 1.4 µmol m^{-2} at pH 4.0 (see Figure 55), and the positions of the adsorption maxima with respect to concentration remain constant, coinciding with a surfactant CMC in 0.1 mol dm^{-3} NaCl (c.f. Section 3.1.1). Figure 56 shows the effect of lowering the solution pH further, where it can be seen that at pH 1.8, the adsorption is some eight times greater than that at pH 4.0. However, in contrast to the higher pHs, the adsorption at pH 1.8 continues above the CMC, suggesting that some mechanism other than adsorption is causing the loss of surfactant from solution (see below).

Figure 57 shows a plot of the plateau adsorption values, obtained from Figures 55 and 56, against solution pH, and emphasises the sharp increase in adsorption on reducing the pH to less than 4.0.

Table 16 summarises the adsorption data, calculated from the results of Figures 55 and 56, and shows how the fraction of surface covered by the surfactant (calculated using a head-group area of 27 $Å^2$ as previously, Section 4.4.1) changes with the solution pH. These results indicate that a bilayer coverage is apparently achieved at pH 1.8 (c.f. Figure 57).

The mechanism by which solution pH controls the surfactant adsorptions found may be explained by two possibilities:

(1) Loss of aluminium ions, as Al^{3+}, from the clay surface forming complexes with the surfactant molecules and precipitating surfactant, or

(2) Increased positive charge density at the clay surface due to adsorption of H^+, or loss of OH^-, ions, thus providing an increase in the number of adsorption sites available for the charged surfactant.

In order to investigate the first possibility, measurements were made of the interaction between the surfactant and aluminium in solution, under varying conditions of pH (section 3.8).

Considering the light transmission of solutions containing a fixed aluminium concentration, 20 and 50 ppm Al, and varying surfactant concentration, Figure 76, it can be seen that light transmission, at a given aluminium concentration, at first decreases, then increases, as the sulphonate concentration is

increased, indicating a precipitation and re-dissolution mechanism.

In addition, the results of Figure 76 show the percent light transmission recorded to depend on wavelength. At 700 nm, the light transmission, for a given point on the curves, is greater than that at 400 nm, possibly reflecting the size of precipitate.

Figure 77 shows the percentage of light transmission, at 700 nm, as a function of surfactant concentration, for aluminium solutions, ranging from 10 to 100 ppm (3.7×10^{-4} to 3.7×10^{-2} mol dm^{-3}) Al. The precipitation re-dissolution behaviour, up to 50 ppm, is clearly seen here. From the results, it is apparent that higher concentrations of aluminium cause greater precipitation of surfactant, and that the amount of surfactant needed to "re-dissolve" the precipitate increases, as the concentration of aluminium increases. These observations are summarised in Figure 89 below which shows a plot of aluminium concentration against the log of surfactant concentration, the points being taken from the minima of Figure 77.

The effect of varying solution pH on the interactions is shown in Figure 78. The results here show that an increase in pH reduces the precipitation.

From the turning points of Figures 78 and 79, the mole ratio of surfactant to aluminium has been determined at each pH, and the solubility products determined for the precipitate, Table 21.

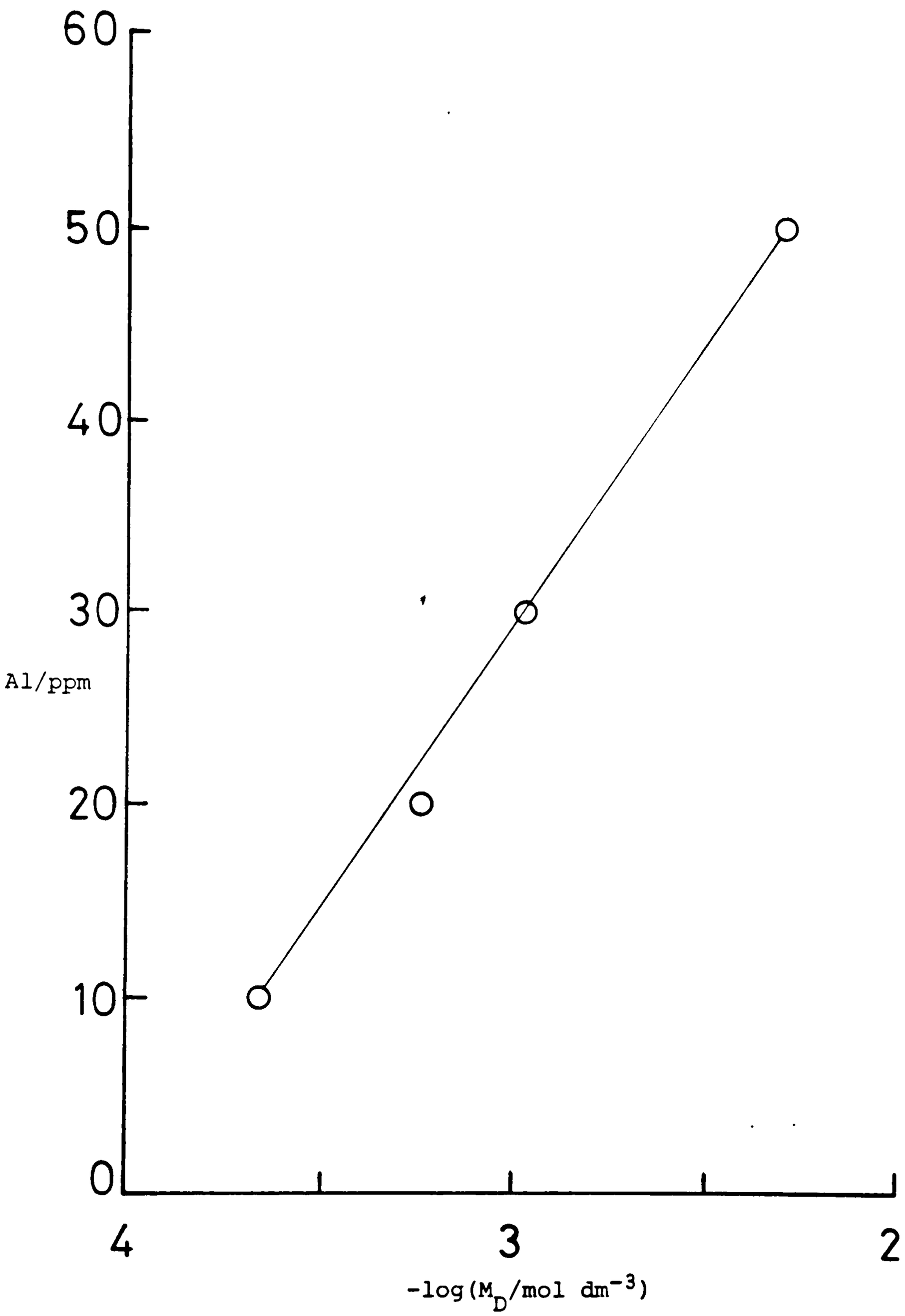

Figure 89: "Turning point" values of 4-ϕ-C_{12} ABS, and aluminium, concentrations, taken from Figure 77, reflecting the point of re-dissolution of precipitate.

Table 21. Calculated values of mole ratio of surfactant to dimension, and pKsp, for different solution pHs.

Solution pH	[Al] / 10^{-3} mol dm^{-3}	[4-ϕ-C_{12} ABS] / 10^{-3} mol dm^{-3}	[4-ϕ-C_{12} ABS] / [Al]	pKsp
1.57	3.70	11.00	2.97	11.0
1.81	1.85	6.31	3.40	12.2
4.24	3.70	3.98	1.08	6.6
4.38	1.85	2.51	1.36	6.2

The data in Table 21 show that at low pH the mole ratio of 4-ϕ-C_{12} ABS to aluminium is about 3:1, indicating a complex of the form:

$$Al^{3+} + 3(4\text{-}\phi\text{-}C_{12}\ ABS)^{-} = Al(4\text{-}\phi\text{-}C_{12}\ ABS)_3$$

and, at pH 4, the mole ratio is about 1:1, giving:

$$Al(OH)_2^{+} + (4\text{-}\phi\text{-}C_{12}\ ABS)^{-} = Al(OH)_2\ (4\text{-}\phi\text{-}C_{12}\ ABS)$$

The pKsp's of these complexes show good agreement at pH 4, but not such good agreement at the lower pH. However, the values obtained at each pH region indicate that the 3:1 complex is much less soluble than the 1:1 complex.

Because sodium chloride addition showed a marked influence on the surfactant adsorption at the kaolin surface (Section 3.3.2), the effect of salt addition on aluminium-surfactant complexation has also been considered (Section 3.8.2.2). From here, Figure 81, it can be seen that the salt addition reduces precipitation, and because the position of the minima remains

almost constant this suggests the nature of the complex to be constant, that is, under the acid conditions employed a complex of structure $Al[4\text{-}\phi\text{-}C_{12}\ ABS]_3$, is formed (see above). Some competition for the surfactant anions may be taking place between Na^+ and Al^{3+} ions. Re-dissolution of the surfactant sodium salt has been observed under increasing surfactant concentrations by other workers [C5].

In addition to any salt effects on aluminium-surfactant precipitation, the further effect of added n-butanol has also been considered (Section 3.9.2.3). The possible influence of the alcohol on the interaction was investigated, because its addition to aqueous solution had shown marked effects on the surfactant adsorption at the solid-liquid interface (Section 3.3.4).

From the results of Section 3.9.2.3, Figure 82, it can be seen that butanol addition reduces precipitation at low surfactant concentrations (ca. 10^{-3} mol dm^{-3}) but increases the loss at higher concentrations (ca. 10^{-2} mol dm^{-3}).

That alcohol addition should affect the surfactant-aluminium interactions, might be explained by the reduction in surfactant CMC induced by n-butanol (Section 3.1). Micelles are known to be important in solubilisation, and suspension, processes [G5] and their presence here may serve to lower the precipitation in the system. At higher surfactant concentrations, however, precipitate formation may exceed this solubilisation capacity.

Adding sodium chloride and n-butanol together to the aluminium-surfactant system, at low pH, reduces precipitation in comparison to the alcohol alone; and slightly reduces the precipitation in comparison to NaCl alone results, suggesting that while NaCl influences on precipitate are greater than those of the alcohol, the presence of alcohol does aid re-dissolution.

At a higher pH (12.0), very little precipitation is observed in any case. Under these solution conditions aluminium is present, as a soluble hydroxide, $Al(OH)_2^+$ or $Al(OH)_4^-$, and the presence of any free aluminium Al^{3+} ions is unlikely [R8], as can be seen from Figure 90 below, thus precipitate formation would be minimal here.

When the above are considered, together with the release of aluminium from the clay, under varying solution conditions (pH) (Section 3.8.3, Figure 84), it becomes obvious that the dissolution of Al occurs at extreme pHs. Sodium chloride inhibits this release rather than ion exchange with the aluminium.

Thus an increase in the solution ionic strength inhibits Al^{3+} ion release from the clay structure. The presence of butanol reduces the effect of ionic strength, possibly by decreasing the permittivity of the solution, although the possibility of uncharged, $Al(OH)_3$, species which may interact favourably with the alcohol-water system, could be considered.

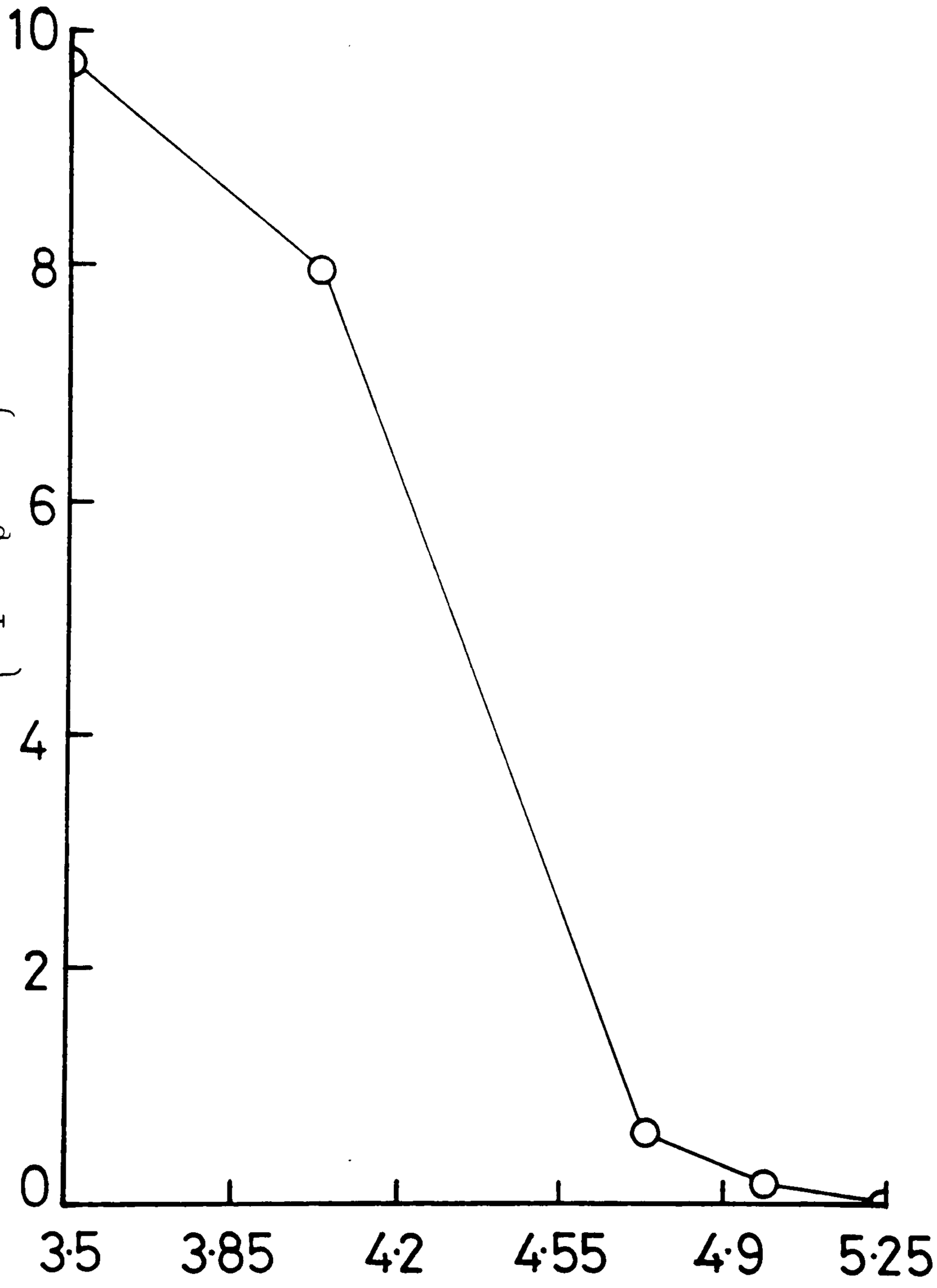

Figure 90: Calculated concentrations of Al^{3+} in 10^{-3} mol dm^{-3} $AlCl_3$ solutions, taken from reference R8.

Another possible explanation for increased surfactant adsorption at lower solution pHs is that of H^+ adsorption, or OH^- release. To further elucidate the mechanisms here, extensive electrophoretic investigations were carried out (Section 3.6). The discussion of these results and, incorporation of them with the above, has been deferred until the thermodynamic aspects of adsorption at the interfaces have been discussed (see below).

4.3.2 The Effect of n-butanol on 4-ϕ-C_{12} ABS Adsorption at the Kaolin-Aqueous Solution Interface (Section 3.3.4)

The results of Section 3.3.4, Figure 58, show the effect of adding n-butanol on the surfactant adsorption at the kaolin surface. These measurements, made at constant salt conditions (0.1 mol dm^{-3} NaCl), show that at low surfactant concentrations the alcohol enhances adsorption, while at higher concentrations the adsorption is reduced.

Increasing the concentration of alcohol in the system also has an effect, the greater alcohol concentration (0.47 mol dm^{-3}) showing marked surfactant adsorption.

These observations can be explained by synergism between the adsorbed surfactant and alcohol molecules at the solid surface, forming mixed hemimicelles [S15]. Such structures would be analogous to mixed micelles which have been observed to form between anionic-nonionic surfactants [S16]. An alternative explanation is the solubilisation of n-butanol by surfactants (see Section 3.1.4). Thus alcohol molecules may be held in hemimicelle structures of the surfactant, encouraging growth

through further adsorption of surfactant molecules.

To test which of these ideas are correct, measurements were made of n-butanol adsorption at the solid-liquid interface, Section 3.3.4.1. From the results obtained (Figure 59 and Tables 17-18), it can be seen that butanol adsorption was not significant until the equilibrium concentration had reached about 0.03 mol dm^{-3}. Below that concentration, no adsorption could be found, by either surface tension measurements, Figure 59, or radiolabelled measurements, Tables 17-18. Above 0.03 mol dm^{-3}, adsorption of the alcohol becomes significant (Figure 59), increasing rapidly up to a plateau at about 0.1 mol dm^{-3}.

That the alcohol should adsorb at all at the solid-aqueous interface may be surprising, although its adsorption at the air-water interface was well established (Section 3.1.3, Figure 45). The adsorption indicates that the clay surface may have some hydrophobicity, i.e. patches onto which alcohol may adsorb. Such behaviour supports the postulate that some surfactant-alcohol interactions may be taking place at the solid-liquid interface, so enhancing adsorption at lower surfactant concentrations. As surfactant concentration is increased, however, release of alcohol may occur, due possibly to more favourable interactions in solution - through micelle formation, for example, providing solubilisation for the alcohol (see Section 3.1.4).

The rapid increase in surfactant loss from solution at the highest alcohol concentration, 1.1 mol dm^{-3}, Figure 58, can be attributed to the formation of a separate alcohol phase, in

which the surfactant is more soluble (×4) than in the aqueous phase, Section 3.3.4.2, Figure 61.

4.3.3 The Effect of Temperature on 4-ϕ-C_{12} ABS Adsorption onto Kaolin (Section 3.3.5)

The results of Figure 62, obtained for the adsorption of 4-ϕ-C_{12} ABS onto kaolin at three different temperatures (25, 60 and 80°C) show that the adsorption decreases as the solution temperature is increased from 25 to 60°C. Above 60°C, however, no further reduction in adsorption could be found.

Using the Clausius-Clapeyron equation [S2]:

$$\frac{\partial \ln M_D}{\partial T} = \frac{-\Delta H_{ads}}{RT^2} \qquad (4.6)$$

in which, ΔH_{ads} = the enthalpy of adsorption, in kJ mol^{-1},

values of the enthalpy of surfactant adsorption at the interface have been calculated, Figure 91. From here, it is apparent that the enthalpy is negative throughout the adsorption range. For adsorption due to electrostatic interactions (region I of the isotherm, Section 3.3, Figure 54), it is reasonable that ΔH be negative since adsorption here is analogous to ionic bond formation.

In addition, sharp changes in ΔH, from region I to region II, are evident (Figure 91), in accordance with hemimicelle formation. The contribution to ΔH due to hemimicelle formation is of the order of 4 kJ mol^{-1}. Changes in ΔH reported for micelle formation exist in a wide range from +20.9 to -12.5 kJ mol^{-i} [R2], showing the value here to be of the order expected for hydrocarbon-tail interactions.

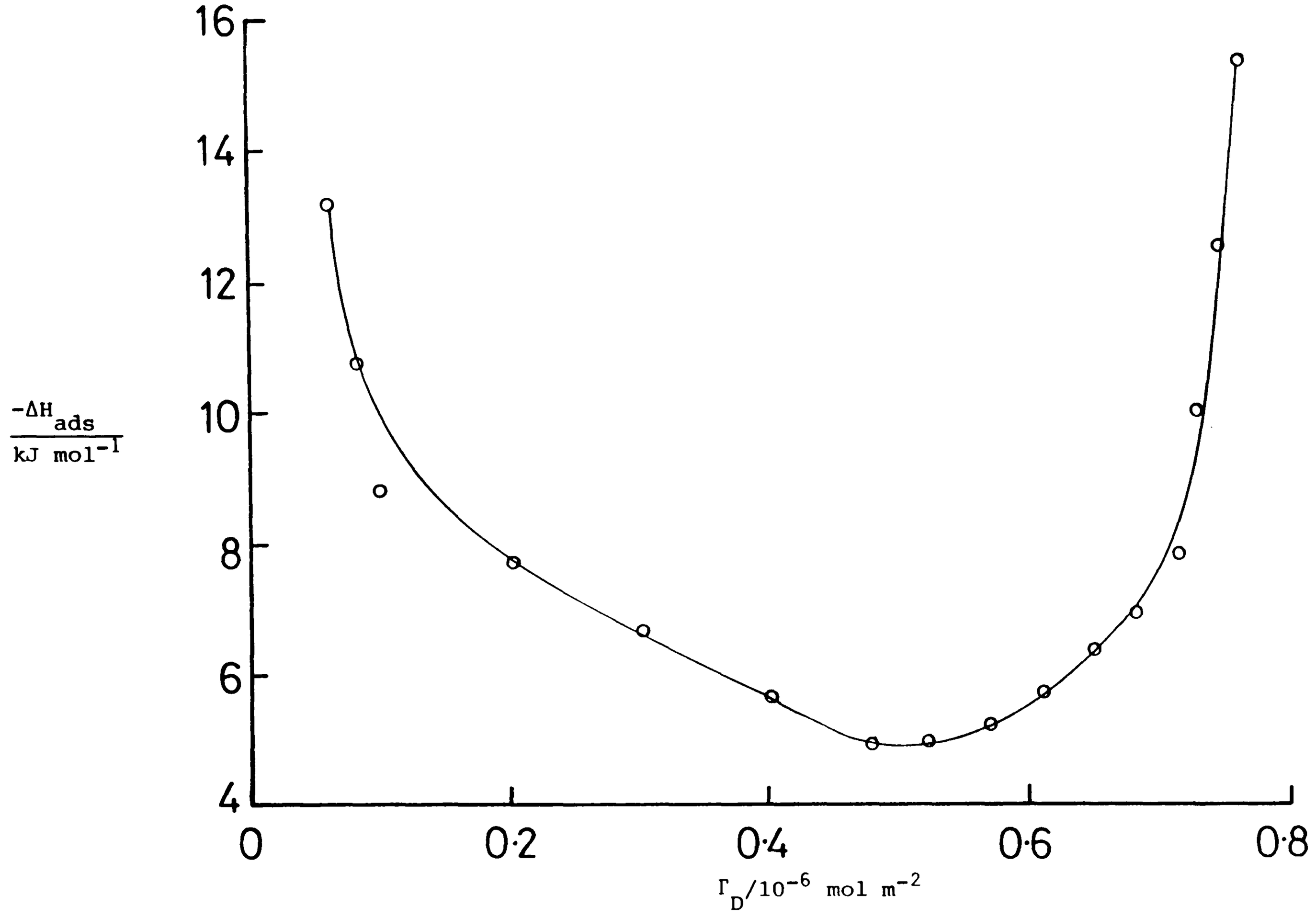

Figure 91: Calculated enthalpy of adsorption, ΔH_{ads}, of 4-ϕ-C_{12} ABS onto kaolin from 0.1 mol dm^{-3} NaCl solution, using data of Figure 62.

4.3.4 Adsorption of 4-ϕ-C12 ABS in the Presence of n-decane and Loss of n-decane (Section 3.3.6)

In the presence of n-decane, Section 3.3.6, Figure 63, the surfactant loss by adsorption depends on the nature of the emulsion formed - that is, oil-in-water, or water-in-oil. Overall, the loss appears to be greater from the water-in-oil emulsion. The hydrophilic nature of the clay may account for this. Water in the emulsion, probably containing surfactant, or having surfactant adsorbed at the oil-interface, can be "gathered" up by clay particles in contact, removing surfactant from solution.

The adsorption of surfactant, over a range of concentrations, in the presence of a fixed amount of decane, has been measured in Section 3.3.6.1, Figure 64. The characteristic isotherm shape (see Section 3.3) is retained; low initial adsorption, followed by a rapid increase to a plateau of adsorption. However, in the isotherm of Figure 64, adsorption has continued above the surfactant CMC under these conditions (ca. 10^{-4} mol dm^{-3}, Figure 39).

Included in Figure 64 are the results of measured oil loss from the system. The process of oil loss onto kaolin effectively mirrors the changing nature of the clay surface - from hydrophilic, in the absence of surfactant, to hydrophobic, due to hemimicelle formation at the solid-liquid interface. The presence of hydrophobic surfactant tail-groups at the interface provides a suitable region for the organic oils to absorb. Above surfactant concentrations, where a maximum (plateau)

has been reached, new ionic head-group-solvent interactions are important (see Section 3.3), oil adsorption is reduced and micelles in solution provide an alternative location for the n-decane molecules.

Whether n-decane is absent, or present in solution, or initially on the clay, the effect of increasing the n-butanol concentration is to reduce the surfactant adsorption. The presence of minima in the plots (Figure 65) is interesting because such minima were apparent in interfacial-tension plots, between n-decane and water when n-butanol was added to the system (Section 3.2.2, Figure 50). In this latter case the minimum interfacial tension was 0.9 mN m^{-1}. In the present system, a very stable emulsion may have formed which would hold the surfactant and prevent surfactant and butanol loss from the solution. Consideration of Figure 50 and Figure 51 (Section 3.2.2) shows that at the minimum of Figure 65 ($\sim$0.5 mol dm^{-3} n-butanol), a stable emulsion does exist, a third phase being present, even after three weeks.

4.3.5 Adsorption of CTAB at the Kaolin-Aqueous Solution Interface Under Varying conditions of Sodium Chloride Concentration (Section 3.4.1) and Solution pH (Section 3.4.2)

The adsorption process of the cationic surfactant (Figure 66) confirms the results and discussion of the anionic surfactant behaviour in terms of charged sites on the particle surface. At pH 6.0, kaolin particles are overall negatively charged (see Section 3.6), the negative sites being located on the face surfaces primarily (see Section 1.7), also additional

sites may exist on the edges. Initial surfactant adsorption (CTAB), at low concentrations (below the hemimicelle concentration (HMC)), will take place primarily at the particle's face surfaces, thus avoiding repulsive interactions at the edges, and being little influenced by salt addition (due to large initial population of available adsorption sites). Above the HMC (> 10^{-5} mol dm^{-3}), the number of suitably charged sites available for adsorption has been reduced, approaching zero, thus edge sites now become important. At the particle edges, there will be a number of positively charged sites inhibiting the ions' approach and so reducing its adsorption. Addition of NaCl, through its influence on electrical double layer thickness (see Section 4.1.2), will aid its surfactant ions' approach and so enhance adsorption. The effect of NaCl on the reduction of the attractive forces of negatively charged sites is offset by the relatively high population of these, over the positively charged sites, at this pH.

Above the surfactant CMC, adsorption is inhibited, both by the lack of available adsorption sites, and by the presence of micelles in solution (cf. Section 4.4.1).

The calculated percentage coverage of the solid surface by CTAB, Table 19, shows that the amount of surfactant adsorbed far exceeds a monolayer coverage. This is, in the main, due to the complete coverage of the large, negatively charged, face areas of the clay particles with a bilayer of ions, a result which masks the existence of any unfilled, positively charged,

sites of the clay edges (cf. electrophoretic measurements, Section 3.6).

The effect of solution pH on the adsorption of CTAB (Figure 67) is to increase the adsorption as the pH is increased, because the hydrophilic group carries a positive charge, in contrast to the behaviour observed for 4-ϕ-C_{12} ABS considered earlier, Section 3.3.3, Figure 55.

From the results, and Table 20, it can be seen that the surface coverage exceeds a monolayer at all pHs, a consequence of the dominant negative charge of the kaolin particle.

4.4 Adsorption of 4-ϕ-C_{12} ABS [^{35}S] onto Clashach Sandstone, BDH Precipitated Silica, and Crosfields Gasil-35 (Section 3.5)

Adsorption of anionic surfactant, 4-ϕ-C_{12} ABS, onto different adsorbents viz. Clashach sandstone and BDH precipitated silica, was less than than that observed on kaolin. The surfactant adsorption is greater on the silica surface than on the sandstone surface, the adsorption on silica increasing rapidly above a surfactant concentration of 1×10^{-3} mol dm^{-3}, continuing above the CMC (cf. Section 3.1), and no plateau of adsorption being reached.

On Gasil-35, the surfactant adsorption is similar to that on sandstone, and ten times lower than that of the precipitated silica, and, like the adsorption on sandstone, a maximum in the adsorption is reached well below the CMC.

Considering first the Clashach sandstone results. The adsorption measurements shown in Figure 68 were obtained using sandstone samples that had been washed with distilled water, to remove adhering clay particles (see Section 3.5). Washing of the particles with 0.1 mol dm^{-3} HCl yielded a material that showed no measurable adsorption. Thus, the adsorption at the sandstone surface can be attributed to incomplete removal of embedded clay particles using water only, the low adsorption levels found (relative to kaolin particles, Section 3.3) reflecting the small amount of clay that must be left.

Considering the BDH precipitated silica, 4-ϕ-C_{12} ABS adsorption reached the levels found previously with impure surfactant but failed to find the plateau adsorption limits observed by Tadros [T6] even at pH 10.0. To "visualise" anionic surfactant adsorption at a silica surface, particularly at pHs above 2 where the silica particle is negatively charged (see Section 3.6), it is necessary to consider hydrophobic interactions between the surfactant tail and silica surface. The surfactant is then adsorbing at the silica surface in an opposite way to that at the kaolin surface (see Section 3.6 for electrophoretic data, and Section 4.7 for a discussion). This adsorption mechanism is well known for systems containing hydrophobic solids in water [R2], however the precipitated silica being used here is very hydrophilic, finding use as a drying agent.

The adsorption results from the second silica (Gasil-35), which were determined via the loss of surfactant from solution (Figure 69), can be used to resolve the apparently anomalous results above. Figures 68 and 69 show that the surfactant adsorption, above 1×10^{-3} mol dm^{-3}, of Gasil-35 is much lower than that of the precipitated silica. This is despite the Gasil-35 having a N_2 surface area more than twice that of the BDH silica (Section 2.1).

In view of the above results, therefore, the loss of surfactant in the silica system is most likely due to the strong affinity of these materials for water, surfactant molecules forming part of the aqueous solution bound to the surface. The amount lost from solution to the BDH silica can be expected to be greater in view of the method by which measurement were made here (see Section 2.4.6.1), in which a drying stage of the solid has been attempted.

The results here do not agree with the findings of Tadros [T6], but can be explained, particularly when the results of the electrophoretic measurements are considered (see Section 4.7 below). From the results presented here, it must be stated that the findings of Tadros are doubtful.

4.5 Microelectrophoretic Studies (Section 3.6)

The results of Figure 70 show that as solution pH is increased, the negative electrophoretic mobility of kaolin particles increases up to a limit (i.e. the number of negative electrical charges increases), the magnitude of mobility depends on the

solution ionic strength.

The pH-dependence of the particle mobility is attributed to the pH-dependent ionisation of exposed alumina (and silica) groups at the edges of the clay particles, which behave amphoterically, adsorbing, or releasing, H^+ (or OH^-) ions according to the solution pH (cf. Section 1.7).

The influence of NaCl addition on the mobilities can be explained by its effect on the double-layer thickness ($\frac{1}{\kappa}$) (equation 1.12) of the charged sites. An increase in ionic strength compresses the double layer (i.e. increases κ) and reduces the surface potential of the particles (equation 1.13).

Zeta Potentials and Surface Charge Density

Using equation (1.2), relating the particle electrophoretic mobility to zeta potential:

$$u_E = \frac{2}{3} \varepsilon \frac{\zeta}{\eta} . f_1(\kappa a) \qquad (1.20)$$

and the values of $f_1(\kappa a)$ shown in Table 22 below, the pH-dependent zeta potential of kaolin was determined for the mobilities shown in Figure 70. The calculated values, from equation 1.20, are shown in Figure 92 below, from which it can be seen that ζ-potential varies from about -10 mV, at low pH, to -120 mV at high pH, for 0.100 and 0.001 mol dm^{-3} NaCl respectively.

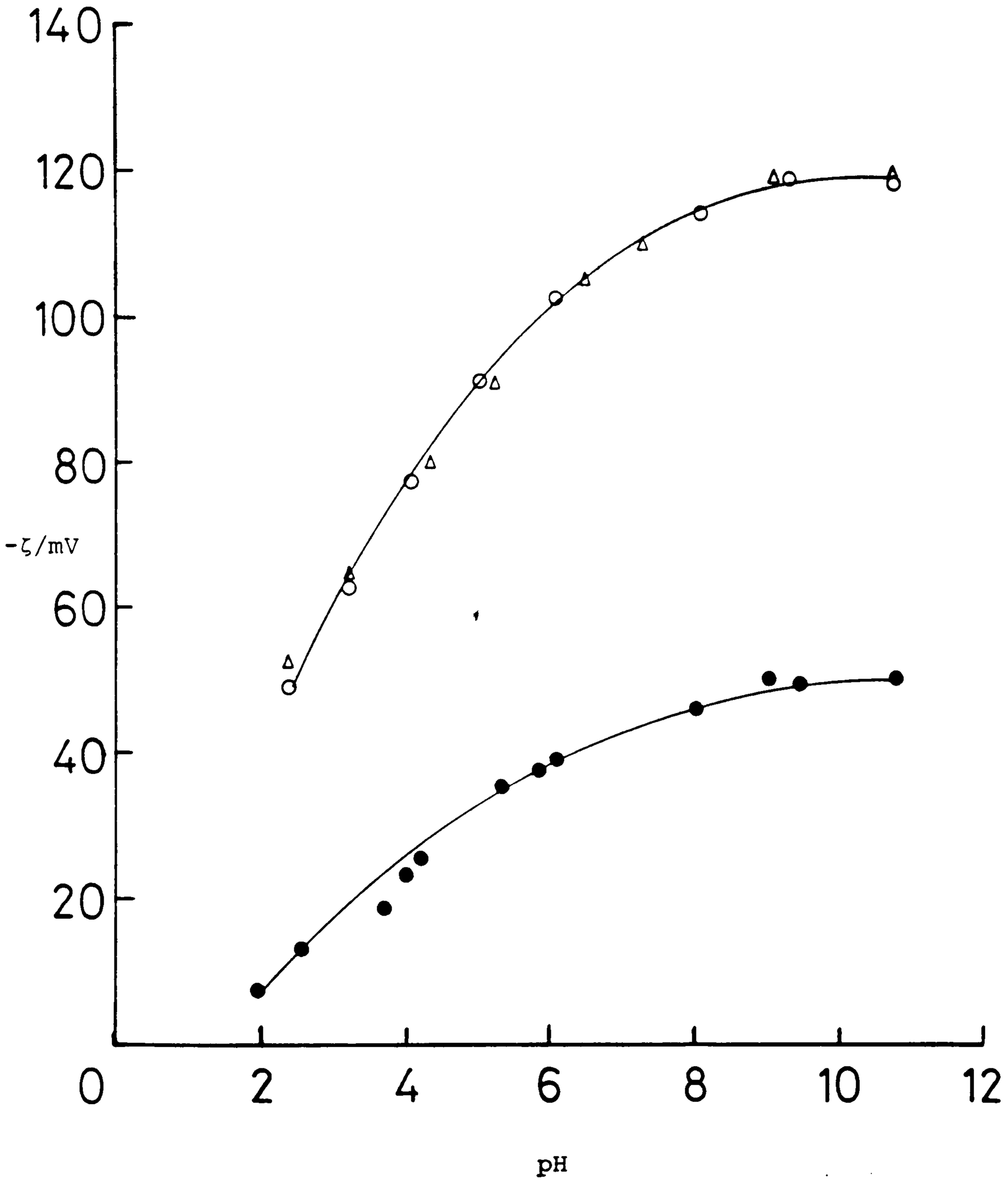

Figure 92: Zeta potential versus pH for kaolin particles calculated using $f_1(\kappa a)$ from Henry.

[NaCl] = 0.01 (●), 0.01 (O), 0.001 (Δ) mol dm^{-3}. T = 25°C.

Table 22. Values of $f_1(\kappa a)$ and mobility equations used to determine the ζ-potential of kaolin particles.

$\frac{[NaCl]}{mol\ dm^{-3}}$	$\frac{\kappa}{m^{-1}}$	$f_1(\kappa a)$	Mobility Equation u_E =
0.100	1.04×10^{-9}	1.49	$7.81 \times 10^{-7}\ \zeta$
0.010	3.28×10^{-8}	1.47	$7.65 \times 10^{-7}\ \zeta$
0.001	1.04×10^{-8}	1.42	$7.42 \times 10^{-7}\ \zeta$

Using equation (1.14), the diffuse layer charge density of the kaolin particles has been determined and calculated for the 0.100 mol dm^{-3} NaCl data of Figure 70. Figure 93 below shows the values of charge density to range from 0.8 $\mu C\ cm^{-2}$ to about 4.5 $\mu C\ cm^{-2}$, giving between 5×10^{12} and 3×10^{13} sites cm^{-2} on the surface, or 2000 to 333 $\AA^2$ per charge site, well above the minimum of 20 $\AA^2$ site^{-1} [H7].

Double Layer Capacitance (Section 1.6.2.2)

The double layer capacitance of a charged kaolin particle can be related to the change in zeta potential with pH [S6] (and Section 1.6.2.2) by:

$$N\ s^{-1} = a + \frac{C_d^0}{K} \exp \kappa\Delta \qquad (4.7)$$

where, $s = \left(\frac{d\zeta}{dpH}\right)_{\zeta \to 0}$ in mV/pH

$$N = -2.303\ \frac{kT}{e}$$

K = the integral capacitance of the inner region of the double layer; $\mu F\ m^{-2}$

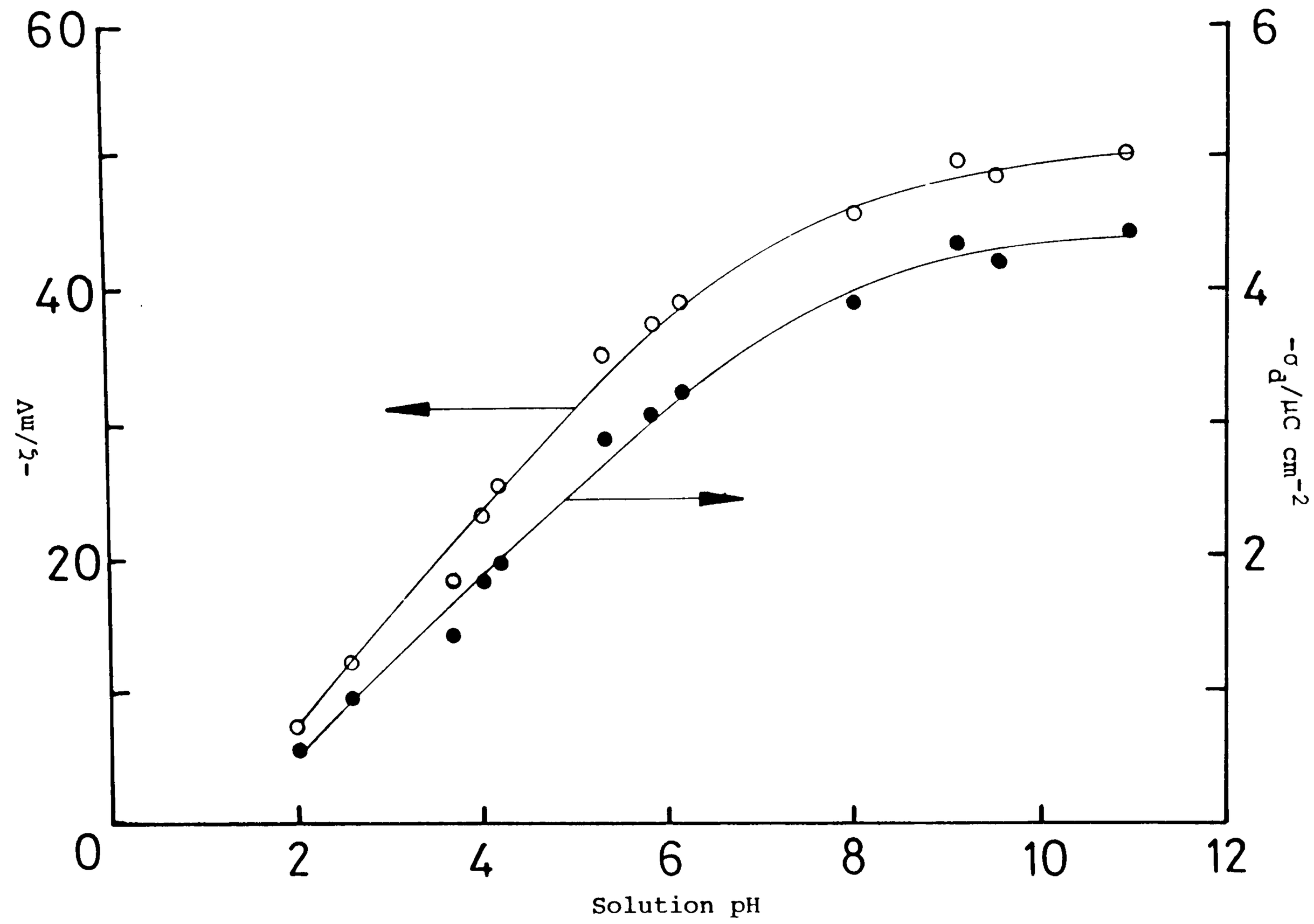

Figure 93: Effect of solution pH on the zeta potential (Smoluchowski) (O), and diffuse charge density (●), of kaolin in 0.1 mol dm^{-3} NaCl, at 25°C.

C_d^0 = the diffuse double layer capacitance as $\zeta \rightarrow 0$; $\mu F\ m^{-2}$

Δ = the distance from the Outer Stern Plane (OSP) to the electrokinetic shear plane (see below).

Note: $C_d = \varepsilon \kappa \cosh \frac{Z\ e\ \zeta}{2kT}$ (Section 1.6)

which, at 25°C gives; $C_d = 228.5Z\ e^{\frac{1}{2}} \cosh(19.46Z\ \zeta)\ \mu F\ cm^{-2}$

Then, as $\zeta \rightarrow 0$, so $\cosh(19.46Z\ \zeta) \rightarrow 1$.

From the results of Figure 92, extrapolated to zero ζ-potential, values of C_d, s, and N s^{-1} have been determined, Table 23, and a plot of N s^{-1} against C_d^0 is shown in Figure 94.

Table 23. Calculated values of C_d^0, s, and N s^{-1} for kaolin at different NaCl concentrations.

[NaCl] / 10^{-3} mol dm^{-3}	C_d / $\mu F\ cm^{-2}$	s / mV/pH	N s^{-1}
0	0	-	1
1	7.2	37.1	1.59
100	7.2	9.0	6.57

This plot gives a straight line, and an intercept of 1.0, as required by equation (4.7) since κ goes to zero with C_d^0. Since K only varies slightly with electrolyte concentration the linearity of the plot shows that Δ is not significant, and the slope gives K = 12.8 $\mu F\ cm^{-2}$.

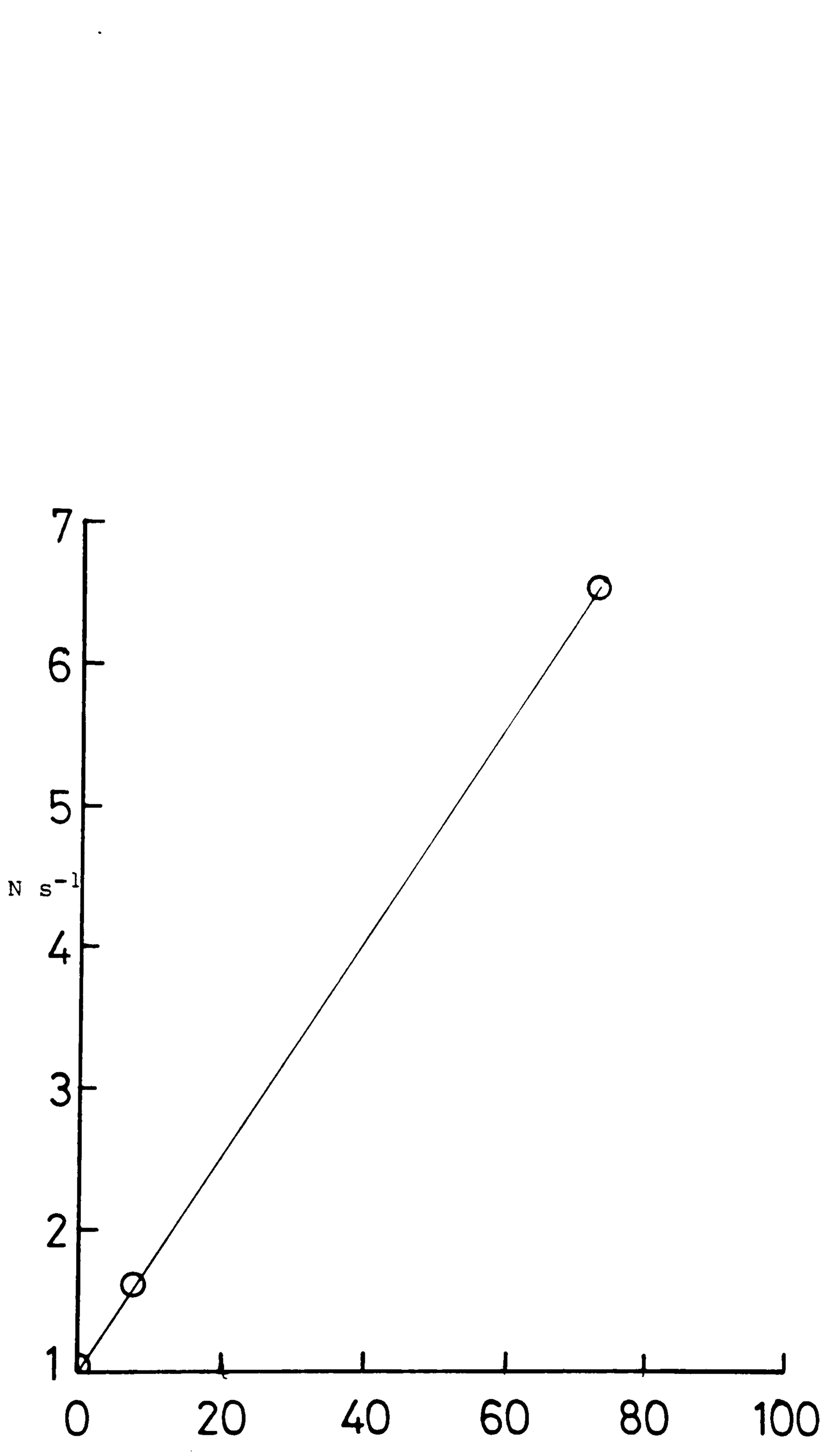

Figure 94: Values of N s^{-1} against C_d^0 for kaolin in solutions of varying pH and salt concentration

The double layer is treated as two capacitors in series, then:

$$\frac{1}{K} = \frac{1}{K_{Stern}} + \frac{1}{K_{diffuse}}$$

where, K_{Stern} = the capacitance of the Stern layer (inner part of the edl), in $\mu F\ cm^{-2}$

$K_{diffuse}$ = the capacitance of the diffuse part of the double layer, in $\mu F\ cm^{-2}$.

Then, taking $K_{Stern} = 30\ \mu F\ cm^{-2}$[H7] gives:

$$\frac{1}{12.8} = \frac{1}{30} + \frac{1}{K_{diffuse}}$$

giving $K_{diffuse} = 22\ \mu F\ cm^{-2}$.

The diffuse layer capacitance can now be related to the fraction of dissociable surface groups whcih are charged at the point-of-zero charge, θ_c [H7]:

$$K_{diffuse} = \frac{2N_s s\ e^2 \theta_c}{kT} .$$

Taking the number of sites per cm^2, $N_s = 5 \times 10^{14}\ cm^{-2}$[S17], gives a value of $\theta_c = 0.04$, indicating that the fraction of dissociable groups which are charged at the pzc is small, which for the low pH involved is a reasonable conclusion.

4.5.1 <u>The Effect of Surfactant Adsorption on the Electrophoretic Mobility of Kaolin Particles (Section 3.6.2)</u>

The results of Figure 71 show the variation of electrophoretic mobility as a function of surfactant concentration. From here it is apparent that the surfactant adsorption increases the

negative charge on the particles, up to a plateau, and yields a mobility plot which is similar in form to the adsorption isotherms found earlier (Section 3.3), consisting of a small initial slope, followed by a marked increase then a plateau of constant mobility.

Zeta Potential and Surface Charge Density

The calculated values of zeta potential and surface charge density for the system, at pH 2.3 and 11.0, are shown in Figure 95.

The results here can be compared to those of Figure 71 to see the effect of surfactant addition. For pH = 2.3, addition of 10^{-5} mol dm^{-3} of surfactant increases the surface charge density from about -0.8 $\mu C\ cm^{-2}$ in the absence of surfactant, to about -2.4 $\mu C\ cm^{-2}$ with surfactant, an increase of 66%. At pH 11.0 the charge density increases from -3.5 $\mu C\ cm^{-2}$ to -4.4 $\mu C\ cm^{-2}$ for the same concentration range, that is an 18% increase, showing the difficulty of adsorbing surfactant onto the more negatively charged surface. At plateau adsorption, the surface charge density is 82% higher for the low pH samples and about 45% greater for the higher pH, relative to the zero surfactant concentration levels.

The variation of the "maximum" surfactant adsorption density with pH, obtained from adsorption isotherms (Figures55 and 56) is shown in Figure 96, together with the surface charge density of kaolin particles in the absence of surfactant. The results clearly show the dependence of surfactant adsorption on solution pH, through the solid's surface charge density. As the pH is

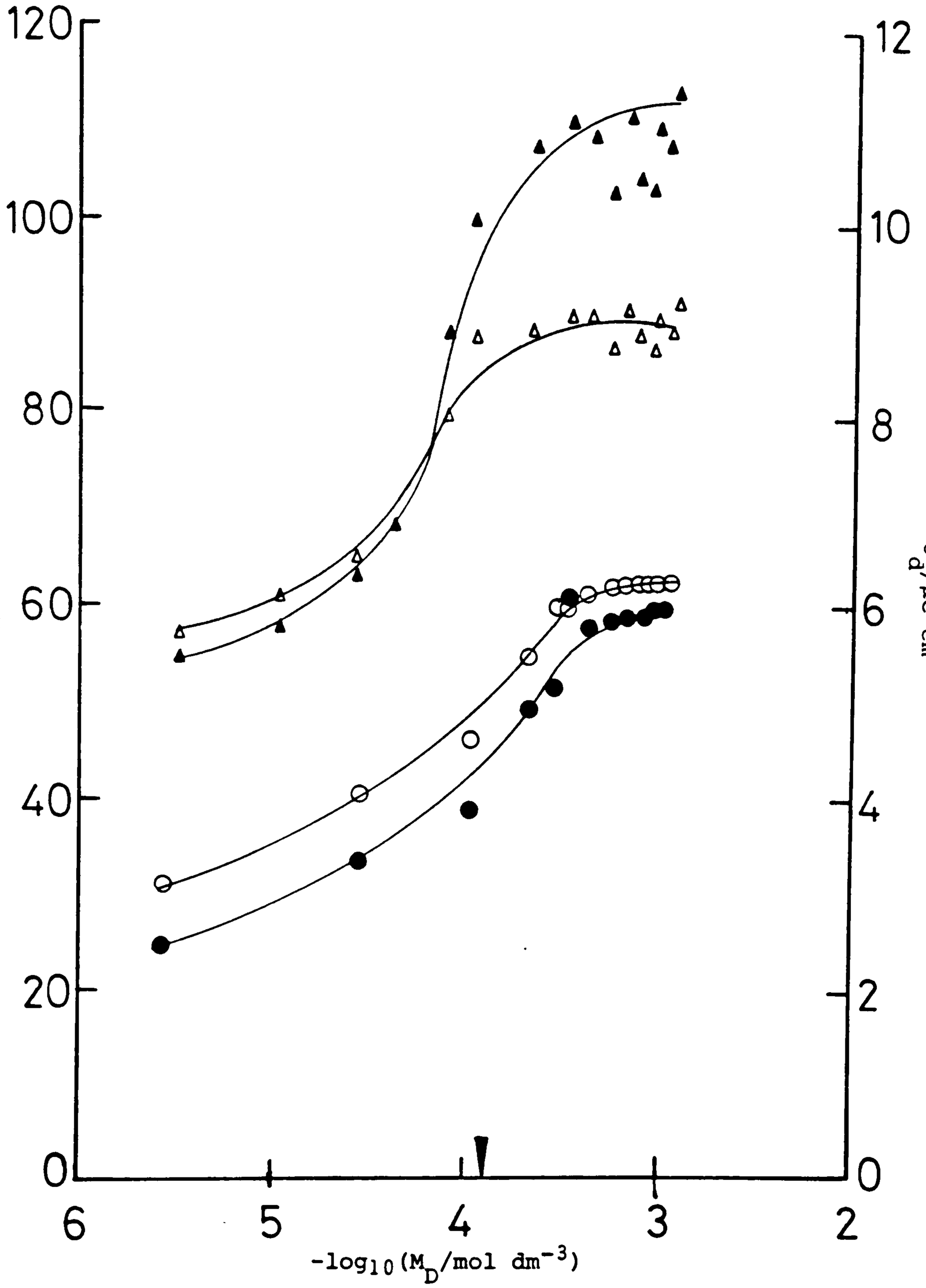

Figure 95 : Effect of 4-ϕ-C_{12} ABS on the zeta potential (Smoluchowski) (○) and diffuse charge density (●) of kaolin particles at pH 2.3, and zeta potential (△) and diffuse charge density (▲), at pH 11.0, in 0.1 mol dm^{-3} NaCl solution, at 25°C.

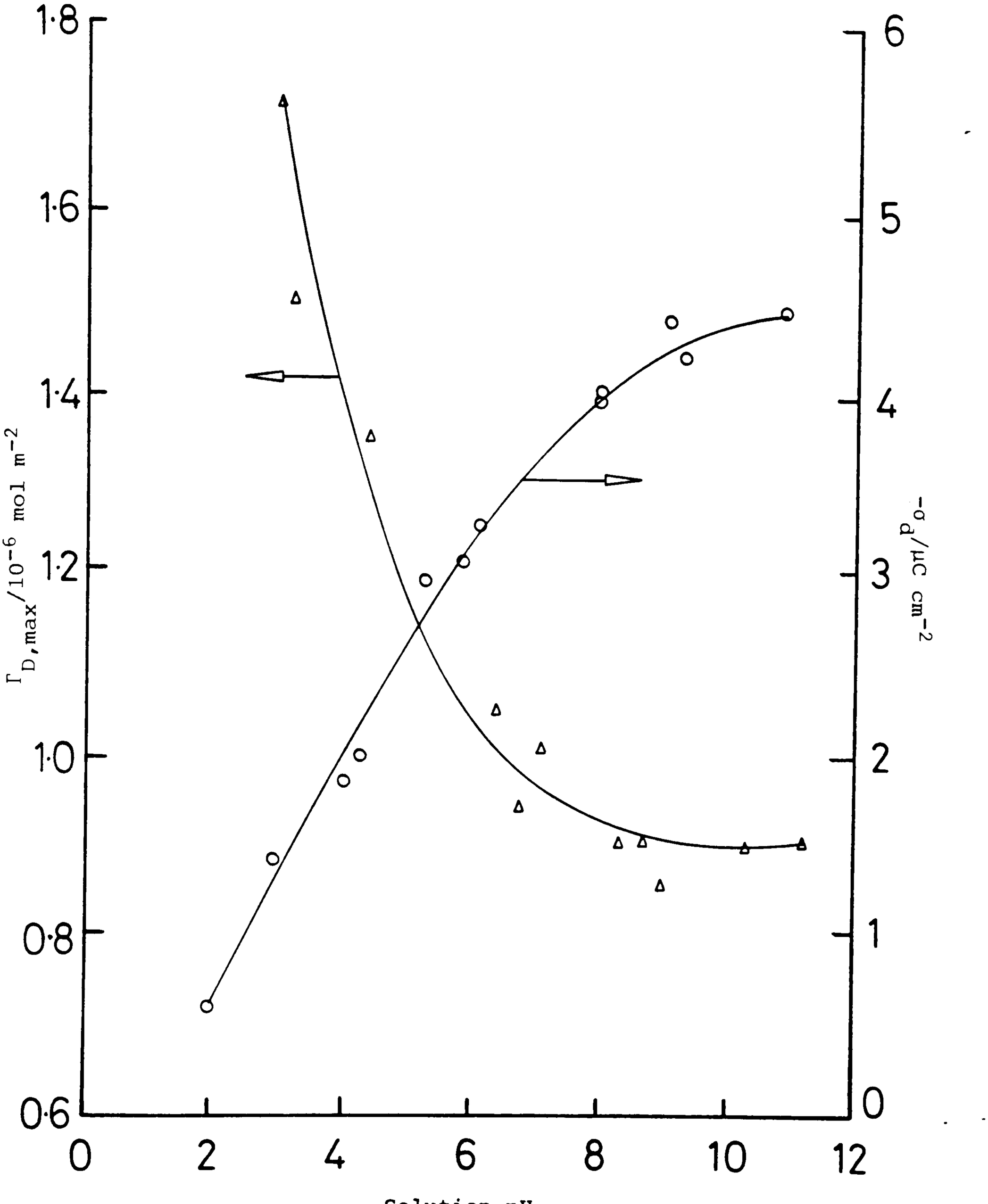

Figure 96: Effect of pH on the plateau adsorption density of 4-ϕ-C_{12} ABS onto kaolin (Δ) and on the diffuse charge density of the clay (O), in 0.1 mol dm^{-3} NaCl, at 25°C.

S/L for adsorption results = 10%.

increased, negative charge density increases and the anionic surfactant adsorption decreases. When surfactant does adsorb, there is effectively a neutralisation of positive surface charge.

Thus at low pH, when the negative charge density of the particle is at a minimum (Figure 93) and surfactant adsorption is highest (Figures 56 and 96), the change in surface charge is larger as discussed above.

Adsorption of the positively charged CTAB surfactant reduces the negative mobility of the particles, and with higher concentrations of surfactant the surface charge is eventually reduced to zero, then reversed (Figure 72). Thus, in contrast to all other measurements (Section 4.1), a point of zero charge has been reached, and exceeded.

These results provide definite evidence of the surfactant head-group-surface interaction, and eventual bilayer coverage. An additional observation that can be made from Figure 72 is that increasing the solution pH requires more surfactant to be adsorbed to reduce the surface charge, a fact which makes sense when the results of Figure 93 are considered, that is, a greater negative charge is to be neutralised at higher solution pHs. Figure 97 shows the calculated ζ-potential and surface charge density.

Considering the results of Figure 72 at zero mobility. For a solution pH of 2.7, the concentration needed to reduce the surface charge is about 3.5×10^{-6} mol dm^{-3}, while for pH 11.0

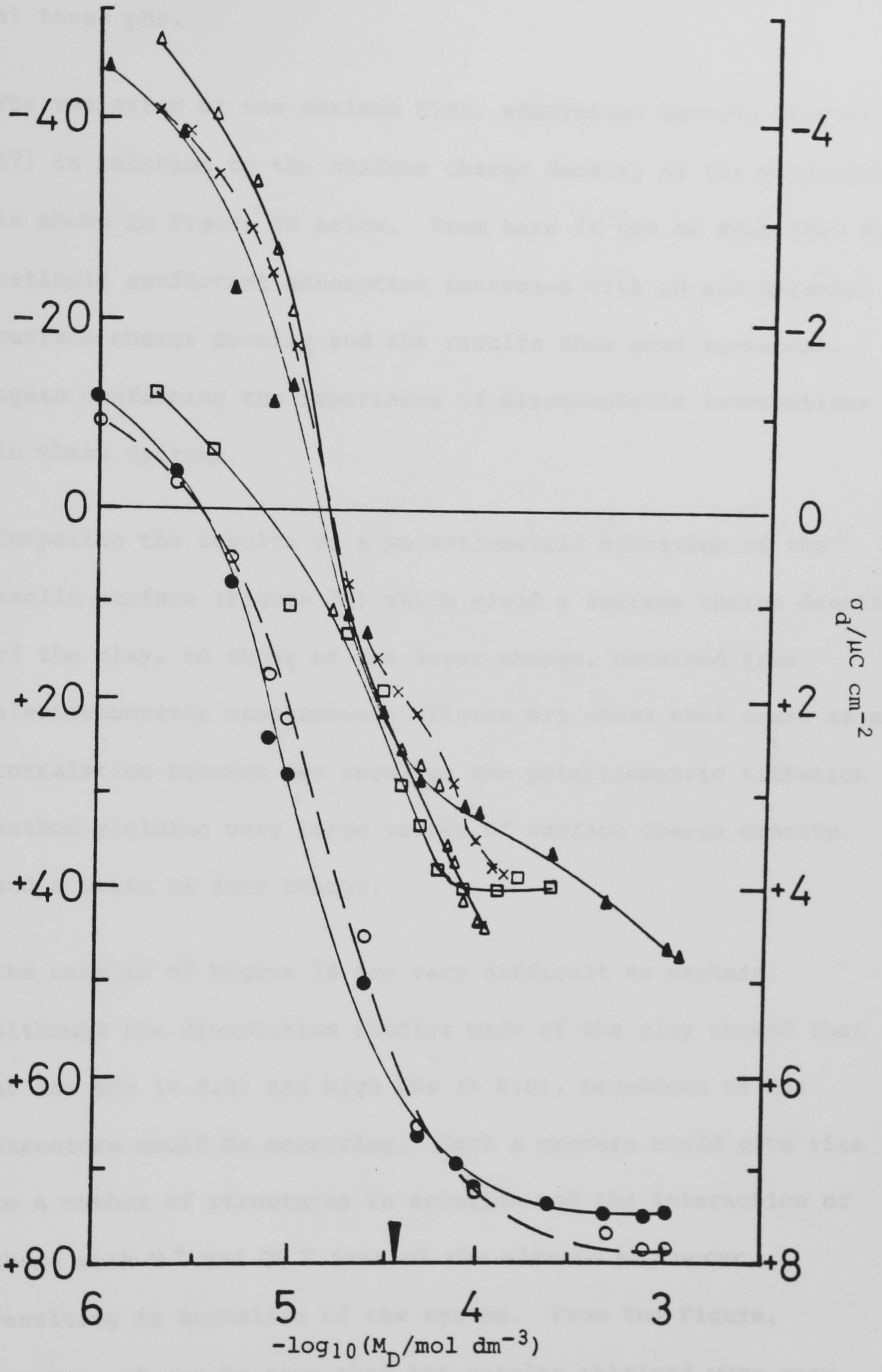

Figure 97: Effect of CTAB on the zeta potential (Smoluchowski) of kaolin particles in 0.1 mol dm^{-3} NaCl, at 25°C, and pH 2.7 (●), 6.0 (□), 8.3 (▲) and 11.0 (△); and on the diffuse charge density at pH 2.7 (O) and 11.0 (x) (dashed lines).

the concentration is about 18.0×10^{-6} mol dm^{-3}, an increase of 80%, showing the large differences in surface charge density at these pHs.

The variation of the maximum CTAB, adsorption density (Figure 67) in relation to the surface charge density of the particles is shown in Figure 98 below. From here it can be seen that the cationic surfactant adsorption increases with pH and negative surface charge density and the results show good agreement, again confirming the importance of electrostatic interactions in these systems.

Comparing the results of a potentiometric titration of the kaolin surface (Figure 74) which yield a surface charge density of the clay, to those of the layer charge, obtained from electrophoretic measurements (Figure 93), shows that there is no correlation between the results; the potentiometric titration method yielding very large values of surface charge density, and a point of zero charge.

The results of Figure 74 are very difficult to explain, although the dissolution studies made of the clay showed that at low pHs (< 3.0) and high pHs (> 8.0), breakdown of the structure could be occurring. Such a process would give rise to a number of structures in solution and the interaction of these with H^+ and OH^- ions of the titrand may occur, resulting in anomalies of the system. From the Figure, however, it can be seen that the results obtained were very consistent, even at different levels of sodium chloride. The potentiometric measurements were made by starting at a high pH

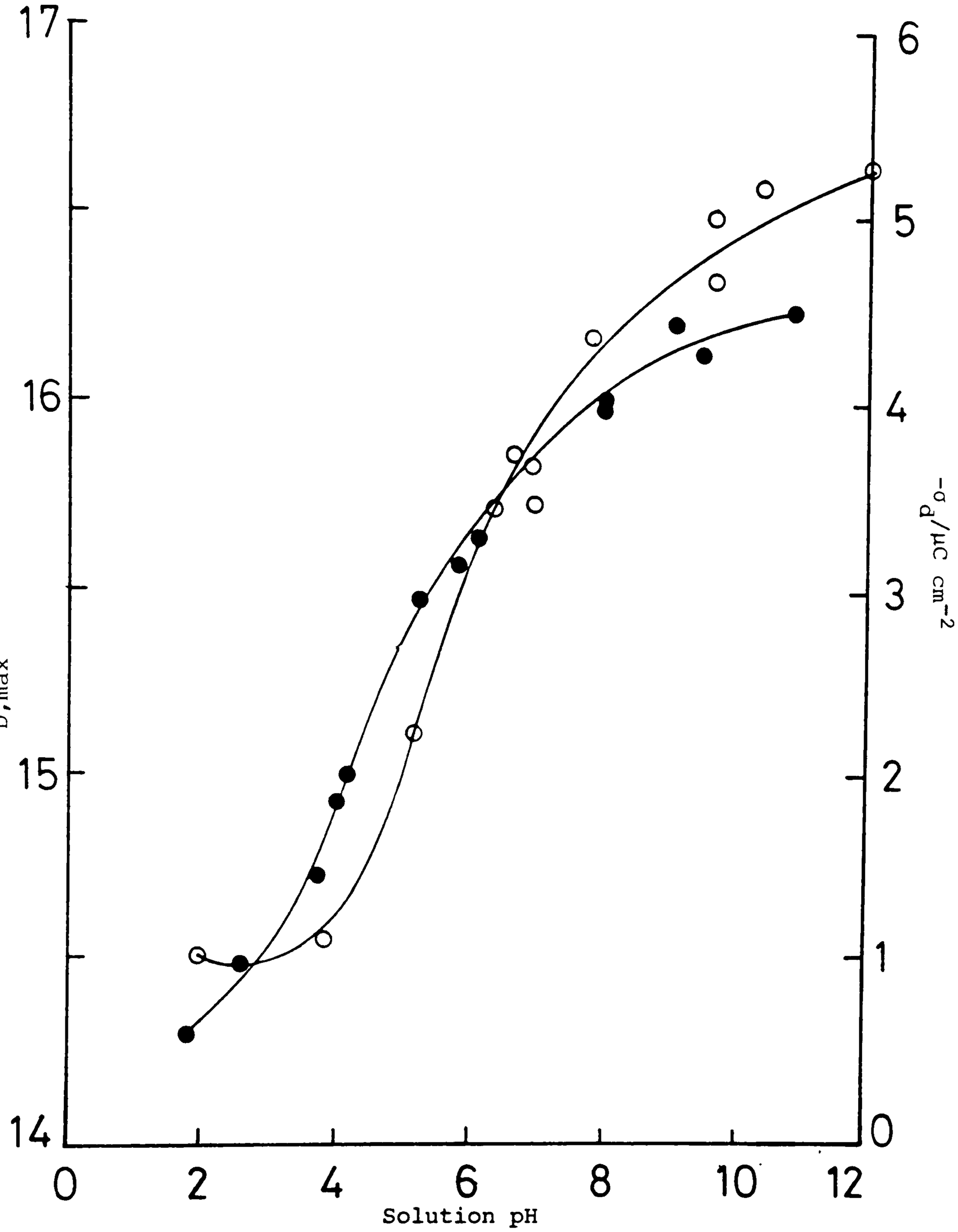

Figure 98: Effect of pH on plateau adsorption of CTAB onto kaolin (O) and on diffuse charge density of the clay (●), in 0.1 mol dm^{-3} NaCl solution, at 25°C. S/L for adsorption measurements = 10%.

and working downwards, and perhaps further data, starting at a neutral solution pH, might reveal some differences. In view of these factors, it is felt that the electrophoretic results, rather than the potentiometric titration data, reflect the true nature of the system.

4.5.2 Electrophoretic Mobility Measurements of Silica (Gasil-35) (Section 3.7)

The importance of positively charged sites on the clay edge to anionic surfactant adsorption is shown particularly when the adsorption results are compared to those of silica (Figures 55 and 69, for kaolin and silica respectively). The amounts of surfactant adsorbed at the clay-solution interface is over 500 × greater than that at the silica surface (pH 2.4, Figure 55 for kaolin, Figure 69 for silica), and yet they have almost the same magnitude of surface charge density (Figures 93 and 99, for kaolin and silica, respectively). Based on electrophoretic studies alone therefore, an erroneous conclusion that anionic surfactants should not adsorb on clay particles might be drawn. Combination of both electrophoresis and adsorption studies is thus very important for the applications considered in this report, since they have mutually shown the existence of positive, as well as negative, sites on clay particles.

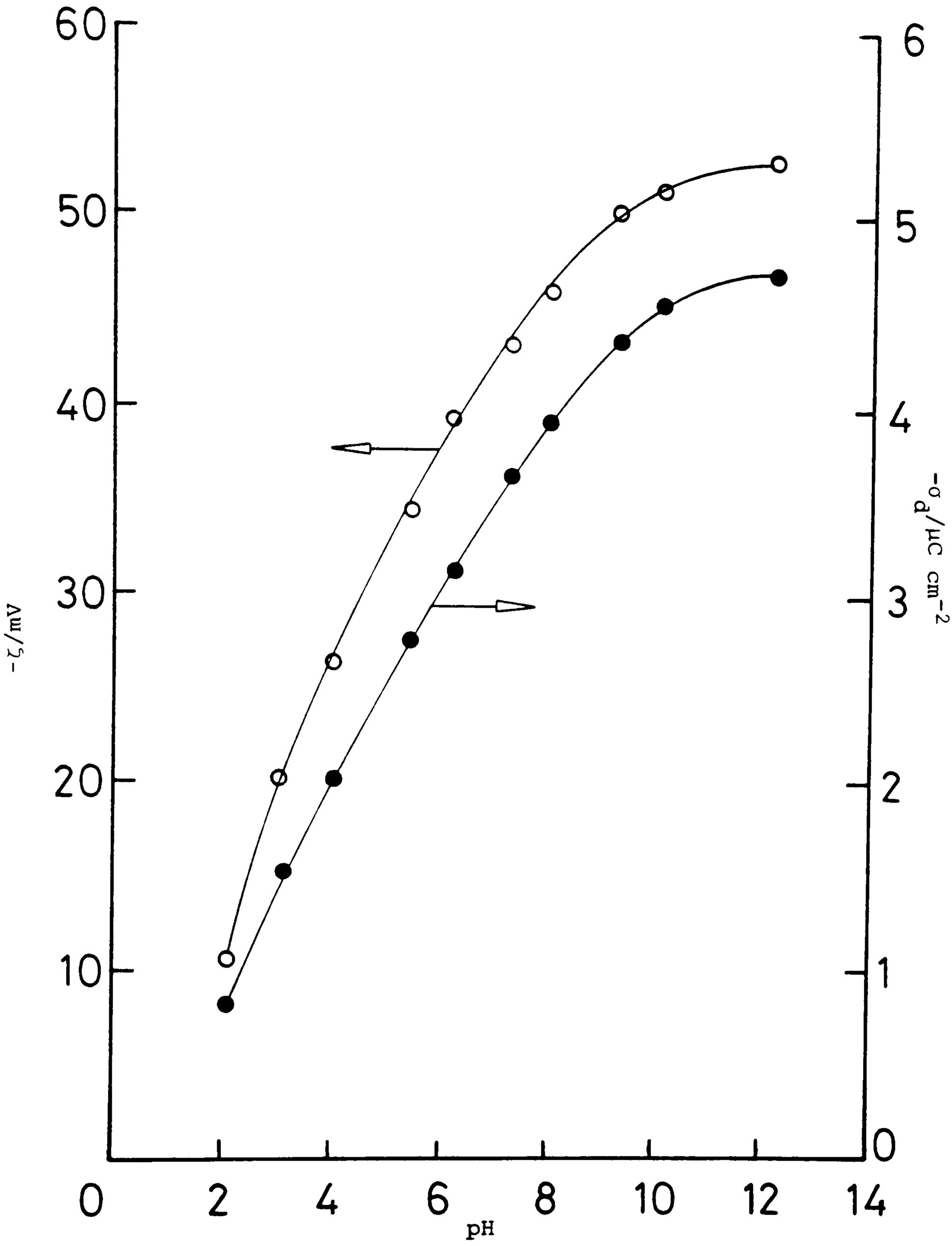

Figure 99: Variation of zeta potential (Smoluchowski), (O), and diffuse charge density (●), of silica (Gasil-35) particles, at 25°C, with pH. NaCl = 0.1 mol dm^{-3}.

FINAL DISCUSSION

The adsorption of both cationic and anionic surfactants, from aqueous solutions, onto a wide variety of mineral surfaces has been extensively studied [B4-B6,D4, for example]. From these works, numerous aspects of the adsorption process have been widely accepted as established.

Most workers [C1,F1,G1,S1,S13-S14, for example] divide adsorption isotherms into three, or four distinct regions, Figure 54. In region I, ionic surfactant adsorption obeys Henry's Law and corresponds to low-surface coverage without surfactant aggregation on the surface [S13]. The region I/region II transition occurs at the onset of surfactant aggregate formation at the mineral surface, as indicated by the sharp increase in the slope of the isotherm [B2,B3,C4,C5,D1,G6,G7, M1,S13,S14]. These aggregates form locally on the surface, i.e. by patchwise adsorption [G8], and are referred to as hemi-micelles [G7,S13], or admicelles [H1], to emphasise the micelle-like aspects of their structure, and are envisaged as two-dimensional analogues of micelles [H2,S14].

The concentration at which the region I/region II transition occurs is referred to as the hemimicelle concentration (HMC) [S13], the critical admicelle concentration (CAC) [H1], or the critical hemimicelle (CHMC) [C6]. Region III begins where the slope of the adsorption isotherm starts to decrease; this decrease is believed to arise from either the electrostatic repulsion of ions at the interface, because of a change in the sign of surface charge [S13,A11], or from the distribution of patch adsorption energies [G8,H1]. The region III/region IV transition occurs either at the critical micelle concentration (CMC) or upon completion of bilayer coverage of the surface [A1,A4,H1,S14,T1].

Region IV is a plateau adsorption region, characterised by almost zero slope, and occurs at concentrations above the CMC [F2].

The primary forces involved in the formation of the surfactant surface aggregates are the same as those involved in micelle formation [C4,G7, G8]. These primary forces are the Coulombic interactions arising from the charges on the surfactant hydrophilic moieties, the mineral surface, and the surfactant tail-tail interactions now explained in terms of the hydrophilic effect [B1,B7,D2,F3,R8,T2,W1]. Various attempts at modelling admicelle formation as a local phase transition have also yielded thermodynamic parameter values that approximate to the analogous quantities found in micelles [S13,S14,H1].

While a certain amount of work has been carried out concerning the influence of alcohol on surfactant adsorption at air-liquid [R2] and liquid-liquid [A3] interfaces, and on micelle formation [M4], very few studies have been made concerning adsorption at the solid-liquid interface. Somasundaran [S15] has made studies of this effect on surfactant adsorption on alumina and found that the addition of alcohol produced marked changes in the adsorption, increasing particularly the adsorption in region I of the isotherm. The present work also concerns the effect of n-butanol on 4-ϕ-C_{12} ABS adsorption onto kaolin, in line with the proposed flooding system for EOR in the North Sea [D7].

Region V, of Figure 54, is a major finding of this study. In this region, surfactant loss onto the solid surface is reduced. Previous work published, concerning surfactant adsorption at the solid-liquid interface, was limited to concentrations of surfactant up to 1×10^{-3} mol dm^{-3} [B2,B3,B9,S13,S14, for example], up to which a plateau of

adsorption was found, in agreement with the present work. However, those other workers did not measure surfactant adsorptions up to 1×10^{-2} mol dm^{-3} as here.

As these higher surfactant concentrations, while experimental error is high, the trend of surfactant adsorption is downward, indicating a reduction in adsorption.

To explain this finding, a surfactant precipitation, re-dissolution mechanism has been postulated. In order to test this postulate, surfactant precipitation with aluminium, and re-dissolution with additional surfactant, was studied, the results here supporting the postulate. Thus, it has been concluded that at high surfactant concentrations ($> 10^{-3}$ mol dm^{-3}), surfactant re-dissolution from kaolin does occur, and that the loss of surfactant from solution is therefore reduced. However, in the solution, the surfactant may be held in the soluble Al complex and not be available to lower the interfacial tension (o/w).

Because H^+ and OH^- are potential determining ions for mineral oxides [S13,F7,F8,D6,R2,T7], the surface potential increases (positively) as the pH is reduced. Thus, the adsorption of ionic surfactants at the mineral oxide surface is markedly affected by the solution pH (see Section 3.3). Past studies which have considered this factor have mainly been confined to anionic surfactant adsorption onto alumina [D6,F8,R2,S12,S13,G10,B8,H12,Y1] or cationic surfactant adsorption onto silica [T6,Z4,L3,L4,G11,C7]. The obvious reason for this is that, with respect to surface charge (as obtained from electrophoretic studies), such adsorbent-adsorbate combinations will show favourable interactions.

In the case of the clay mineral, kaolin, however, the situation is not quite so straightforward. Electrophoretic studies of this material show that the particles carry a negative charge over a wide pH range, and yet this and other studies have shown that anionic surfactant adsorption takes place at their surface [S12,C6,G7,S15,R5]. The explanation for this apparent anomaly lies with the different natures of the edge, and faces, of clay particles, which are pseudo-hexagonal plates (see Section 1.6 and Figure 15 [V1]). While the edges carry a pH-dependent charge density, the faces carry a net-negative charge which is effectively independent of the solution conditions [V1] and dominates the electrophoretic mobility of the particle (see Section 3.6). Previous workers [S12,C6] have acknowledged this face-edge difference in electrical charge distribution, but have made no efforts to link electrophoretic and adsorption measurements.

Conclusions

CONCLUSION

The present work has shown a very good correlation between electrophoretic mobility measurements and adsorption studies. Using this combined information it has been shown that charged surfactant-charged surface interactions occur through an electrophoretic mechanism, even for an anionic surfactant and an "apparently" negatively charged surface. Multi-valent cations (Al^{3+}) in the solid surface appear to be responsible for the primary attraction of the anionic surfactant. What appears to form on the surface are insoluble aluminium salts of the anionic surfactant. Adsorption is greater in the presence of salt (NaCl) which prevents aluminium ions dissolving out of the surface into aqueous solution.

Clay (kaolin) contains multivalent cations while sandstone (and silica) does not. It follows therefore that adsorption of anionic surfactant is much greater on clay than that on sand. The clay fraction of an oil-well is the major cause of surfactant loss from aqueous solution during surfactant-enhanced oil recovery.

At high surfactant concentrations, greater than about 10^{-5} mol dm^{-3} and less than about 10^{-3} mol dm^{-3}, adsorption occurs through surfactant tail-tail interactions with the formation of hemi-micelles and admicelles at the solid surface. Before complete surface coverage limiting adsorption is reached due to micelle formation in solution, limiting the availability of monomer for adsorption.

Finally, it was discovered that at the highest surfactant concentrations ($> 10^{-2}$ mol dm^{-3}) when the number of anionic micelles is large, the amount of surfactant adsorbed decreases. This drop in adsorption

is considered to occur because the multivalent cations are drawn out of the kaolin surface into aqueous solution and solubilised as counterions to the micelles. The presence of other counterions (e.g. sodium from salt) retards this process until higher concentrations of surfactant micelles are formed (i.e. a plateau).

Further studies here of the interfacial tension between n-decane and aqueous surfactant solutions have shown that it is possible to achieve (with suitable concentrations of n-butanol, sodium chloride, and surfactant) very low interfacial tensions, although measurements were hampered by the limitations of the method employed.

From all of the evidence gathered in this thesis, some statements may be made to help those using surfactant flooding as an "enhanced oil recovery":

(i) Anionic surfactant (4-ϕ-C_{12} ABS) loss from aqueous solution, by adsorption, takes place on the clay surfaces of the well and such losses can be minimised by suitable adjustment of the flooding solution through:

(a) ionic strength,

(b) alcohol addition,

(c) improved emulsion stability,

(d) solution pH.

(ii) Loss of surfactant from solution by precipitation with aluminium ions is likely to be low, interactions with sites at the clay surfaces being of greater importance.

(iii) Loss of surfactant is "reduced" at high surfactant concentrations (>> CMC), due to a re-dissolution, or desorbing, mechanism of precipitated, or adsorbed, surfactant.

REFERENCES

A1 Aveyard, R., Binks, B.P., Clark, S., and Mead, J., J. Chem. Soc., Faraday Trans. I, 82, 125 (1986).

A2 Aveyard, R., and Haydon, D.A., "An Introduction to the Principles of Surface Chemistry", Cambridge University Press (1973), p.50.

A3 Aveyard, R., Binks, B.P., and Mead, J., J. Chem. Soc., Faraday Trans. I, 83 (8), 2347 (1987).

A4 Adamson, A.W., "Physical Chemistry of Surfaces", 34th Ed., Wiley Interscience, New York (1976), p.115.

A5 Abuin, E.B., and Lissi, E.A., J. Colloid Interface Sci., 95, 198 (1983).

A6 Almgren, M., Greiser, F., and Thomas, J.K., J. Chem. Soc., Faraday Trans. I, 75, 1674 (1979).

A7 Almgren, M., and Swarup, P., J. Colloid Interface Sci., 91, 256 (1983).

A8 Attwood, D., Mosquera, V., and Perez-Villa, V., J. Colloid Interface Sci., 127 (no. 2), 532 (1989).

A9 Aveyard, R., Binks, B.P., and Mead, J., J. Chem. Soc., Faraday Trans. I., 81, 2169 (1985).

A10 Aveyard, R., Binks, B.P., and Mead, J., J. Chem. Soc., Faraday Trans. I, 82, 1755 (1986).

A11 Ananthapadmanabhan, K.P., and Somasundaran, D., Colloids Surf., 77, 105 (1983).

B1 Bae, J.H., Petrick, C.B., and Ehrlich, R., "A Comparative Evaluation of Microemulsions and Aqueous Systems", SPE Paper 4749, presented at the Improved Oil Recovery Group of SPE, Tulsa (1974).

B2 Beeson, D.M., and Ortloff, G.D., Trans. AIME, 216, 388 (1959).

B3 Bansal, V.K., and Shah, D.O., in "Microemulsions", (L.M. Prince, Ed.), Academic Press, New York, p.159 (1977).

B4 Buchanan, A.S., and Oppenheim, R.C., Aust. J. Chem., 21, 2367 (1968).

B5 Ball, B., and Fuerstenau, D.W., Disc. Faraday Soc., 52, 371 (1971).

B6 Bitting, D., and Harwell, J.H., Langmuir, 3 (4), 500 (1987).

B7 Banwell, C.N., "Fundamentals of Molecular Spectroscopy", 2nd Ed., McGraw-Hill (1972).

B8 Bisio, P.D., Cartledge, J.G., Keeson, W.H., and Radke, C.J., J. Colloid Interface Sci., 78, 225 (1980).

B9 Bazin, B., and Defives, D., Collect. Colloq. Seminar (Inst. Fr. Pet.), 42, 537-556 (1985).

C1 Chan, K.S., and Shah, D.O., J. Disperson Sci Technol., 1, 55 (1980).

C2 Cayais, J.L., Schecter, R.S., and Wade, W.H., "Adsorption at Interfaces", p.234, ACS Symp. Series No. 8 (1975).

C3 Cayais, J.L., Schecter, R.S., and Wade, W.H., Soc. Petrol. Eng. J., 16, 351 (1976).

C4 Cross, A., PhD Thesis, Liverpool Polytechnic (1987).

C5 Chapman, D.L., Philos, Mag., 25, 475 (1913).

C6 Cases, J.M., Goujou, G., and Smani, S., AIChE Symp. Ser., 71, 100 (1975).

C7 Chander, S., Fuerstenau, D.W., and Stigter, D., in "Adsorption from Solution" (R.H. Ottewill, C.H. Rochester, and A.L. Smith, Eds.), Academic Press, London, p.197 (1983).

C8 Cox, B.G., Garcia Rosar, J., and Schneider, H., J. Am. Chem. Soc., 103, 1384 (1981).

D1 Dupeyrat, M., Minssieux, L., and Naggar, A.El., European Symp. Enhanced Oil Recovery, Edinburgh, p.161 (1978).

D2 Doe, P.H., Wade, W.H., and Schecter, R.S., J. Colloid Interface Sci., 59, 525 (1977).

D3 Dukhin, S.S., and Deryaguin, B.V., in "Surface and Colloid Science" (E. Matijevic, Ed.), 7, 52, John Wiley, New York (1986).

D4 Doe, P.H., El-Emary, M., Wade, W.H., and Schecter, R.S., J. Amer. Oil Chem. soc., 54, 570 (1977).

D5 Danil de Namor, A.F., Ghousseini, L., and Lee, W.H., J. Chem. Soc., Faraday Trans. I, 81, 2495 (1985).

D6 Dick, S.G., Fuerstenau, D.W., and Healy, T.W., J. Colloid Interface Sci., 37 (3), 595 (1971).

F1 Foster, W.F., J. Pet. Technol., 25, 205 (1973).

F2 Franses, E.I., Puig, J.E., Talmon, Y., Miller, W.G., Scriven, L.E., and Davis, H.T., J. Phys. Chem., 84, 1547 (1980).

F3 Franses, E.I., Talmon, Y., Scriven, L.E., David, H.T., and Miller, W.G., J. Colloid Interface Sci., 86, 449 (1982).

F4 Foulser, R.W.S, Dept. of Energy Seminar on Enhanced Oil Recovery Research, Imperial College, London, June 1987.

F5 Flegman, A.W., Goodwin, J.W., and Ottewill, R.H., Proc. Brit. Ceram. Soc., 13, 31 (1969).

F6 Frumkin, A.Z., Z. Phys. Chem., 116, 466 (1925).

F7 Fuerstenau, D.W., Pure Appl. Chem., 24, 135 (1970).

F8 Fuerstenau, D.W., and Wakamatsu, T., Faraday Disc. Chem. Soc., 59, 157 (1976).

G1 Gogarty, W.B., J. Pet. Technol., 35, 1168 (1983).

G2 Gouy, G., J. Phys. chem., 9, 457 (1910).

G3 Gregg, S.J., and Sing, K.S.W., "Adsorption, Surface Area, and Porosity", Academic Press (1983), p.22.

G4 Graham, D.C., Chem. Rev., 41, 441 (1947).

G5 Gettins, W.J., Rassing, J.E., and Wyn-Jones, E., in "Micellisation, Solubilisation, and Microemulsions", Vol.1 (K.J. Mittal, Ed.), Plenum Press, New York (1977), p.270.

G6 Gale, W.W., and Sandvik, E.I., Soc. Pet. Eng. J., 13, 191 (1973).

G7 Goujon, G., Cases, J.M., and Mutaftschiev, B., J. Colloid Interface Sci., 56, 587 (1976).

G8 Gu, T., Gao, Y., and He, L., J. Chem. Soc., Faraday Trans. I, 84 (12), 4471 (1988).

G9 Gao, Y., Du, J., and Gu, T., J. Chem. Soc., Faraday Trans. I, 83 (8), 2671 (1987).

G10 Geer, R.D., Eylar, E.H., and Anacker, E.W., J. Phys. Chem., 75, 369 (1971).

G11 Gao, Y., Yue, C., Lu, S., Gu, W., and Gu., T., J. Colloid Interface Sci., 100, 581 (1984).

G12 Guggenheim, E.A., Trans. Faraday Soc. 36, 407 (1940).

H1 Hanna, M.S., and Somasundaran, D., in "Improved Oil Recovery by Surfactant and Polymer Flooding", Academic Press, New York, p.253 (1977).

H2 Healy, R.N., Reed, R.L., and Carpenter, C.W., Soc. Pet. Eng. J., 15, 87 (1975).

H3 Haydon, D.A., and Phillips, J.N., Trans. Faraday Soc., 54, 698 (1958).

H4 Hanson, K.H., and Froelich, E.M., Chem. Times Trends, 1 (4), 44 (1878).

H5 Haydon, D.A., in "Recent Progress in Surface Science" (J.F. Danielli, K.G.A. Pankhurst, and A.C. Riddiford, Eds.), Vol. 1, Academic Press, London (1964), p.100.

H6 Hunter, R.J., in "Zeta Potential in Colloid Science" (R.H. Ottewill, and R.L. Rowell, Eds.), Academic Press, London (1981), p.75.

H7 Healy, T.W., and White, L.R., Adv. Colloid Interface Sci., 9, 303 (1978).

H8 Høiland, H., Ljosland, E., and Backlund, S., J. Colloid Interface Sci., 101, 467 (1984).

H9 Hayase, K., and Hayano, S., Bull. Chem. Soc. Japan, 50, 83 (1977).

H10 Hayase, K., Hayano, S., and Tsubuta, H., J. Colloid Interface Sci., 101, 336 (1984).

H11 Hayase, K., and Hayano, S., J. Colloid Interface Sci., 63, 446 (1978).

H12 Harwell, J.H., Hoskins, J.C., Schecter, R.S., and Wade, W.H., Langmuir, 1, 251 (1985).

J1 Jewett, R.L., and Schurz, G.E., J. Petrol. Tech., 22, 675 (1970).

J2 Jayson, G.G., J. Appl. Chem., 9, 422 (1959).

J3 Johnson, V.J., "A Compendium of the Properties of Materials at Low Temperatures (Phase I). WADD Technical Report, 60-56, October (1960).

L1 Lee-Tuffnell, C., Dept. of Energy Seminar on Enhanced Oil Recovery Research, Imperial College, London, June (1986).

L2 Leibner, J.E., and Jacobus, J., J. Phys. Chem., 81, 130 (1977).

L3 Langevin, D., Guest, D., and Meunier, J., Colloids and Surfaces, 19, 159 (1986).

L4 Levine, P.L., Levine, S., and Smith, A.L., J. Colloid Interface Sci., 34, 549 (1970).

L5 Levine, P.L., and Smith, A.L., Disc. Faraday Soc., 52, 290 (1971).

L6 Lange, H., 4th Int. Congr. Surface Active Substances, Brussels, 2, 497 (1964).

M1 Melrose, J.C., and Brandner, C.F., J. Can. Pet. Tech., 54-62, October-December (1974).

M2 Micrometrics, Accusorb. Phsyical Adsorption Analyser Handbook (1978), ref. P/N 210/42801/00.

M3 Mukerjee, P., Advan. Colloid Interface Sci., 1, 264 (1967).

O1 Oil and Gas, Oct. 9, p.10 (1989).

O2 Oil and Gas, Jan. 15, p.18 (1990).

O3 Overbeek, J.Th.G., and Bijsterbosch, B.H., in "Electrokinetic Separation Methods" (P.G. Righetti, C.J. van Oss, and J.W. Vanderhoff, Eds.), Elsevier/North Holland Biomedical Press (1979), p.75.

O4 Ohshima, H., Healy, T.W., and White, L.R., J. Colloid Interface Sci., 90, 17 (1982).

O5 Overbeek, J.Th.G., de Brujn, D.L., and Verhoek, F., in "Surfactants", (Th.F. Tadros, Ed.), Academic Press, London (1984), p.125.

P1 Parsons, R.W., J. Pet. Tech., 26, 550 (1974).

P2 Parrish, D.R., and Craig, F.F. Jr., J. Petr. Technol., 753-761, June (1969).

P3 Puig, J.E., Franses, E.I., and Miller, W.G., J. Colloid Interface Sci., 89, 441 (1982).

P4 Parks, G.A., in "Equilibrium Concepts in Natural Water Systems" (W. Stumm, Ed.), Am. Chem. Soc., New York (1967), p.202.

P5 Prince, L.M., in "Microemulsions" (L.M. Prince, Ed.), Academic Press, New York (1977), p.127.

R1 Reed, R.L., and Healy, R.N., in "Improved Oil Recovery by Surfactant and Polymer Flooding" (D.O. Shah, and R.S. Schecter, Eds.), Academic Press, p.383 (1977).

R2 Rosen, M.J., in "Surfactants and Interfacial Phenomena", Wiley Interscience, New York (1978), p.150.

R3 Rand, B., and Melton, I.E., Nature, 257, 214 (1975).

R4 Reid, V.W., Longman, G.F., and Heinerth, E., Tenside, 4, 292 (1967).

R5 Rosen, M.J., and Nakamura, Y., J. Phys. Chem., 81, 873 (1977).

R6 Rosen, M.J., J. Colloid Interface Sci., 56, 320 (1976).

R7 Rao, I.V., and Ruckenstein, E., J. Colloid Interface Sci., 113, 375 (1986).

R8 Rahbain, R., and Francois, J., Polymer, 29, 845 (1988).

S1 Stalkup, F.I., SPE Monograph, 8 (1983).

S2 Shaw, D.J., "Introduction to Colloid and Surface Chemistry", 3rd ed., Butterworths (1980), p.75.

S3 Stern, O., Z. Electrochem., 30, 508 (1924).

S4 Smith, A.L., in "Dispersions of Powders in Liquids", Chapter 3, (G.D. Parfitt, Ed.), Applied Sciences Pub., Barking (1973).

S5 Shaw, D.J., "Electrophoresis", Academic Press, London (1969), p.60.

S6 Smith, A.L., J. Colloid Interface Sci., 55 (3), 525 (1976).

S7 Schofield, R.K., and Samson, H.R., Disc. Faraday Soc., 18, 135, (1954).

S8 Street, N., and Buchanan, A.S., Aust. J. Chem., 9, 450 (1956).

S9 Staples, E.J., and Tiddy, G.J.T., J. Chem. Soc., Faraday Trans. I, 74, 2530 (1878).

S10 Socrates, G., "Infrared Characteristic Group Frequencies", John Wiley and Sons, Chichester (1980).

S11 Stilbs, D., J. Colloid Interface Sci., 87, 385 (1982).

S12 Stephen, H., and Stephen, T. (Eds.), "Solubilities of Inorganic and Organic Compounds", Pergamon Press, Oxford (1969).

S13 Scamehorn, J.F., Schecter, R.S., and Wade, W.H., J. Colloid Interface Sci., 85, 463 (1982).

S14 Somasundaran, P., Healy, T.W., and Fuerstenau, D.W., J. Phys. Chem., 68, 3562 (1964).

S15 Somasundaran, P., and Fuerstenau, D.W., J. Phys. Chem., 79, 90 (1966).

S16 Somasundaran, P., "Adsorption from Flooding Solutions in Porous Media", Annual Report submitted to the Dept. of Energy, Columbia, New York (1983-1987); also Colloids and Surfaces, 26, 55 (1987).

T1 Taber, J.J., Soc. Petrol. Eng. J., 3-12, March (1969).

T2 Taber, J.J., Kirby, J.C., and Schroeder, F.U., AlChE Symp. Ser., No. 127, 69, 53 (1973).

T3 Trapnell, B.M.W., and Hayward, D.O., "Chemisorption", 2nd Ed., Butterworths, London (1964), p.60.

T4 Trogus, F.J., Schecter, R.S., and Wade, W.H., J. Colloid Interface Sci., 70, 293 (1979).

T5 Tschapek, M., Tcheichvili, L., and Wasowski, C., Clay Miner, 10, 219 (1974).

T6 Tadros, Th.F., J. Colloid Interface Sci., 46, 528 (1974).

T7 Tamamuschi, B., and Tamaki, K., Trans. Faraday Soc., 55, 1007 (1959).

V1 van Olphen, H., Disc. Faraday Soc., 11, 82 (1951).

V2 van Olphen, H., "An Introduction to Clay Colloid Chemistry", Wiley Interscience, New York (1963), p.16.

V3 Vestier, D., Sci. Terre., 14, 289 (1969).

V4 Vogel, A.I., "Textbook of Quantitative Inorganic Analysis", 4th Ed., Longmans (1978), p.116.

V5 Vogel, A.I., "Textbook of Practical Organic Chemistry", 4th Ed., Longmans (1978), p.206.

W1 Wagner, O.R., and Leach, R.O., Soc. Pet. Eng. J., 335-344, December (1966).

W2 Wakamatsu, T., and Fuerstenau, D.W., Adv. Chem. Ser., 79, 161 (1968).

W3 Wasik, S.P., and Roscher, N.M., J. Phys. Chem., 74, 2784 (1970).

W4 Williams, D.J.A., and Williams, K.P., J. Colloid Interface Sci., 65 (1), 79 (1978).

W5 Wiggins, J.L., Soc. Pet. Eng. J., 29 (5), 347 (1957).

W6 Weise, G.R., James, R.O., Yates, D.E., and Healy, T.W., "Electrochemistry" (M.T.P. Int. Rev. Sci.), Butterworths, London (1976), p.350.

Y1 Yoon, R., and Salman, T., Proc. Int. Conf. Colloid Interface Sci., 50th, 233 (1976).

Z1 Zettlemoyer, A.C., Ind. Eng. Chem., 57, 2, 27 (1965).

Z2 Ziegler, W.T., and Mullins, J.C., Report No. 1 to the National Bureau of Standards, Project A-663, Georgia Institute of Technology, Atlanta, April (1963).

Z3 Zana, R., Yio, S., Strazielle, C., and Lianos, P., J. Colloid Interface Sci., 80, 208 (1981).

Z4 Zhao, Z., and Gu, T., J. Chem. Soc., Faraday Teans. I, 81, 185 (1985).

APPENDIX I

Derivation of the Gibbs, Langmuir, Freundlich and Tempkin Equations

A.1.1 The Gibbs Equation (1878)

The Gibbs equation quantitatively relates the amount of surfactant adsorbed at an interface to the reduction in interfacial tension produced. Gibbs considered the surface as a matheamtical plane dividing two phases. This is illustrated in Figure A1, where the composition of the α and β phases are homogeneous up to the planes AA' and BB' respectively. The dividing plane is taken at some arbitrarily chosen location.

The general form of the Gibbs equation, which describes changes in surface tension between the limits AA' and BB' can be written (A2):

$$(d\gamma)_T = - \sum_i \Gamma_i . d\mu_i \qquad (1)$$

where, γ = the surface tension of the surfactant solution, mN m^{-2}

μ_i = the chemical potential of the i^{th} component

and Γ_i = the surface excess concentration of the i^{th} component per unit area of the interface, mol m^{-2}.

Thus, for a two-component liquid mixture, equation (1) becomes:

$$-d\gamma = \Gamma_1 \, d\mu_1 + \Gamma_2 \, d\mu_2 \qquad (2)$$

where subscripts 1 and 2 refer to the solvent and solute respectively. Whilst equation (2) describes the surface excesses for any given position of the dividing plane, SS' is usually set such that the surface excess concentration of the solvent is zero ($\Gamma_1 = 0$). Equation (2) may now be written:

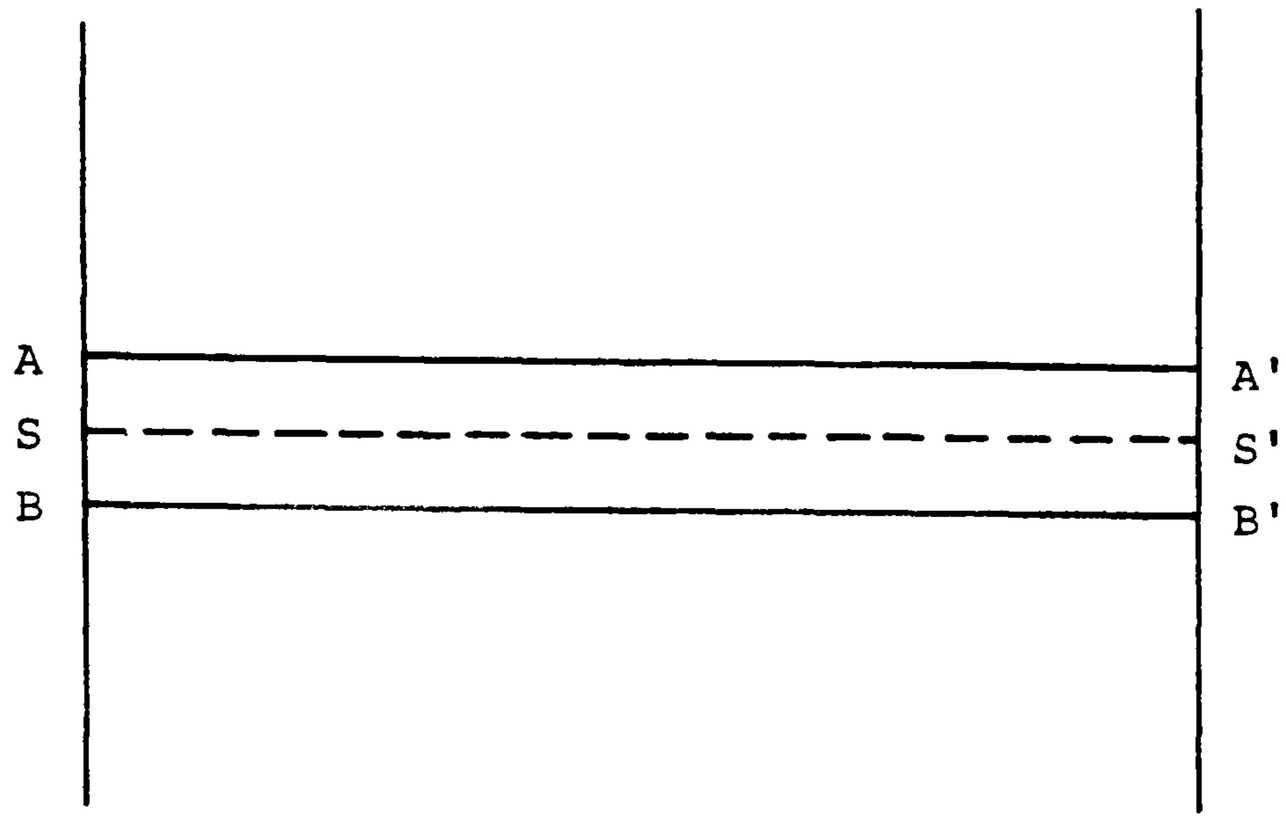

Figure A1: The Gibbs dividing plane model

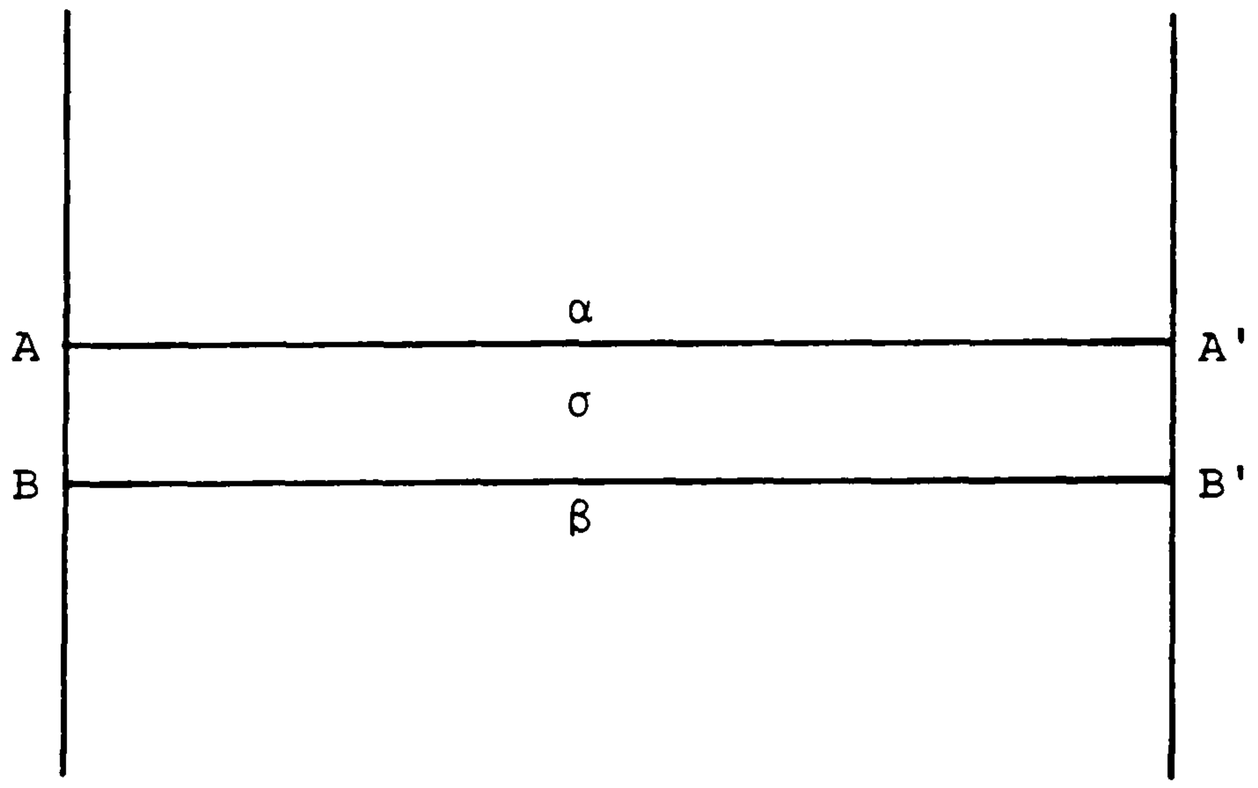

Figure A2: The surface phase model

$$-d\gamma = \Gamma_2 \, d\mu_2 \qquad (3)$$

(where Γ_2 is more accurately defined as the "relative" surface excess concentration).

Noting that $$\mu_2 = \mu_2^{\ominus} + RT \ln a_2 \qquad (4)$$

and $$d\mu_2 = RT \, d\ln a_2 \qquad (5)$$

where a_2 = the activity of component 2 in the bulk solution.

Substitution of this into equation (3) gives:

$$-d\gamma = RT \, \Gamma_2 \, d\ln a_2 \qquad (6)$$

which on rearrangement gives:

$$\Gamma_2 = \frac{1}{RT} \cdot \frac{d\gamma}{d\ln a_2} \qquad (7)$$

Using equation (7), surface excess concentrations can be determined from changes in the surface tension of aqueous surfactant solutions with increasing bulk activity.

The main criticism of the Gibbs dividing plane approach is that the interface will have a finite thickness (possibly up to several hundred Å), and may thus be better considered as a separate phase (σ in Figure A2) of not less than one molecular layer in depth (A2).

The surface phase approach (e.g. Guggenheim [G12]), illustrated in Figure A2, again considers the bulk phases, α and β, to be homogeneous up to the planes AA' and BB' respectively, but that the change from one phase to the other occurs over the distance AB (the surface phase σ). Thus, rewriting equation (1), and considering the interface as a separate phase, we have:

$$-d\gamma = \Gamma_1^{\sigma}.d\mu_1 + \Gamma_2^{\sigma}.d\mu_2 \qquad (8)$$

where, Γ_1^{σ} and Γ_2^{σ} are the total concentrations of components 1 and 2 in the surface phase.

Since the Gibbs-Duhem relationship for a two-component liquid mixture (at constant temperature and pressure) is given as:

$$N_1.d\mu_1 = -N_2.d\mu_2 \qquad (9)$$

where, N_1 and N_2 denote the bulk mole fractions of components 1 and 2 respectively, then equation (8) may be expressed as:

$$-d\gamma = \Gamma_2^{\sigma} - \frac{N_2}{N_1} \cdot \Gamma_1^{\sigma} \ .d\mu_2 \qquad (10)$$

Substitution of equation (10) into (3) gives:

$$\Gamma_2 = \Gamma_2^{\sigma'} - \frac{N_2}{N_1} \cdot \Gamma_1^{\sigma} \qquad (11)$$

The quantity Γ_2 is thus defined as the total surface concentration of component 2, less that which is present in the bulk region which contains an equivalent number of moles of component 1 [A2]. Clearly, at dilute solutions of a strongly-adsorbing surfactant, the last term in the bracket of equation (10) is small compared to the first and the equation reduces to that of the dividing plane model (equation (3).

A.1.2 The Langmuir Equation

The Langmuir adsorption isotherm is based on the characteristic assumptions that:

(i) only monolayer adsorption takes place

(ii) adsorption is localized, and

(iii) the heat of adsorption (ΔH) is independent of surface coverage (θ).

As a result of the first assumption, the rate of adsorption is proportional to the fraction of surface which is bare, $(1 - \theta)$, as well as the number of molecules striking the surface (Z). Gas kinetic theory predicts that the collision rate of molecules with a surface per cm^2 per second is given by:

$$Z = PN \left(\frac{1}{2\pi\ MRT}\right)^{\frac{1}{2}} \qquad (12)$$

where P = pressure in N m^{-2}

N = the number of molecules considered

M = the relative molecular mass.

Thus, the rate of adsorption per unit area is:

$$R_a = k_1\ X(1 - \theta) \qquad (13)$$

The rate of desorption of molecules from the surface is proportional to the surface coverage and inversely proportional to a desorption energy term (exp $\Delta H/RT$). The rate of desorption per unit area is therefore:

$$R_d = k_2\ \theta \exp \frac{\Delta H}{RT} \qquad (14)$$

At equilibrium, $R_a = R_d$, giving:

$$k_1 Z(1 - \theta) = k_2 \, \theta \exp \frac{\Delta H}{RT} \qquad (15)$$

Rearranging equation (15):

$$\theta = \frac{bP}{1 + bP} \qquad (16)$$

in which,

$$b = \frac{k_1}{k_2} \cdot \frac{N}{(2\pi \, MRT)^{\frac{1}{2}}} \cdot \exp \frac{\Delta H}{RT}$$

Alternatively, θ can be replaced by V/V_m, where V denotes the volume of gas adsorbed and V_m represents the monolayer volume, thus:

$$V = V_m \, bP/1 + bP \qquad (17)$$

and rearranging equation (17) gives:

$$\frac{P}{V} = \frac{1}{V_m \, b} + \frac{P}{V_m} \qquad (18)$$

so that the plot of P/V versus P gives a straight line with a slope of $1/V_m$.

For adsorption from solution, the equation (18) may be expressed by:

$$\frac{M_D}{\Gamma_D} = \frac{1}{\Gamma_m . b} + \frac{M_D}{\Gamma_m} \qquad (19)$$

where M_D = the equilibrium bulk concentration of solute, in mol dm^{-3}

Γ_D = the amount of solute adsorbed per unit area of adsorbent, in mol m^{-2}

Γ_m = the monolayer capacity, in mol m^{-2}

b = a constant, given above, in dm^{-3} mol^{-1}.

A.1.3 The Freundlich Equation

The Freundlich equation can be derived theoretically from the Langmuir equation if certain assumptions are made concerning the nature of the surface and the mechanism of adsorption [S2].

Expressing the Langmuir equation as:

$$\theta = \frac{bP}{1 + bP} \quad .$$

This equation is true if the quantity "b" is independent of θ. If this is not so, the total surface coverage can be obtained by a process of summation. Thus, dividing the surface into a number of groups of identical sites, designated as "i", each of which has a particular value of "b", the above equation can be expressed as:

$$\theta_i = \frac{b_i P}{1 + b_i P} \tag{20}$$

and the total coverage is given by:

$$\theta = \Sigma\ \theta_i\ n_i \tag{21}$$

where n_i = the fraction of sites of type "i".

If the "b" values are sufficiently close in value to form a continuous distribution then equation (21) can be reduced to:

$$\theta = \int n_i\ \theta_i\ d_i \tag{22}$$

where $n_i d_i$ is the frequency of occurrence of θ_i between i and $i + d_i$. In general this integration cannot be carried out because the distribution function n_i is unknown. However, if the variation of b_i is simply due to the variation of ΔH, i.e. the heat of adsorption,

then equations (20) and (22) may be expressed as:

$$\theta_H = \frac{b_{\Delta H} P}{1 + b_{\Delta H} P} \tag{23}$$

and

$$\theta = \int n_{\Delta H} . \theta_{\Delta H} . d\Delta H \tag{24}$$

If $n_{\Delta H}$ is exponentially dependent on ΔH then:

$$n_{\Delta H} = n_o \exp \frac{-\Delta H}{\Delta H_m} \tag{25}$$

where, n_o and ΔH_m = constants representing the total number of adsorption sites, and the minimum heat of adsorption respectively.

Substitution of equations (23) and (25) into equation (24) gives an expression that can be solved:

$$\theta = \int_0^\infty n_o \exp \frac{-\Delta H}{\Delta H_m} \cdot \frac{b_{\Delta H} P}{1 + b_{\Delta H} P} . \, d\Delta H \tag{26}$$

Now, expressing $b_{\Delta H} = b_o \exp(\Delta H/RT)$, equation (26) becomes, after rearranging:

$$\theta = \int_0^\infty \frac{n_o \exp {}^{-\Delta H/}{}_{\Delta H_m}}{1 + \exp \frac{-\Delta H/RT}{b_o P}} . d\Delta H \tag{27}$$

which upon integration gives:

$$\theta = b_o P^{RT/\Delta H_m} . n_o \, \Delta H_m \tag{28}$$

or,

$$\theta = k \, P^{\frac{1}{n}} \tag{29}$$

where

$$k = b_o \, n_o \, \Delta H_m$$

and, $$\frac{1}{n} = \frac{RT}{\Delta H_m} \quad .$$

This is the Freundlich equation. Therefore the Freundlich equation represents the summation of a distribution of Langmuir equations, however, the amount of adsorbate adsorbed (i.e. the surface coverage) is not depicted as approaching a limiting value as in a single Langmuir equation.

A.1.4 The Tempkin Equation

The Tempkin equation may be derived by inserting in the Langmuir equation, the condition that the heat of adsorption decreases directly with surface coverage [B10]. Such a reduction can arise either on a uniform surface from lateral (repulsive) interactions, or from surface heterogeneity.

(a) Derivation for a uniform surface

Expressing the Langmuir equation in the form:

$$\theta = \frac{bP}{1 + bP}$$

and substituting for b gives, upon rearrangement, the expression:

$$\frac{\theta}{1 - \theta} = P.b_o \exp \frac{\Delta H}{RT} \qquad (30)$$

Since all sites are identical it is sufficient to insert into equation (30) the condition that ΔH varies with θ according to the equation:

$$\Delta H = \Delta H_o(1 - \beta\theta) \qquad (31)$$

in which, ΔH_o = the heat of adsorption at $\theta = 0$ in J mol^{-1}

and β = a constant, in J mol^{-1}.

Thus,

$$\frac{\theta}{1 - \theta} = P.b_o \exp \frac{\Delta H_o(1 - \beta\theta)}{RT} \qquad (32)$$

Taking logarithms and rearranging:

$$\ln P = \frac{\ln \theta}{1 - \theta} - \ln b_o \exp \frac{\Delta H_o}{RT} + \frac{\Delta H_o \beta\theta}{RT} . \qquad (33)$$

For $0.2 < \theta < 0.8$, variations in $\ln \frac{\theta}{(1 - \theta)}$ may be neglected and thus equated to zero (its value at $\theta = 0.5$).

Thus, equation (33) simplifies to:

$$\theta = \frac{RT}{\Delta H_o \beta} \ln P.b_o \exp \frac{\Delta H_o}{RT} , \qquad (34)$$

the Tempkin equation.

(b) Derivation for a non-uniform surface

Here, it is necessary to divide the surface into a number of uniform elements, ds, on each of which the heat of adsorption is constant, and the Langmuir equation is expressed as:

$$\theta = \frac{bP}{1 + bP}$$

therefore,

$$\theta_s = \frac{b_o \exp(\Delta H/RT).P}{1 + b_o \exp(\Delta H/RT).P} \qquad (35)$$

and the value of θ over the whole surface is obtained by integration:

$$\theta = \int \theta_s . ds \qquad (36)$$

Since ΔH falls linearly with s:

$$\Delta H = \Delta H_o (1 - \beta s) \qquad (37)$$

Inserting (35) and (37) in (36) and assuming the total surface area is unity:

$$\theta = \int_0^1 \frac{b_o \exp(\Delta H_o (1 - \beta s)/RT) . P . ds}{1 + b_o \exp(\Delta H_o (1 - \beta s)/RT) . P} \qquad (38)$$

which gives:

$$\theta = \frac{RT}{\Delta H_o \beta} \ln \frac{1 + b_o \exp(\Delta H_o/RT) . P}{1 + b_o \exp(\Delta H_o/RT) . P . \exp(-\Delta H_o \beta/RT)} \qquad (39)$$

Now, assuming that for $0.2 < \theta < 0.8$, P is sufficiently large for $[b_o \exp(\Delta H_o/RT) . P]$ to be much greater than unity but still low enough for $[b_o \exp(\Delta H_o/RT) . P \times \exp(-\Delta H_o \beta/RT)]$ to be less than unity, equation (39) simplifies to:

$$\theta = \frac{RT}{\Delta H_o \beta} \ln . P . b_o \exp(\Delta H_o/RT) \qquad .. \text{ (equation (34))}$$

i.e. the Tempkin equation, which may then be written as:

$$\theta = A \ln B + A \ln P \qquad (40)$$

in which $A = \frac{RT}{\Delta H_o \beta}$

and $B = b_o \exp(\Delta H_o/RT) .$

The Tempkin equation is thus valid for $0.2 < \theta < 0.8$ [T3].

APPENDIX 2

Program to calculate various BET Parameters

In order to calculate the figures required to plot the BET line a calculation sheet was used. The process was time consuming and prone to errors induced by mis-calculations. A program, listed below, was written to overcome these problems.

```
10   REM CALCULATION OF BET PARAMETERS P N BROWN 8.6.84
20   PRINT "THIS IS A PROGRAM TO CALCULATE THE VARIOUS"
30   PRINT "FIGURES IN THE BET CALCULATION SHEET."
40   PRINT "*****************************************"
50   PRINT "PLEASE INPUT SAMPLE ID, SAMPLE WEIGHT, H1 AND H2"
60   INPUT N$, W, H1, H2
70   PRINT "NOW INPUT TS AND PS"
80   INPUT TS, PS
90   REM THIS IS END OF MAIN DATA INPUT
100  PRINT "*****************************************"
110  LET VD = 28.47
120  LET Q = 130.6
130  LET Z = 6.6E-5
140  LET S = 16.2
150  LET T! = (307.2 + TS) /2
160  LET K = 0
170  LET VS = TS * ((VD * (H1 - H2)/307.2) - (3.65 * H2)/T1/H2
180  LET A1 = (0.001169 * (VD + Q)/W
190  LET A2 = (0.001169 * VD)/W
200  PRINT VS
```

```
210  LET B = (0.3593 * VS)/(TS * W) + 1.311/(T1 * W)

220  LET C = (0.3593 * VS * Z)/(W * TS)

230  PR#1

240  PRINT "**************************************************"

250  PRINT "T1 VALUE=";T1"K"

260  PRINT "VS VALUE =";VS"mls"

270  PRINT "A1 VALUE =";A1

280  PRINT "A2 VALUE =";A2

290  PRINT "B VALUE =";B

300  PRINT "C VALUE =";C

310  PR#0

320  REM THIS IS THE END OF THE PARAMETER DETERMINATION

330  PRINT "PLEASE INPUT NUMBER OF DATA POINTS"

340  INPUT N

350  FOR I = 1 TO N

360  PRINT "PLEASE INPUT EXTRA VOLUME CODE, 1 IF USED"

370  PRINT "= IF NOT"

380  INPUT J

390  IF J = 1 GOTO 410

400  IF J = = GOTO 430

410  LET O = A1

420  GOTO 440

430  LET O = A2

440  PRINT "PLEASE INPUT P1(";I),P2(";I"),PE(";I")"

450

460  LET D = P1 - P2

470  LET E = P2 - PE

480  LET F = P2↑2 - PE↑2
```

```
490  LET G = O * D

500  LET H = B * E

510  LET J = C * F

520  LET VA = G - H - J

530  GOTO 2000

540  LET V = VA + U

550  LET K = VA

560  LET X = P2/PS

570  LET Y = X?(V * (1-X)

580  PR#3

590  PR#1

600  PRINT "**********************************************"

610  REM THIS IS THE END OF THE CALCULATION SECTION

620  PRINT "P1(";I") =", P1

630  PRINT "P2(";I") =", P2

640  PRINT "PE(";I") =", PE

650  PRINT "D(";I")  =", D

660  PRINT "E(";I")  =", E

670  PRINT "F(";I")  =", F

680  PRINT "G(";I")  =", G

690  PRINT "H(";I")  =", H

700  PRINT "J(";I")  =", J

710  PRINT "VA/WS(";I") =", VA

720  PRINT "V(";I")  =", V

730  PRINT "X(";I")  =", X

740  PRINT "Y(";"I") =", Y

750  REM END OF PRESENTATION SECTION

760  PRINT "**********************************************"
```

```
770  PR#0

780  IF I = N GOTO 2020

790  NEXT I

2000 LET U = K

2010 GOTO 540

2020 PRINT "CALCULATION COMPLETE.  DO YOU WANT ANOTHER RUN?"

2030 PRINT "IF YES TYPE 1, IF NO TYPE 0"

2040 INPUT R

2050 IF R = 1 GOTO

2060 END
```